AD-A090 546 GENERAL MOTORS CORP INDIANAPOLIS IN DETROIT DIESEL A--ETC F/G 21/5
THE EFFECTS OF SOLIDITY, INTERBLADE PHASE ANGLE AND REDUCED FRE--ETC(U)
JUN 80 R L JAY, W A BENNETT F49620-78-C-0070
UNCLASSIFIED DDA-EDR-10339 AFOSR-TR-80-1041 NL

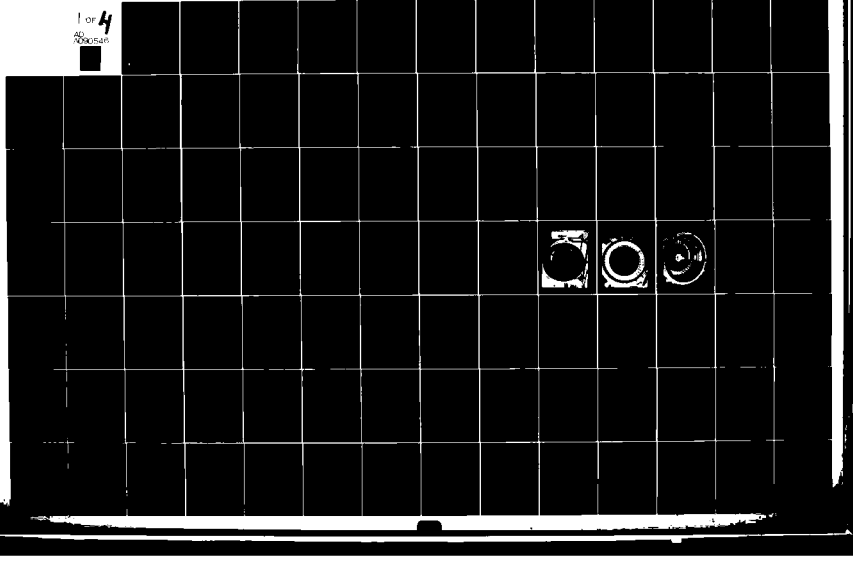

THE EFFECTS OF SOLIDITY, INTERBLADE PHASE ANGLE AND REDUCED FREQUENCY ON THE TIME-VARIANT AERODYNAMIC RESPONSE OF A COMPRESSOR STATOR

EDR 10339

ROBERT L. JAY

WILLIAM A. BENNETT

JUNE 1980

Research Sponsored by the
Air Force Office of Scientific Research
(AFSC) United States Air Force
under Contract F49620-78-C-0070

Detroit Diesel Allison
Division of General Motors Corporation
P.O. Box 894 Indianapolis, Indiana 46206

"Qualified requestors may obtain additional copies from the Defense Technical Information Center, all others should apply to the National Technical Information Service"

Unclassified

SECURITY CLASSIFICATION OF THIS PAGE (When Data Entered)

REPORT DOCUMENTATION PAGE

READ INSTRUCTIONS BEFORE COMPLETING FORM

1. REPORT NUMBER: AFOSR-TR-80-1041	2. GOVT ACCESSION NO.: AD-A090 546
3. RECIPIENT'S CATALOG NUMBER:	
4. TITLE (and Subtitle): THE EFFECTS OF SOLIDITY, INTERBLADE PHASE ANGLE AND REDUCED FREQUENCY ON THE TIME-VARIANT AERODYNAMIC RESPONSE OF A COMPRESSOR STATOR.	5. TYPE OF REPORT & PERIOD COVERED: INTERIM (ANNUAL rpt.) 1 May 79 — 1 May 80
	6. PERFORMING ORG. REPORT NUMBER: DDAEDR-77337
7. AUTHOR(s): ROBERT L. JAY, WILLIAM A. BENNETT	8. CONTRACT OR GRANT NUMBER(s): F49620-78-C-0070
9. PERFORMING ORGANIZATION NAME AND ADDRESS: DETROIT DIESEL ALLISON Div. P. O. BOX 894 INDIANAPOLIS, INDIANA 46206	10. PROGRAM ELEMENT, PROJECT, TASK AREA & WORK UNIT NUMBERS: 2307A4 61102F A4
11. CONTROLLING OFFICE NAME AND ADDRESS: AIR FORCE OFFICE OF SCIENTIFIC RESEARCH/NA BLDG 410 BOLLING AIR FORCE BASE, DC 20332	12. REPORT DATE: Jun 80 — 13. NUMBER OF PAGES: 103
14. MONITORING AGENCY NAME & ADDRESS (if different from Controlling Office)	15. SECURITY CLASS. (of this report): UNCLASSIFIED
	15a. DECLASSIFICATION DOWNGRADING SCHEDULE

16. DISTRIBUTION STATEMENT (of this Report)

Approved for public release; distribution unlimited

17. DISTRIBUTION STATEMENT (of the abstract entered in Block 20, if different from Report)

18. SUPPLEMENTARY NOTES

19. KEY WORDS (Continue on reverse side if necessary and identify by block number)

FORCED VIBRATION
AERODYNAMICALLY INDUCED VIBRATION
TURBO MACHINERY
UNSTEADY FLOW
AXIAL FLOW COMPRESSOR

20. ABSTRACT (Continue on reverse side if necessary and identify by block number)

An experimental investigation was conducted to provide basic unsteady pressure distributions on a stationary vane row, with the primary source of excitation being the wakes generated from an upstream rotor. This was accomplished over a wide range of key parameters in a large-scale, low-speed, single stage compressor. The excitation, the velocity defect created by the rotor blade wakes, was measured with a crossed hot wire. The resulting time-variant aerodynamic response was measured by means of flush mounted high response

DD FORM 1 JAN 73 1473

UNCLASSIFIED

SECURITY CLASSIFICATION OF THIS PAGE (When Data Entered)

pressure transducers mounted on a stator vane over a wide range in incidence angles. The dynamic data were analyzed to determine the chordwise distribution of the dimensionless dynamic pressure coefficient and aerodynamic phase lag as referenced to the transverse gust at the vane leading edge.

Parametric changes were accomplished by changing the number of rotor blades and stator vanes. Data for reduced frequencies from 3.0 to 20 were obtained, while solidity was varied between .758 and 1.516. The interblade phase angles were determined as a function of the number of rotor blades and number of stator vanes and varied as either was changed. The data obtained from the experimental portion of this study were correlated with a compressible, thin, uncambered airfoil cascade analysis. Comparisons were good for low incidence flow at reduced frequencies less than 15. Grid spacing chosen for the analysis resulted in large deviations between theory and experimental data at the higher reduced frequencies. Of the variables considered, the steady flow field affected the time-variant pressure distribution on the stator vane most greatly.

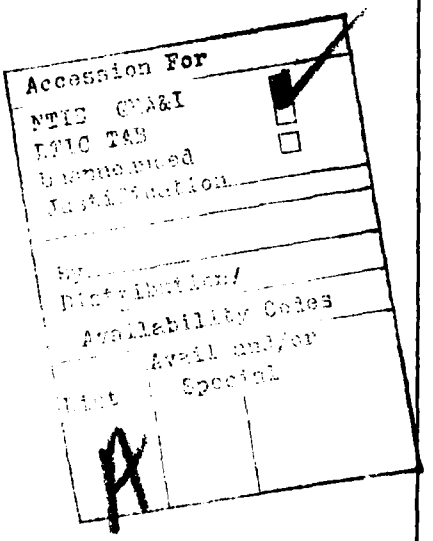

THE EFFECTS OF SOLIDITY, INTERBLADE PHASE ANGLE AND REDUCED FREQUENCY ON THE TIME-VARIANT AERODYNAMIC RESPONSE OF A COMPRESSOR STATOR

EDR 10339

JUNE 1980

ROBERT L. JAY
WILLIAM A. BENNETT

RESEARCH SPONSORED BY THE
AIR FORCE OFFICE OF SCIENTIFIC RESEARCH (AFSC)
UNITED STATES AIR FORCE
UNDER CONTRACT F49620-78-C-0070

ABSTRACT

An experimental investigation was conducted to provide basic unsteady pressure distributions on a stationary vane row, with the primary source of excitation being the wakes generated from an upstream rotor. This was accomplished over a wide range of key parameters in a large-scale, low-speed, single stage compressor. The excitation, the velocity defect created by the rotor blade wakes, was measured with a crossed hot wire. The resulting time-variant aerodynamic response was measured by means of flush mounted high response pressure transducers mounted on a stator vane over a wide range in incidence angles. The dynamic data were analyzed to determine the chordwise distribution of the dimensionless dynamic pressure coefficient and aerodynamic phase lag as referenced to the transverse gust at the vane leading edge.

Parametric changes were accomplished by changing the number of rotor blades and stator vanes. Data for reduced frequencies from 3.0 to 20 were obtained, while solidity was varied between .758 and 1.516. The interblade phase angles were determined as a function of the number of rotor blades and number of stator vanes and varied as either was changed. The data obtained from the experimental portion of this study were correlated with a compressible, thin, uncambered airfoil cascade analysis. Comparisons were good for low incidence flow at reduced frequencies less than 15. Grid spacing chosen for the analysis resulted in large deviations between theory and experimental data at the higher reduced frequencies. Of the variables considered, the steady flow field affected the time-variant pressure distribution on the stator vane most greatly.

TABLE OF CONTENTS

LIST OF TABLES

LIST OF ILLUSTRATIONS

NOMENCLATURE

b	Airfoil semi-chord
c	Airfoil chord
C_p	Dynamic pressure coefficient ($\Delta P/(\rho V^2 v/V)$)
L	Length
R	Radius
R_c	Compressor pressure ratio
V	Absolute velocity
$W\sqrt{\theta}/\delta$	Corrected mass flow
S	Vane spacing
T	Blade pass period
X	Distance from rotor trailing edge
K	Reduced frequency ($K = \omega b/V$)
u	Longitudinal perturbation velocity
v	Transverse perturbation velocity
β	Inlet angle
ϕ	Phase lag
ρ	Inlet air density
ω	Blade passing angular frequency
ΔP	Suction to pressure surface pressure differential on a vane

Subscripts

1	First harmonic
2	Second harmonic
ABS	Absolute
R	Rotor
Ax	Axial
REL	Relative

INTRODUCTION

Aerodynamically induced vibration of fan, compressor and turbine airfoils is a commonly encountered problem in the development of gas turbine engines. Vibrations occur when a periodic aerodynamic forcing function has a frequency equal to the natural frequency of a blade. These frequency correspondences are typically plotted on a frequency/speed diagram which relates the natural frequencies of a particular blade and its forcing function frequencies at varying rotor speeds.

Current technology is sufficient to predict with a fair degree of accuracy the natural frequencies of bladed disk systems. The knowledge of the source of various aerodynamic stimuli acting on the airfoils is also well substantiated by experience. However, these tools are used only to locate, in terms of rotor speed, the resonant points on a frequency/speed diagram. Design rules are used typically to determine if a particular intersection will be detrimental to engine operation. At present, the actual values of the resonant stresses are unknown until the first testing of the assembled rig or engine. If stresses in excess of a predetermined allowable value are measured, then life requirements dictate that such stresses must be reduced. This reduction can be effected by altering frequencies, changing the magnitude of the forcing function, increasing allowables for the airfoil, and other demonstrated techniques. Systematic as this procedure may seem, it still requires that test iteration be performed until design goals are met. Hence, a predictive methodology for determining the stress levels of a blade in resonance with an aerodynamic forcing function is needed.

The predictive model would include a description of the pressure distribution created by the disturbance being swept past an assumed nonresponding airfoil and of the pressure distribution created by the movement of the airfoil in the aerodynamic field. The first of these effects has been labeled the "gust" loading, the second termed the "aerodynamic damping." An iterative solution which relates the gust loading, the ensuing blade motion, and

the generated aerodynamic damping is necessary to properly predict the total response of a particular airfoil.

The aerodynamic "gust" problem has been analyzed by several investigators. Kemp and Sears[1]*, Horlock[2], Naumann and Yeh[3], and Goldstein and Atassi[4] considered isolated airfoils acted on by various input gust profiles to determine unsteady or time-variant loadings of the airfoils. These investigators contributed to the overall understanding of the gust problem, yet the results were not amenable for application to turbomachinery blading rows.

D. S. Whitehead[5] analyzed a cascade of flat-plate airfoils subjected to a wake resulting from periodic obstructions far upstream and presented the induced gust loading as functions of cascade variables for incompressible flow. Smith[6] extended this analysis to include the effects of compressibility in the subsonic flow regime. Henderson and Daneshyar[7] used thin airfoil theory to derive an expression for the unsteady lift acting on a two-dimensional cascade of thin, slightly cambered airfoils moving through a sinusoidal disturbance in an incompressible velocity field. In a later analysis, Henderson and Horlock[8] analytically investigated a moving cascade of airfoils experiencing a sinusoidal disturbance in inlet axial velocity. Two-dimensional, inviscid, and incompressible flow was assumed for highly cambered, small-lift-coefficient blading. The purpose of these analyses was to describe analytically the time-variant loading of an airfoil attributable to wake-type disturbances. On-going analytical investigations by Verdon and Caspar[9] and Caruthers[10] are designed to properly consider realistic airfoil geometries in a loaded cascade operating in a two dimensional compressible flow field.

Because of the limiting assumptions in these and other analyses, experimental data to validate results and indicate needed improvements in the analytical models were needed. Such investigators as Commerford and Carta[11], Ostdiek[12], Henderson and Franke[13], and Fleeter, Novick, and Riffel[14]

*Numbers in parentheses correspond to references listed at end of this report.

furnished sets of initial correlative data. Fleeter, Bennett, and Jay [15, 16, 17, 18] have provided measurements of rotor wake-induced time-variant surface pressures on a highly cambered stator vane. The pressures were related to the strength of the incoming velocity defect typifying the rotor wake. Variations of parameters including reduced frequency, solidity, axial spacing, and interblade phase angle have provided an extensive data bank for correlation of gust analyses in the subsonic flow regime.

The aerodynamic damping portion of the overall forced vibration problem has been analytically investigated by several of these mentioned previously. Because the aerodynamic damping analyses are necessary to predict flutter, this area of research has been vigorously attacked. Whitehead[5], Smith[6], and Fleeter[19] are but a few of those who have presented analyses for the subsonic flow regime. The common assumption in many of these analyses has been that of a zero-thickness flat plate. Atassi and Akai[20] presented an analytical formulation for analyzing oscillating airfoils in cascade in uniform incompressible flows. The theory accounts for the geometry of the airfoils. Experimentally, the efforts of Carta and St. Hilaire[21], Fleeter and Riffel[22], and Riffel and Rothrock[23] in two-dimensional, rectilinear wind tunnels have furnished basic experimental damping for correlations in the low subsonic and supersonic flow regimes. The effect of loading on aerodynamic damping was identified by Riffel and Rothrock for torsional motion of thin, low camber airfoil operating in a supersonic cascade.

Jay, Rothrock, Riffel and Sinnet[24] have obtained benchmark experimental data from large turning airfoils operating in a cascade. A five blade cascade was oscillated in the torsional mode with prescribed interblade phase angles at varying levels of cascade loading (expansion ratio). Two high subsonic cases and two transonic cases were investigated in this study. This chordwise complex time-variant pressure field was correlated with existing thin, flat plate airfoil analysis.

Platzer[25] presented a review of unsteady flows in turbomachinery which included the efforts of investigators in the areas of both gust response

and aerodynamic damping. This survey was concluded with an emphasis on the need for evaluation of the various analytical formulations by comparison with experimental data, specifically in the area of highly loaded, transonic cascades.

Blade failures due to a "lyre," "stripe," or chordwise bending mode have become particularly troublesome in low aspect ratio blading. A schematic of the first three chordwise bending modes of a low aspect ratio airfoil is presented in Figure 1. These modes are excited, in general, by adjacent blade rows, thus have relatively high reduced frequencies. These type modes have been experienced in the reduced frequency range of 3 to 10. An examination of these modes indicates that the time-variant lift and moment coefficients are not sufficient to determine the energy input during forced response, a chordwise description of the unsteady loading must be obtained.

The purpose of the experimental research program described in this report is to provide basic unsteady aerodynamic data relevant to forced response with particular emphasis on expanding the data base with respect to the reduced frequency, loading interblade phase angle and solidity. This was accomplished in the Detroit Diesel Allison (DDA) low speed compressor research facility with variations in the above key parameters achieved by varying the number of rotor blades and stator vanes. The results of various operating conditions, i.e., compressor loading at a constant speed, on the measured unsteady chordwise vane surface pressures are presented along with a correlation of the data with an existing analysis.

DISCUSSION

EXPERIMENTAL FACILITY

The wakes from the upstream rotor blades are the source of the aerodynamically induced fluctuating surface pressure distributions on the stator vanes, i.e., the rotor wakes define the forcing function to the downstream stator vanes. Hence, it is necessary to experimentally model the significant features which define this forcing function. These include the wave form, the velocity variation, and the reduced frequency ($k = \omega C/2V_{axial}$). The above described features are simulated in the DDA large-scale, low speed, single stage research compressor. A schematic of the overall facility is shown in Figure 2 and a view of the assembled test rig in Figure 3.

This 48.01 inch inlet diameter research compressor features blading (42 rotor blades and 40 stator vanes, NACA 65 Series) that is aerodynamically loaded to levels that are typical of advanced multi-stage compressors and is also large enough to provide for large quantities of instrumentation. Table 1 presents the airfoil mean section properties as well as the compressor design point conditions. As indicated, the airfoils are large with the rotor and stator chords being equal to 4.589 and 5.089 inches (11.66 and 12.93 cm), respectively. In this facility the flow, the rotor speed and the pressure ratio can be varied independently.

The rotor blades were designed to have aerodynamic loading levels representative of aft stages of modern multi-stage compressors. At the design point, approximately 27° of turning is accomplished near the blade hub, diminishing to about 13° near the tip. The geometric characteristics of the rotor blade include high camber with fairly large deviation angle near the hub region, and a maximum thickness-to-chord ratio which varies from nearly 7% at the hub to 4% at the tip. The rotor solidity varies from about 1.6 at the hub to 1.3 at the tip. Figure 4 shows a view of the rotor.

The 40 vane stator row, seen in Figure 5, results in a nearly uniform axial exit flow direction. Again, the airfoil loss and aerodynamic loading levels are typical of those of aft stages of modern multistage compressors. The vane features a large camber angle variation in the hub region, a radially constant maximum thickness-chord distribution, and design point incidence that varies from about zero to minus one degree. Vane solidity varies from 1.68 at the hub to 1.35 at the tip.

INSTRUMENTATION

The research compressor steady-state instrumentation, indicated schematically in Figure 6, permits the inlet and exit flow fields to be defined and the compressor map determined. The inlet temperature is measured by means of four thermocouples equally spaced circumferentially in the large stagnation chamber. The rotor inlet velocity profile is determined from the pressure measurements obtained from three, eleven-element total pressure rakes equally spaced circumferentially, and the average of four hub and four tip static pressure taps. The exit flow field downstream of the stator row is determined from six total pressure rakes, uniformly spaced across an equivalent vane passage together with hub and tip static pressure taps. The exit temperature is measured with an eleven element rake located circumferentially at the center of the vane passage. The overall compressor aerodynamic performance is evaluated by examining the stagnation tank and stator exit temperature and pressure measurements, with the flow rate computed from the stagnation tank static pressure and total temperature and pressure measurements.

The time-variant quantities of fundamental interest in the proposed experimental investigations include the fluctuating aerodynamic forcing function -- the rotor wake, and the chordwise distributions of the complex time-variant pressure distribution on the downstream stator vane.

The blade surface dynamic pressure measurements are obtained by flush mounted Kulite thin-line design dynamic pressure transducers on a pair of the NACA

Series 65 stator vanes. These vanes are located in the stator row such that one flow passage is instrumented.

The time-variant wake measurements are obtained by means of a cross-wire probe calibrated and linearized up to 200 feet per second and ±25° angular variation. The probe is located at mid-stator circumferential spacing with axial location corresponding to mid rotor-stator axial spacing in a passage adjacent to the pressure instrumented one, as schematically depicted in Figure 7. The mean absolute exit flow angle from the rotor is determined by rotating the probe until a zero voltage difference is obtained between the two hot-wire channels. This mean angle is then used as a reference for calculating the instantaneous absolute and relative flow angles. The output from each channel is corrected for tangential cooling effects and the individual fluctuating velocity components parallel and normal to the mean flow angle calculated from the corrected quantities.

DATA ACQUISITION AND ANALYSIS

In this investigation, both steady and time-variant data were acquired. The steady state data define the points of compressor operation, in terms of overall pressure ratio and corrected mass flow rate, at which the unsteady velocity and surface pressure measurements will be obtained. Both the steady and time-variant data acquisition are controlled by an on-line digital computer. The rotor speed is manually controlled by varying the power to the DC drive motor; a digital readout of the rotor speed is provided via a tachometer generated signal.

Figure 8 presents a schematic of the steady state and time-variant instrumentation modules as related to the on-line remote digital computer. Only one mode of data acquisition operation can be performed at a time. The steady state corrected data is output on the teletype at the rig site as well as on a line printer. The time-variant data acquisition is controlled through the CRT terminal. On-line monitoring of this time-variant data is accomplished by means of a dual beam storage oscilloscope synchronized to

the speed of the rotor by a rotor shaft mounted optical encoder. The unsteady data are presented on the line printer, and stored in digital form on a magnetic disk and/or punched paper tape for off-line analysis.

The steady state data acquisition follows the standard compressor evaluation procedure. At a selected corrected speed, the compressor is stabilized for approximately 5 minutes. Following this period, the on-line computer is used to initiate the acquisition of the temperatures and pressures necessary to generate the corrected mass flow rate, overall pressure ratio, and corrected speed. A scanning of the reduced data is then made to assure data uniformity and to ascertain the operating point.

The time-variant data acquisition and analysis technique used is based on a data averaging or signal enhancement concept. The key to such a technique is the ability to sample data at a preset time. For this investigation the signal of interest is being generated at the blade passing frequency. Hence, the logical choice for a time or data initiation reference is the rotor shaft. An optical encoder is mounted on the rotor shaft for this purpose. This encoder delivers a square wave voltage signal having a duration of 40 microsconds. The computer analog-to-digital converter is triggered from the positive voltage at the leading edge of the pulse, thereby initiating the acquisition of the time unsteady data at the rate of up to 100,000 points per second. The data will be sampled for N blade passages and over M rotor revolutions. These rotor revolutions will not be consecutive because a finite time is required to operate on the N blade passage data before the computer returns to the pulse acceptance mode which initiated the gathering of the data.

At each steady operating point an averaged time-variant data set, consisting of the two hot-wire and the 22 Kulite signals, is obtained. Each of these signals is digitized, stored on a punched paper tape, and Fourier decomposed into its harmonics. In this investigation only the first two harmonics of the data are examined through the entirety of the data analysis process. The

reduced frequencies of these data are in the range of turbomachinery experience with forced response problems.

From the Fourier analyses performed on the data both the magnitude and phase angles referenced to the data initiation pulse are obtained. To then relate the wake generated velocity profiles with the surface dynamic pressures on the instrumented vanes, the rotor exit velocity triangles are examined.

Figure 9 shows the change in the rotor relative exit velocity which occurs as a result of the presence of the blade. A deficit in the velocity in this relative frame creates a change in the absolute velocity vector as indicated. This velocity change is measured via the crossed hot-wires. From this instantaneous absolute angle and velocity, the rotor exit relative angle and velocity and the magnitude and phase of the perturbation quantities are determined.

As noted previously, the hot-wire probe is positioned at mid rotor-stator axial spacing. To relate the time based events as measured by this hot wire probe to the pressures on the vane surfaces, the following assumptions are made: (1) the wakes are identical at the hot-wire and the stator leading edge planes; (2) the wakes are fixed in the relative frame. Figure 10 presents a schematic of the rotor wakes, the instrumented vanes, and the hot-wire probe. The rotor blade spacing, the vane spacing, the length of the probe, and the axial spacing between the vane leading edge plane and the probe holder centerline are known quantities. At a steady operating point the hot-wire data is analyzed to yield the absolute flow angle and the rotor exit relative flow angle. Using the two assumptions noted, the wake is located relative to the hot-wires and the leading edges of the instrumented vane suction and pressure surfaces. From this, the times at which the wake is present at various locations can be determined. The incremented times between occurrences at the hot-wire and the vane leading edge plane are then related to phase differences between the perturbation velocities and the vane surface pressures.

To simplify the experiment-theory correlation process, the data is adjusted in phase so that the transverse perturbation is at zero degrees at the vane suction surface leading edge.

From the geometry indicated in Figure 10, the time at which this would occur is calculated and transposed into a phase difference. This difference is then used to adjust the pressure data from the suction surface. A similar operation is performed on the pressure surface data so that the surfaces of the vanes are time related; i.e., time relating the data resulted in data equivalent to that for a single instrumented vane.

Following this procedure the pressure differences across a single vane at all transducer locations are calculated. These data, along with the individual surface pressure data, are normalized with respect to the quantity $\rho \cdot V^2 \cdot \frac{v}{V}$; where ρ is the density, V is the absolute velocity, and v is the transverse perturbation velocity at the vane inlet. This unsteady pressure differential data will be correlated with predictions obtained from an appropriate state-of-the-art unsteady aerodynamic cascade analysis.

CALIBRATION PROCEDURES

Calibrations of the two primary data sensors, the crossed hot wire and the Kulites, were performed before the time variant data was obtained so that the transfer functions throughout the measurement system could be determined. Included in these measurements were Kulite static sensitivities, amplitude and phase shift of the Kulite signals due to amplifier and signal conditioner gains and temperature and directional sensitivities of the crossed hot wire. The following paragraphs briefly delineate the calibration procedure used on the Kulite pressure transducers and the crossed hot wire system.

The Kulite pressure transducer static sensitivities were obtained using a vacuum-jar calibration rig. A quartz manometer-controller was used to evacuate the jar containing the Kulite-instrumented blade to the desired pressure. The d-c voltage of each Kulite was measured over a range of pressures, resulting

in plots of voltage versus pressure. The sensitivities in mV/psi were the slopes of these linear plots. These sensitivities compared closely with manufacturer-supplied data.

The crossed hot wire is calibrated in a standard DISA 55D44 hot wire calibrator system. The velocity range is chosen such that the anemometer output during operation is on the highly sloped part of the voltage output curve as shown in Figure 11. This procedure ensures a high sensitivity of velocity change for a given anemometer voltage variation. Due to the fact that the sensor wires are physically placed at a 45 degree angle to the plane normal to the velocity vector of the rotor field, the anemometer output must be corrected for tangential cooling effects. The complete analysis for obtaining this correction is found in reference (26). The crossed wire signal is further corrected for temperature deviation from the original calibration temperature. This is accomplished on the DISA 55D44 calibration rig whereby the temperature of the calibration air is controlled by inline heaters. As the temperature of the fluid increases the output from the constant temperature anemometer (CTA) decreases due to the inherent decrease in the heat transfer from the wire to the fluid, i.e., the fluid temperature approaches the sensor temperature. A typical output of a linearized anemometer voltage plotted as fluid velocity is shown in Figure 12. The fall off in linearizer voltage output as a function of increasing fluid temperature is programmed into the online analysis code and is used in velocity correction. The crossed hot wire system is also calibrated for directional sensitivity, i.e., the output or response of each wire does not follow the same cosine cooling curve due to small differences in wire alignment, wire linearity and wire to probe support junctions. A typical directional sensitivity plot for one sensor on a crossed wire probe is shown in Figure 13. This type of plot is utilized in the acquisition program to make the necessary corrections to the measured velocity and angle deviations of the rotor wake.

ANALYTICAL MODEL

Forced vibration of a cascade of airfoils comprising either a rotor stage or stator occurs when the frequency of a forcing function corresponds to one of

the natural frequencies of the assembly of airfoils. Most generally in turbomachinery applications, the concept of engine order excitation is used to describe the potential forced vibration areas on a plot of airfoil frequency versus engine speed. In a plot of this type the integer orders corresponding to excitation sources are superimposed on a plot of airfoil frequencies. To establish the airfoil frequencies beam and finite element techniques are used depending on the depth of analysis desired. For rotor airfoils the temperature, steady state loading and centrifugal field effects are considered in the analyses at the rotor speeds where frequencies are desired. For a non-rotating stage only temperature and steady state loadings need to be considered. For the excitation sources, experience has shown that adjacent blade rows, either upstream or downstream, are main sources of excitation. One, two, three and four per revolution loading can be important to inlet rotor stage excitation and generally these occur due to non-symmetry in the inlet velocity profile to the compressor. Other sources of excitation are possible, but are not discussed here.

To understand the engine order concept for turbomachinery, imagine a rotor blade rotating in a flow downstream of four struts. As the blade traverses the wake created by each strut, a perturbation in the aerodynamic loading occurs. This occurs four times for each blade revolution. Thus, the frequency generated relative to the blade is four times the rotational speed expressed in revolutions per second. This example of calculating engine order excitation lines demonstrates the construction of the frequency-speed diagram shown in Figure 14.

At each intersection between known engine order excitations and airfoil natural frequencies a forced response problem is possible. Whether this response is a problem or not is dependent on the level of excitation generated by the source, the structural and aerodynamic damping due to the motion of the airfoil, and the agreement between the chordwise and spanwise distribution of the forcing function and the mode shape of the vibrating airfoil. Unfortunately, a predictive capability which considers all these elements has not been established at this point in time.

A separation of the forced response problem into various elements of technical discipline has been made by investigators to enable a building block solution of the overall problem to be accomplished. Under the two main areas of aerodynamics and structural dynamics lie particular elements such as gust-induced loading, aerodynamic damping, steady state loading, structural damping, and frequency and mode shape predictions. Each of these elements are subdivided even farther so that particular techniques can be used for solutions. A schematic of this approach is shown in Figure 15.

The particular area of investigation for the effort reported herein is that of wake-induced gust loading of a stator vane in a subsonic flow field. The wakes generated by a rotor stage create a time-variant loading of the downstream stator vanes. As previously described in the INTRODUCTION section, several investigators have presented analytical formulations to describe this loading. The analytical results used in data correlation for this report were obtained using analytical formulation following Smith[6].

In this formulation the cascade under consideration is assumed to be composed of infinitely thin, flat airfoils operating in a two-dimensional compressible flow aligned parallel with the airfoils. The cascade loading is of course zero. The cascade is described analytically by the setting angle and the solidity. Operating conditions are described by the inlet Mach number, the reduced frequency, and the interblade phase angle, which relates corresponding events on neighboring airfoils. The results from the analysis are presented as a complex pressure field along the airfoil chord. The complex pressures are normalized by the velocity deficit and the inlet dynamic head.

In the solution scheme for the analytical model a choice of the number of grid points must be made. As a check on the convergence of the analysis a data set typical of that presented later in this report was analyzed. The reduced frequency was varied systematically and varying number of grid points were chosen. The results are presented in Figure 16 in terms of the real and imaginary parts of the non-dimensional lift coefficient. Of interest to note is the variation

in this lift coefficient as the number of grid points are increased. This basically presents a warning to check convergence for each particular case. For the experimental/analytical correlations presented in this report, the analytical data was generated using 15 grid points, thus at extremely high reduced frequencies convergence is not assured.

The "in-house" developed analytical model for wake-induced loading of a loaded cascade of airfoils with arbitrarily shaped cross-sections became available at the end of the work period of this effort. The cascade is described by defining a suction surface and the pressure surface of the adjacent airfoil, i.e., a flow passage. The unsteady flow field is treated as a small nonpotential perturbation about a mean nonlinear potential flow field. The unsteady velocity field is further split into potential and non-potential parts. Linearized field equations are obtained for the perturbation entropy, vorticity, rotational velocity, and perturbation potential which are solved successively using a combination of analytical and numerical methods. The pressure distributions on the airfoil surfaces are obtained after solution of the field equations from the integrated linearized momentum equation.

Two test cases using the experimental data generated in previous AFOSR studies were analyzed. The geometry analyzed is shown in Figure 17. A comparison of the experimental data, the flat-plate analysis, and the thick airfoil analysis is shown in Figure 18. The second case analyzed used a reduced frequency of twice that of the presented case. Problems in the analytical results were noted and truncation errors due to grid size was suspected. No further attempts of correlation were made. However, the relatively good agreement in the lower reduced frequency case provides encouragement for the continuation of this analytical development. Additionally, complementary studies have indicated the credibility of the thick airfoil model in aeroelastic predictions at low reduced frequencies by comparisons with Smith[6] and Verdon and Caspar[9] published results.

TEST CONFIGURATIONS

The original design of the DDA low speed rotating rig featured 42 rotor blades operating upstream of a stator row of 40 airfoils. In order to perturb the variables of reduced frequency, solidity, and interblade phase angle, configurations having every other rotor airfoil and every other stator airfoil removed were evaluated.

A total of three test configurations were used in this study. Configuration 1 used 42 rotor blades operating in front of 20 stator vanes. In Configuration 2 every other rotor blade and every other stator vane was removed yielding a 21 blade rotor and a 20 vane stator row. In Configuration 3 the missing stator vanes were replaced, thus a 21 blade rotor operated in front of 40 stators.

For the variations in the several variables resulting from these configuration changes, the comparison is presented in Table 2.

Since more than one variable was altered simultaneously, cross-plots of data must be used. Additionally, the effect of variables concerned with the steady loading of the cascade must be recognized for each configuration. This is consistent with the previous conclusion from prior studies that the operating incidence angle plays a major role in determining the unsteady loading of the stator vanes.

RESULTS

STEADY STATE OPERATION

The primary goal of this experimental investigation was to obtain time-variant surface pressures on downstream stator vanes due to the aerodynamic excitation created by the wakes from the upstream rotor blades for three specific compressor configurations. In order to establish a logical sequence in the testing procedure a compressor map for each configuration is required. Figures 19 through 21 present the steady state operating points for each configuration as compared to the baseline configuration which was previously investigated under AFOSR sponsorship[17]. The particular steady state operating points for each configuration were determined by matching the stator incidence angle at a similar point on the baseline operating curve. The data point identification shown in Figures 19 through 21 will be used in categorizing the various runs. The first digit will refer to the particular build with 0 designating the baseline configuration. The second digit will refer to the particular point on the operating curve with points 1 through 4 designating 100% corrected speed with the incidence angle varying from highly negative at 1 to approximately zero at 4, while 5 through 8 will refer to the 70% corrected speed line with incidence varying as before from highly negative at 5 to zero at point 8. This particular identification is used in Table 3 which lists the relevant aerodynamic parameters for each configuration.

TIME-VARIANT DATA

A cursory examination of Table 3 quickly reveals that the specific effects due to a single parameter change cannot be isolated due to the fact that at least two key parameters change with each configuration. For example, the baseline configuration has an interblade phase angle of -18 degrees and a solidity of 1.516. Configuration 1 has a greatly reduced solidity of .758, but the interblade phase angle has also been changed. Comparing the base-

line to Configuration 2 reveals that the interblade phase angle is the same, the solidity has been reduced, but the reduced frequency has also been reduced which precludes a strict separation of parameter effects on the unsteady behavior of the cascade.

The data does provide several checks on the completeness of the parameter group insofar as its importance to the analytical model is concerned. For example, the first harmonic data of the baseline should compare to the second harmonic data of Configuration 3. Also, the first harmonic data of Configuration 1 should also compare with the second harmonic data of Configuration 2 at a lower solidity and larger interblade phase angle. The following paragraphs will discuss the comparisons made between the various configurations as well as the correlation for the non-dimensional pressure coefficient and the pressure phase lag with a current analytical model.

Figures 22 through 85 present the entire block of data obtained during the course of this investigation. For completeness of reporting the baseline data has been included and is presented in Figures 22 through 37. Since this data has been discussed[17], it will only be used during the discussion on configuration comparison. The data set has been prepared in the standard non-dimensional form with the pressure coefficient and the aerodynamic phase lag being plotted along the vane chord. Also plotted are the predicted pressures from the current analysis discussed previously. On occasion the phase lag data will appear at the top of the graph at about 40 degrees, at other times it appears at the 400 degree value. This is done to maintain all the phase lags negative and on the chosen scale; therefore, when any phase lag increases to a positive value, the entire data set is shifted 360° along with the theory line.

At large values of reduced frequency, i.e., greater than approximately 15, the flat plate cascade theory can fail to properly converge; as was noted previously. The second harmonic baseline and the second harmonic Configuration 1 theory line behaves badly and does not correlate well with the data, this is felt to be a result of not using sufficient grid points in the analysis.

Figures 38 through 53 present the first and second harmonic data of Configuration 1. The first harmonic data correlates well with the theory both in amplitude and phase shift for the 100% speed line condition. The amplitude shows a noticeable increase toward the trailing edge of the blade, as has been reported previously on the baseline data. The effect of loading, i.e., incidence angle change, is not as pronounced at this condition as it is in the other configurations investigated. The amplitude of the pressure coefficient does exhibit a tendency to remain at a high finite level across the entire length of the blade for both the first and second harmonic as the incidence angle is decreased from a high negative value (point 1) to a low value (Point 4).

The 70% speed line data, Figures 46 through 53, exhibits a sharp change in phase angle at approximately the 60% chord position for the first harmonic data only. The second harmonic data experiences a rapid shift in phase at the 30% chord position and high negative incidence. The rapid change in phase shift decreases for both the first and second harmonic data as the blade is loaded and the incidence angle decreases. The magnitude of the pressure coefficient matches the theory quite well with the rapid decrease in amplitude occurring over the first 25% of the vane chord.

Figures 54 through 69 present the first and second harmonic data for Configuration 2. The overall correlation between theory and the experimental data is not as good as it was for Configuration 1 particularly in the phase lag data. The 100% speed line data experiences large differences at the leading edge (Figure 54). This leading edge difference decreases as the incidence angle is decreased (Figure 57), but at the same time the apparent presence of a convected wave is seen beginning at the leading edge Kulite. The second harmonic data of the 100% speedline fairs no better in that large phase shifts occur early on the blade with the presence of a convected wave appearing as the incidence angle is decreased to zero. The 70% speed line data (Figures 62 through 69) exhibits a different characteristic altogether in that the first harmonic phase data appears to line up in a pattern characteristic of a convected wave traveling down the blade at high incidence and completely disappears at zero incidence. This behavior is repeated in the second harmonic data (Figures 66 through 69).

Figures 70 through 85 present the first and second harmonic data for Configuration 3. The effect of incidence angle on the behavior of the pressure coefficient is very evident on this configuration. The first harmonic pressure data for this configuration yields an almost constant value across the blade at high negative incidence (Figure 70). The phase lag is also seen to decrease rapidly down the first half of the blade in the chordwise direction. This trend in pressure coefficient and phase lag changes noticeably as the incidence angle is decreased as shown in Figure 73. Here the pressure coefficient and the phase both match very well with the theory line. The second harmonic phase data indicates a noticeable correlation between the theory line and phase angle as evidenced by Figure 74 and 77. As the incidence angle is decreased, the amplitude and phase lag data correlates very well with the predicted value.

The 70% speed line data, Figures 78 through 85, indicate the same behavior as the 100% speed line data with the data/theory correlation being poor at high negative incidence and improving as the incidence angle is decreased to approximately zero. The amplitude of the pressure coefficient is seen to remain above the theory line for the first harmonic data while the second harmonic data matches quite well at low incidence values. The phase lag data follows a similar trend with the difference being a sharp tailing off in phase lag toward the trailing edge of the vane.

The analytical model used in the data comparisons utilizes three main variables as key parameters in the forced vibration analysis. They are the reduced frequency, the interblade phase angle and the solidity. This group of parameters contributes the majority control over the unsteady pressure distribution and phase lag in the analytical model. The purpose of this investigation was not only to provide a data base of extended range in all of these variables, but also to provide data that would seek to quantify the effects of solidity, reduced frequency and interblade phase angle on the unsteady pressure amplitude and phase of a vane row experiencing forced vibration.

Figures 86 through 89 present a comparison between the first harmonic data of the baseline configuration and the second harmonic data of configuration three, all at 100% corrected speed. These points were chosen due to the fact that the key parameters for both builds are the same. Examination of these plots reveals a very close similarity in both amplitude and phase, particularly at the high and moderate incidence levels where it is felt the pressure field on the blade surface is being dominated by a convected wave phenomena. At zero incidence the phase lags compare remarkably well, indicating that for two dissimilar builds where the rotor flow characteristics are not the same, i.e., build 3 has only 21 rotor blades, the key parameters involved suffice to sufficiently quantify the amplitude and phase lags on the vane surface. What appears to be an almost constant differential of about 40 degrees between the two data sets could very well be the result of a cross wire probe placement error either in Configuration 1 or 3 or both. It has been shown previously[17] that a small error in probe placement could very well lead to this type of error in phase lag. This comparison is of particular importance in that it underscores the need for the analytical model to account for off-incidence flow conditions and a more accurate method of determining a zero phase reference point for purposes of data acquisition. The problem of cross wire placement could possible be improved by a vane leading edge reference point such as a hot film signal. Such a zero reference point could be explored in future investigations.

In order to quantify the effect of a single parameter on the pressure and phase distribution of a vane surface, that particular parameter would have to be varied while holding all others constant. For a given rig of fixed geometry this proves to be unobtainable. The best one could do is vary a given parameter such as solidity and then allow the other connected parameters to vary in a controlled manner. Figures 90 through 93 compare the effect of solidity reduction at the same interblade phase angle and approximately the same reduced frequency. The model indicates that little difference is to be seen in the phase and pressure distribution. The data would tend to confirm this as indicated in Figure 93 where at zero incidence the

amplitudes are quite similar and the phase agreeing in a trendwise manner with the same sharp phase shift experienced at the 50% chord position. Again the effect of incidence effects are noted, particularly at the high incidence value on the baseline data.

Figures 94 through 97 present the comparison between the baseline first harmonic data and configuration one first harmonic data. This comparison involves a change of two parameters, the interblade phase angle and the vane solidity. The data indicates clearly that little difference exists between the two configurations insofar as the normalized pressure coefficient and phase lag are concerned. This conclusion agrees well with theory where only a small difference in both the pressure coefficient and the phase lag exists.

Since more than one variable was altered in each configuration, a presentation whereby the major variables would become apparent was desired. The effect of incidence angle which has been discussed in previous investigations [15, 16, 17, 18] is such a dominant factor in the time-variant loading of the vanes that the near zero incidence data alone was examined. Figures 98 through 103 present the near zero incidence angle experimental and analytical data as functions of solidity, interblade phase angle and reduced frequency. For this data presentation the time variant pressures in the near leading edge region (3% and 10% chord) have been used since they are the most dominant pressures on the airfoil.

In Figures 98 and 99 all data, irrespective of interblade phasing and reduced frequency, was plotted against solidity of the vane row. A banding of the data was performed as indicated on the figure. No clear trend exists with vane solidity at either the 3% or 10% chord position. Seemingly other variables create larger deviations in the measured pressures than does the effect of solidity.

In Figures 100 and 101, the trend of the leading edge time-variant pressures with interblade phase angle is presented. Again, all near zero incidence data,

irrespective of solidity and reduced frequency, was plotted as a function of interblade phase angle alone. The theory grouping and the experimental data grouping both indicate the same trend — the unsteady pressures in the leading edge region are affected little by interblade phase angle over the low incidence range (-18 to -72°) investigate but are affected when the interblade phase angle is near 180°. The maximum gust induced pressures occur with the 171° interblade phase angle.

Figures 102 and 103 present the trend of the analytical and experimental data with reduced frequency. The theoretical and experimental data groupings both indicate that the leading edge region time-variant pressures are reduced at increased reduced frequencies.

The discussion presented in this section reflect analysis of both the flat plate mode analytical results and experimental results from the test program. The effects of solidity, interblade phase angle and reduced frequency on the time-variant pressure distribution existing on a stator vane surface due to gust induced loading have been presented. As a further aid to those investigators needing more detailed pressure measurements — namely, time-variant data from both surfaces of the airfoil, Appendix A is presented. In this Appendix, tabulations of the measurements made from each individual Kulite for each data point are presented.

CONCLUSIONS AND RECOMMENDATIONS

From the investigation performed under the auspices of this contract the following major conclusions are presented:

1. The largest time-variant pressures on an airfoil subjected to gust induced loading are found in the leading edge region.
2. The time-variant pressures in the leading edge region of the airfoil were found to be:
    a. Little affected by solidity over the range of solidities investigated,
    b. Influenced by interblade phase angle with the maximum change with respect to interblade phase angle occurring at a near 180° phase angle,
    c. Reduced in level as the reduced frequency of the gust was increased.
3. The trends noted in the leading edge region for the measured time-variant pressures are in agreement with flat plate airfoil predictions.
4. The level of measured time-variant pressures over the airfoil surface are, in general, larger than the predicted levels from the flat plate model.
5. The variation of chordwise phase lag and time-variant pressures over the surface of the airfoil is affected most dramatically by variations in the incidence angle at which the airfoil operates.
6. Comparisons of first and second harmonic data obtained from varied configurations which yielded equal values of solidity and interblade phase angle and near identical values of reduced frequency for the same airfoil shape have validated the parametric grouping to obtain aeroelastic similarity, provided incidence angle is held constant during the comparisons. Additionally, these comparisons provide a check of data reduction techniques and data repeatability over a number of years.

7. At low incidence angles, the flat plate analysis used for correlation provides a good qualitative insight into the gust induced loading of the stator vane.

From the investigation reported herein there are secondary conclusions which, although not related to the primary objective of the investigation, are important to note. These are as follows:

1. The choice of the number of grid points used for the analytical results had a major effect both for the flat plate and the thick airfoil model results.
2. The breakdown in chordwise phase lag at high negative incidence angle is possibly due to separation occurring on the airfoil surface, thus existing analyses are not capable of adequate predictions unless modifications are made.

Based on these conclusions, the following recommendations are presented.

1. Following the development of analytical models such as described in References 9 and 10, the ability to properly assess the effects of separation on the gust-induced loading should be made.
2. A detailed study to quantify the three-dimensional interactions through the entire vane passage should be undertaken to both address the validity of the strip assumption and to assess wake decay characteristics through the passage.
3. An experimental study similar to this investigation should be performed at inlet Mach numbers in the high subsonic range to properly assess compressibility effects for validation of the various analytical models.
4. A technique to better relate the time-variant pressures with the gust in terms of phase lag should be established. A suggested method would be to place a heated film gage at the airfoil leading edge.

These conclusions and recommendations are presented as a result of the analysis of the experimental and analytical results obtained in this investigation. The data used in these analyses are presented, so that other investigators can formulate their separate conclusions.

REFERENCES

1. Kemp, N. H. and Sears, W. R., "Aerodynamic Interference Between Moving Blade Rows," Journal of the Aeronautical Sciences, Vol 20, No. 9, September 1953.

2. Horlock, J. H., "Fluctuating Lift Forces on Airfoils Moving Through Transverse and Chordwise Gusts," Transactions of the ASME, Journal of Basic Engineering, Vol 90, Series D, No. 4, December 1968.

3. Naumann, H. and Yeh, H., "Lift and Pressure Fluctuations of a Cambered Airfoil Under Periodic Gusts and Applications in Turbomachinery," Transactions of the ASME, Journal of Engineering for Power, Vol 95, Series A, No. 1, January 1973, pp 1-10.

4. Goldstein, M. E. and Atassi, H., "A Complete Second-Order Theory for the Unsteady Flow About an Airfoil Due to a Periodic Gust," Journal of Fluid Mechanics, Vol 74, 1976.

5. Whitehead, D. S., Force and Moment Coefficients for Vibrating Airfoils in Cascade, Aeronautical Research Council R and M 3254, February 1960.

6. Smith, S. M., Discrete Frequency Sound Generation in Axial Flow Turbomachines, University of Cambridge, Department of Engineering Report CUED/A-Turbo/TR 29, 1971.

7. Henderson, R. E. and Daneshyar, H., Theoretical Analysis of Fluctuating Lift on the Rotor of an Axial Turbomachine, Aeronautical Research Council R and M 3684, September 1970.

8. Henderson, R. E. and Horlock, J. H., "An Approximate Analysis of the Unsteady Lift on Airfoils in Cascade," Transactions of the ASME, Journal of Engineering for Power, October 1972.

9. Verdon, J. M. and Caspar, J. R., Subsonic Flow Past an Oscillating Cascade with Finite Mean Flow Deflection, AIAA Paper No. 79-1516, July 1979.

10. Caruthers, J. E., Analysis of Aerodynamically Forced Vibration of Airfoil Cascades, Final Report prepared for Detroit Diesel Allison Division of General Motors Corporation, March 31, 1980.

11. Commerford, G. L. and Carta, F. O., "Unsteady Aerodynamic Response of a Two-Dimensional Airfoil at High Reduced Frequency," AIAA Journal, Vol 12, No. 1, 1974.

12. Ostdiek, F. R., A Cascade in Unsteady Flow, Ph.D. Thesis, The Ohio State University, 1975.

13. Henderson, R. E. and Franke, G. F., Investigation of the Unsteady Pressure Distribution on the Blades of an Axial Flow Fan, Final Report, NASA Grant No. NGR 39-009-275, March 1978.

14. Fleeter, S., Novick, A. S., and Riffel, R. E., "The Unsteady Aerodynamic Response of an Airfoil Cascade to a Time-Variant Supersonic Inlet Flow Field," Unsteady Phenomena in Turbomachinery, AGARD-CP-177, 1975.

15. Fleeter, S., Jay, R. L., and Bennett, W. A., Rotor Wake Generated Unsteady AErodynamic Response of a Compressor Stator, ASME Paper No. 78-GT-112, April 1978.

16. Fleeter, S., Bennett, W. A., and Jay, R. L., "Time-Variant Aerodynamic Measurements in a Research Compressor," Proceedings of the Dynamic Flow Conference 1978, September 1978.

17. Fleeter, S., Jay, R. L., and Bennett, W. A., "Wake Induced Time-Variant Aerodynamics Including Rotor-Stator Axial Spacing Effects," ASME Journal of Non-Steady Fluid Dynamics, December 1978.

18. Fleeter, S., Bennett, W. A., and Jay, R. L., The Time-Variant Response of a Stator Row Including the Effects of Airfoil Camber, ASME Paper No. 79-GT-110, March 1979.

19. Fleeter, S., "Fluctuating Lift and Moment Coefficients for Cascaded Airfoils in a Nonuniform Compressible Flow," AIAA Journal of Aircraft, Vol 10, No. 2, February 1973.

20. Atassi, H. and Akai, T. J., Aerodynamic and Aeroelastic Characteristics of Oscillating Loaded Cascades at Low Mach Number, ASME Paper No. 79-FT-111, March 1979.

21. Carta, F. O. and St. Hilaire, A. O., An Experimental Study on the Aerodynamic Response of a Subsonic Cascade Oscillating Near Stall, ASME Paper No. 77-GT-47.

22. Fleeter, S. and Riffel, R. E., Aerodynamic Phenomena in an Oscillating Transonic MCA Airfoil Cascade Including Loading Effects, AGARD-CP-227, September 1979.

23. Riffel, R. E., and Rothrock, M. D., Experimental Determination of Unsteady Blade Element Aerodynamics in Cascades — NASA 1 - Torsion Mode Cascade Data Report, Contractor Report NASA CR-159831 prepared for NASA-Lewis Research Center under Contract NAS3-20055, November 1979.

24. Jay, R. L., Rothrock, M. D., Riffel, R. E., and Sinnet, G. T., Time-Variant Aerodynamics for Torsional Motion of Large-Turning Airfoils, Contractor Final Report DDA EDR 10192 prepared for Naval Air Systems Command under Contract N00019-79-C-0087, January 1980.

25. Platzer, M. F., Unsteady Flows in Turbomachines - A Review of Recent Developments, AGARD-CP-227, September 1977.

26. Jorgensen, F. E.,"Directional Sensitivity of Wire and Fiber-film Probes," DISA Information, No. 11, May 1971, pp 31-37.

Type of Airfoil	65 Series	65 Series
Number	42	40
Chord, C-in. (Cm.)	4.589(11.66)	5.089(12.93)
Solidity, σ = C/S	1.435	1.516
Camber, ϕ - Deg.	20.42	48.57
Aspect Ratio, AR = S/C	1.046	0.943
Leading Edge Radius/C	0.0044	0.0049
Trailing Edge Radius/C	0.0028	0.0030
Inlet Air Angle, β_1 - Deg.	59.38	37.84
Exit Air Angle, β_2 - Deg.	42.41	0.00
Loss Coefficient	0.043	0.056
Diffusion Factor	0.449	0.410
Rotor-Stator Axial Spacing-in.(Cm.)	1.485(3.772)	
Flow Rate	31.02 lb/sec. (14.07 Kg/Sec)	
Tip Speed	183.5 ft/sec. (5593.1 Cm/Sec)	
Rotational Speed	876.3 rpm	
Stage Pressure Ratio	1.0125	
Inlet Tip Diameter	48.01 in. (121.95 Cm)	
Hub/Tip Radius Ratio	0.80	
Stage Efficiency, Percent	88.1	

Table 1. Airfoil mean section characteristics and compressor design point conditions.

CONFIGURATION	NUMBER OF ROTOR BLADES / NUMBER OF STATOR BLADES	INTERBLADE PHASE ANGLE FOR FIRST HARMONIC/SECOND HARMONIC	SOLIDITY AT MEAN - SPAN	REDUCED FREQUENCY* FOR FIRST HARMONIC/ SECOND HARMONIC
Baseline	42/40	-18°/-36°	1.516	10.0/20.0
1	42/20	-36°/-72°	.758	9.3/18.6
2	21/20	-18°/-36°	.758	5.16/10.32
3	21/40	171°/-18°	1.516	4.91/9.82

*REDUCED FREQUENCY AT NEAR ZERO INCIDENCE ANGLE

Table 2. Test configurations used in parametric evaluation.

	DATA POINT IDENTIFICATION	% SPEED	MACH #	INTERBLADE * PHASE ANGLE	VANE SOLIDITY	β_{ABS}	K_1 AX	K_2 AX	$v/V)_1$	$v/V)_2$
BASELINE	01	100	.103	-18	1.516	25	6.95	13.90	.03148	.03203
	02	100	.099	-18	1.516	28	7.27	14.54	.03306	.03452
	03	100	.080	-18	1.516	33	8.96	17.92	.07811	.06258
	04	100	.071	-18	1.516	36	10.05	20.10	.10798	.07397
	05	70	.071	-18	1.516	25	6.95	13.90	.03388	.03622
	06	70	.068	-18	1.516	28	7.40	14.80	.03630	.03826
	07	70	.056	-18	1.516	33	8.91	17.82	.07803	.06462
	08	70	.051	-18	1.516	36	9.82	19.64	.12118	.08612
CONFIGURATION ONE	11	100	.1025	-36	.758	25	7.13	14.26	.04911	.04899
	12	100	.09816	-36	.758	28	7.48	14.96	.05055	.04984
	13	100	.0987	-36	.758	33	8.35	16.70	.06457	.06024
	14	100	.07921	-36	.758	36	9.26	18.52	.1412	.1159
	15	70	.0719	-36	.758	24	7.13	14.26	.05145	.05257
	16	70	.0697	-36	.758	27	7.38	14.76	.0549	.0539
	17	70	.0628	-36	.758	32	8.24	16.48	.07218	.06679
	18	70	.0577	-36	.758	36	8.98	17.96	.12857	.10752

*FIRST HARMONIC DATA

Table 3. Steady state data point identifications and relevant time-variant parameters.

Table 3 (continued)

	DATA POINT IDENTIFICATION	% SPEED	MACH #	INTERBLADE* PHASE ANGLE	VANE SOLIDITY	β_{ABS}	$K_{1\ AX}$	$K_{2\ AX}$	$v/V)_1$	$v/V)_1$
CONFIGURATION TWO	21	100	.0899	-18	.758	25	4.09	8.18	.03246	.03281
	22	100	.0840	-18	.758	29	4.38	8.76	.03980	.06138
	23	100	.0746	-18	.758	33	4.93	9.86	.07213	.09832
	24	100	.0712	-18	.758	36	5.16	10.32	.1090	.1230
	25	70	.0737	-18	.758	25	3.50	7.00	.03473	.01516
	26	70	.0695	-18	.758	27	3.72	7.44	.03124	.02449
	27	70	.0643	-18	.758	32	4.02	8.04	.05663	.08198
	28	70	.0582	-18	.758	36	4.44	8.88	.1040	.1231
CONFIGURATION THREE	31	100	.0977	171	1.516	25	3.75	7.50	.01727	.02066
	32	100	.0897	171	1.516	29	4.09	8.18	.02522	.04082
	33	100	.0844	171	1.516	32	4.34	8.68	.04447	.06619
	34	100	.0746	171	1.516	38	4.91	9.82	.08626	.10513
	35	70	.0615	171	1.516	25	4.19	8.38	.01965	.02474
	36	70	.0499	171	1.516	29	5.16	10.32	.03172	.05031
	37	70	.0437	171	1.516	33	5.90	11.80	.07051	.09085
	38	70	.0409	171	1.516	36	6.29	12.58	.10614	.10456

*FIRST HARMONIC DATA

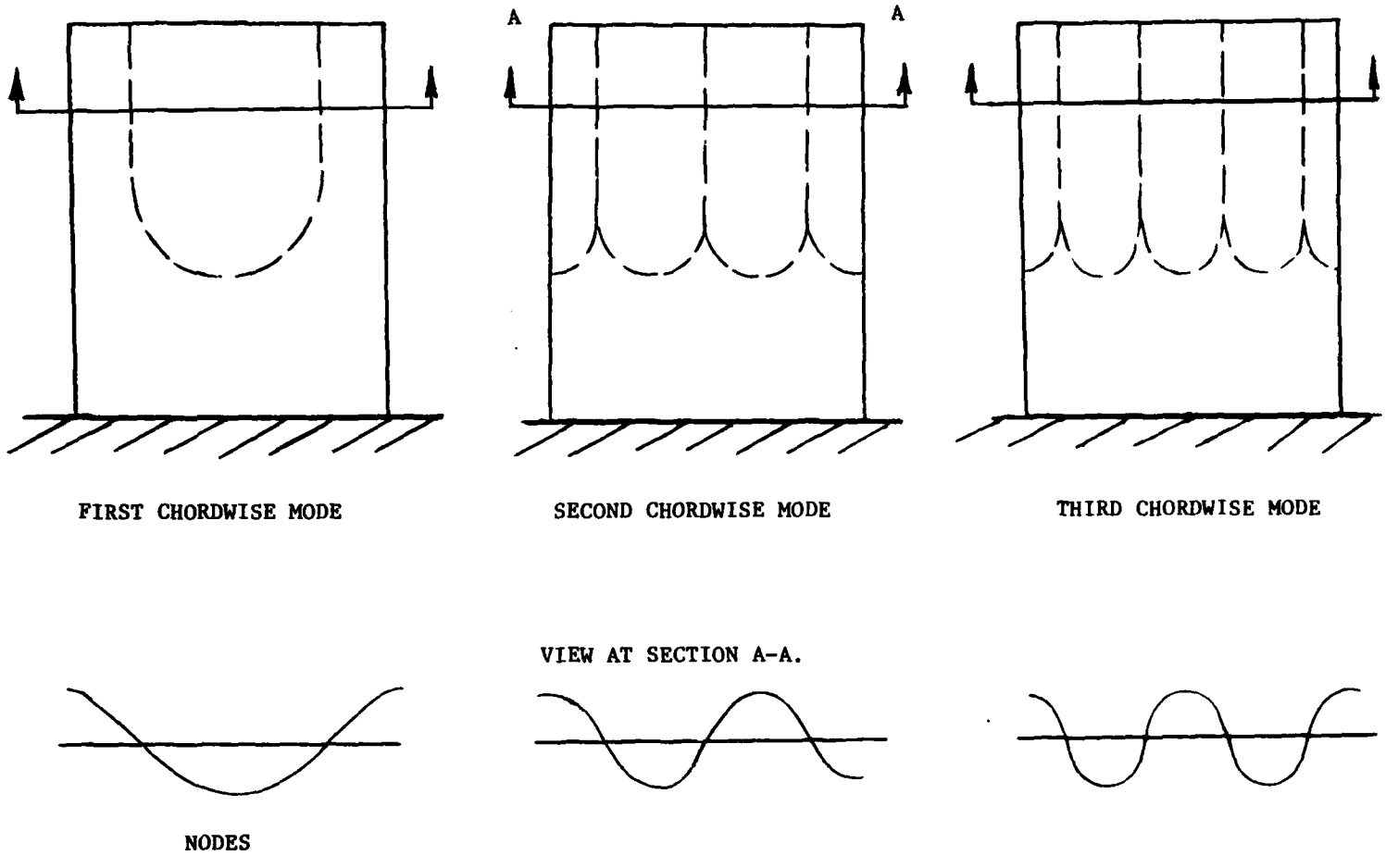

Figure 1. First three chordwise bending modes of a low aspect ratio blade.

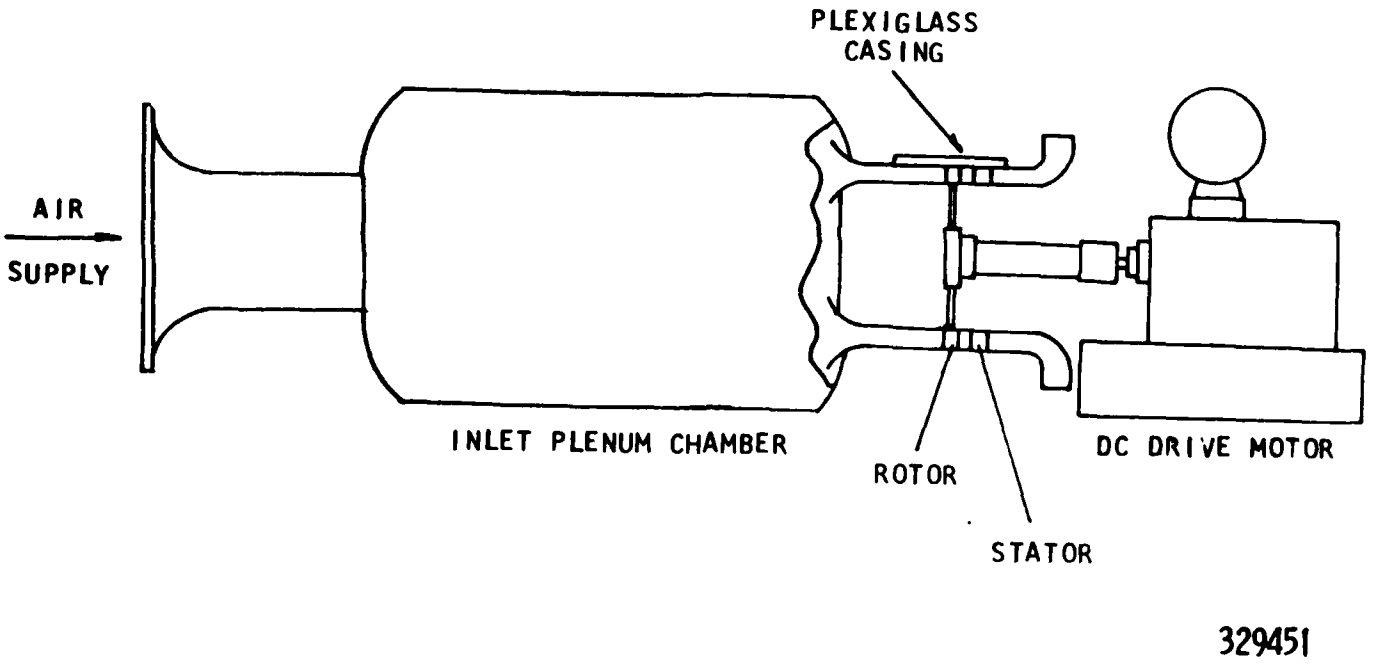

Figure 2. View of large-scale, low-speed, research compressor.

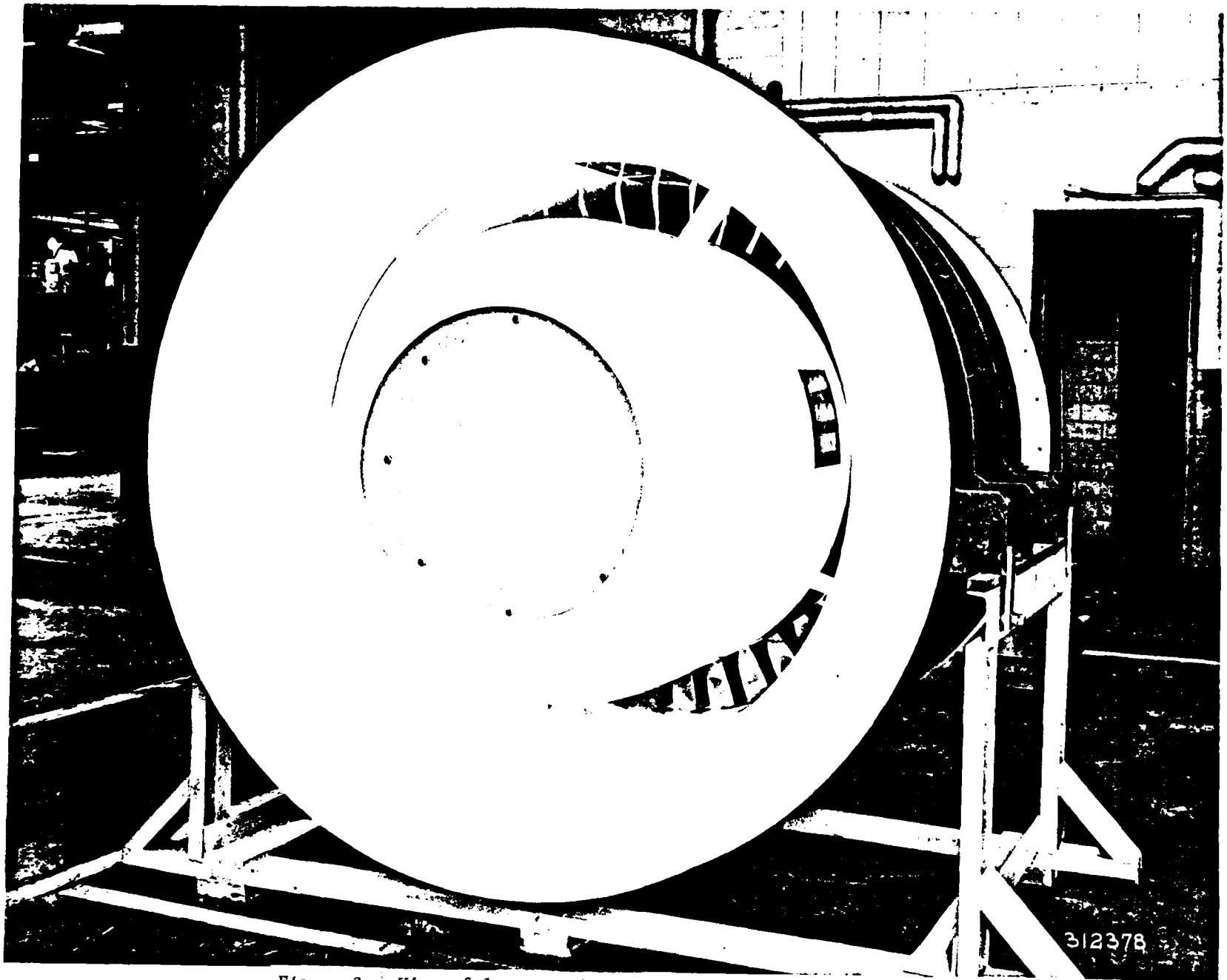

Figure 3. View of large-scale, low speed, research compressor.

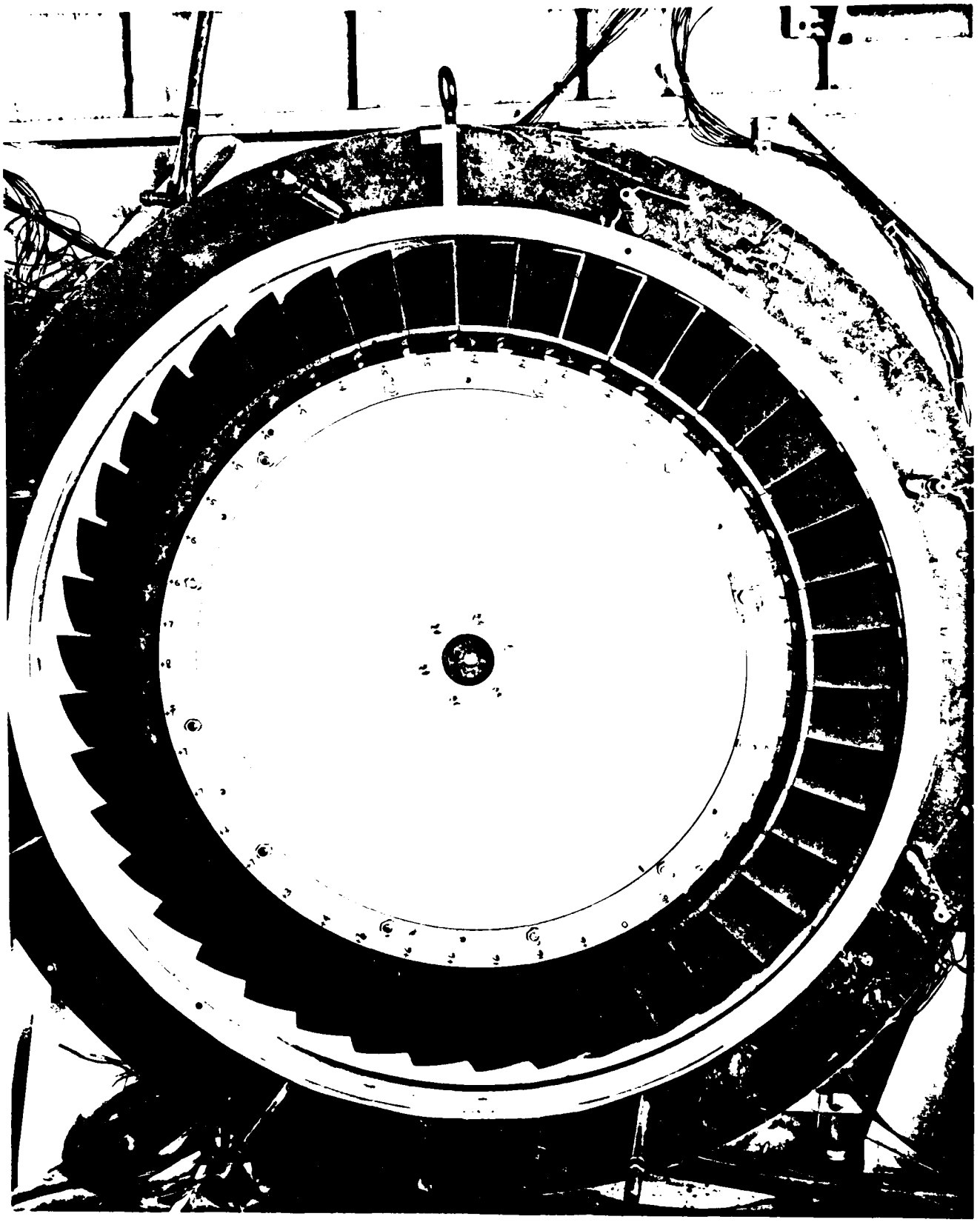

Figure 4. View of single stage research compressor rotor.

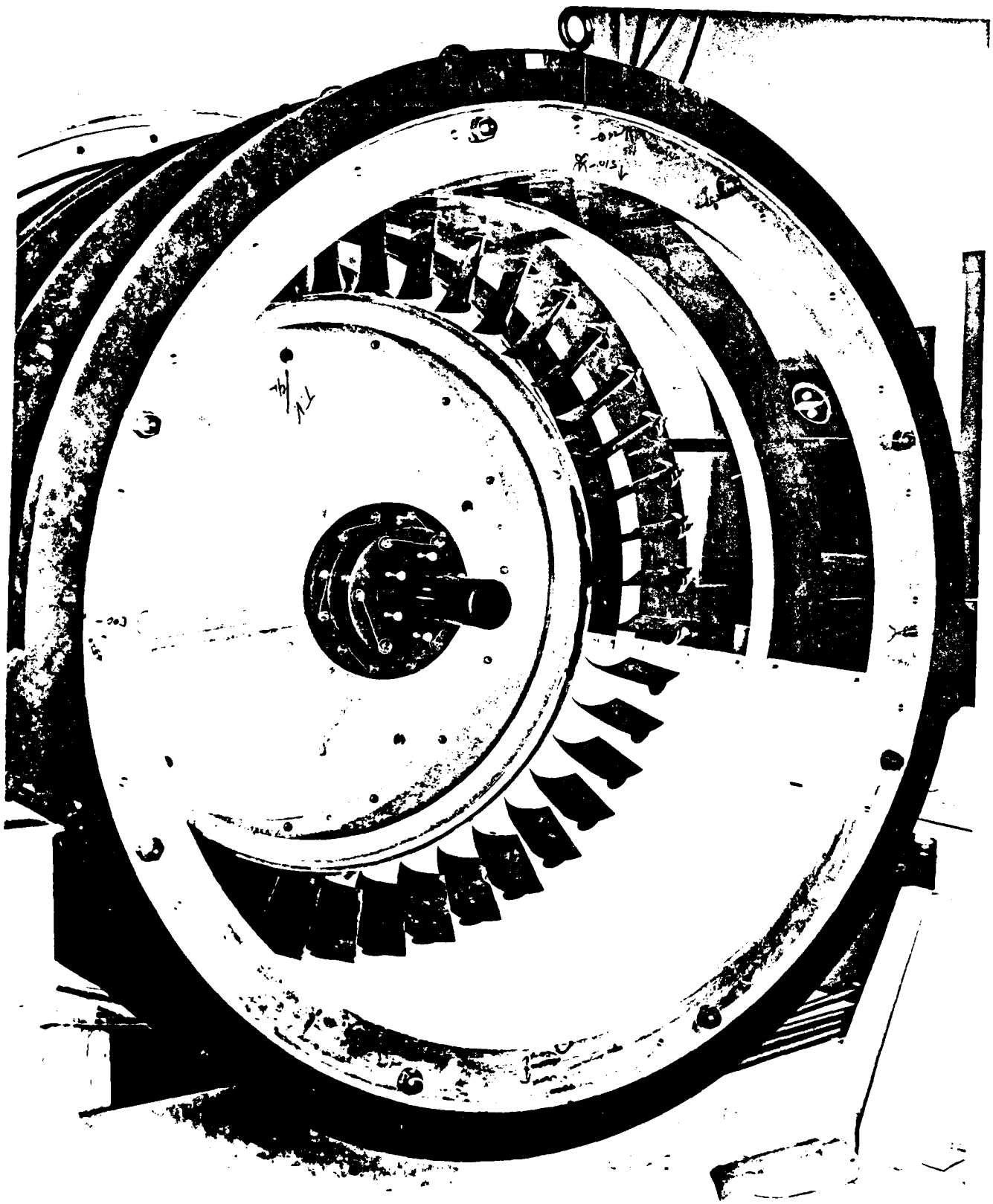

Figure 5. View of single stage research compressor stator row.

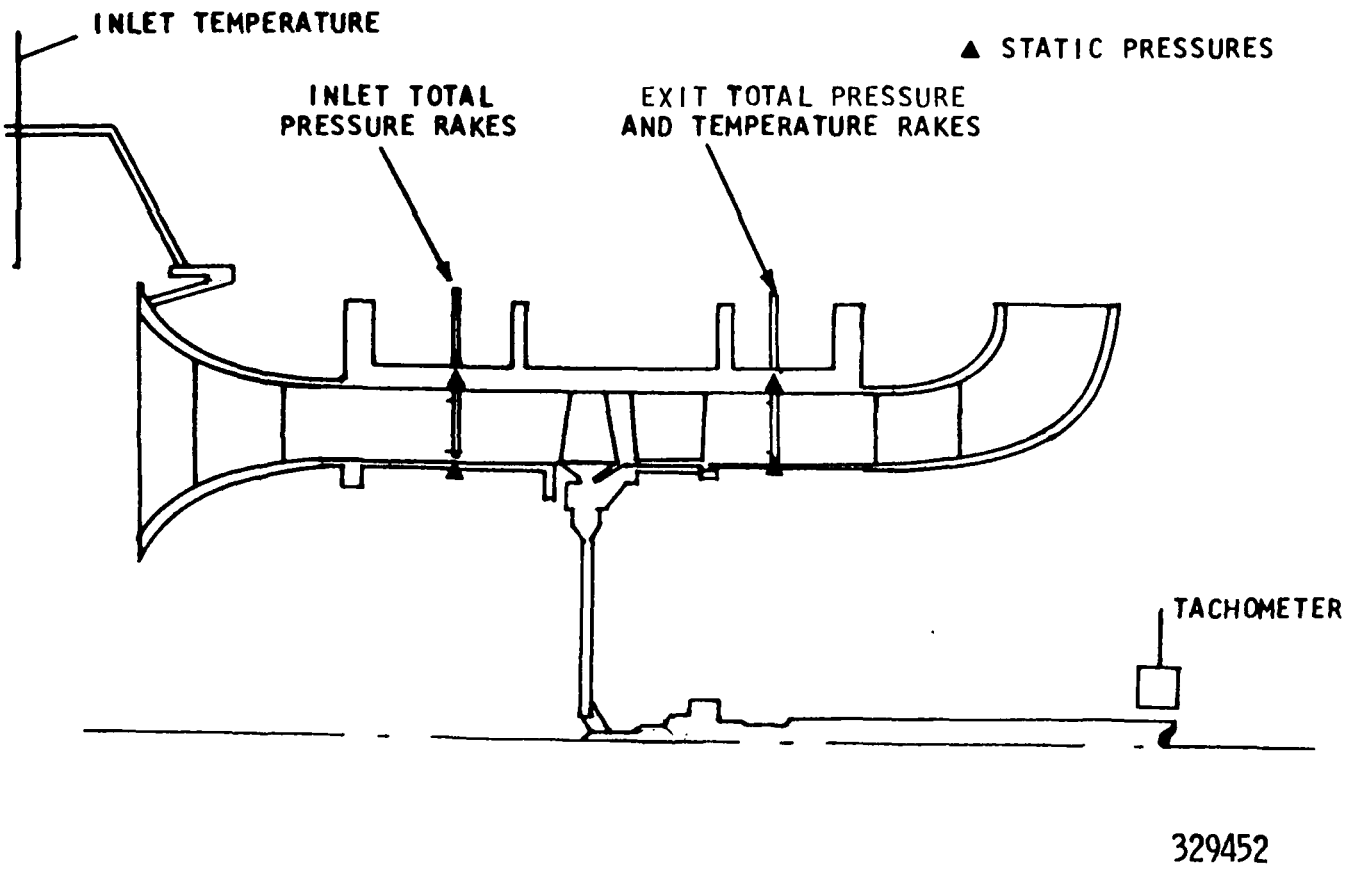

Figure 6. Schematic of steady-state instrumentation and compressor flow path.

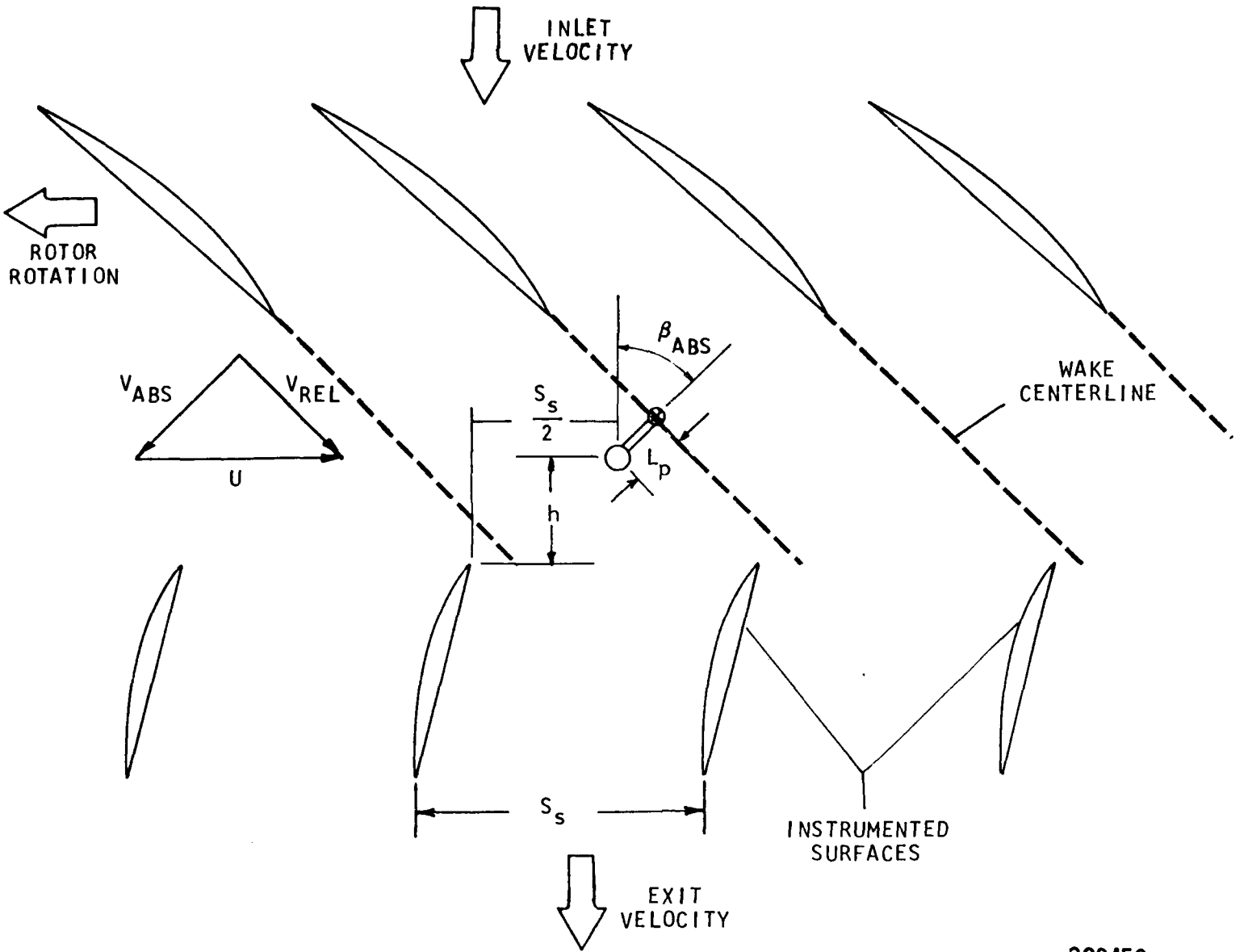

Figure 7. Schematic of dynamic instrumentation.

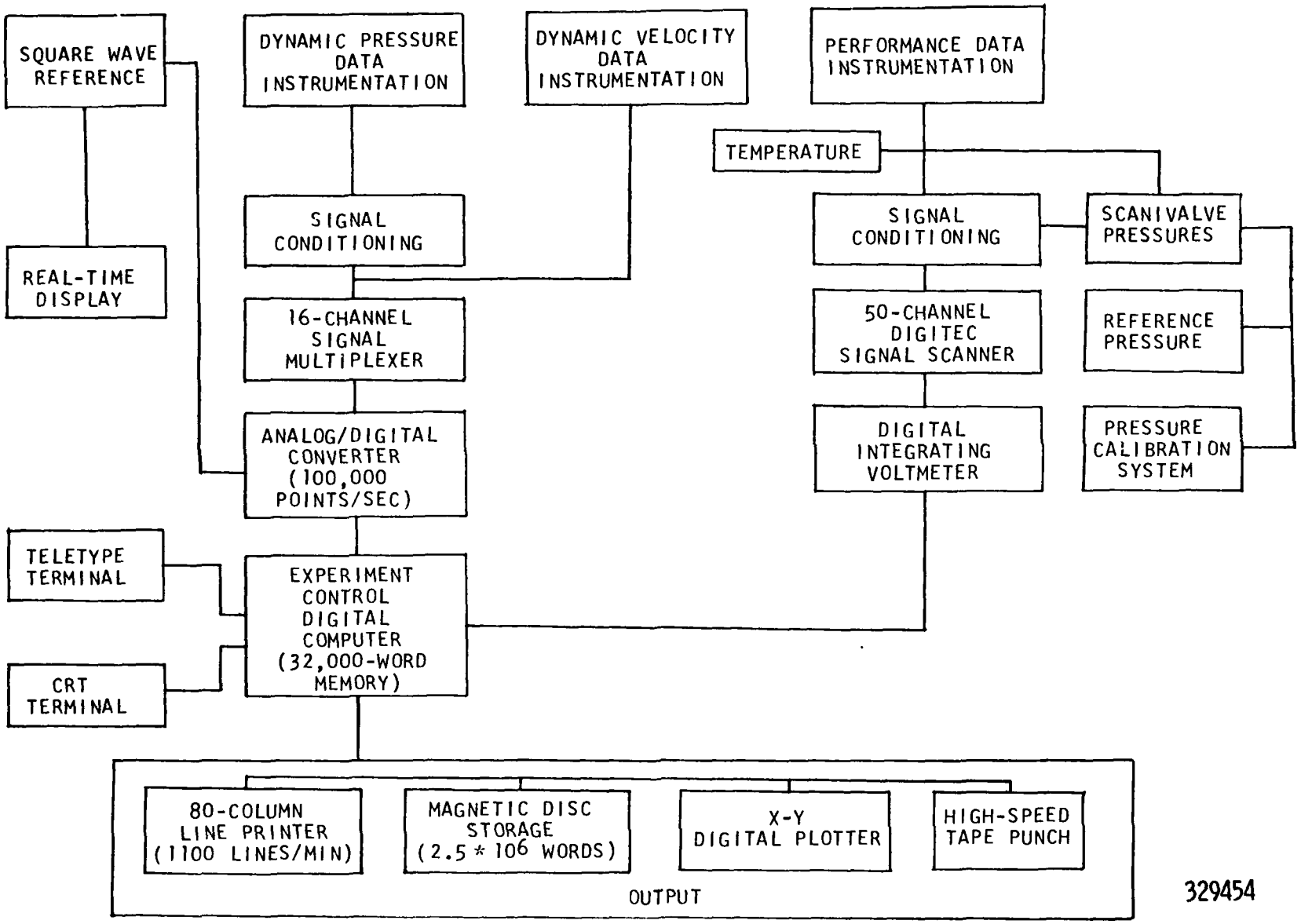

Figure 8. Schematic of on-line computer controlled data acquisition system.

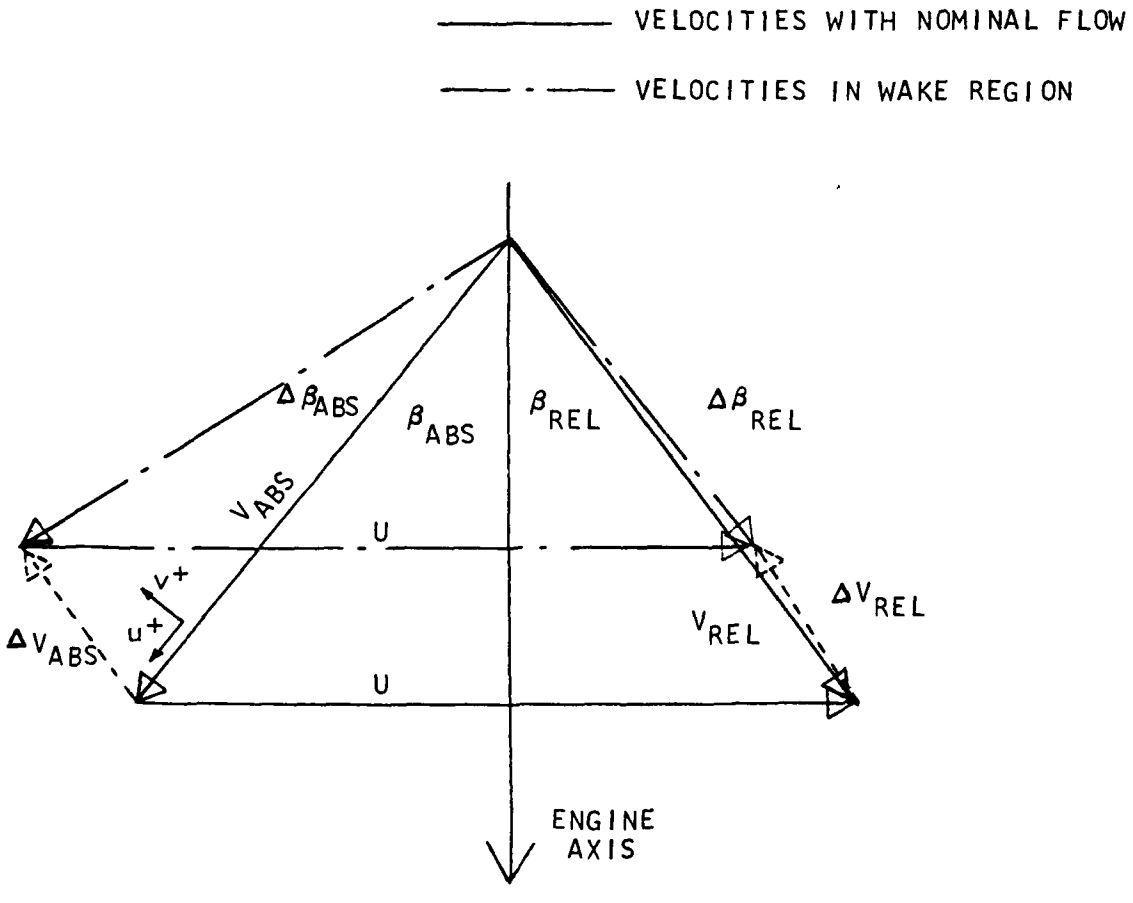

Figure 9. Reduction in relative velocity created by blade wake creates corresponding velocity and angular change in absolute frame.

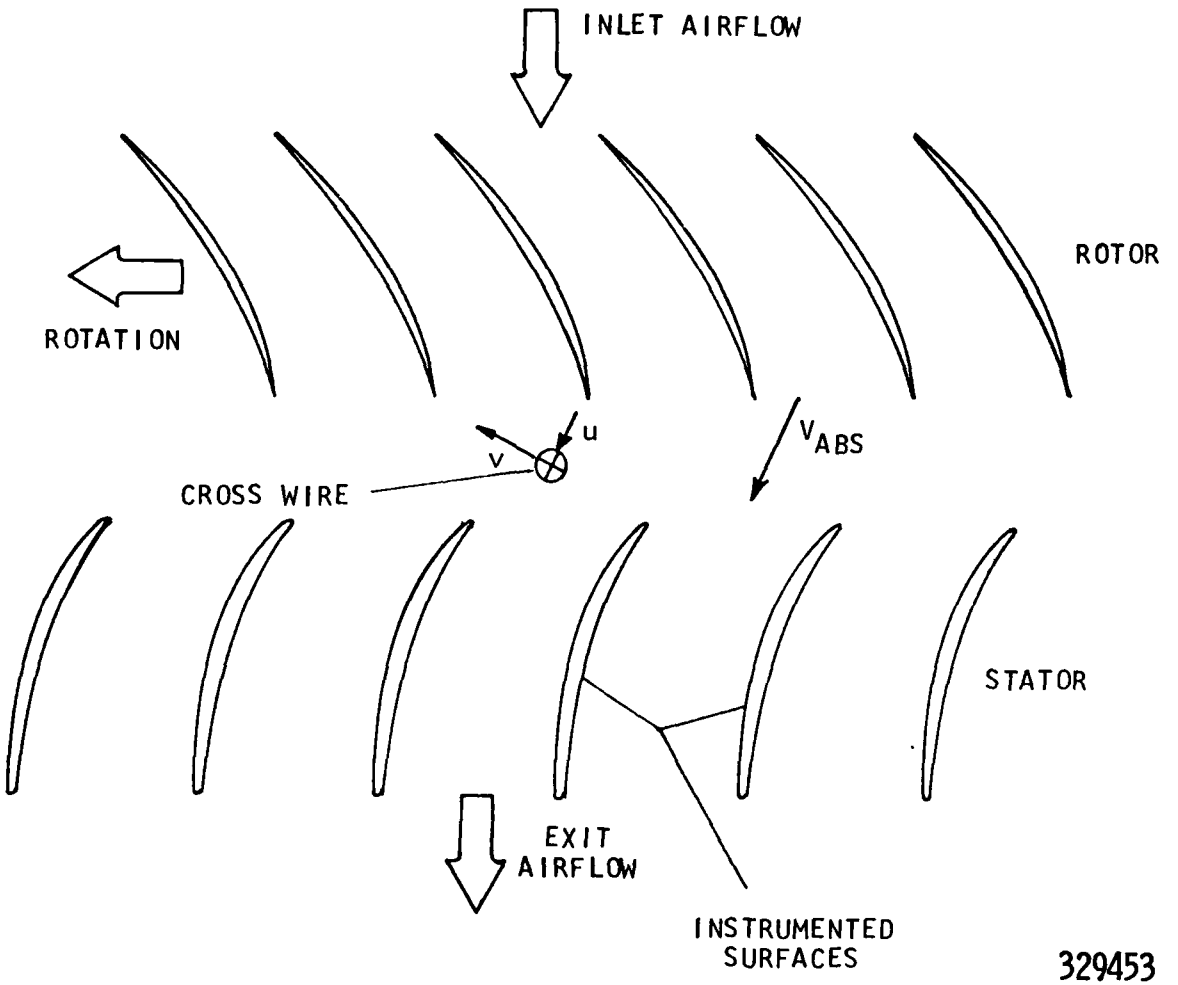

Figure 10. Schematic of flow field used in dynamic data analysis.

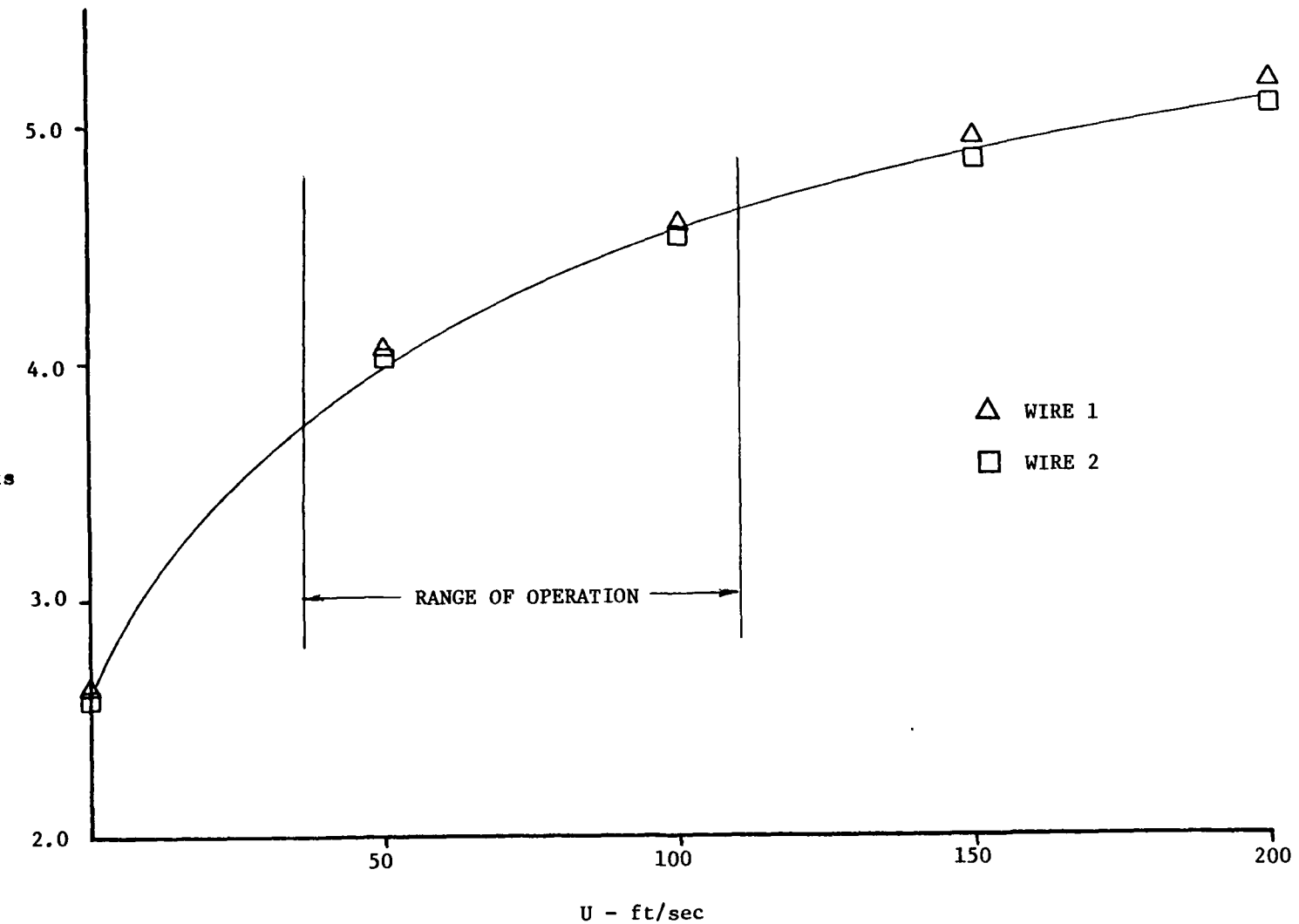

Figure 11. Typical output of hot wire anemometer as a function of fluid velocity.

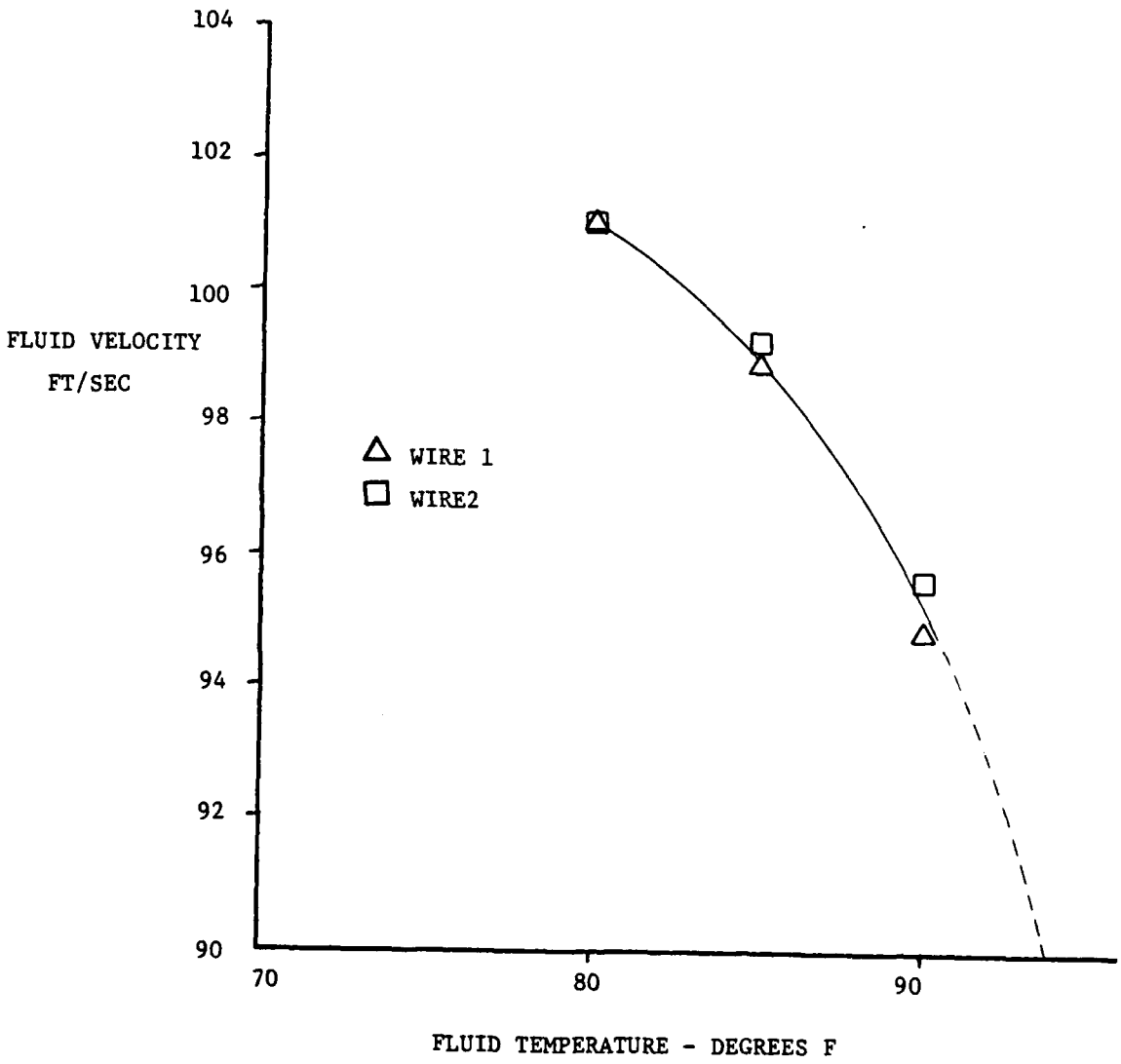

Figure 12. Typical linearized anemometer output of fluid velocity shown as a function of fluid temperature.

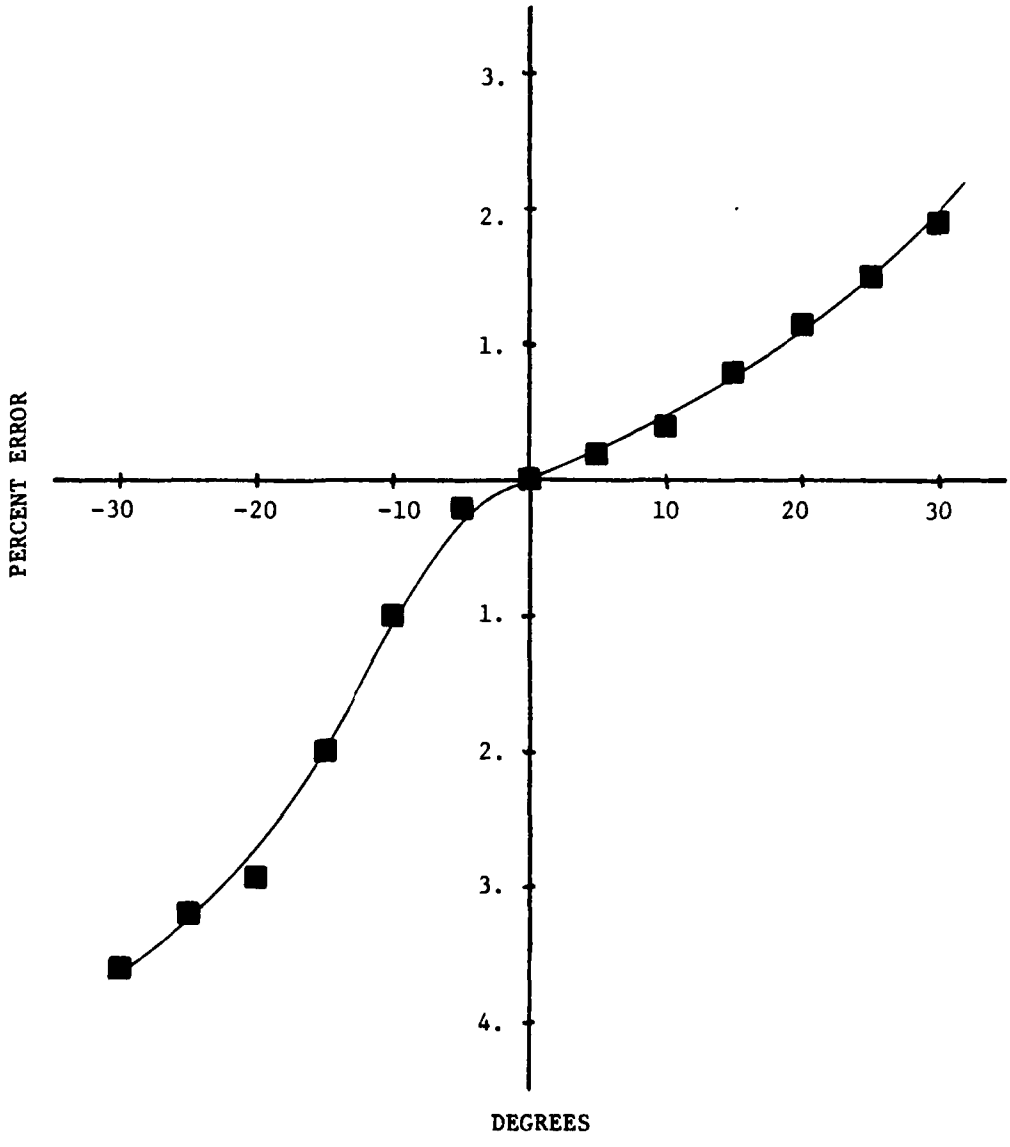

Figure 13. Typical directional sensitivity of a crossed hot wire probe.

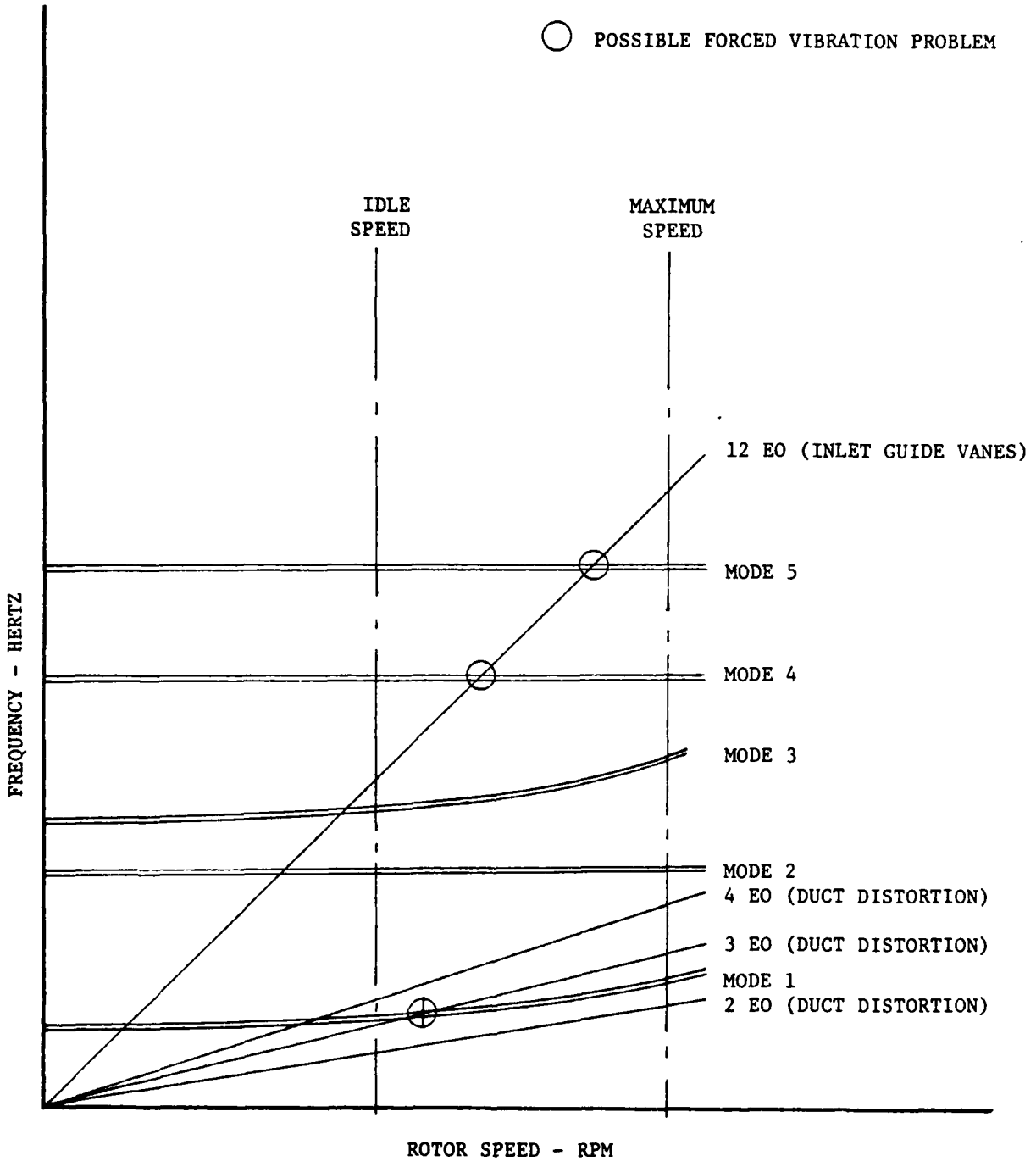

Figure 14. Typical frequency-speed chart for inlet compressor stage.

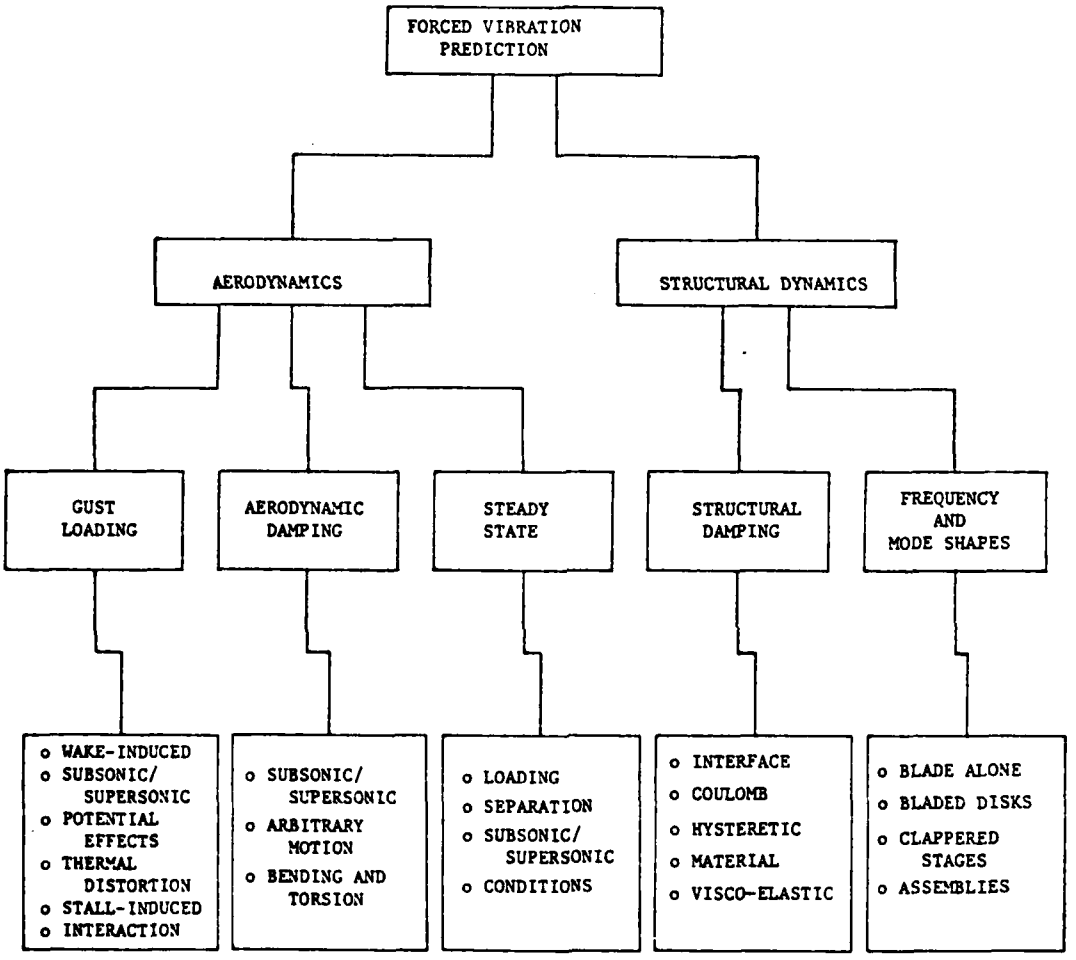

Figure 15. Elements of forced vibration problem.

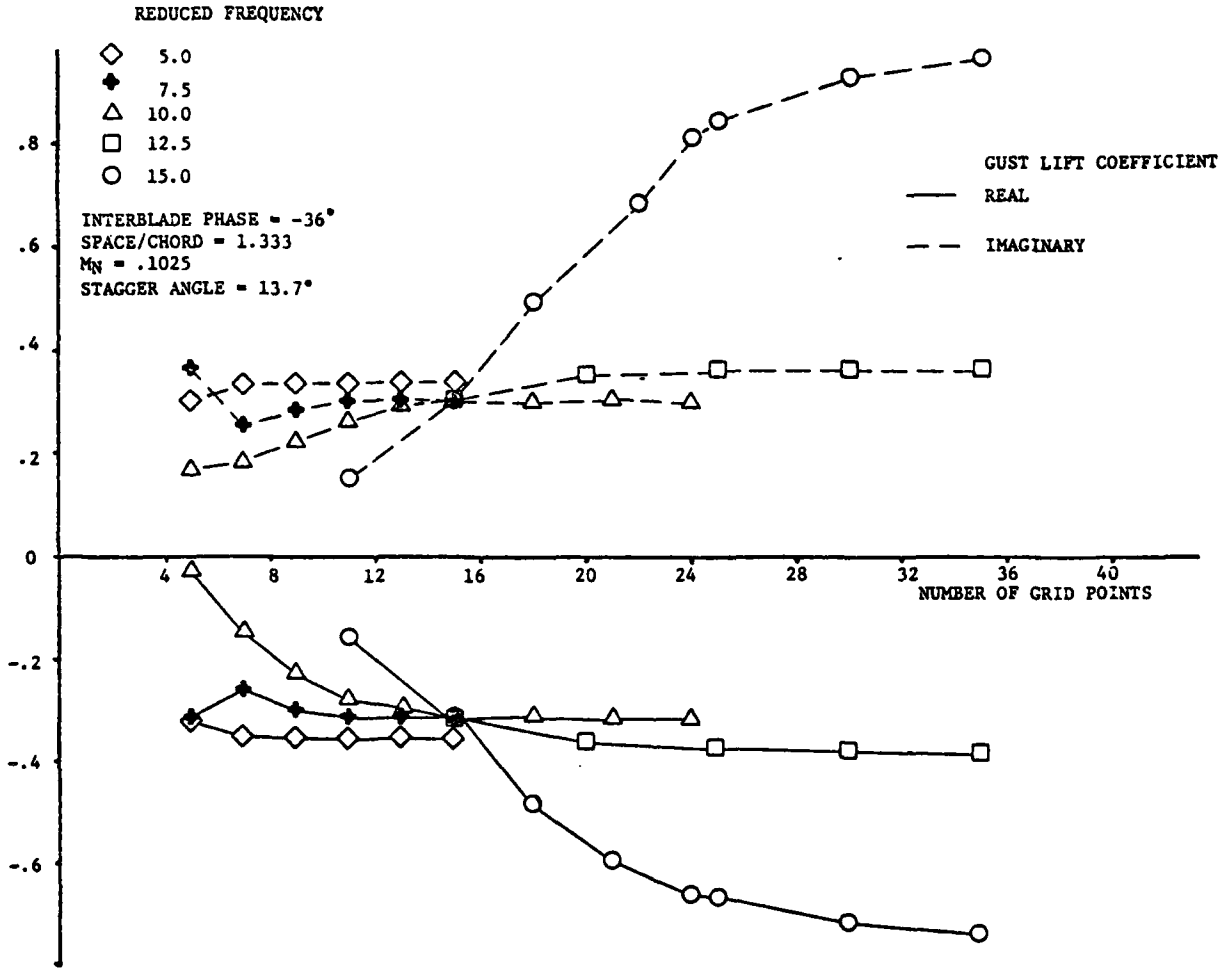

Figure 16. Variation in lift coefficient with number of grid points at varying reduced frequency.

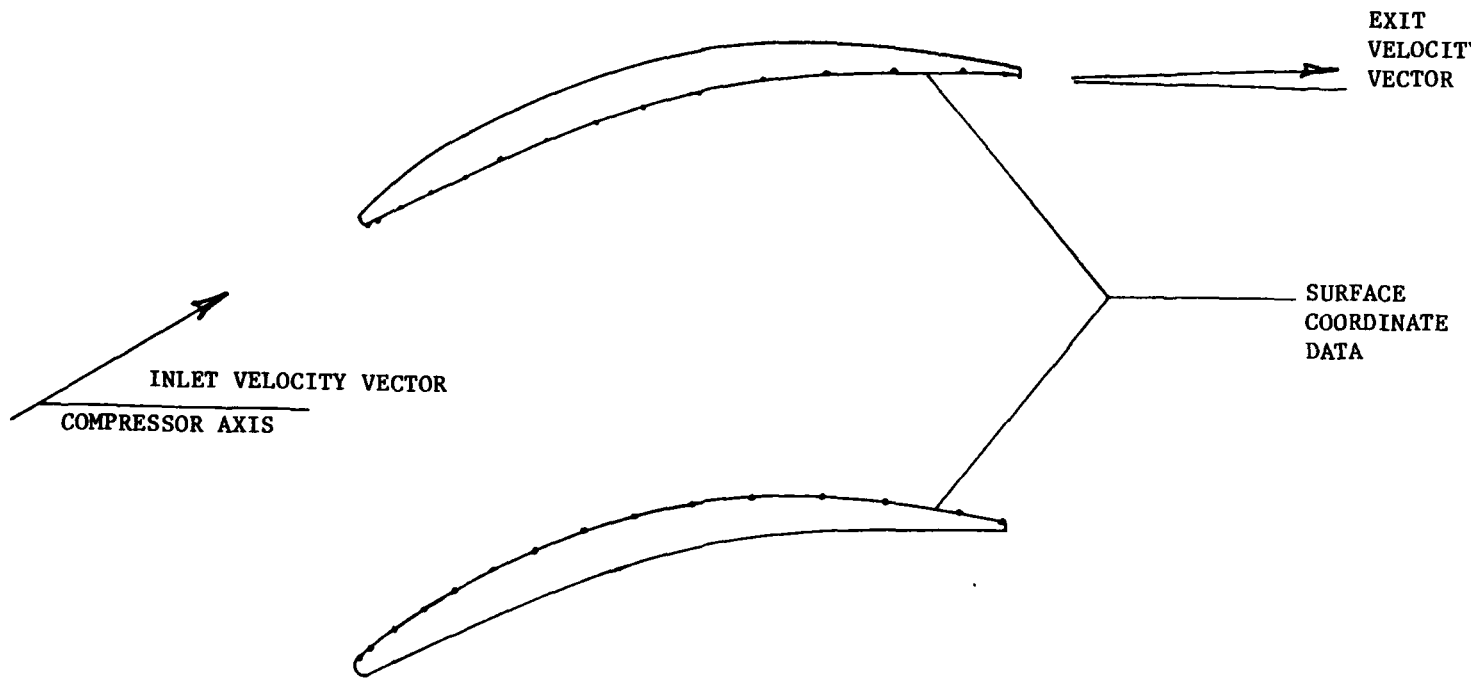

Figure 17. Cascade geometry for use in thick airfoil analysis per Reference 10.

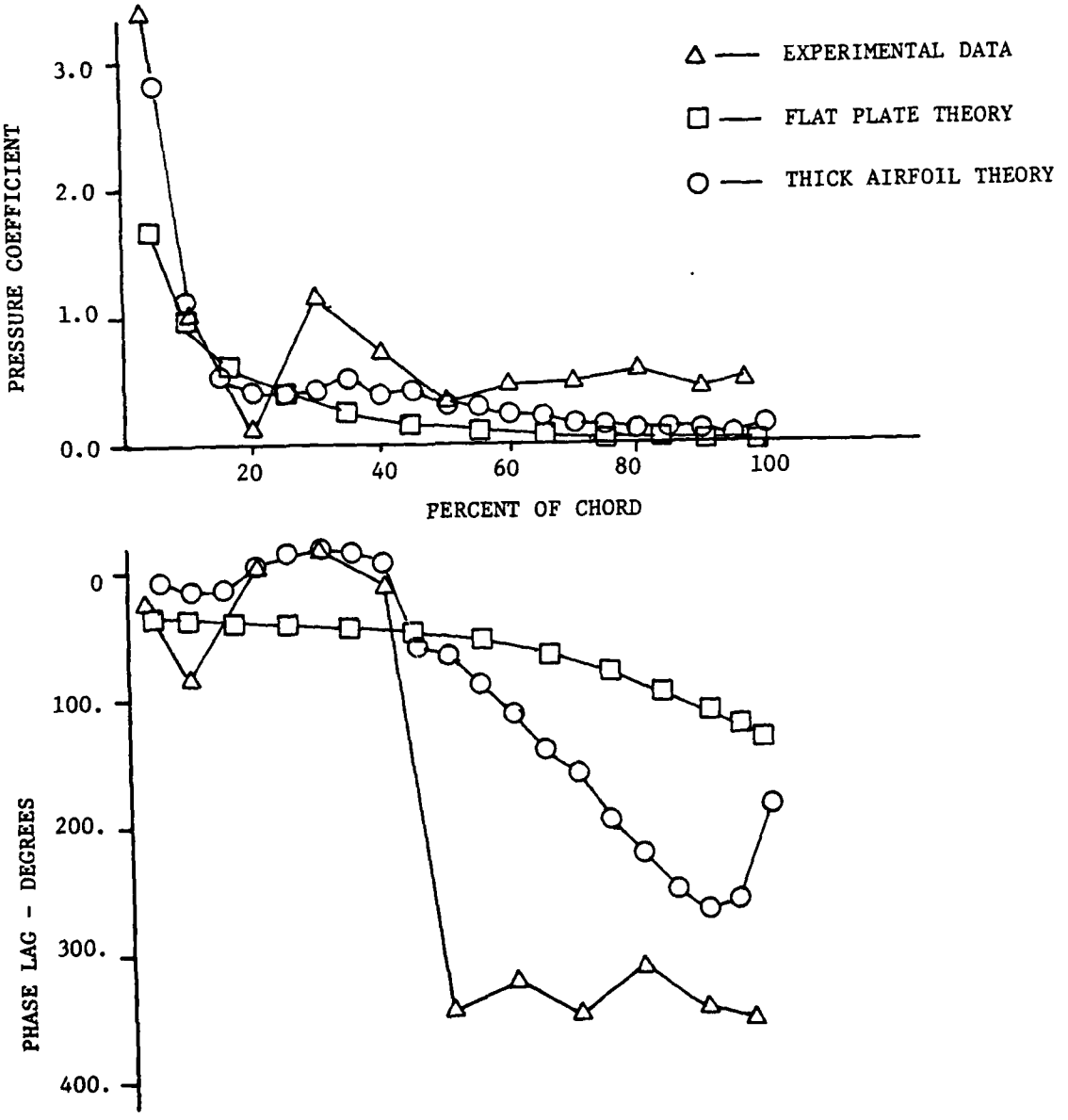

Figure 18. Comparisons of flat plate, thick airfoil and experimental results.

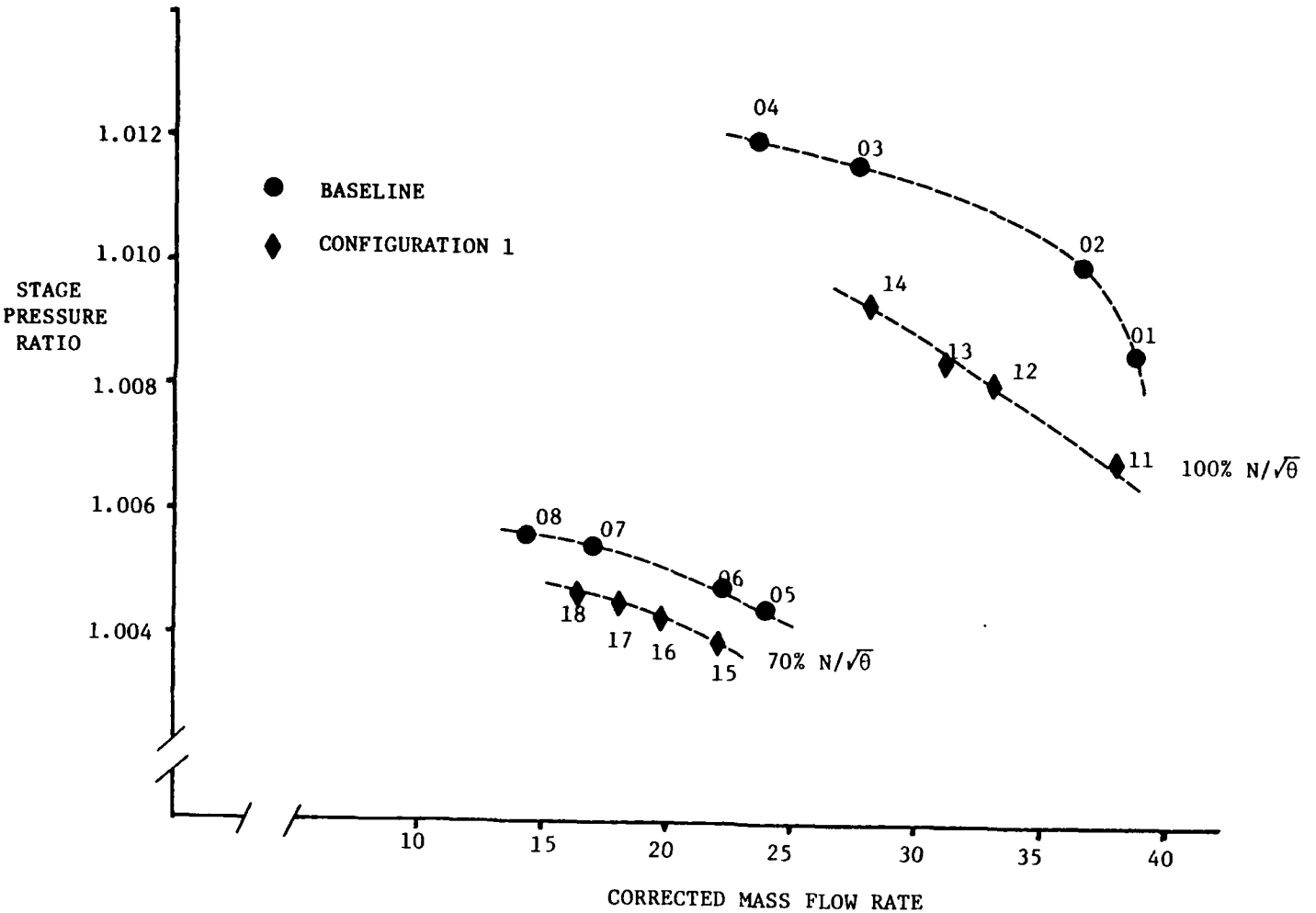

Figure 19. Data point identification for baseline and configuration 1.

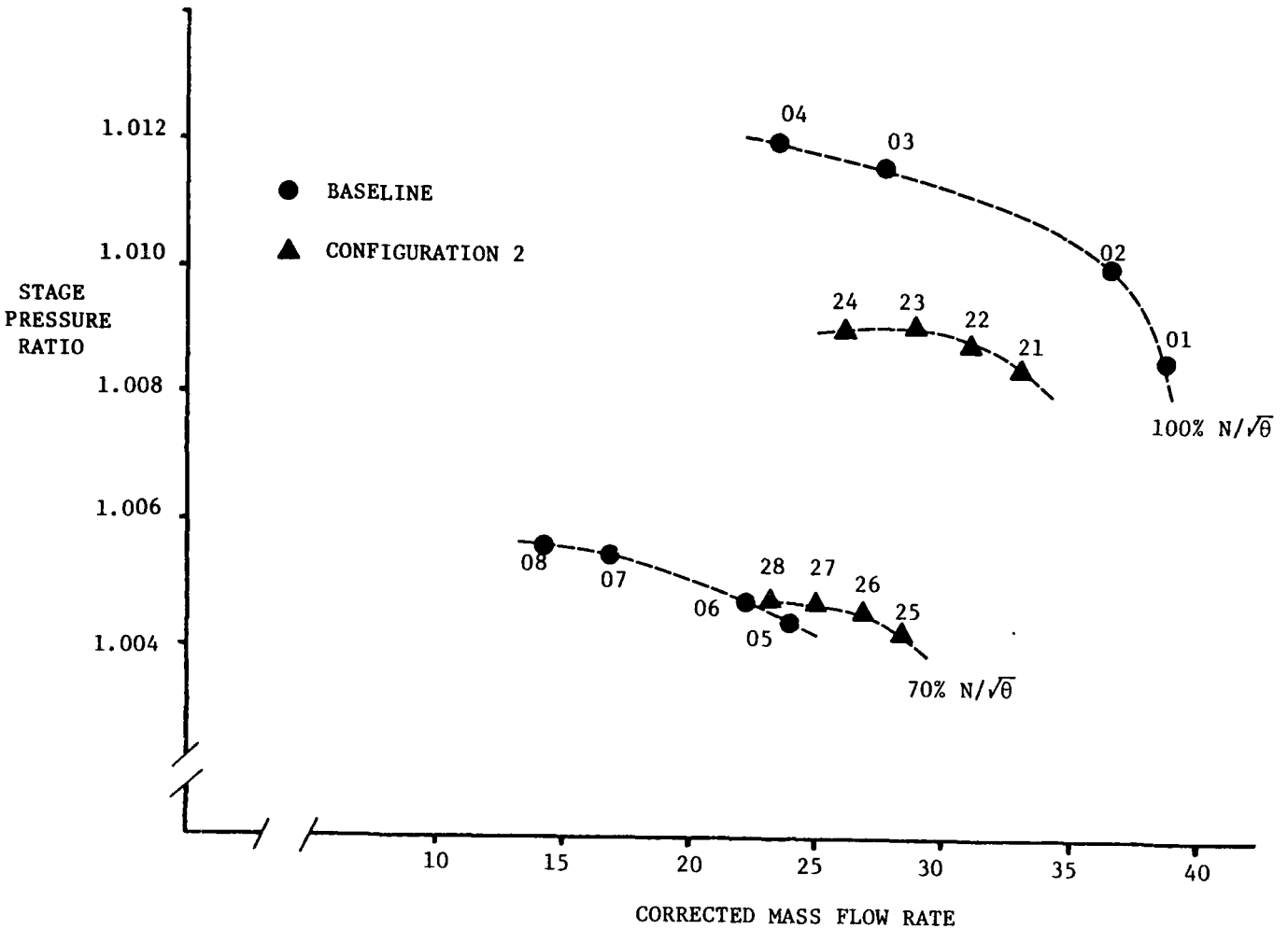

Figure 20. Data point identification for baseline and configuration 2.

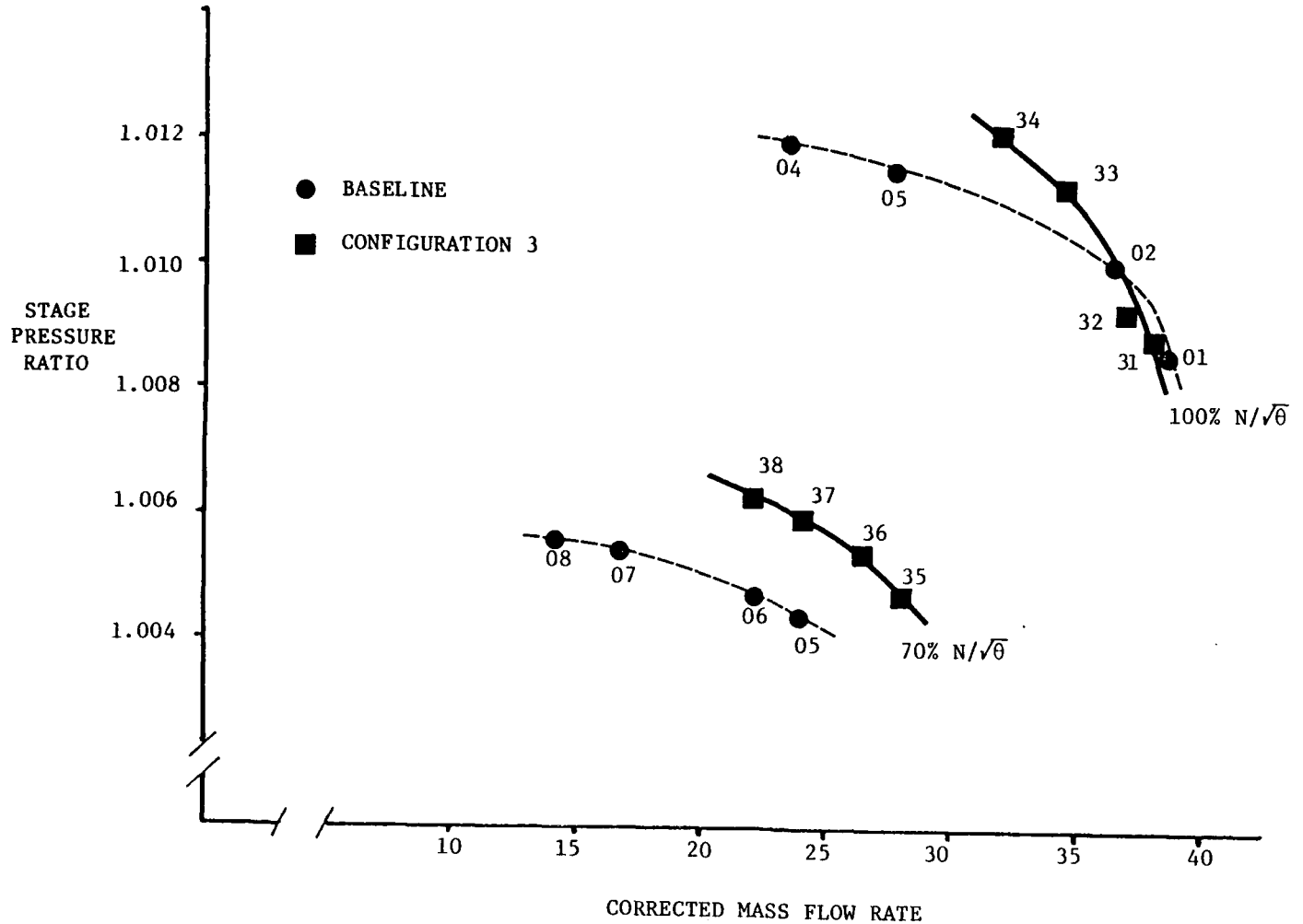

Figure 21. Data point identification for baseline and configuration 3.

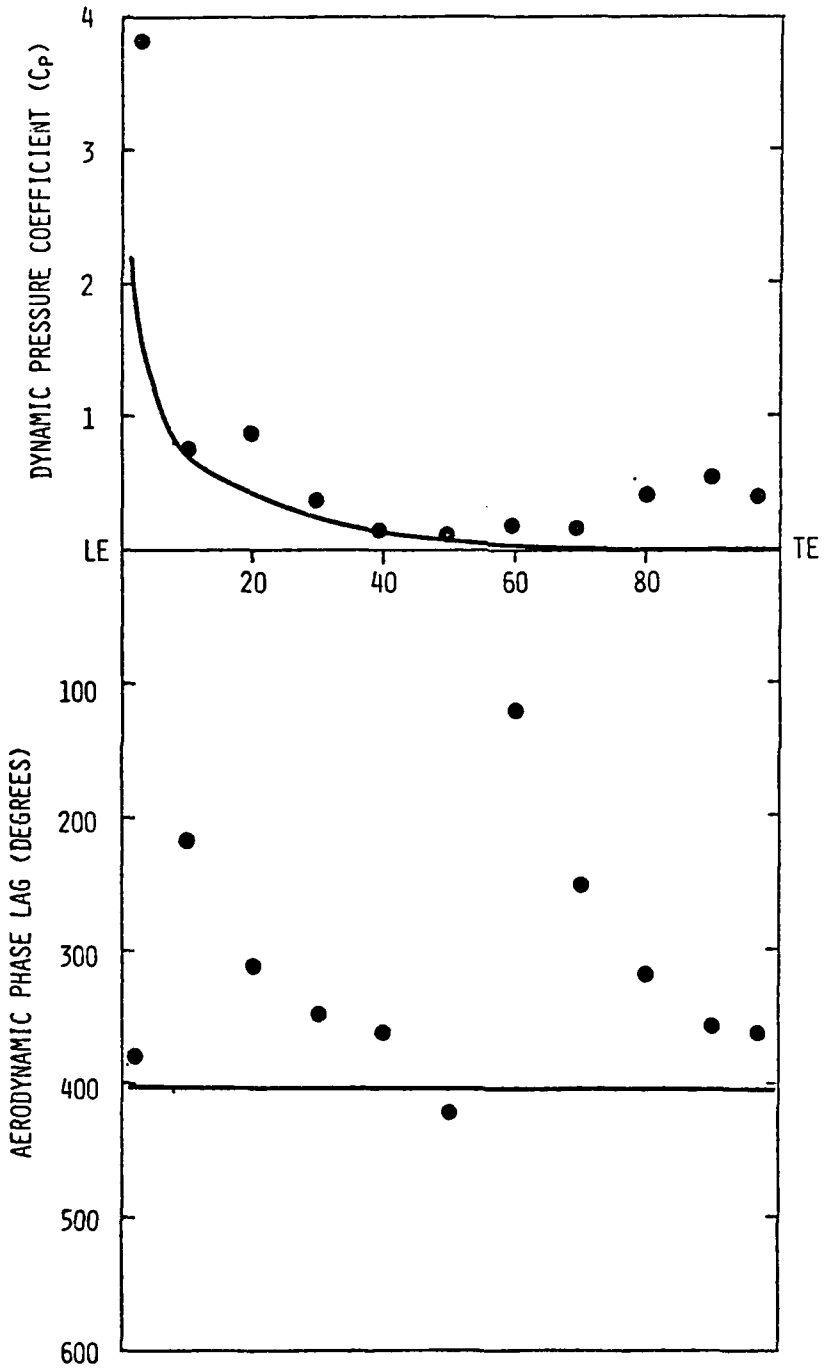

Figure 22. Chordwise data for first harmonic pressure difference and phase lag and prediction from reference 6 for point 01.

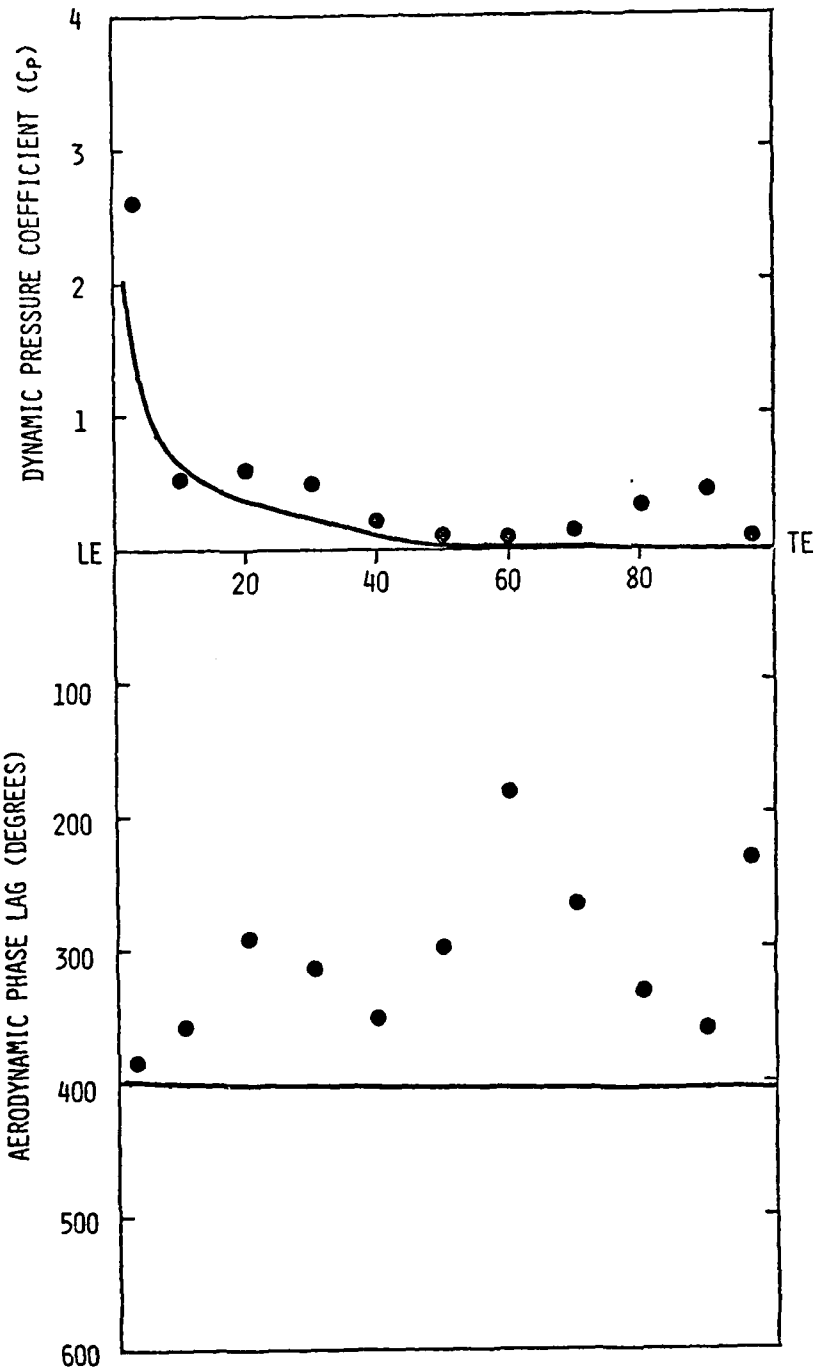

Figure 23. Chordwise data for first harmonic pressure difference and phase lag and prediction from reference 6 for point 02.

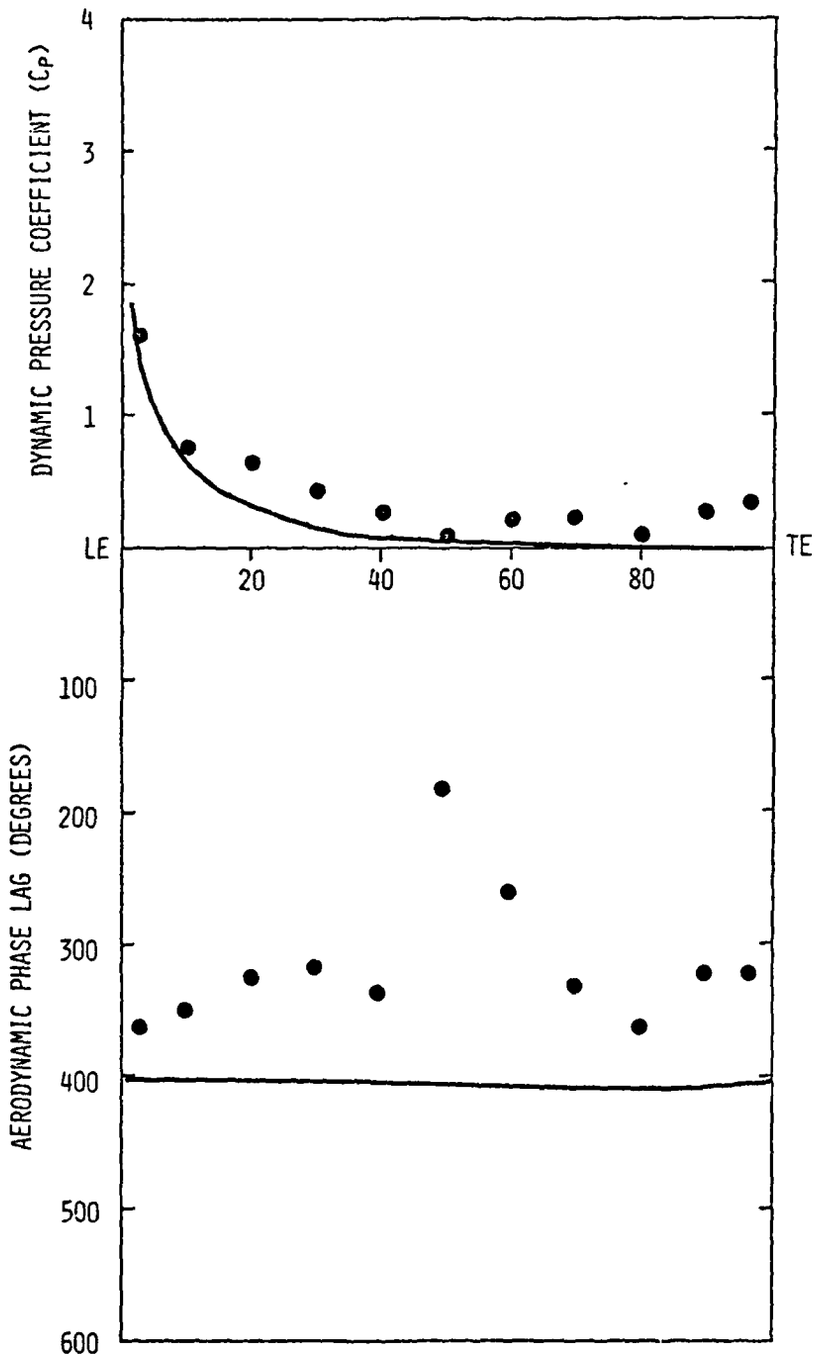

Figure 24. Chordwise data for first harmonic pressure difference and phase lag and prediction from reference 6 for point 03.

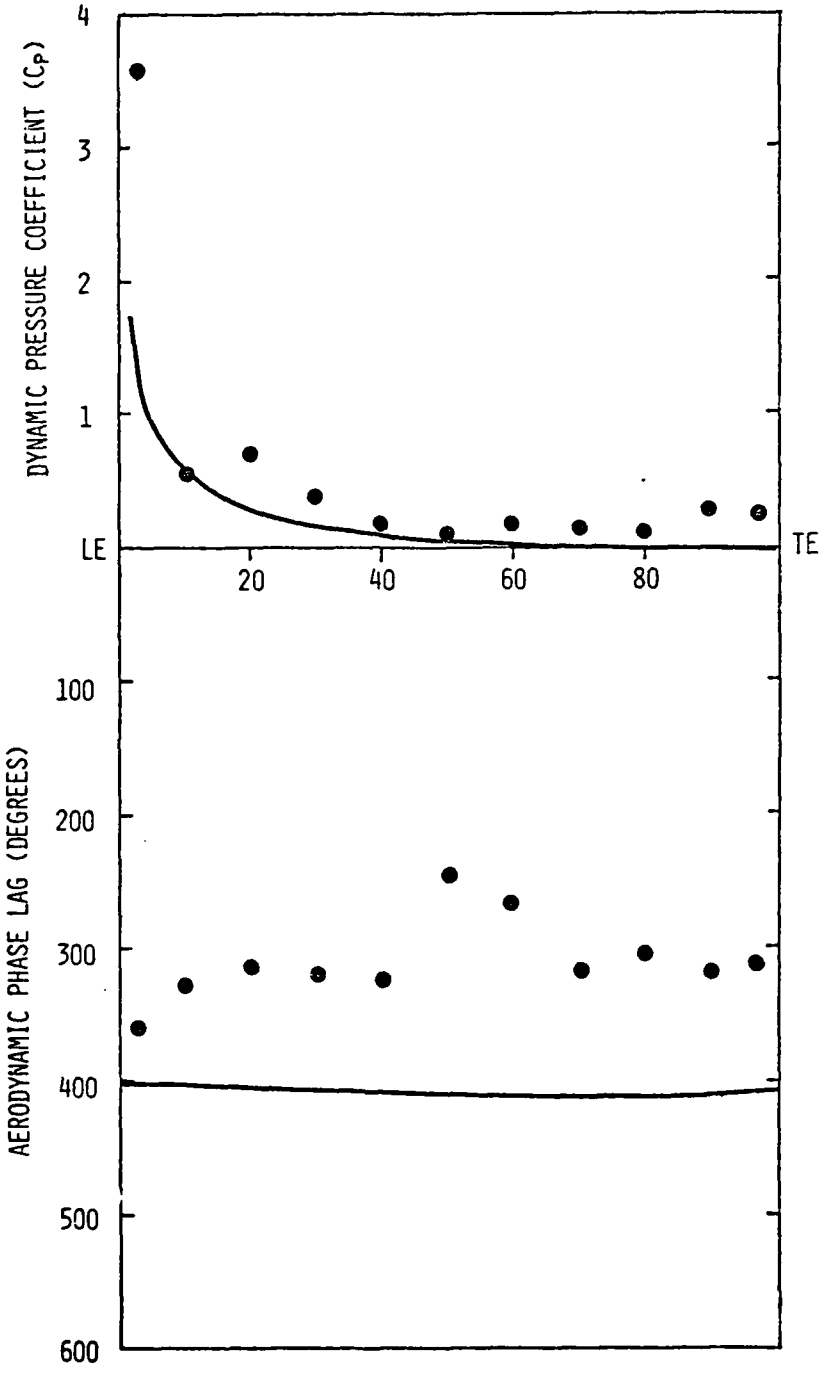

Figure 25. Chordwise data for first harmonic pressure difference and phase lag and prediction from reference 6 for point 04.

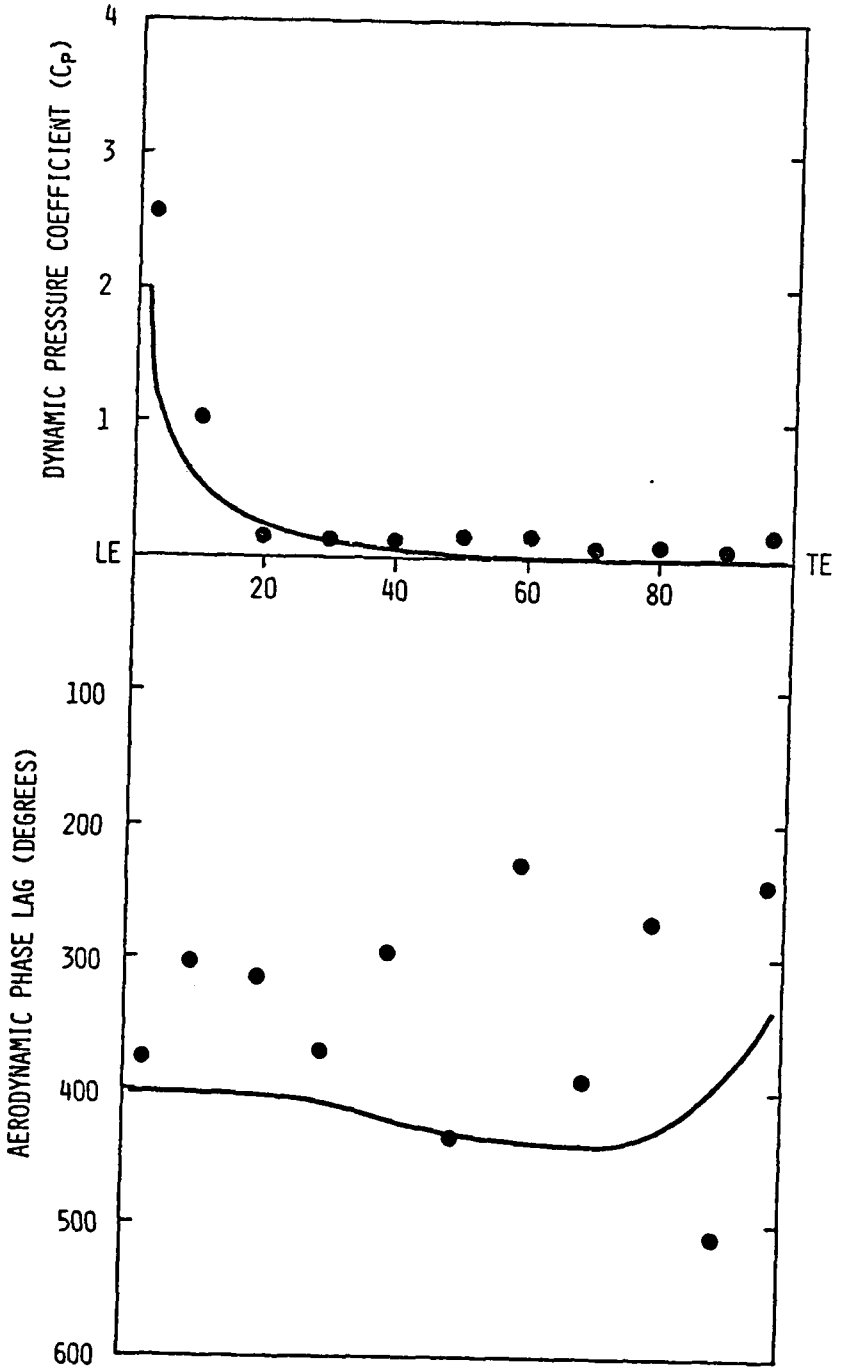

Figure 26. Chordwise data for second harmonic pressure difference and phase lag and prediction from reference 6 for point 01.

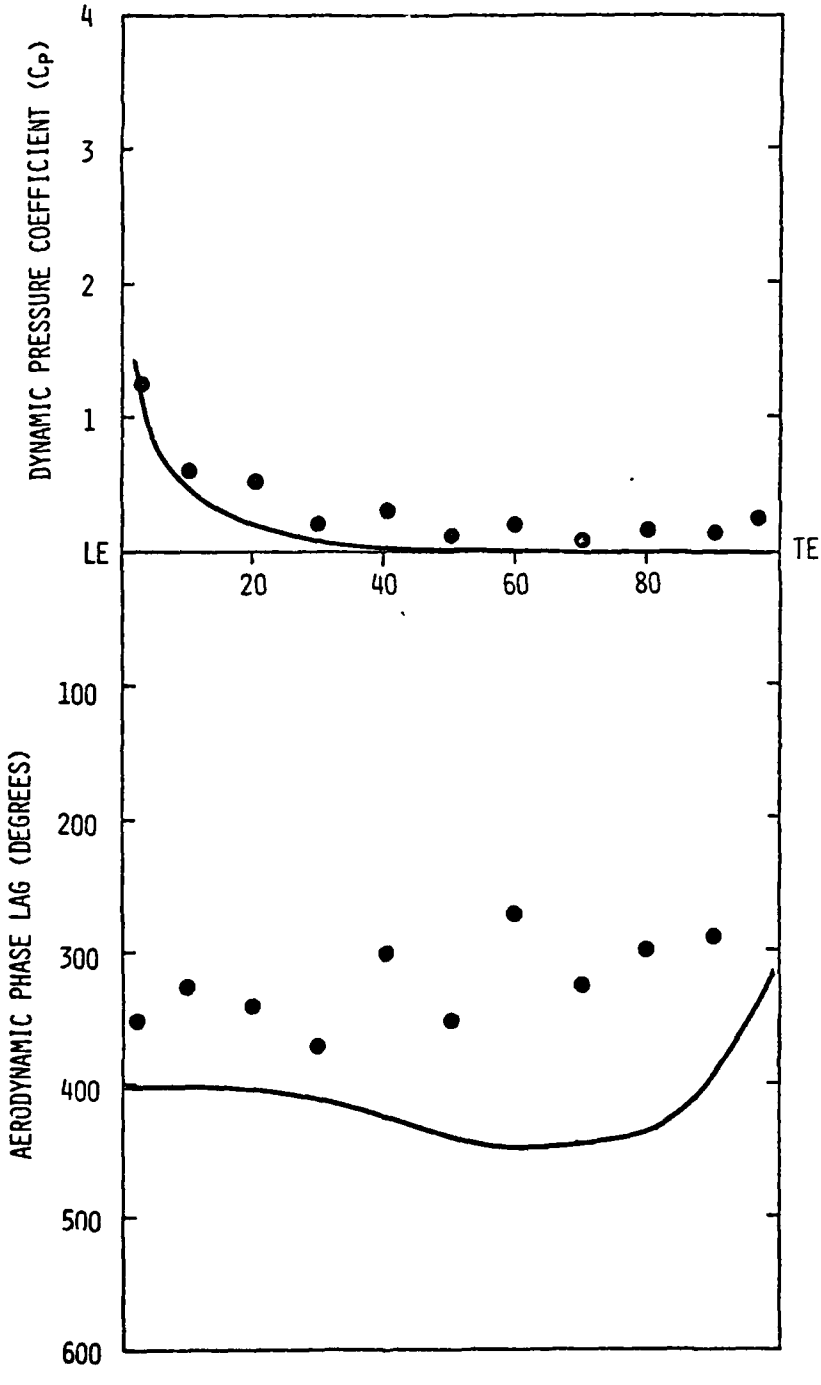

Figure 27. Chordwise data for second harmonid pressure difference and phase lag and prediction from reference 6 for point 02.

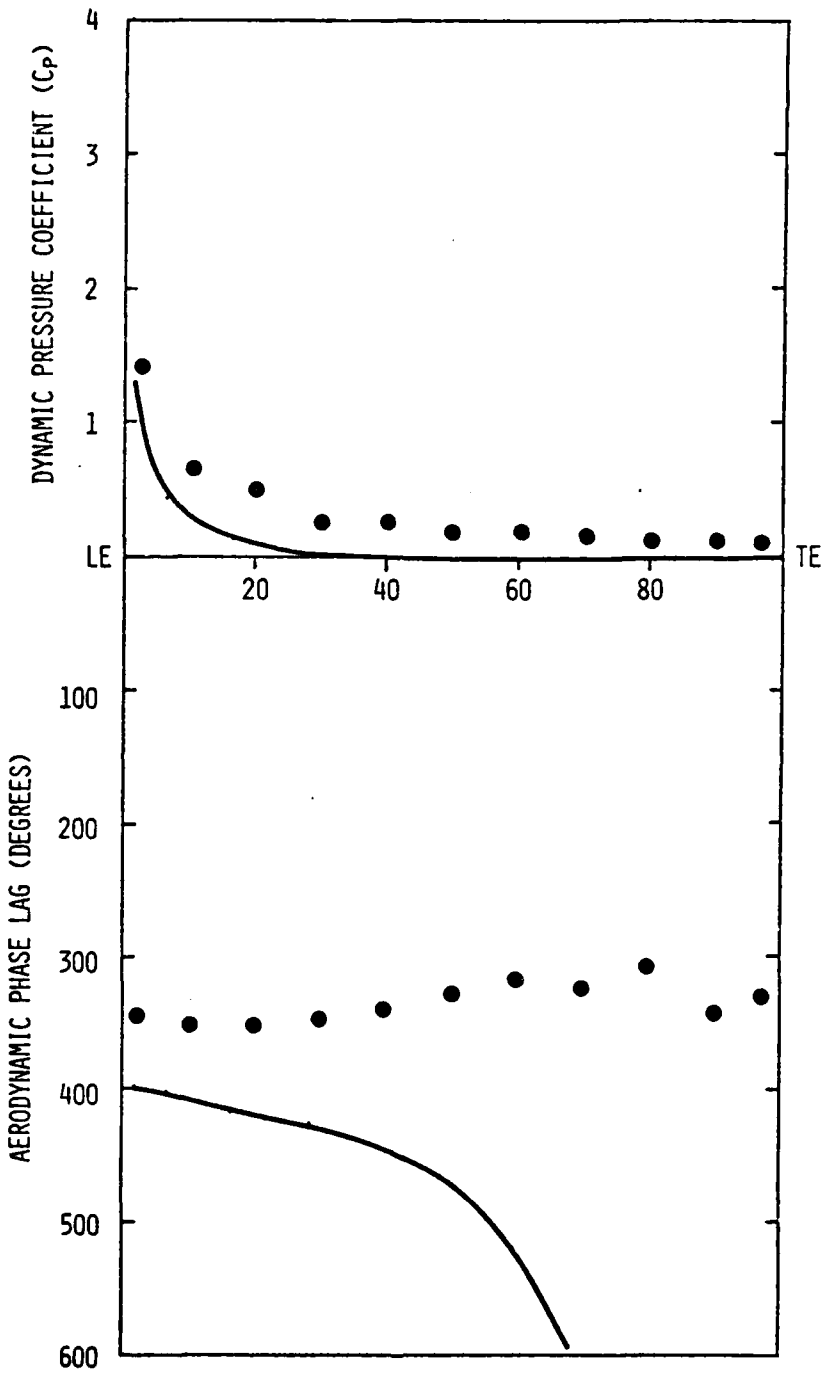

Figure 28. Chordwise data for second harmonic pressure difference and phase lag and prediction from reference 6 for point 03.

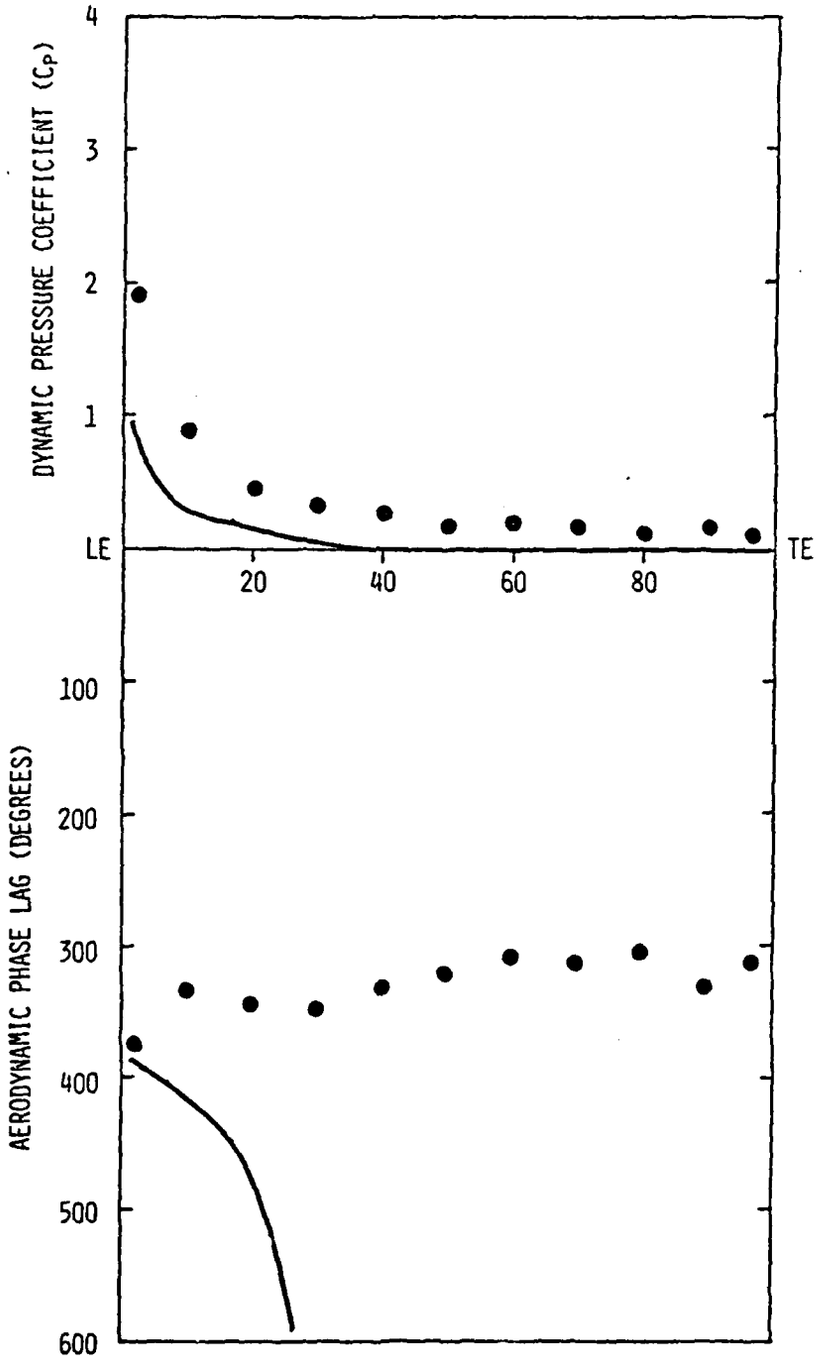

Figure 29. Chordwise data for second harmonic pressure difference and phase lag and prediction from reference 6 for point 04.

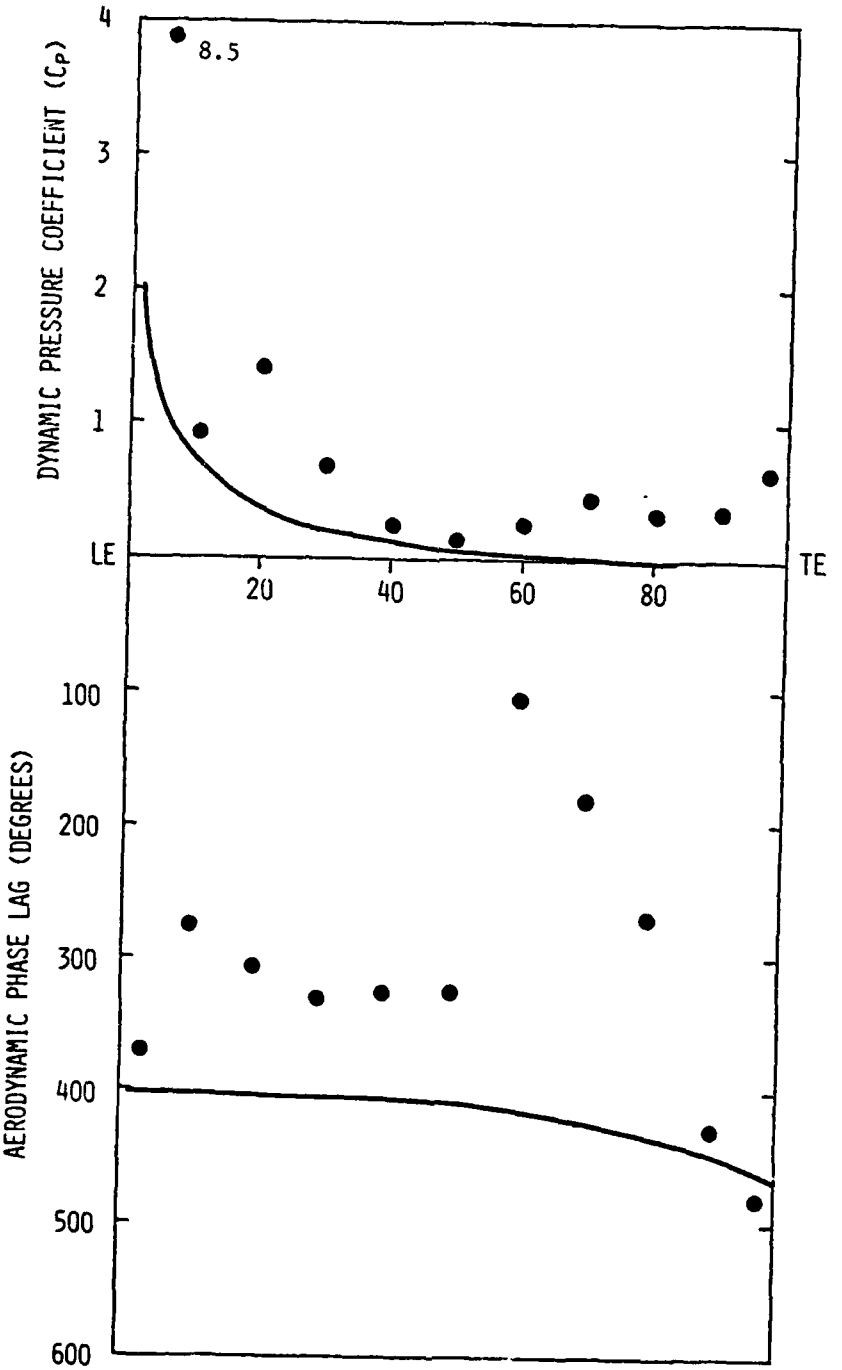

Figure 30. Chordwise data for first harmonic pressure difference and phase lag and prediction from reference 6 for point 05.

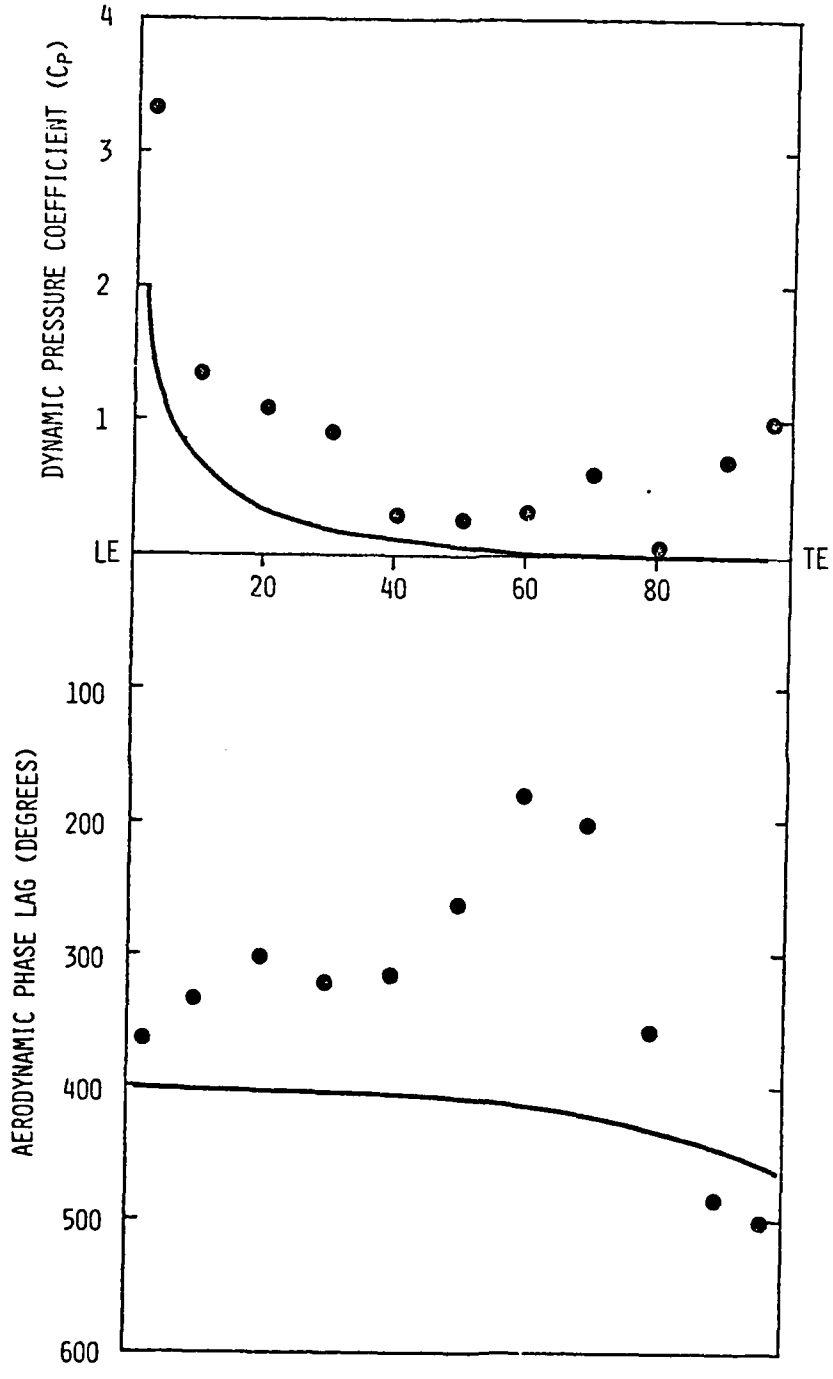

Figure 31. Chordwise data for first harmonic pressure difference and phase lag and prediction from reference 6 for point 06.

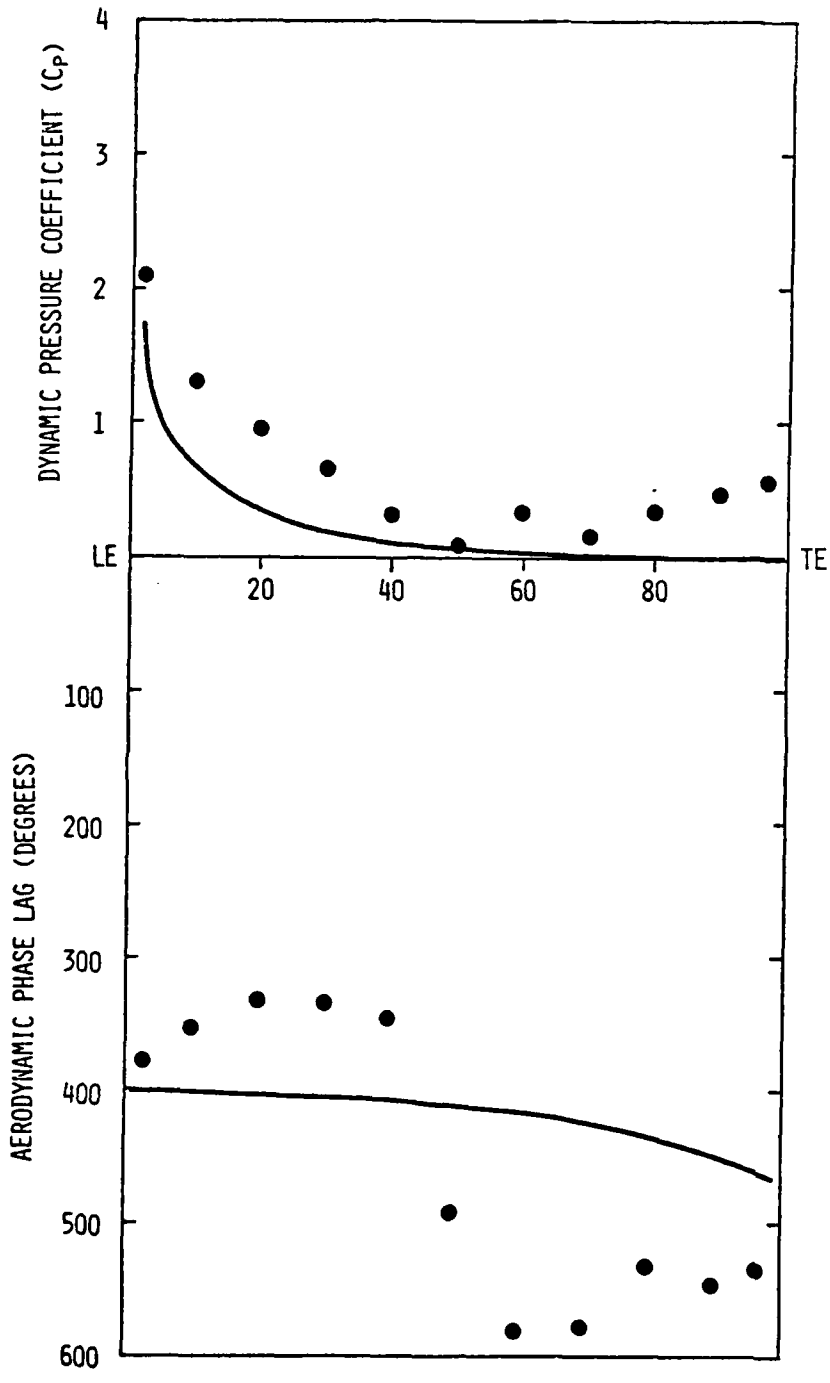

Figure 32. Chordwise data for first harmonic pressure difference and phase lag and prediction from reference 6 for point 07.

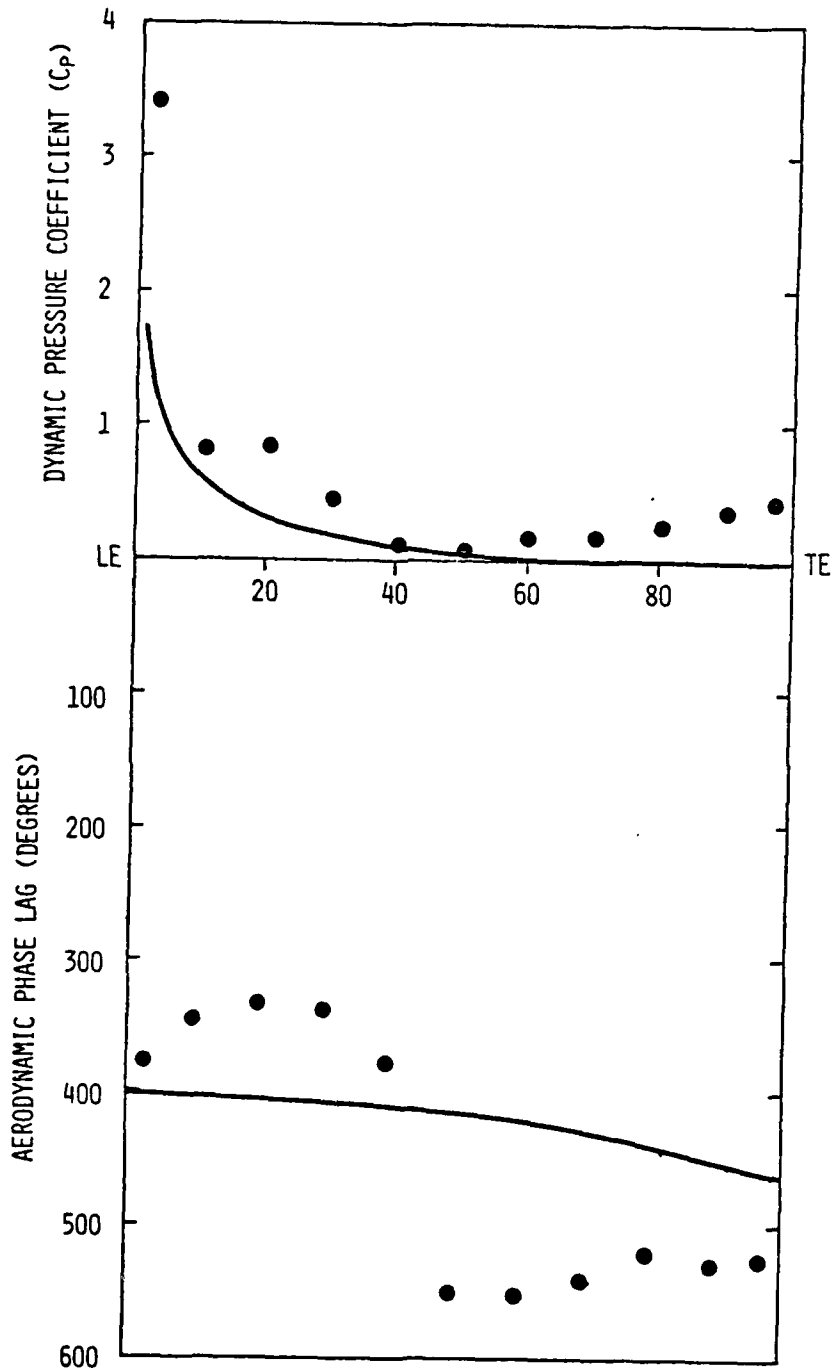

Figure 33. Chordwise data for first narmonic pressure difference and phase lag and prediction from reference 6 for point 08.

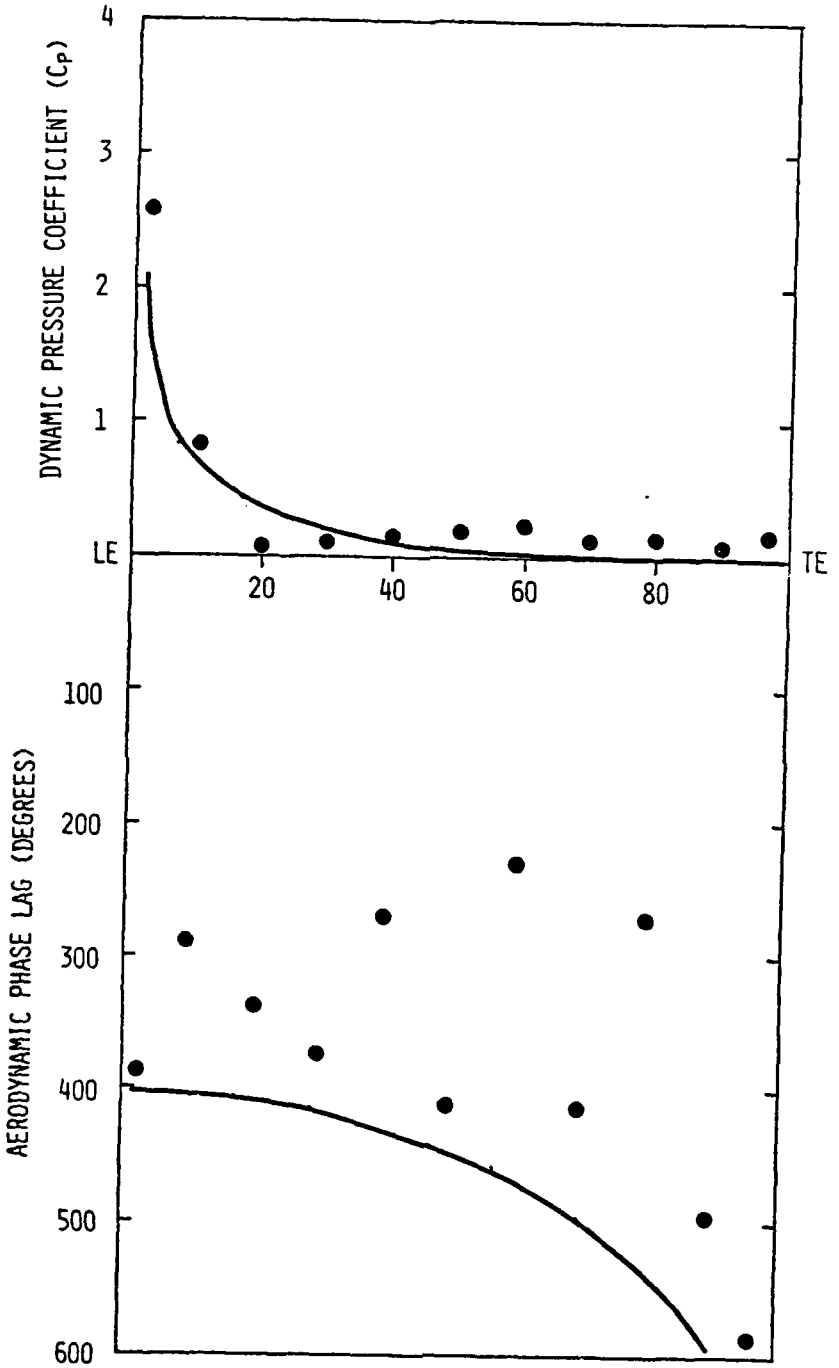

Figure 34. Chordwise data for second harmonic pressure difference and phase lag and prediction from reference 6 for point 05.

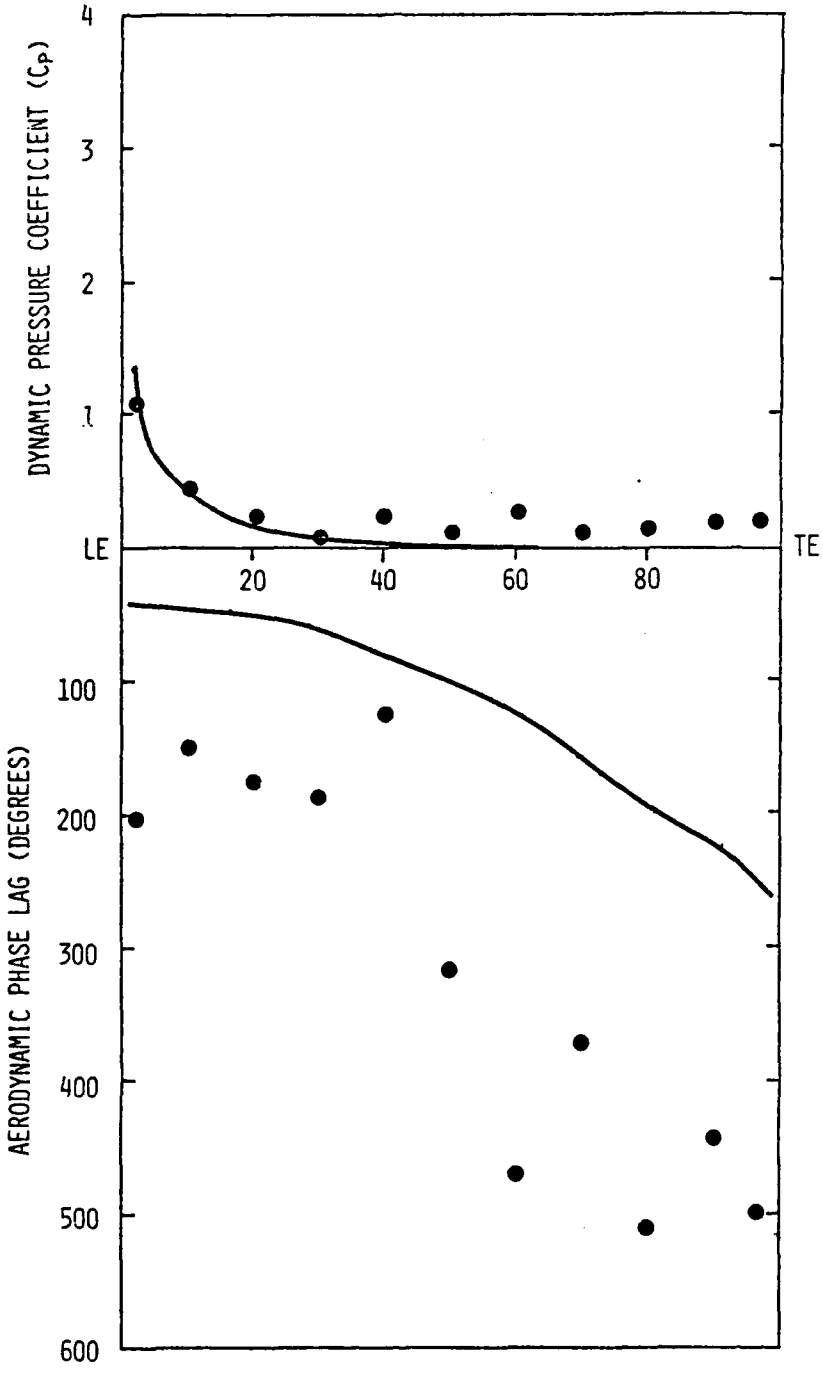

Figure 35. Chordwise data for second harmonic pressure difference and phase lag and prediction from reference 6 for point 06.

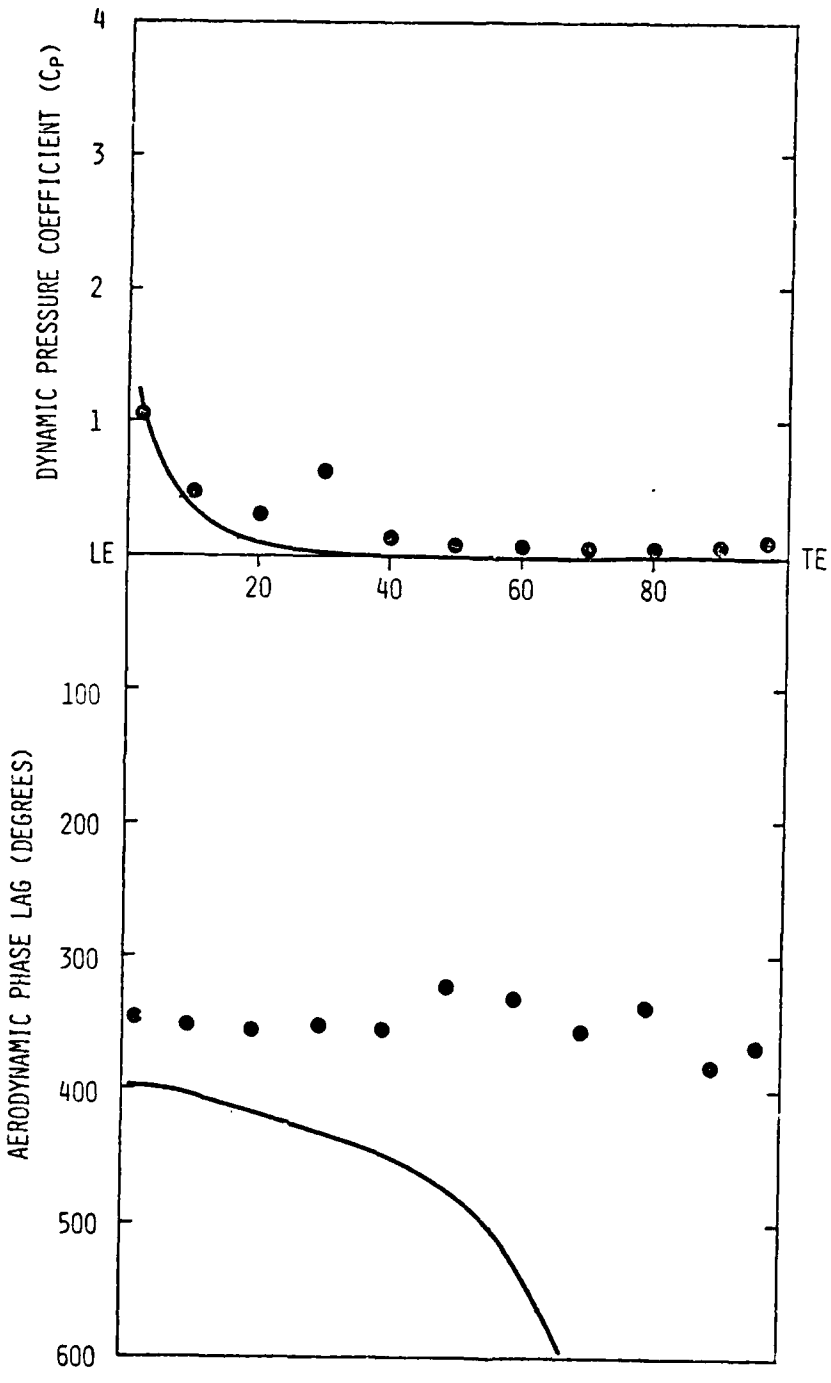

Figure 36. Chordwise data for second harmonic pressure difference and phase lag and prediction from reference 6 for point 07.

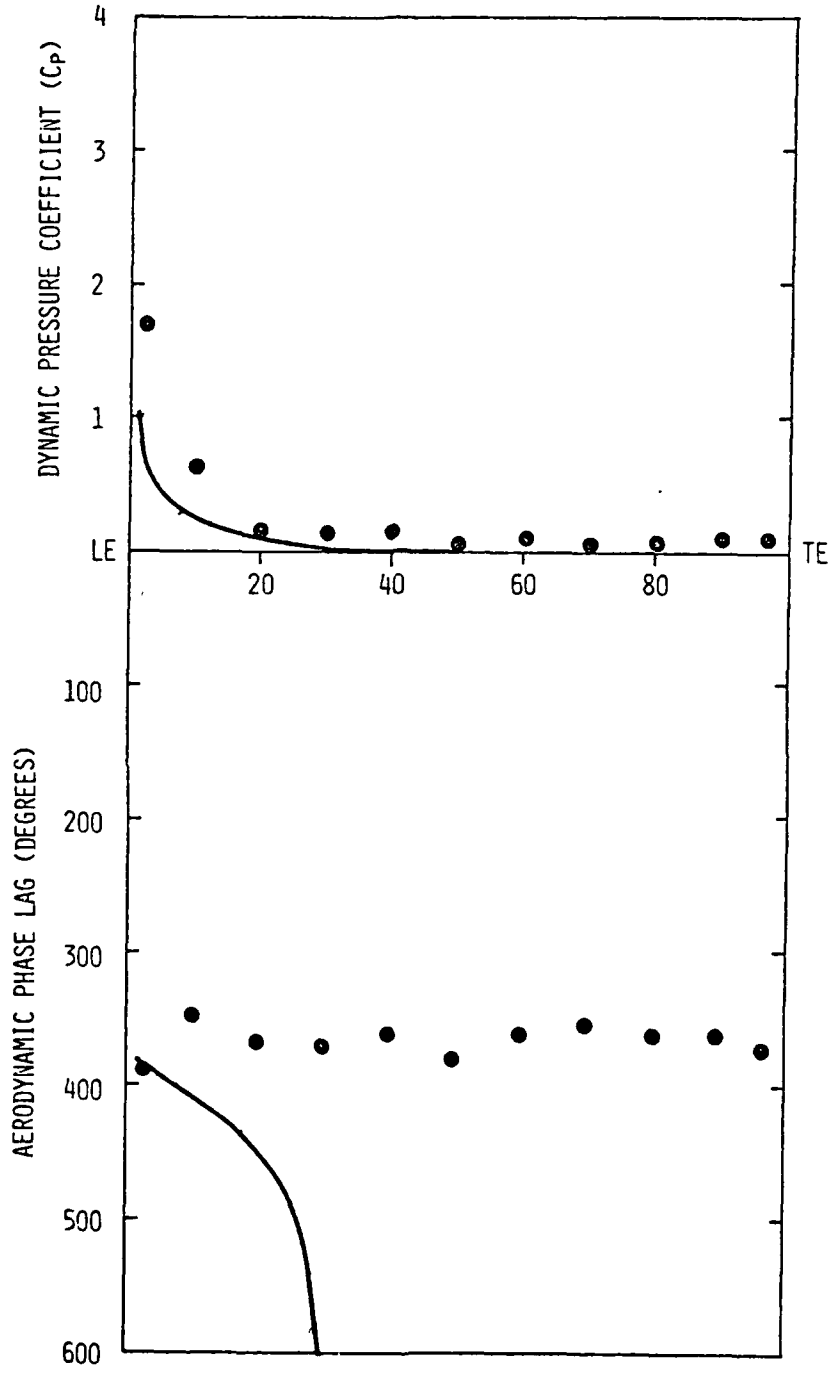

Figure 37. Chordwise data for second harmonic pressure difference and phase lag and prediction from reference 6 for point 08.

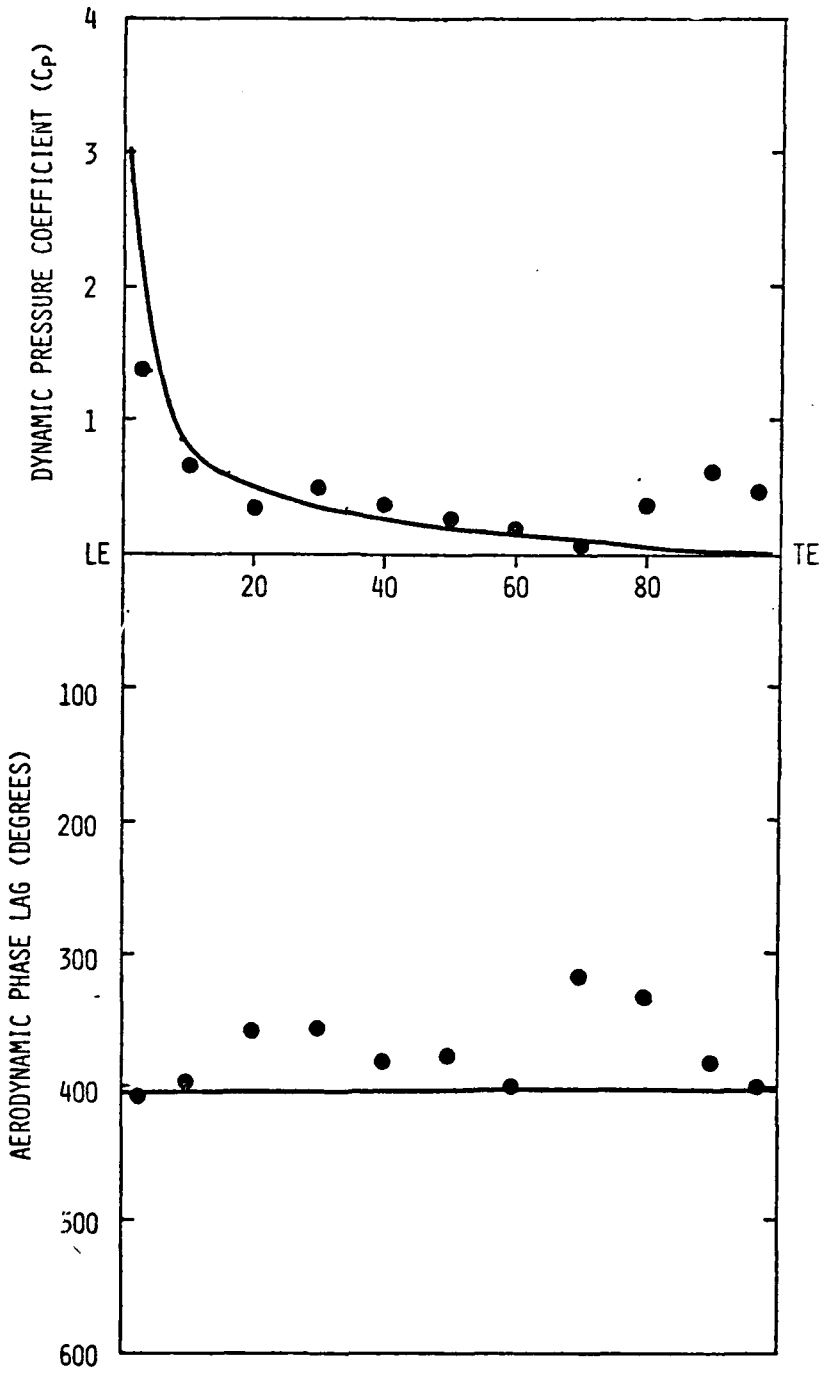

Figure 38. Chordwise data for first harmonic pressure difference and phase lag and prediction from reference 6 for point 11.

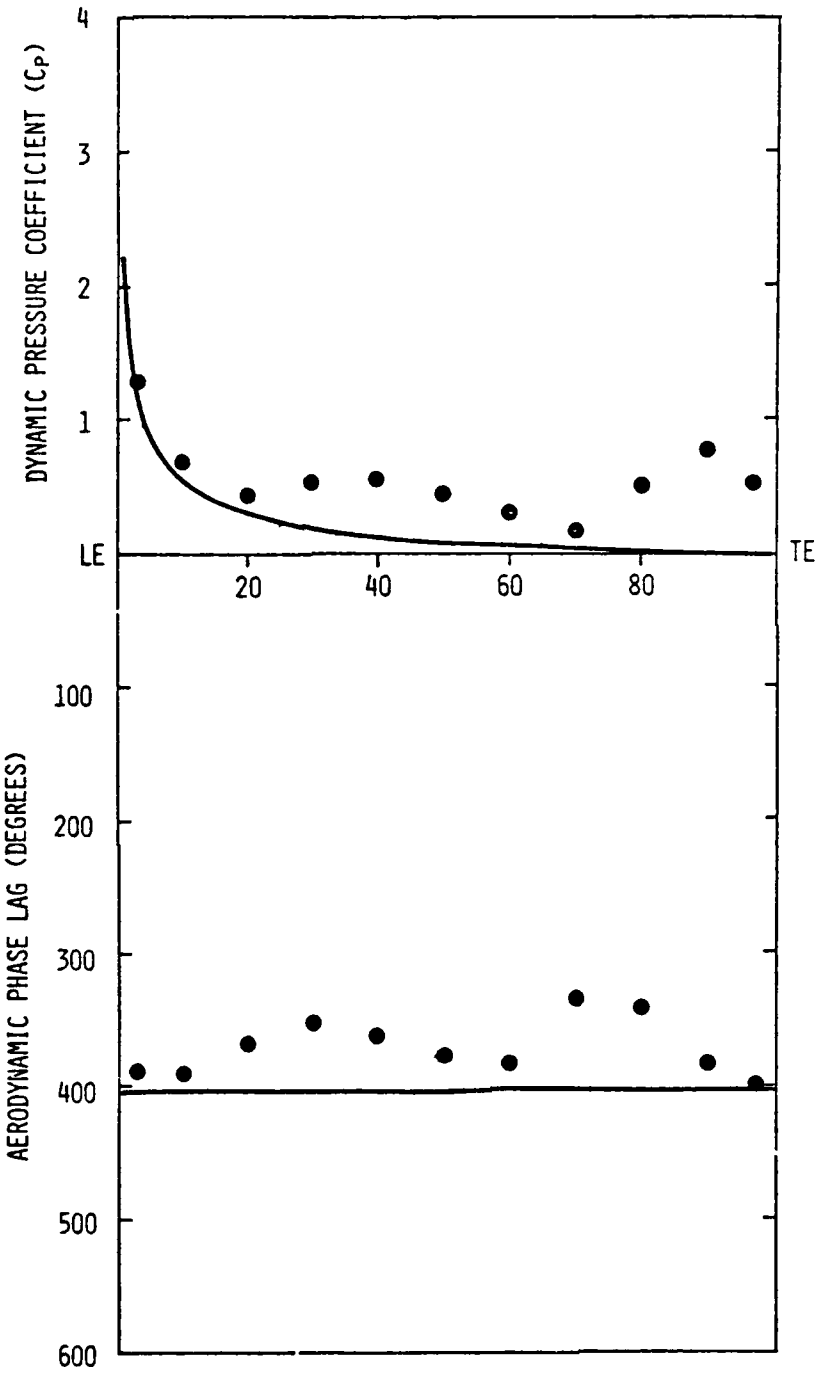

Figure 39. Chordwise data for first harmonic pressure difference and phase lag and prediction from reference 6 for point 12.

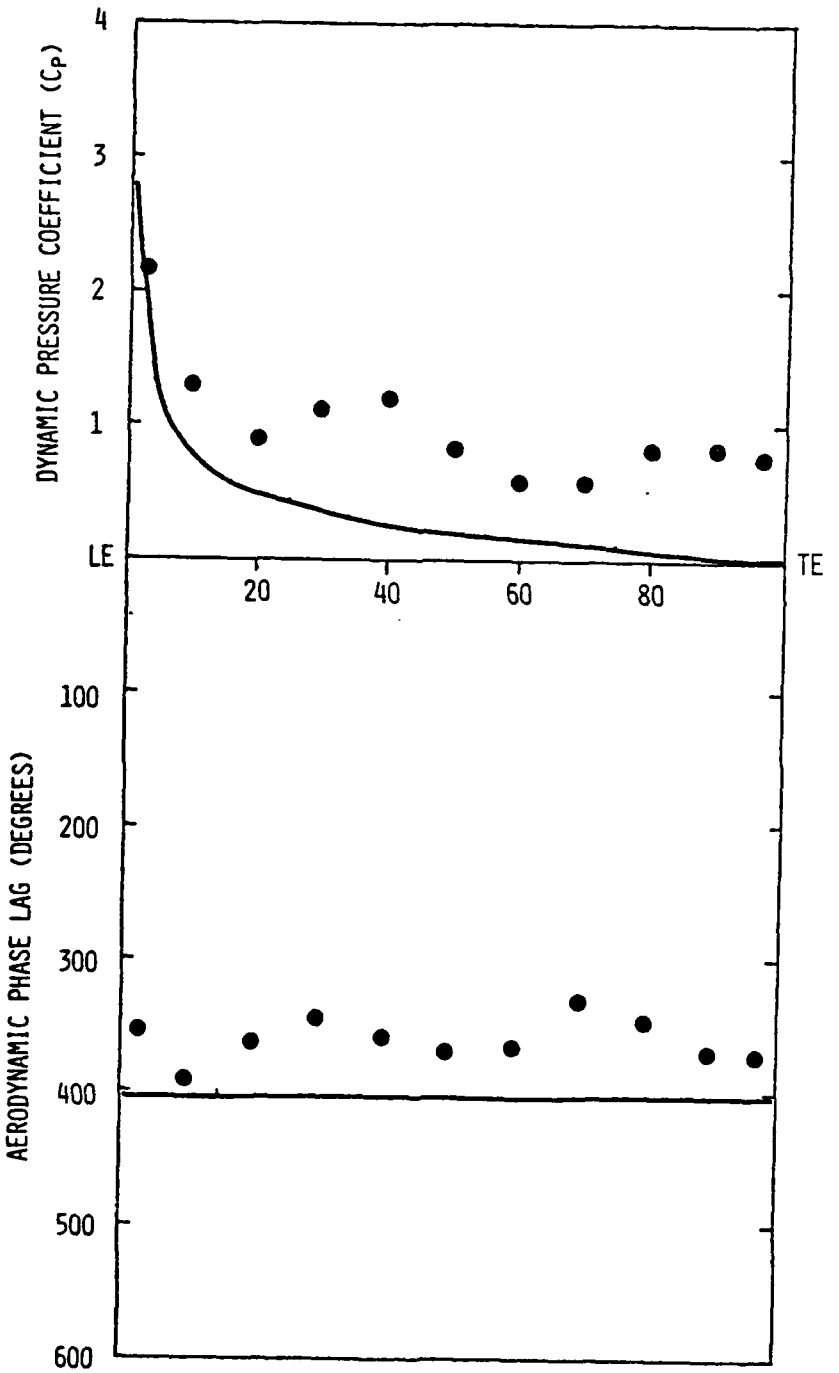

Figure 40. Chordwise data for first harmonic pressure difference and phase lag and prediction from reference 6 for point 13.

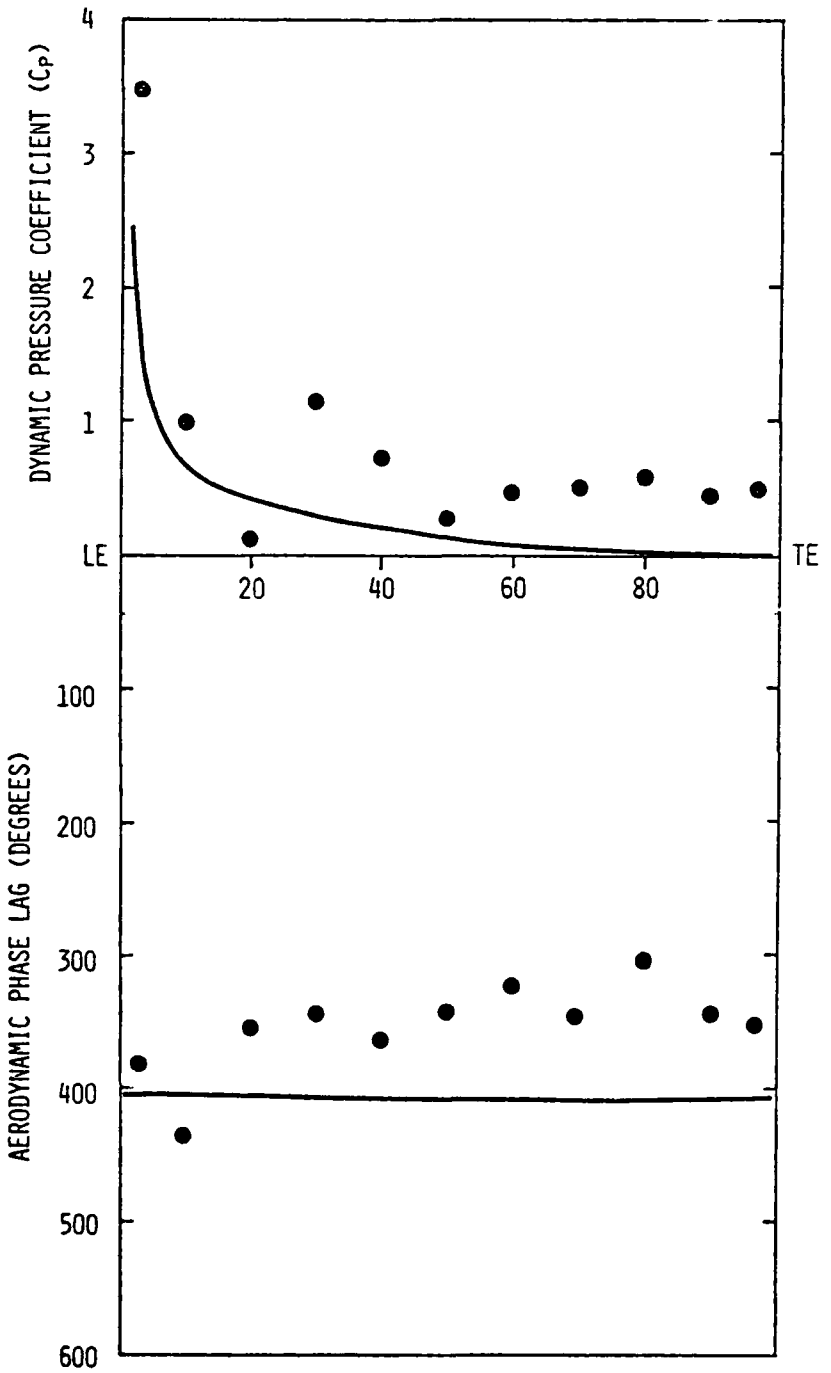

Figure 41. Chordwise data for first harmonic pressure difference and phase lag and prediction from reference 6 for point 14.

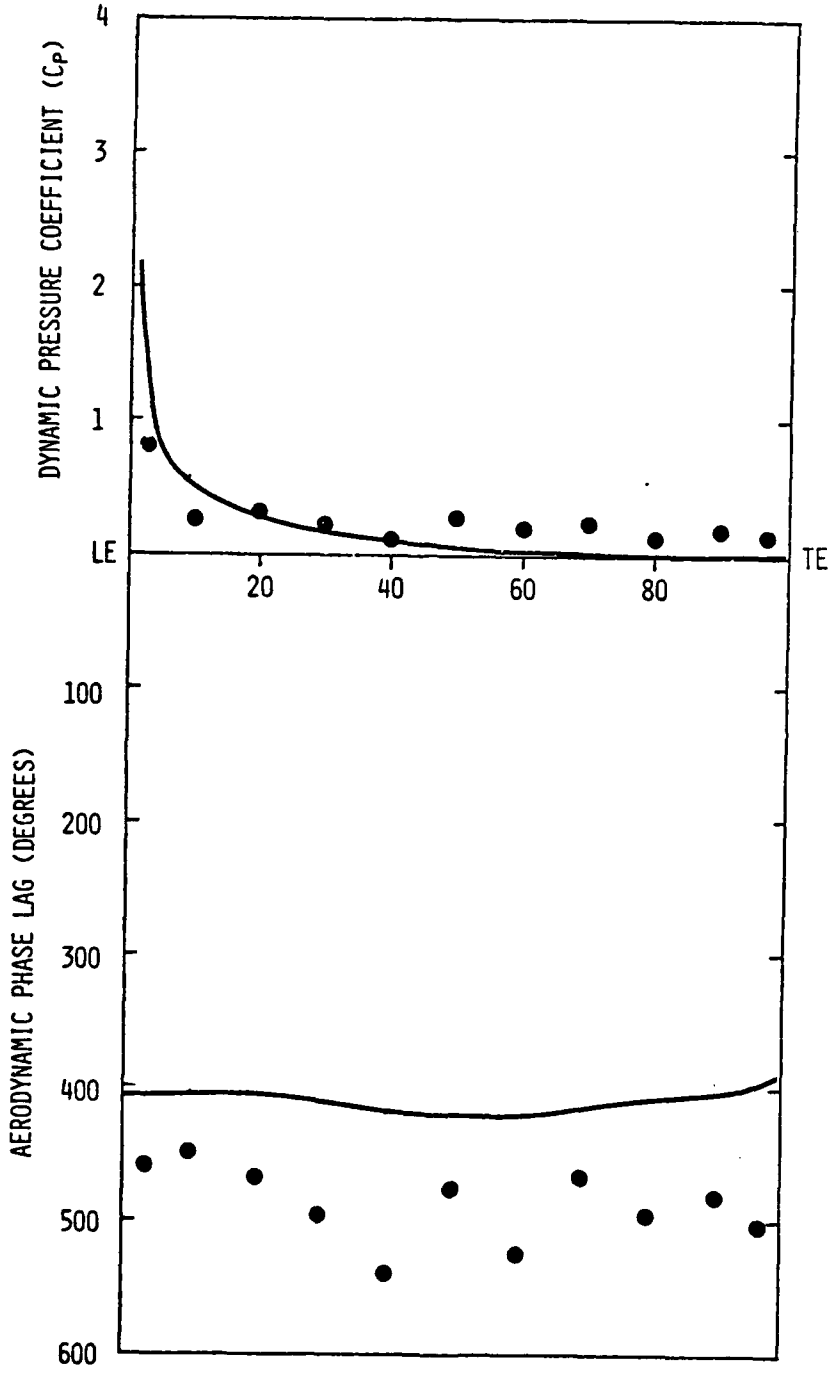

Figure 42. Chordwise data for second harmonic pressure difference and phase lag and prediction from reference 6 for point 11.

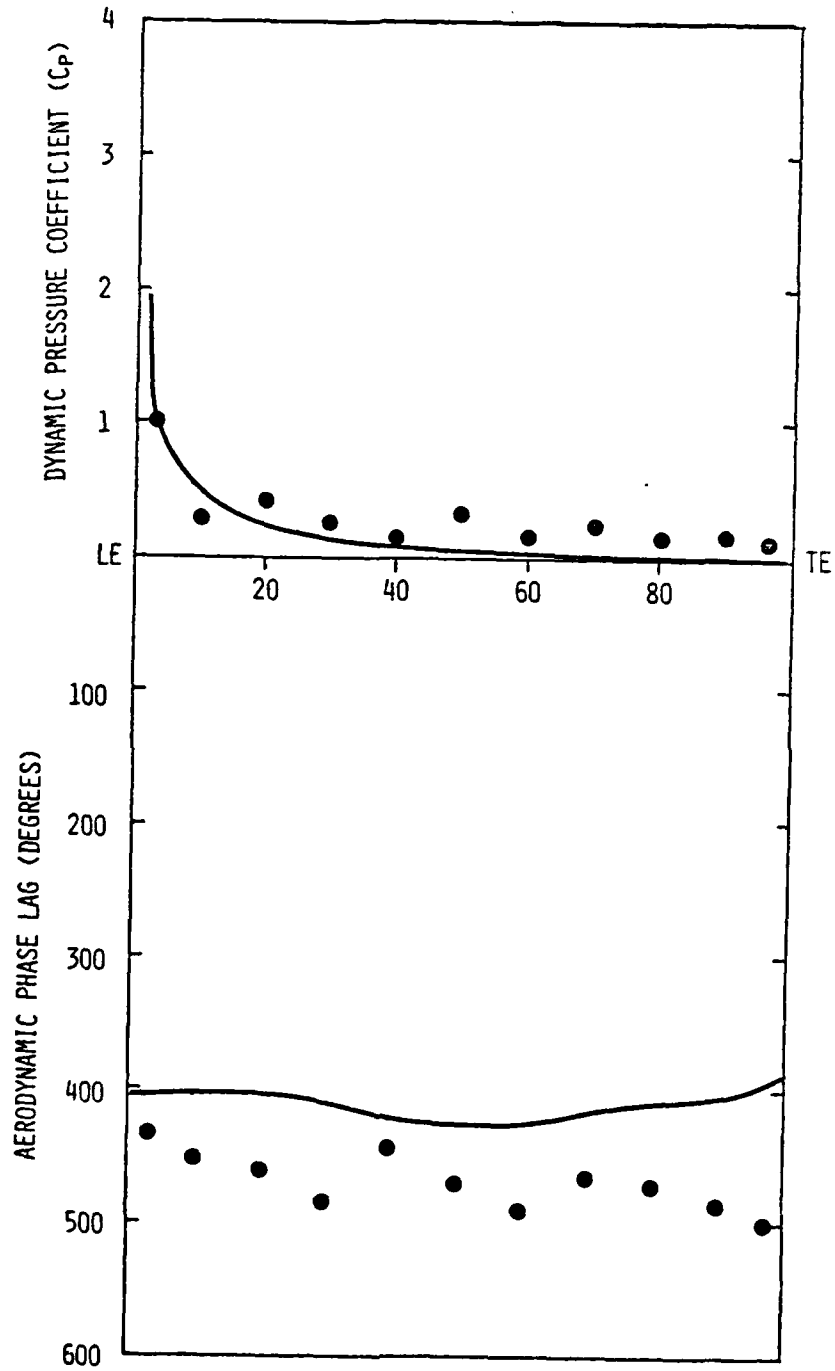

Figure 43. Chordwise data for second harmonic pressure difference and phase lag and prediction from reference 6 for point 12.

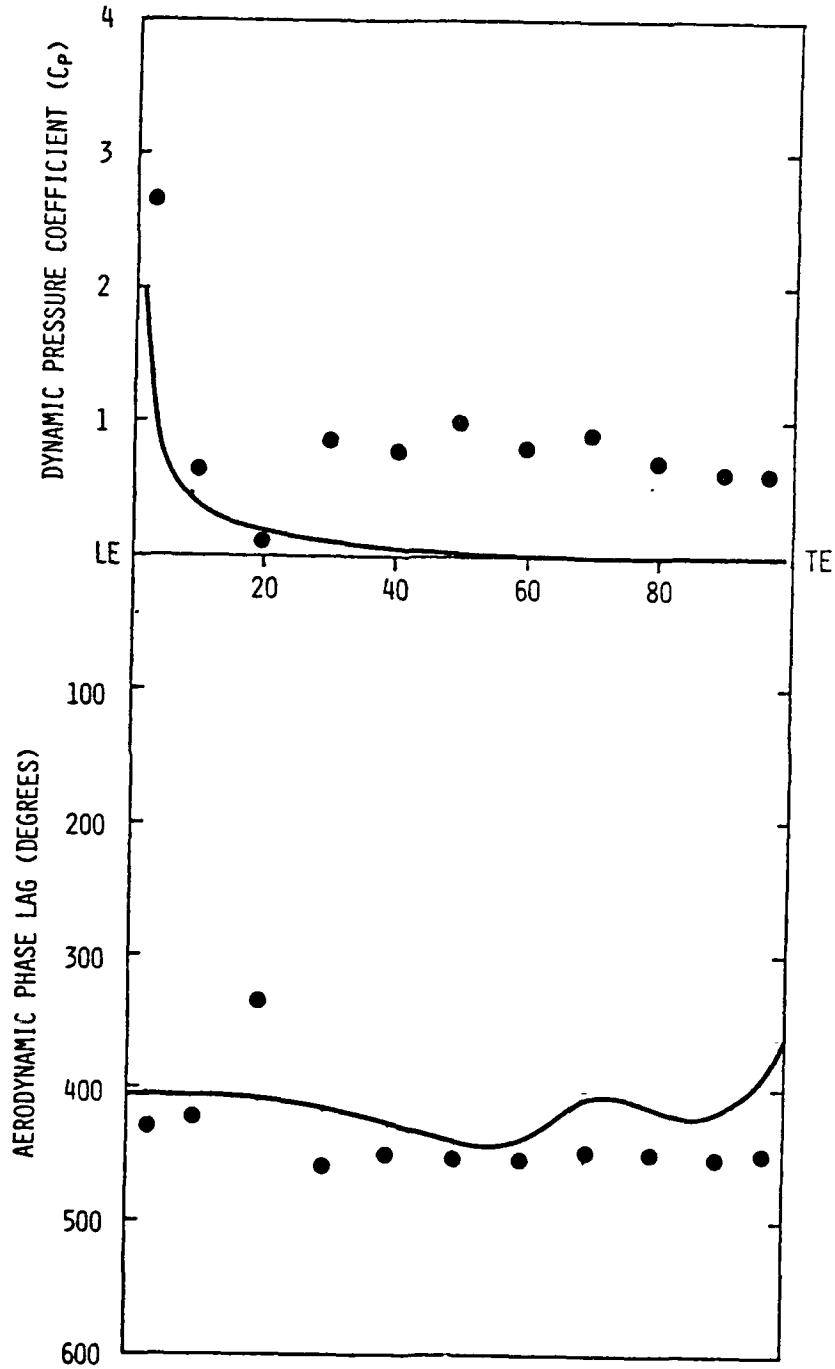

Figure 44. Chordwise data for second harmonic pressure difference and phase lag and prediction from reference 6 for point 13.

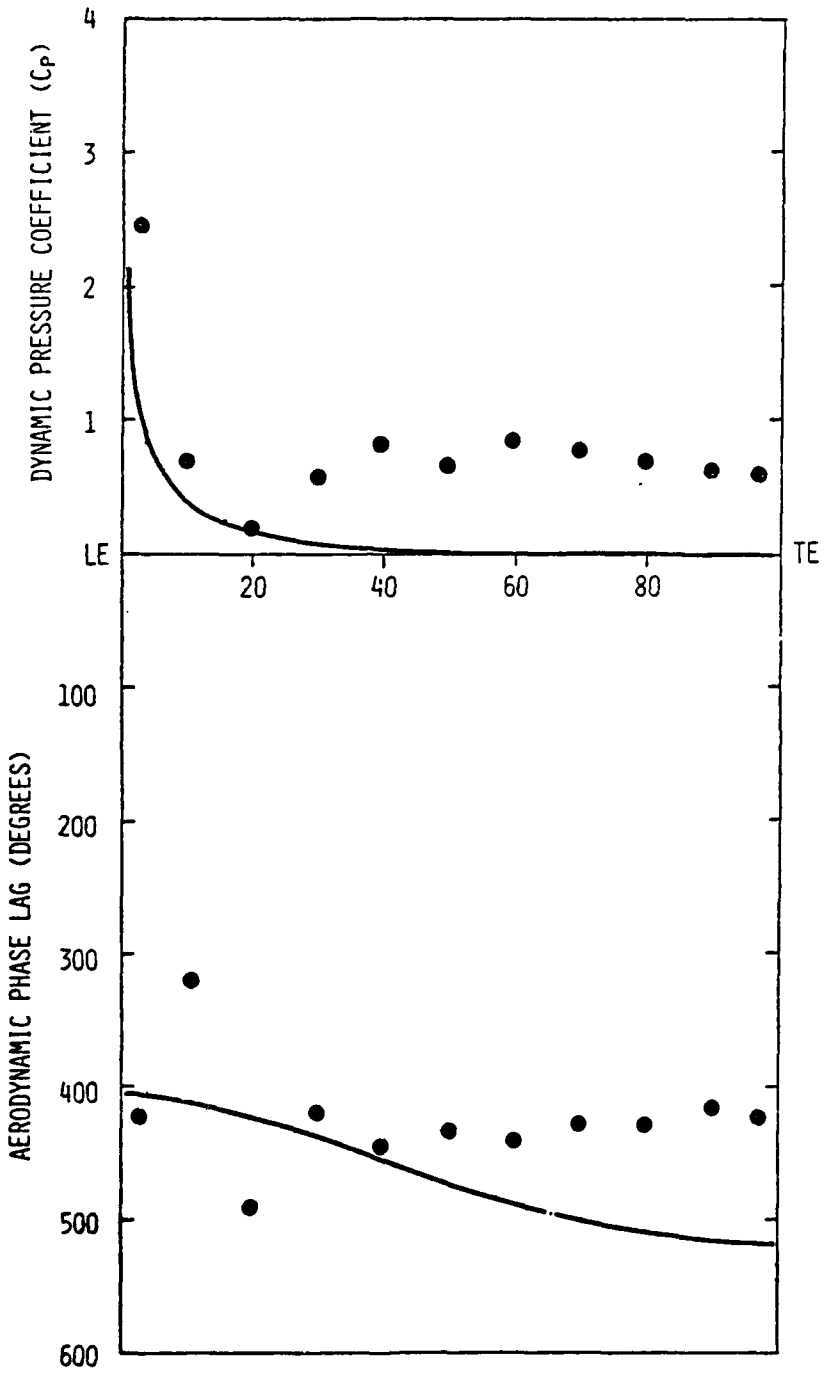

Figure 45. Chordwise data for second harmonic pressure difference and phase lag and prediction from reference 6 for point 14.

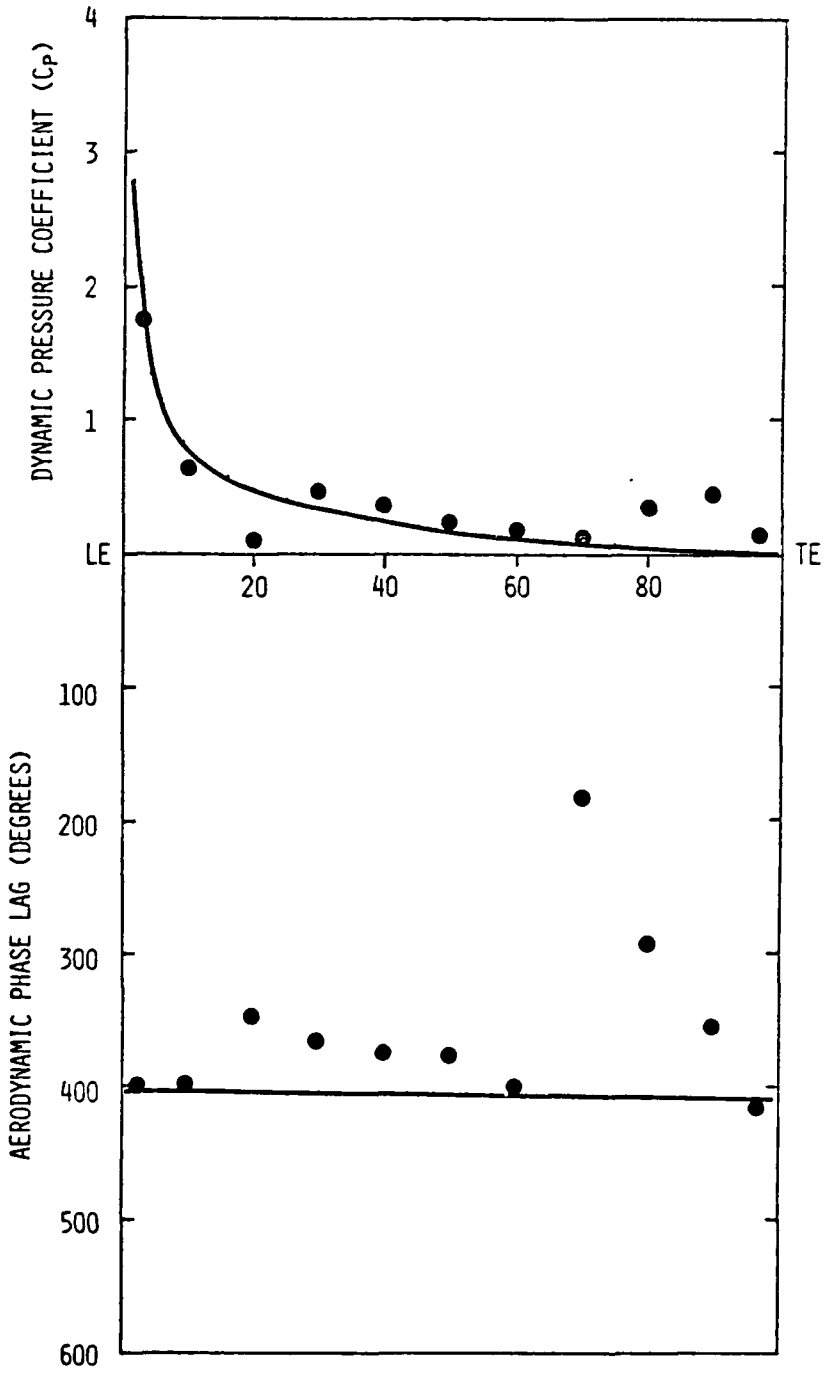

Figure 46. Chordwise data for first harmonic pressure difference and phase lag and prediction from reference 6 for point 15.

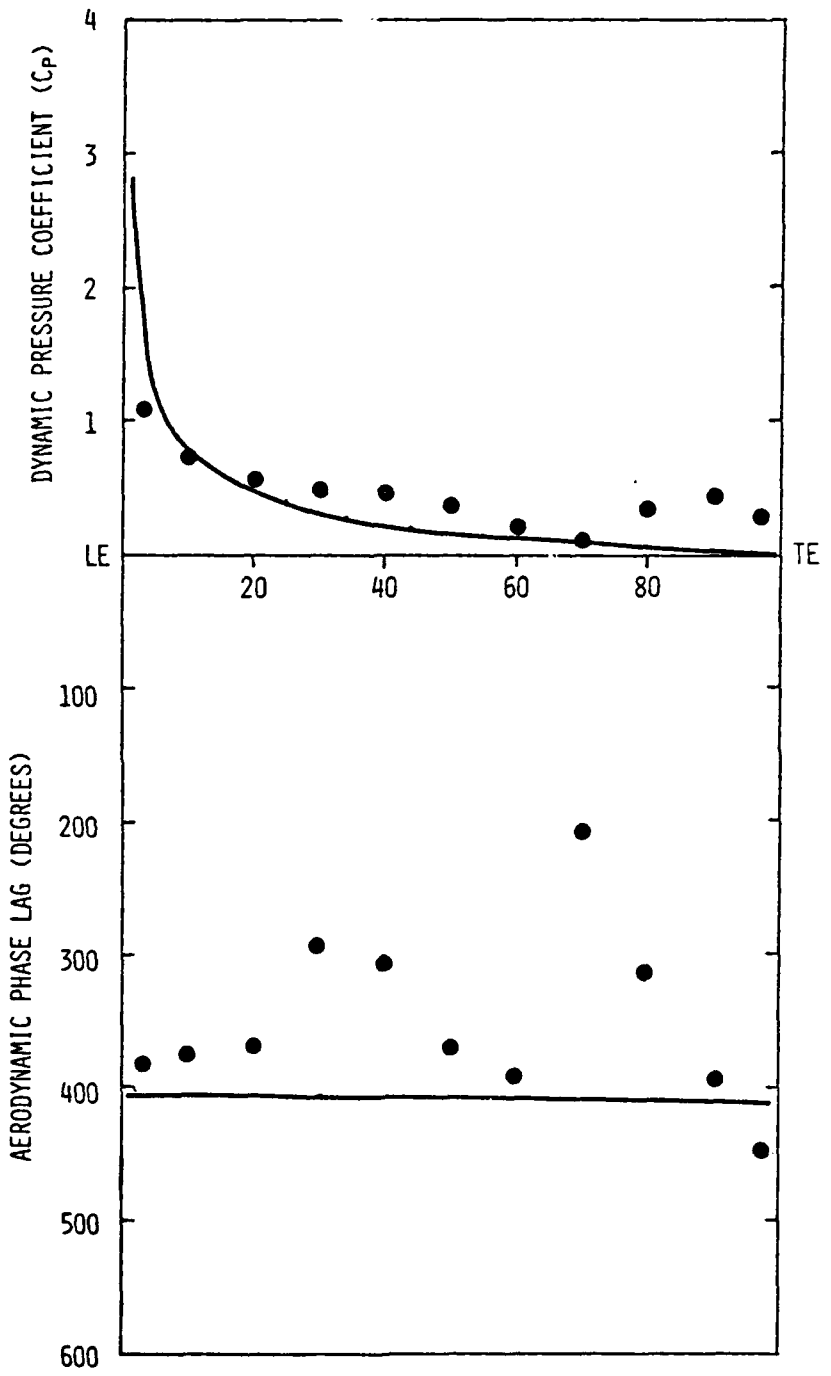

Figure 47. Chordwise data for first harmonic pressure difference and phase lag and prediction from reference 6 for point 16.

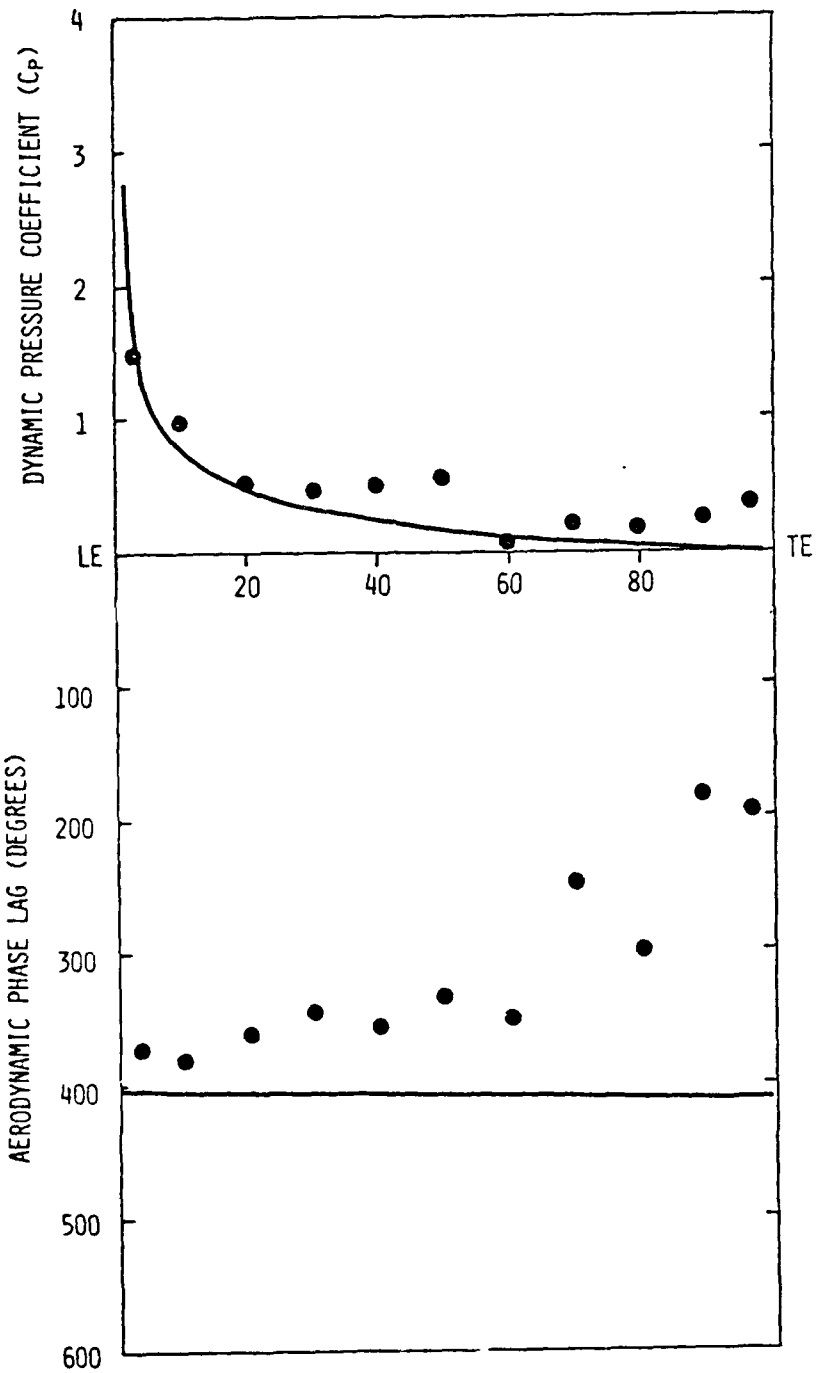

Figure 48. Chordwise data for first harmonic pressure difference and phase lag and prediction from reference 6 for point 17.

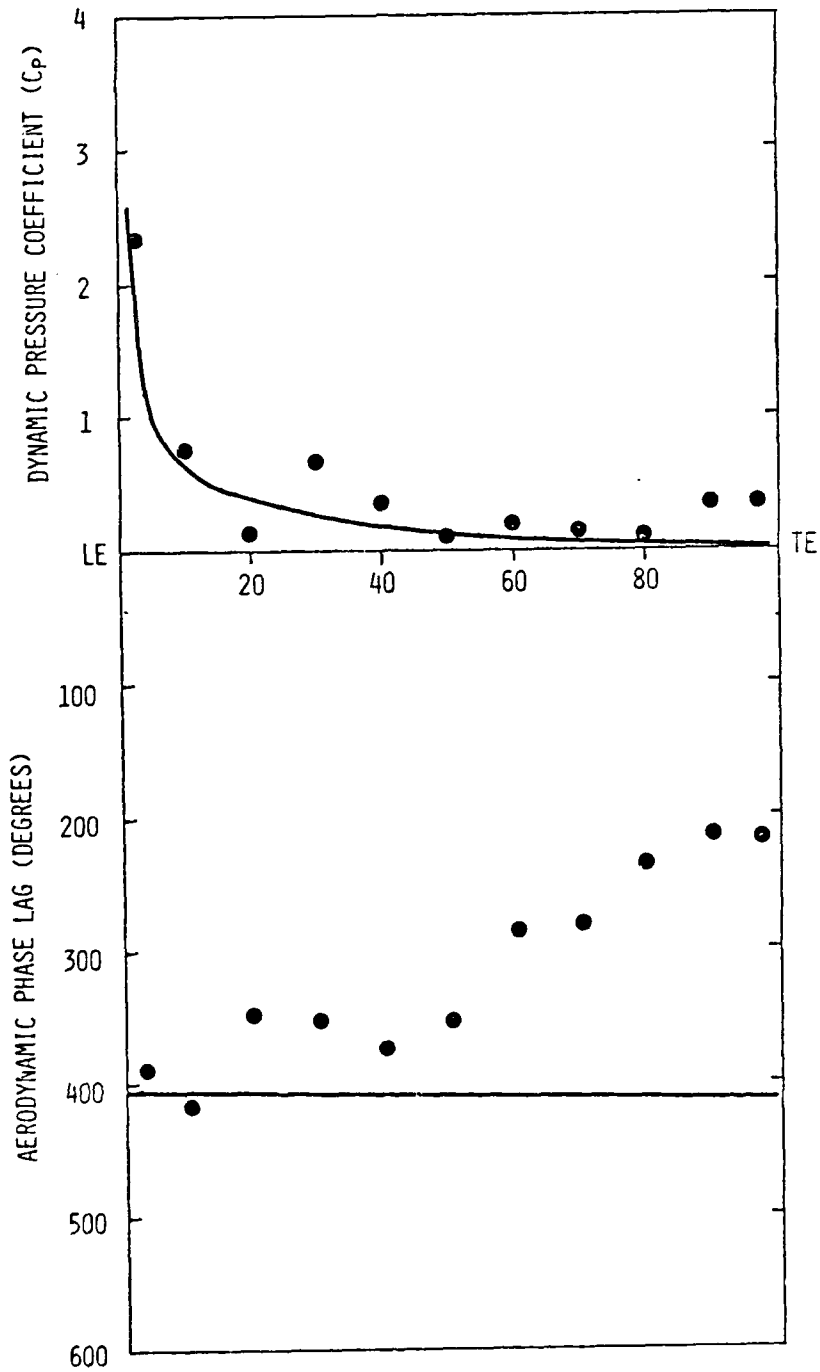

Figure 49. Chordwise data for first harmonic pressure difference and phase lag and prediction from reference 6 for point 18.

AD-A090 546 GENERAL MOTORS CORP INDIANAPOLIS IN DETROIT DIESEL A--ETC F/G 21/5
THE EFFECTS OF SOLIDITY, INTERBLADE PHASE ANGLE AND REDUCED FRE--ETC(U)
JUN 80 R L JAY, W A BENNETT F49620-78-C-0070
UNCLASSIFIED DDA-EDR-10339 AFOSR-TR-80-1041 NL

2 OF 4
AD A090546

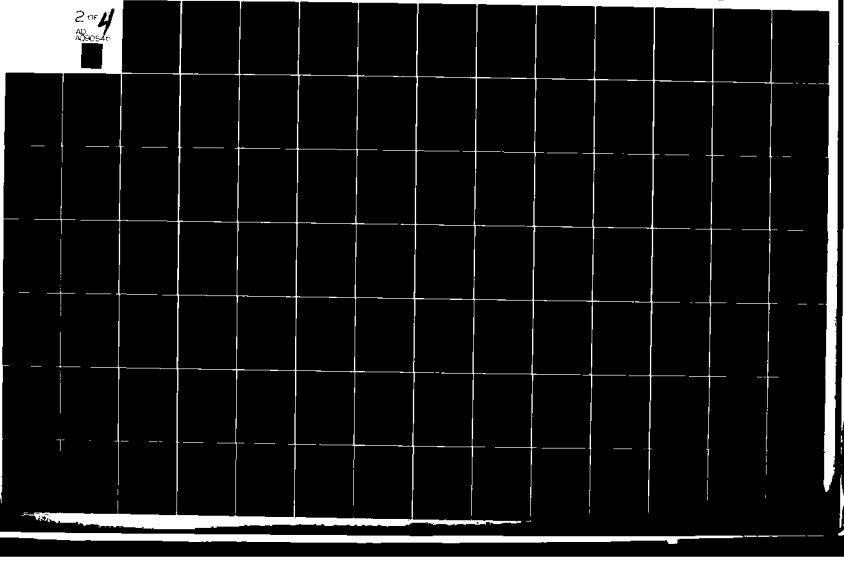

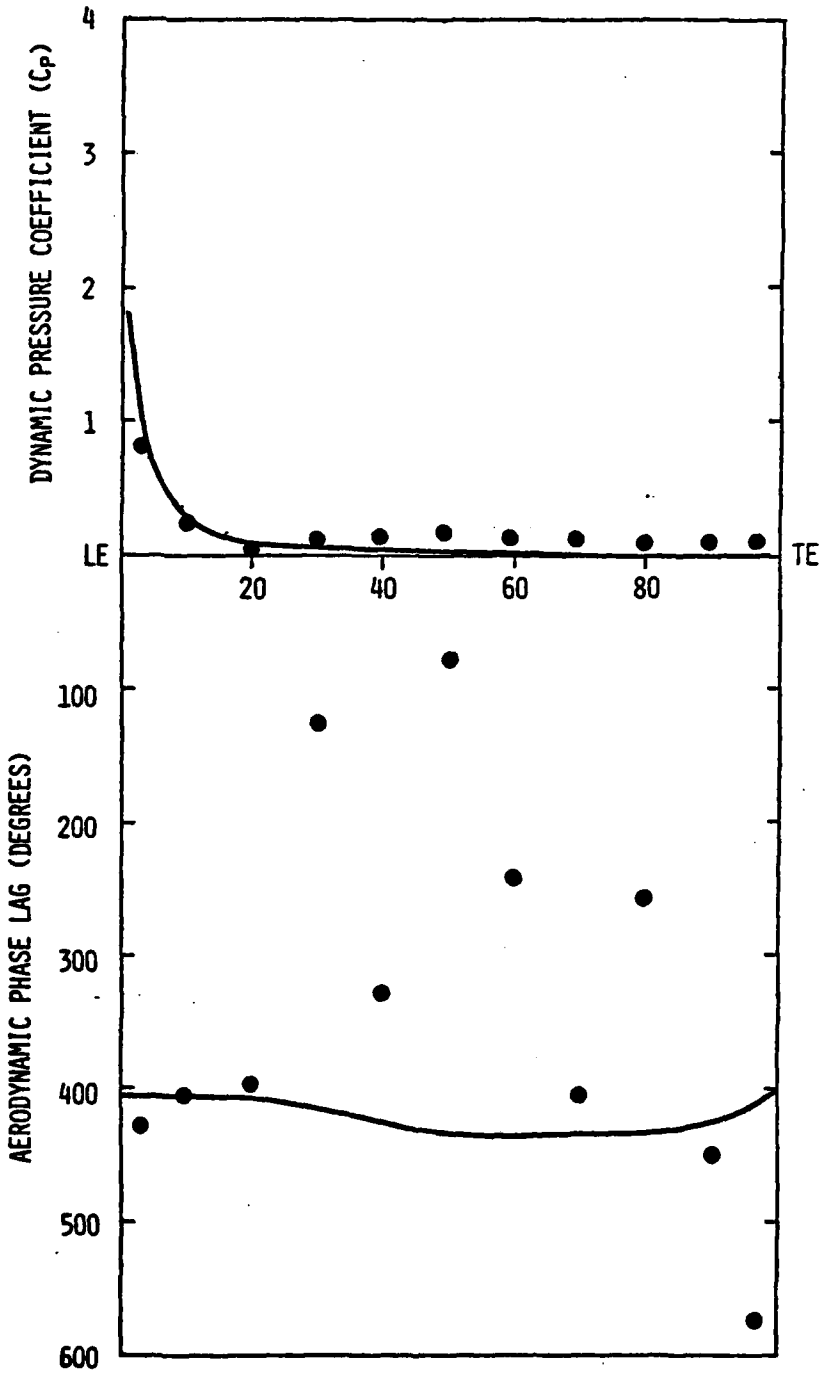

Figure 50. Chordwise data for second harmonic pressure difference and phase lag and prediction from reference 6 for point 15.

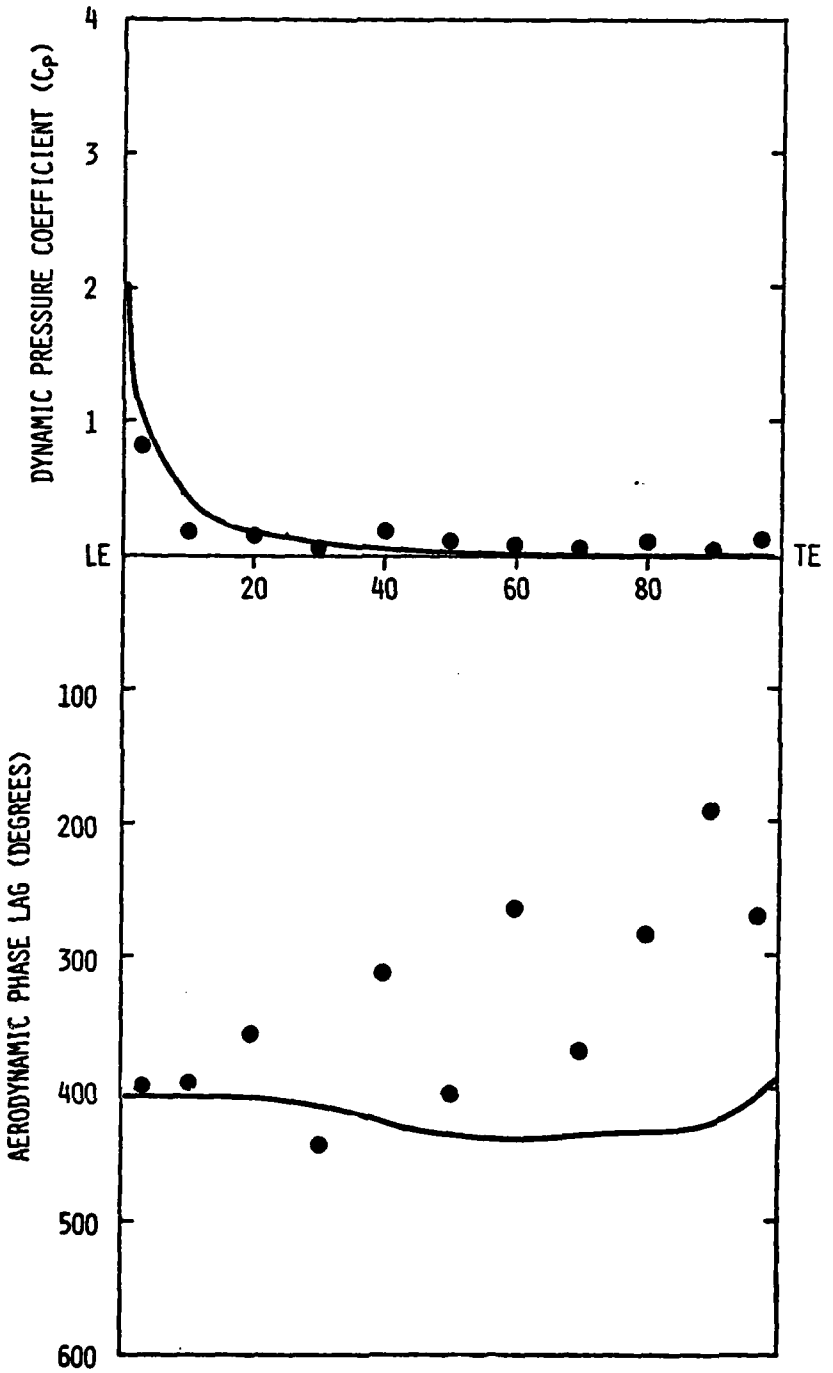

Figure 51. Chordwise data for second harmonic pressure difference and phase lag and prediction from reference 6 for point 16.

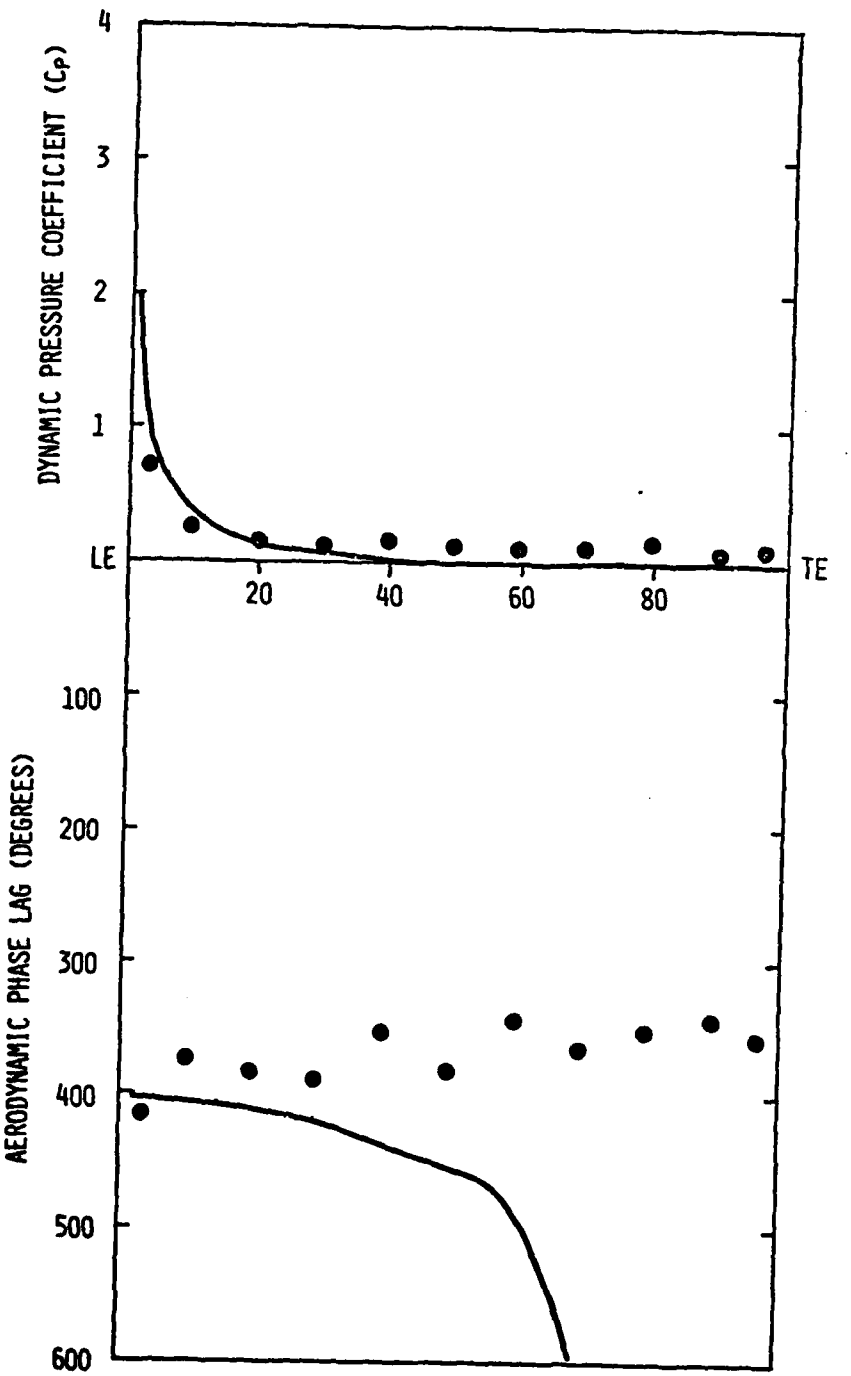

Figure 52. Chordwise data for second harmonic pressure difference and phase lag and prediction from reference 6 for point 17.

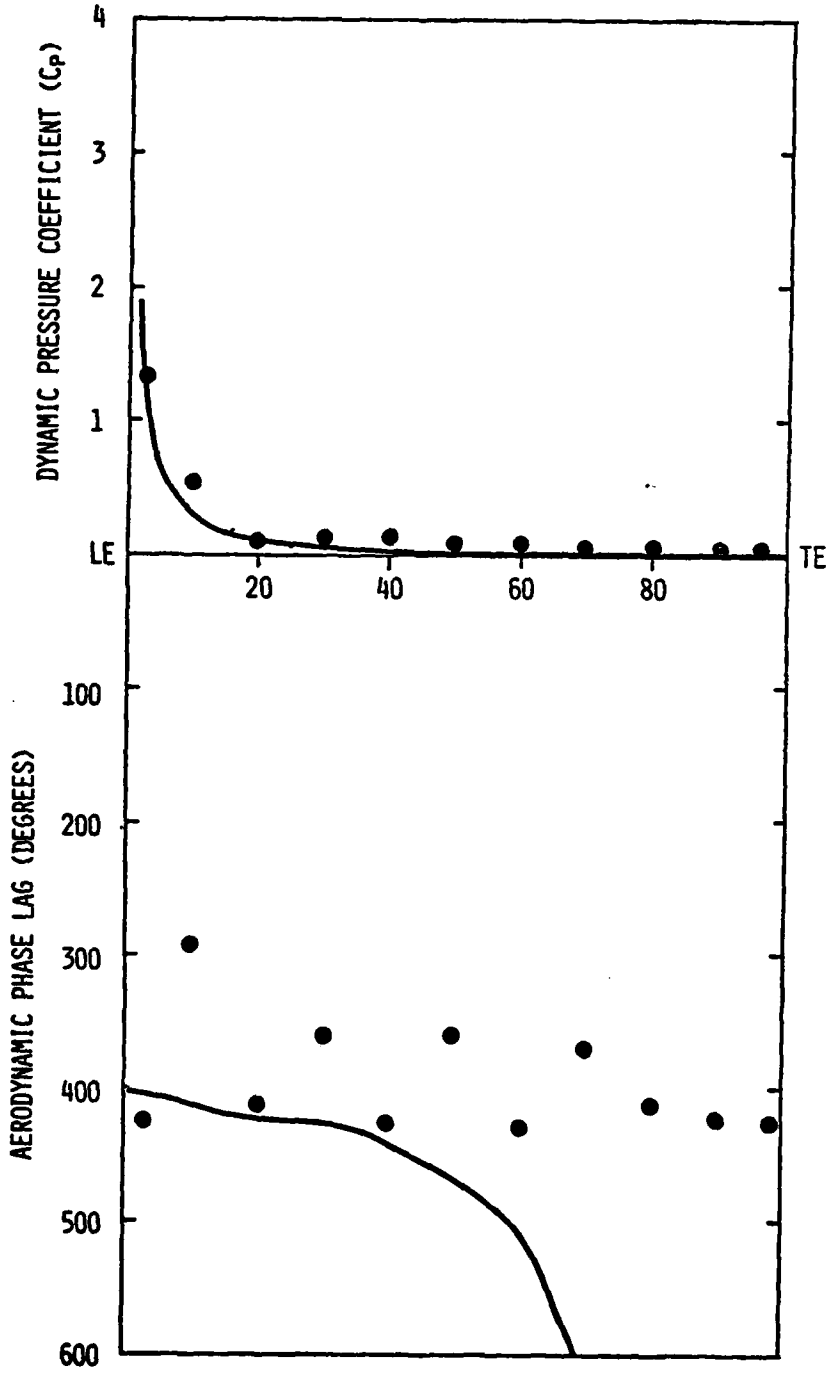

Figure 53. Chordwise data for second harmonic pressure difference and phase lag and prediction from reference 6 for point 18.

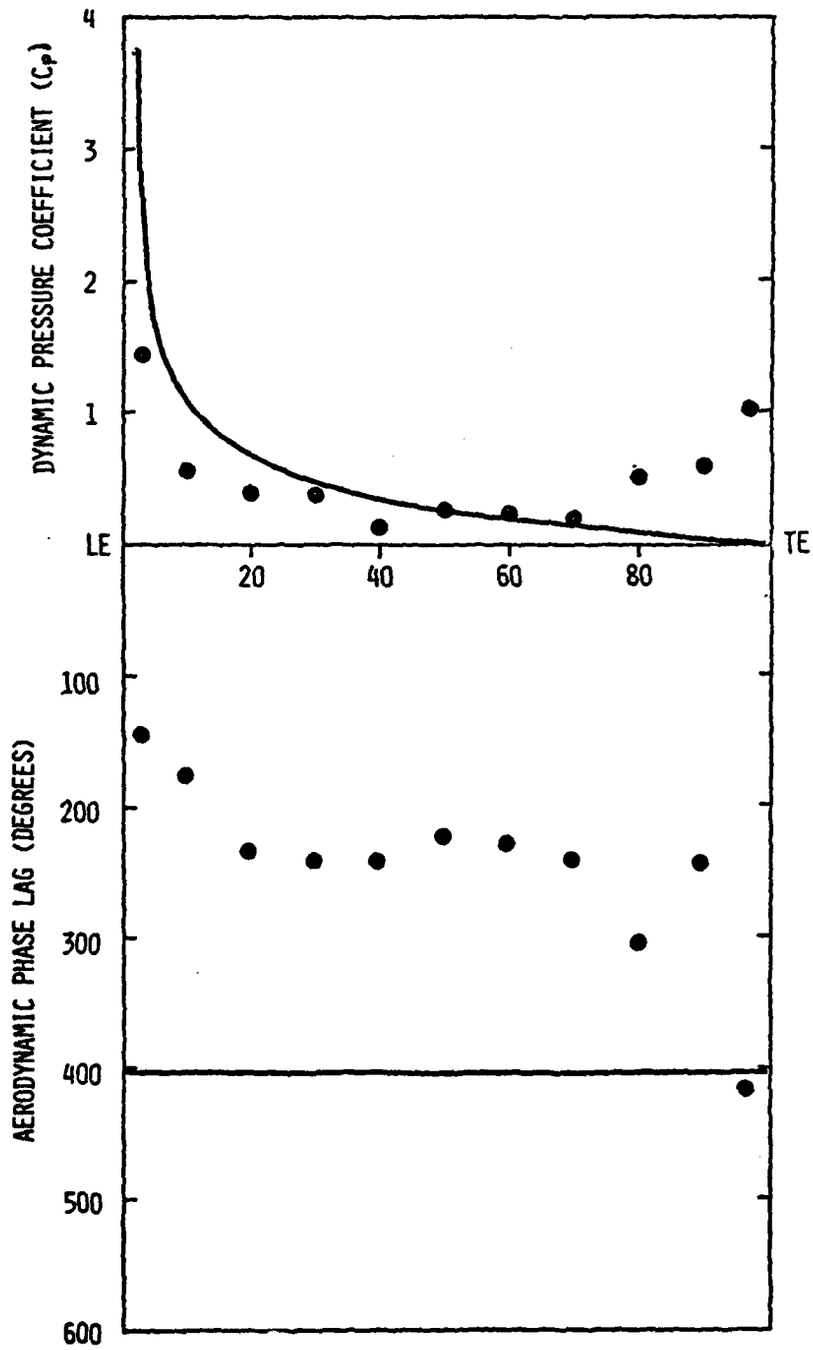

Figure 54. Chordwise data for first harmonic pressure difference and phase lag and prediction from reference 6 for point 21.

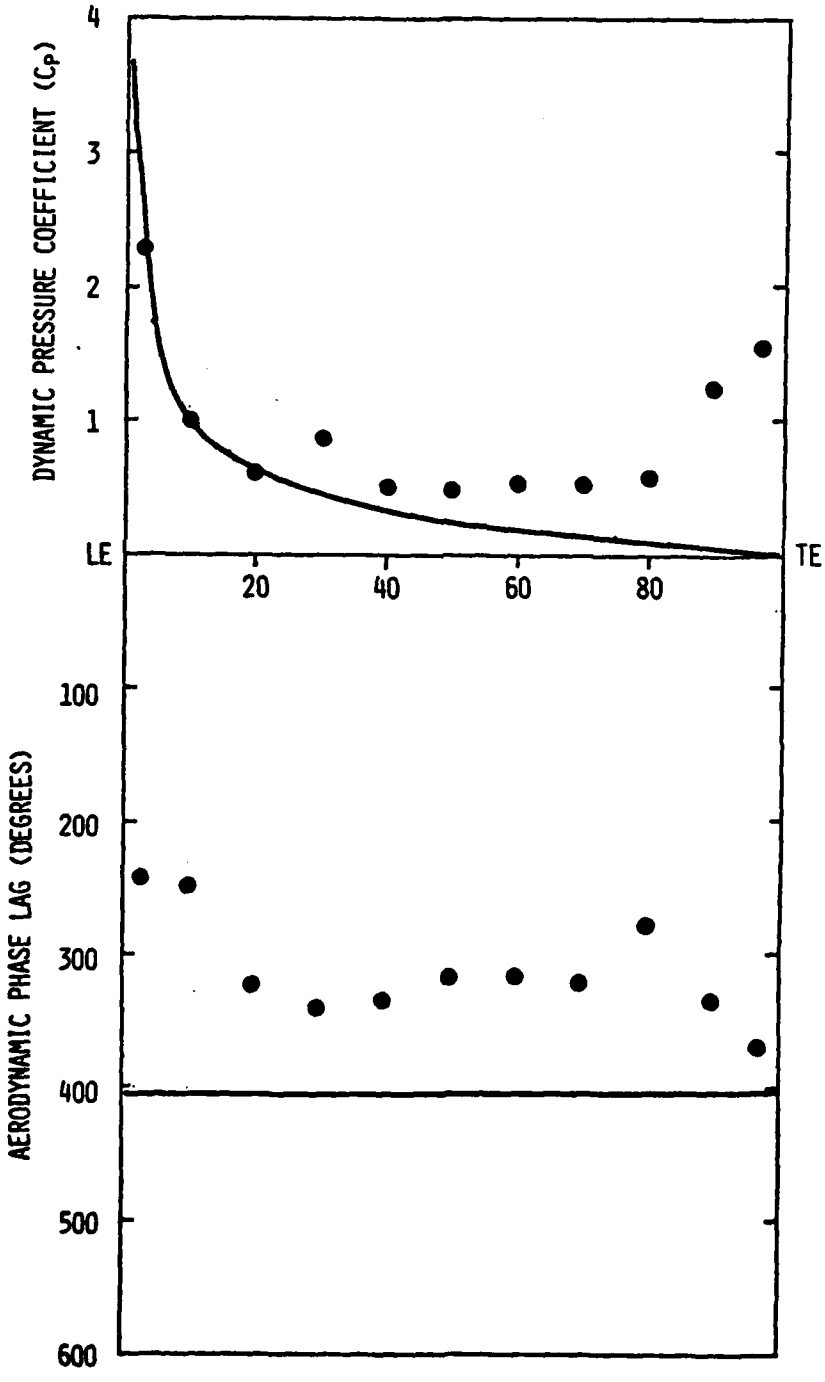

Figure 55. Chordwise data for first harmonic pressure difference and phase lag and prediction from reference 6 for point 22.

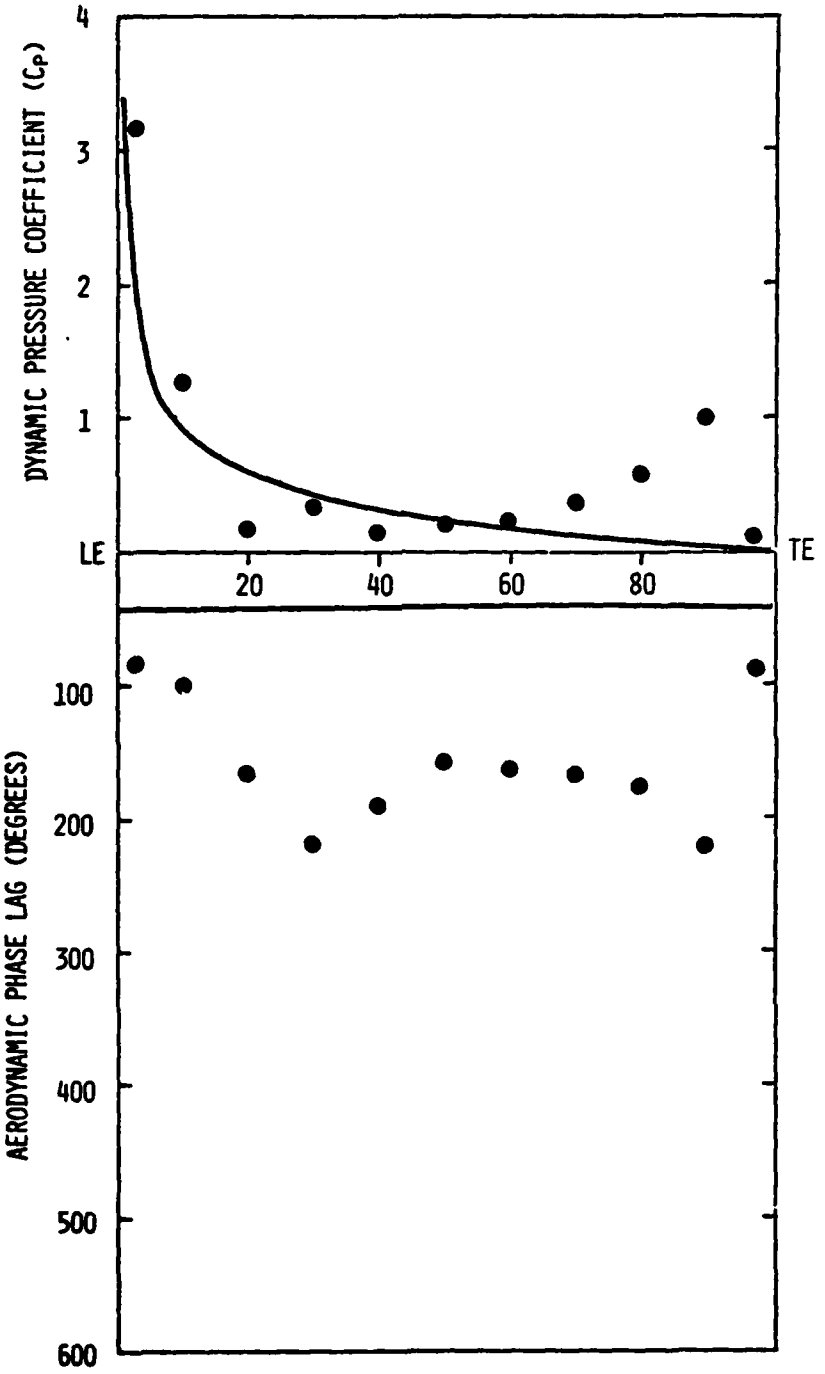

Figure 56. Chordwise data for first harmonic pressure difference and phase lag and prediction from reference 6 for point 23.

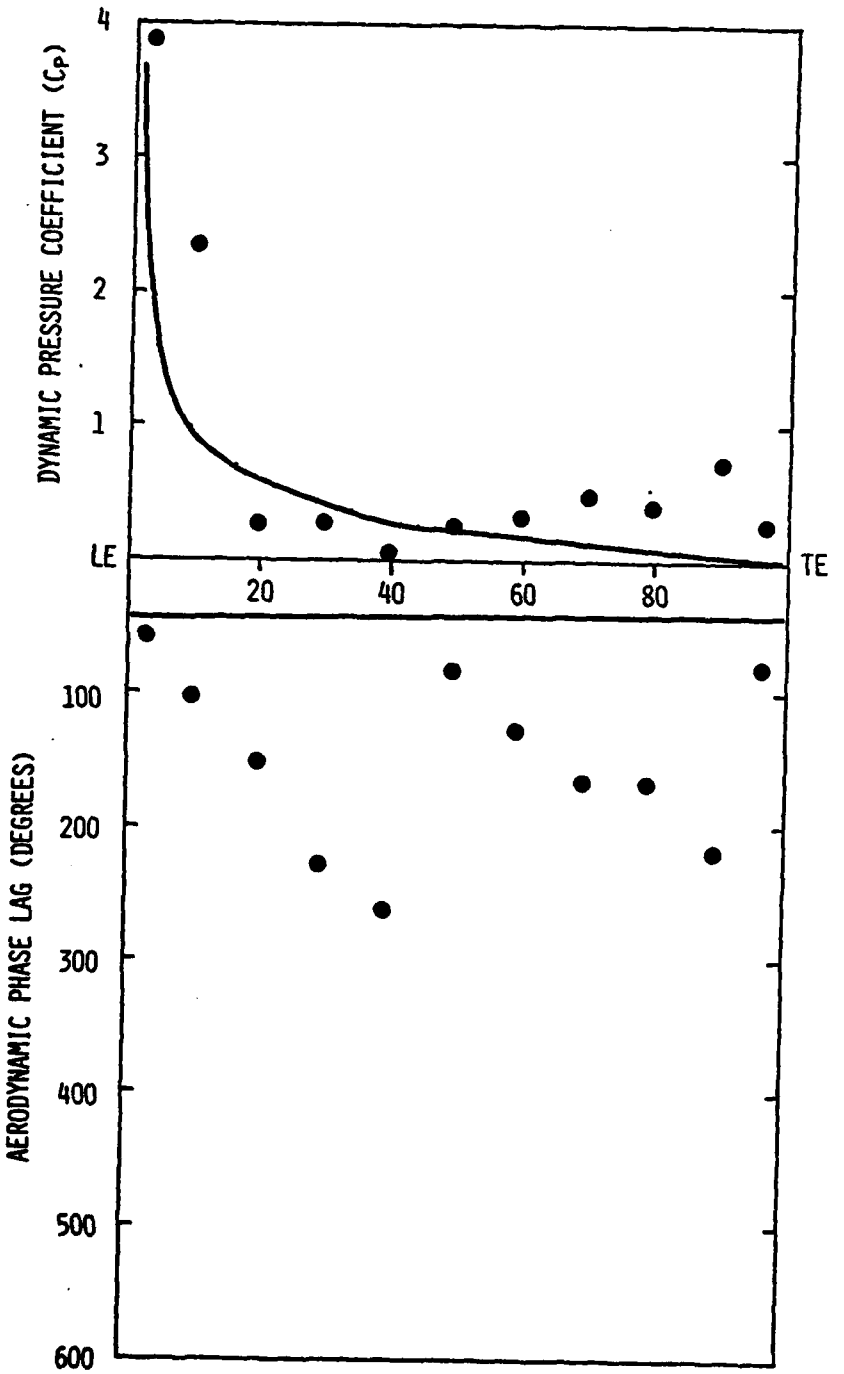

Figure 57. Chordwise data for first harmonic pressure difference and phase lag and prediction from reference 6 for point 24.

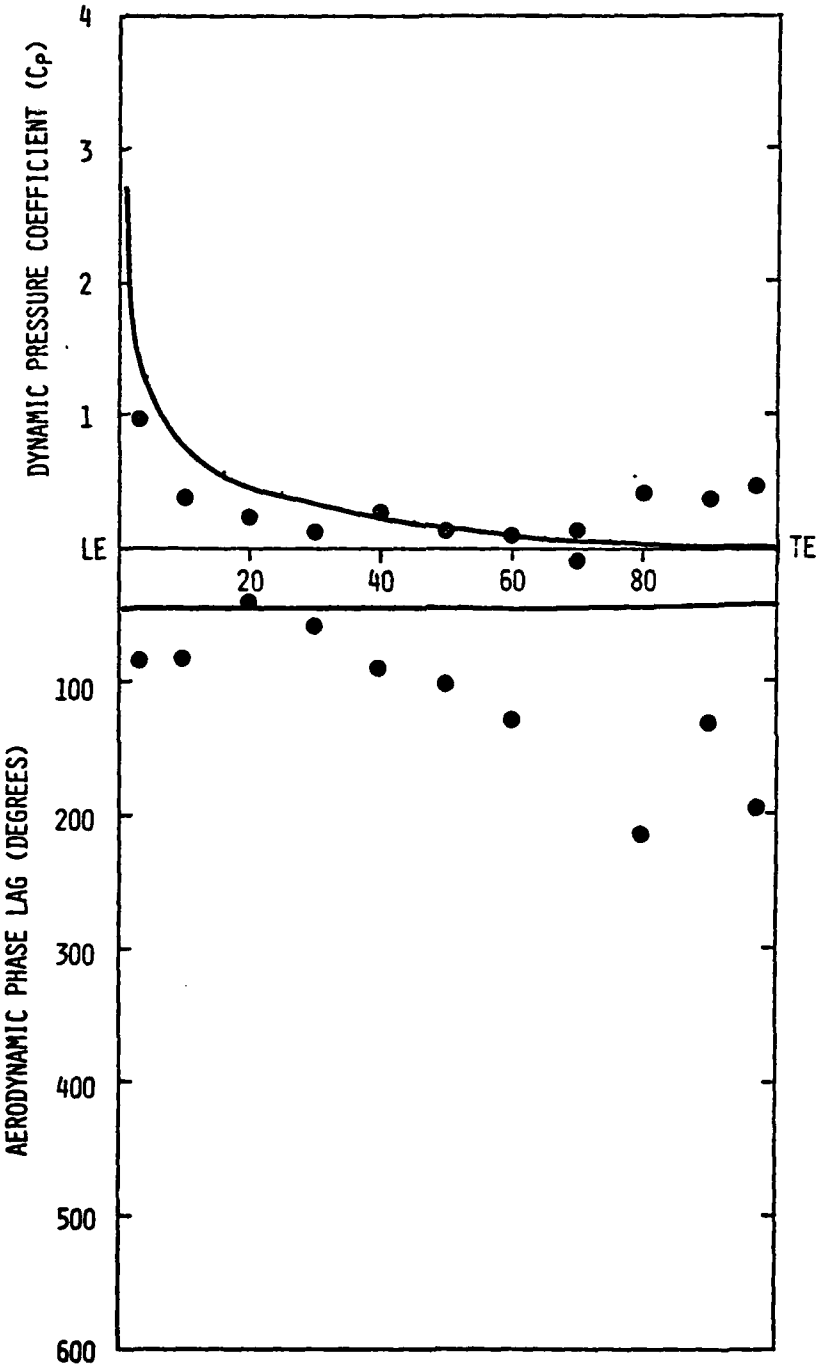

Figure 58. Chordwise data for second harmonic pressure difference and phase lag and prediction from reference 6 for point 21.

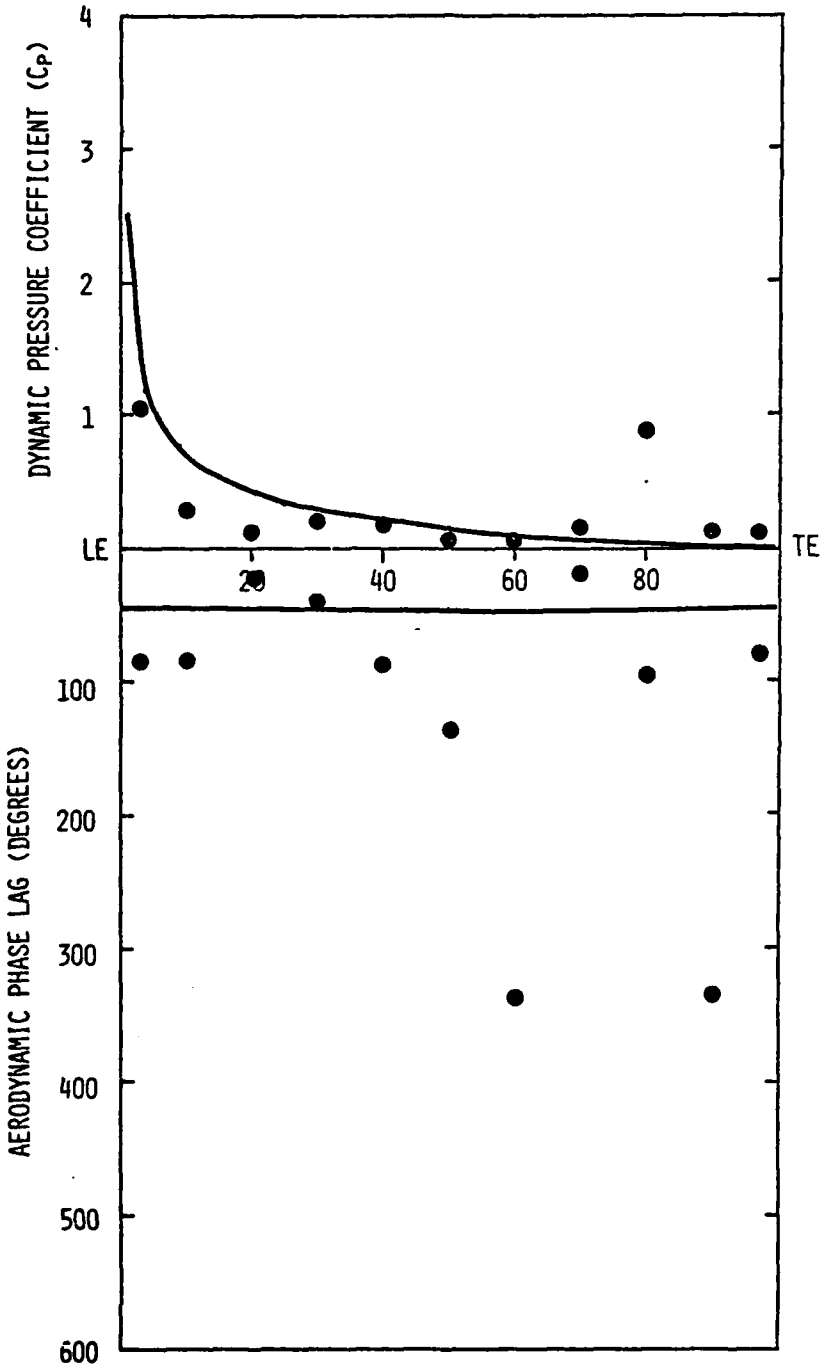

Figure 59. Chordwise data for second harmonic pressure difference and phase lag and prediction from reference 6 for point 22.

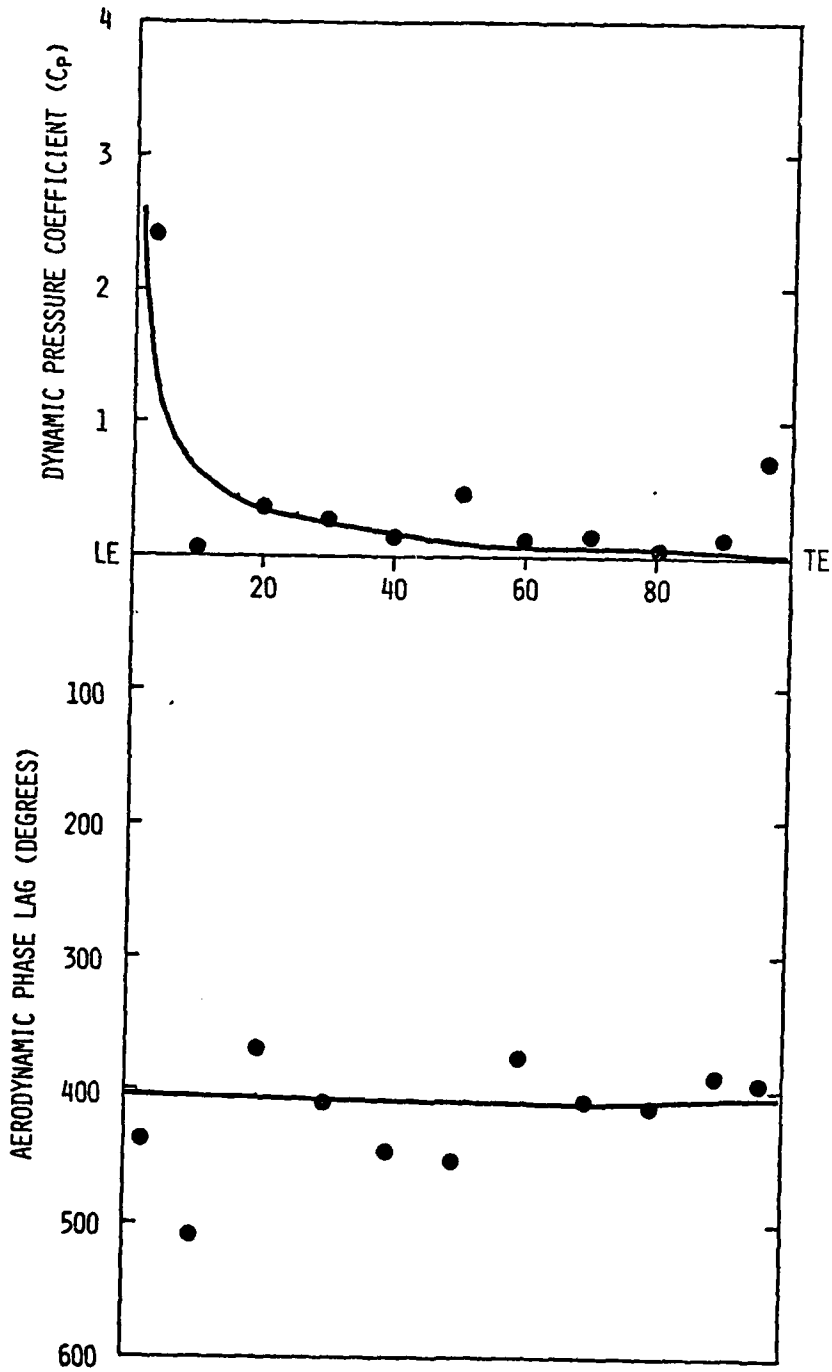

Figure 60. Chordwise data for second harmonic pressure difference and phase lag and prediction from reference 6 for point 23.

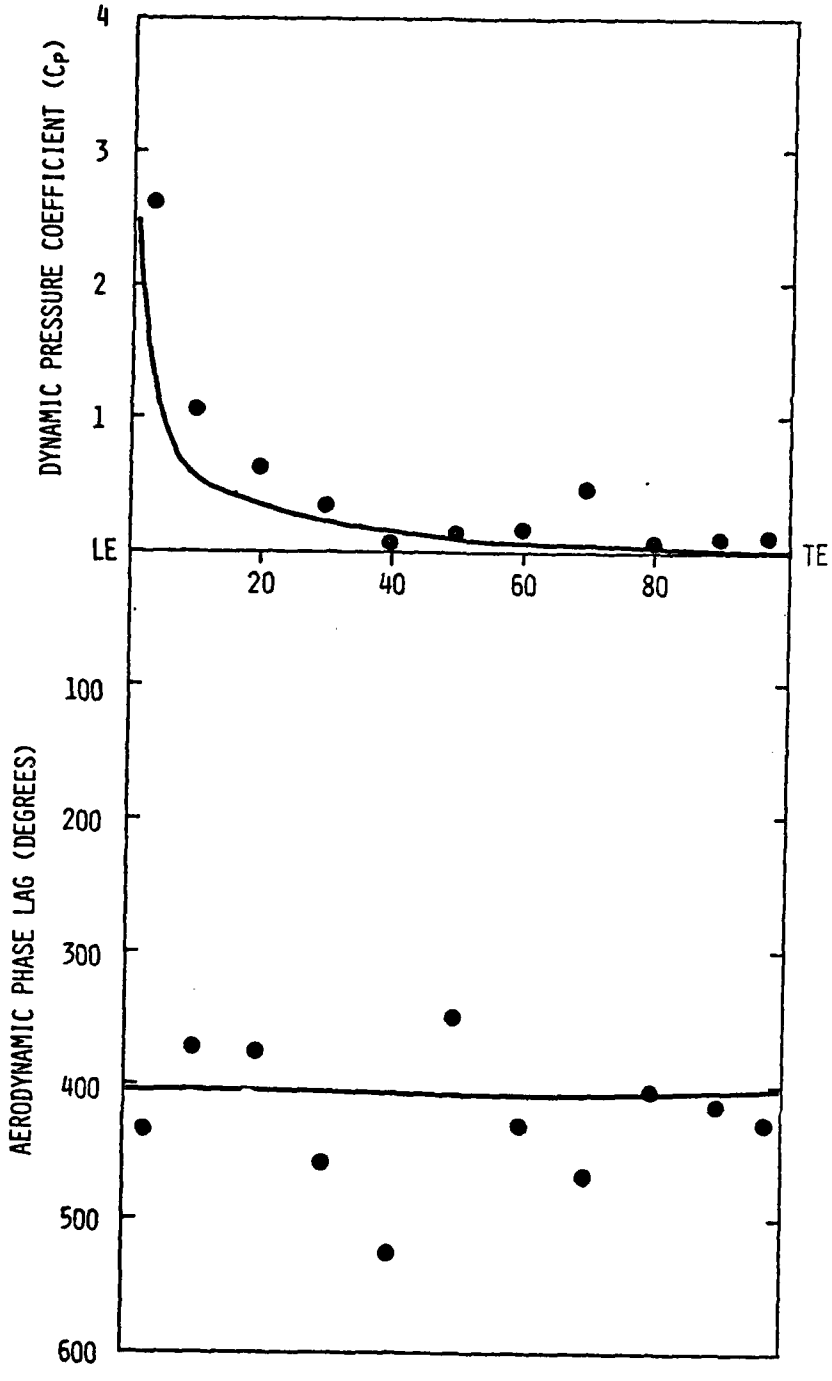

Figure 61. Chordwise data for second harmonic pressure difference and phase lag and prediction from reference 6 for point 24.

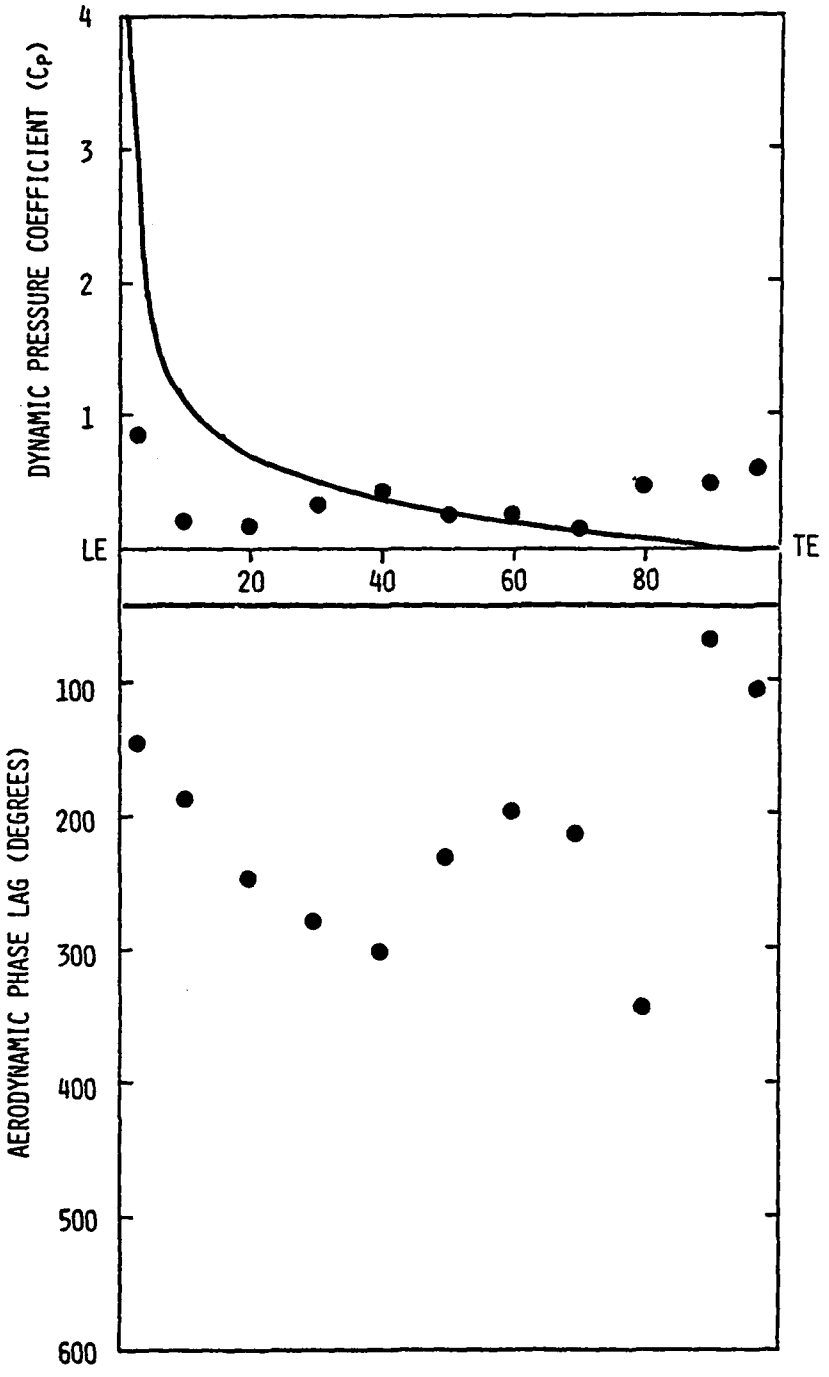

Figure 62. Chordwise data for first harmonic pressure difference and phase lag and prediction from reference 6 for point 25.

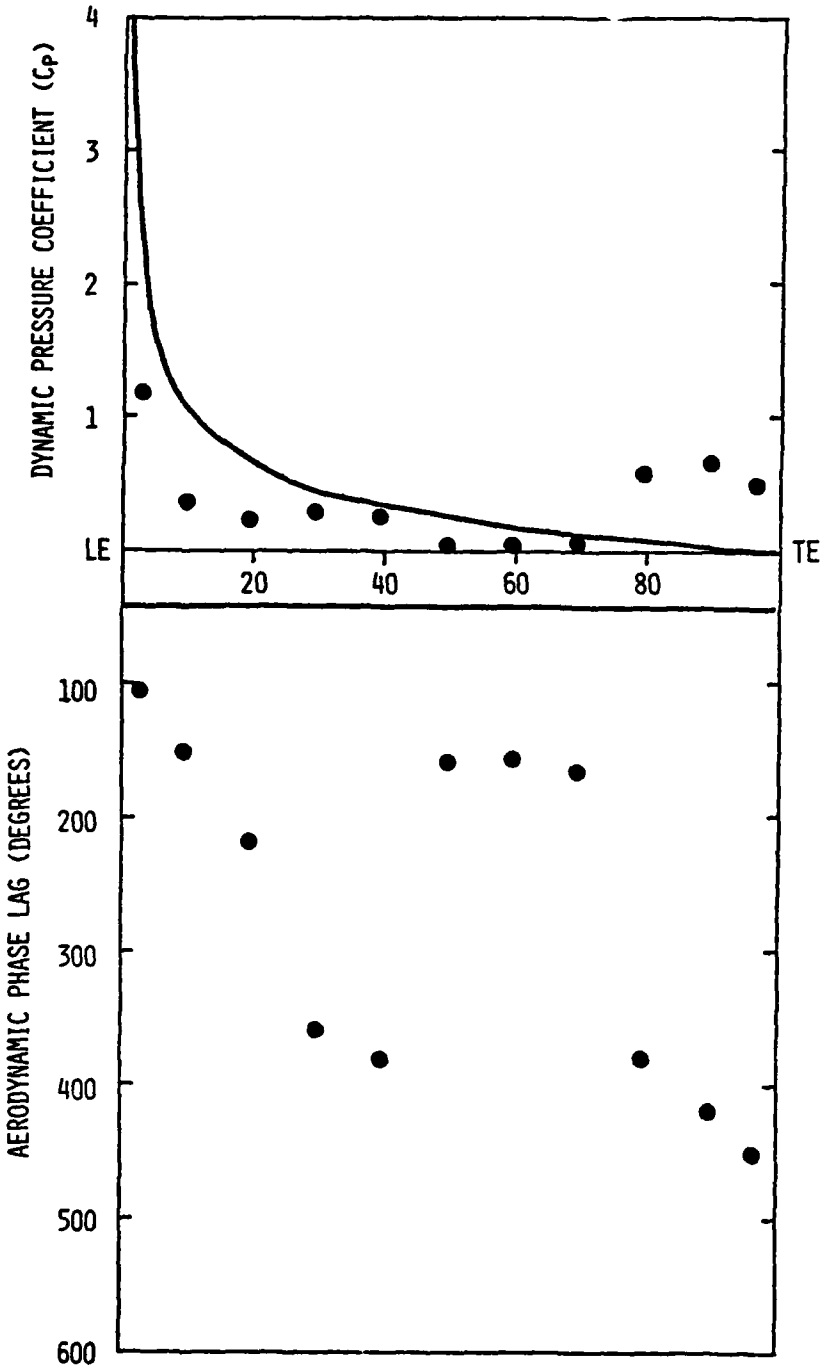

Figure 63. Chordwise data for first harmonic pressure difference and phase lag and prediction from reference 6 for point 26.

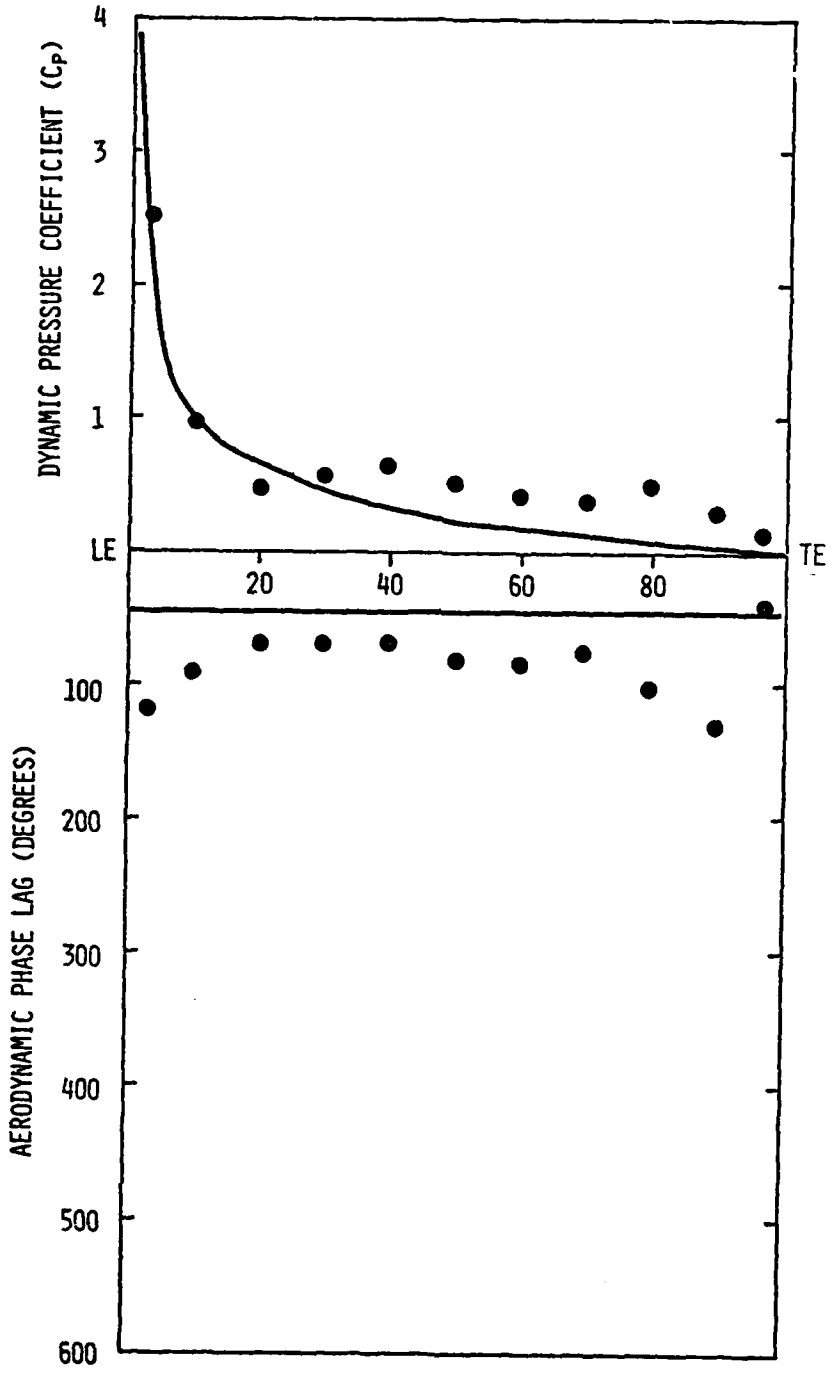

Figure 64. Chordwise data for first harmonic pressure difference and phase lag and prediction from reference 6 for point 27.

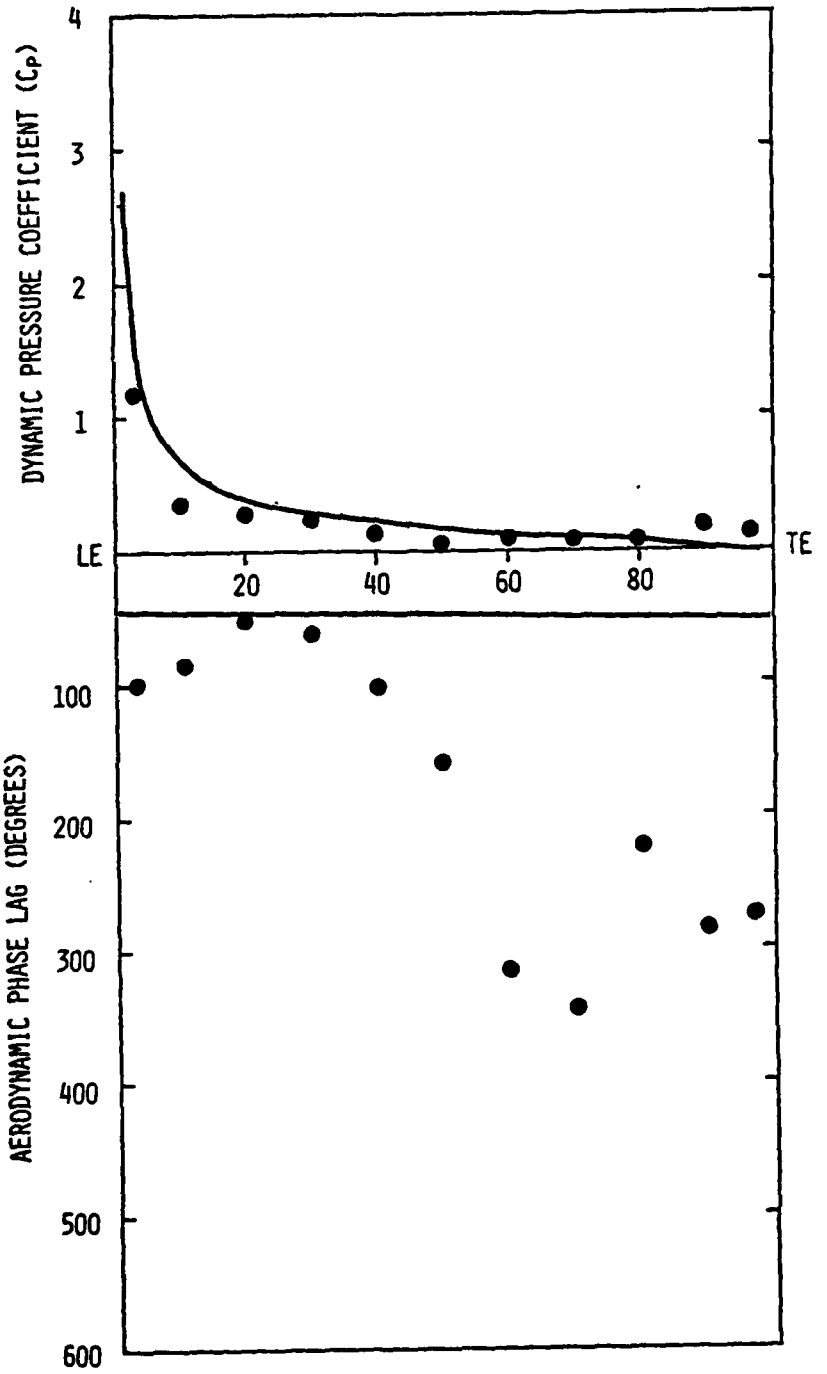

Figure 68. Chordwise data for second harmonic pressure difference and phase lag and prediction from reference 6 for point 27.

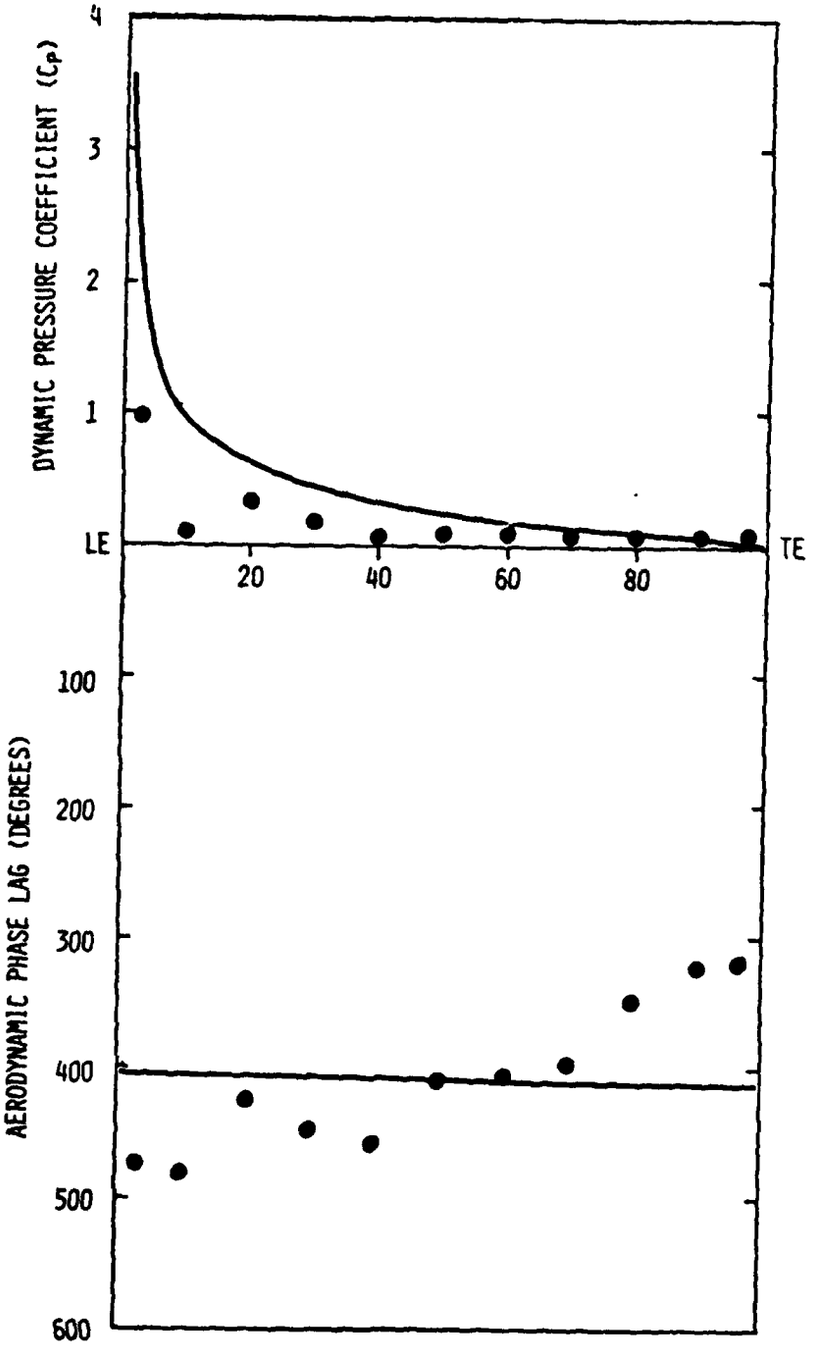

Figure 69. Chordwise data for second harmonic pressure difference and phase lag and prediction from reference 6 for point 28.

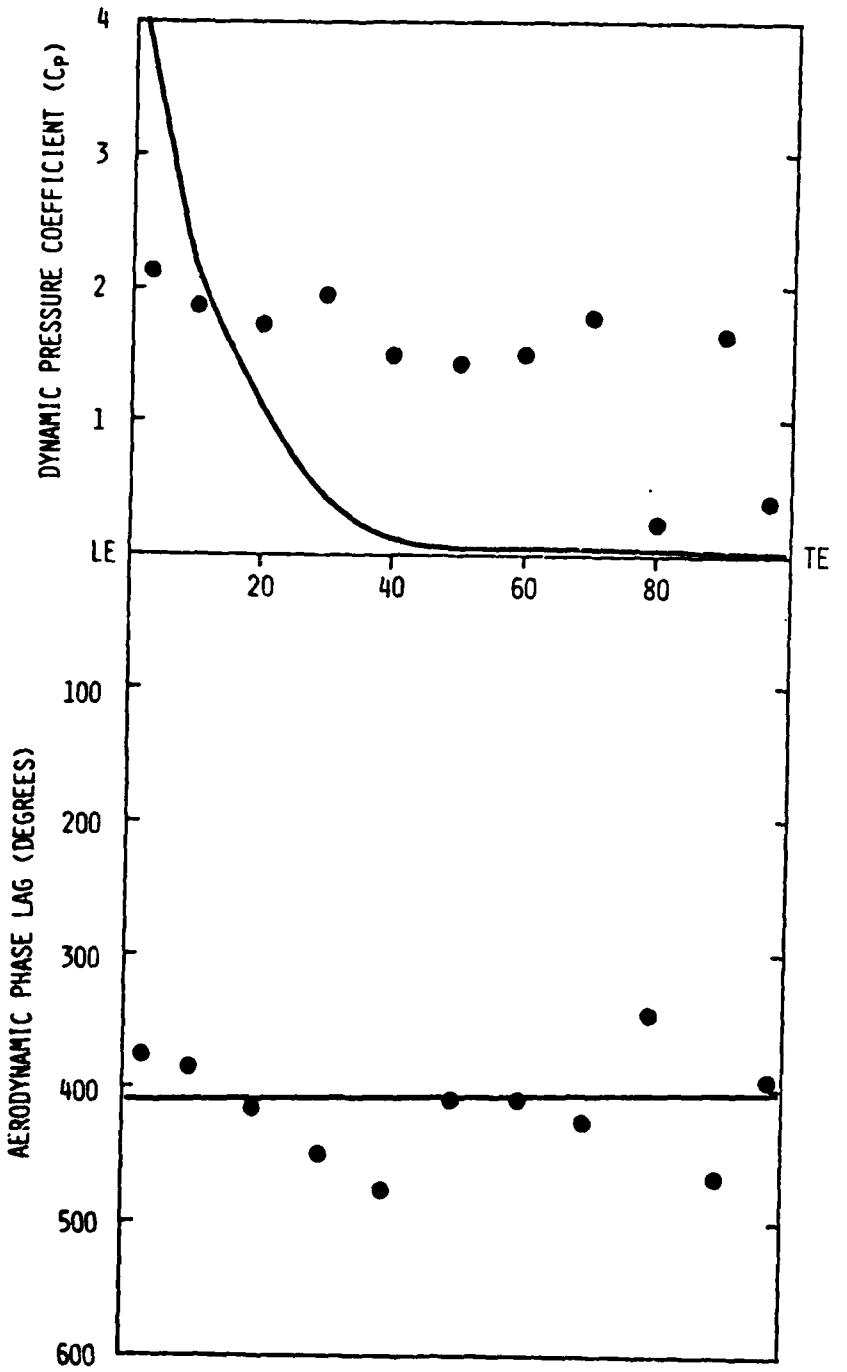

Figure 70. Chordwise data for first harmonic pressure difference and phase lag and prediction from reference 6 for point 31.

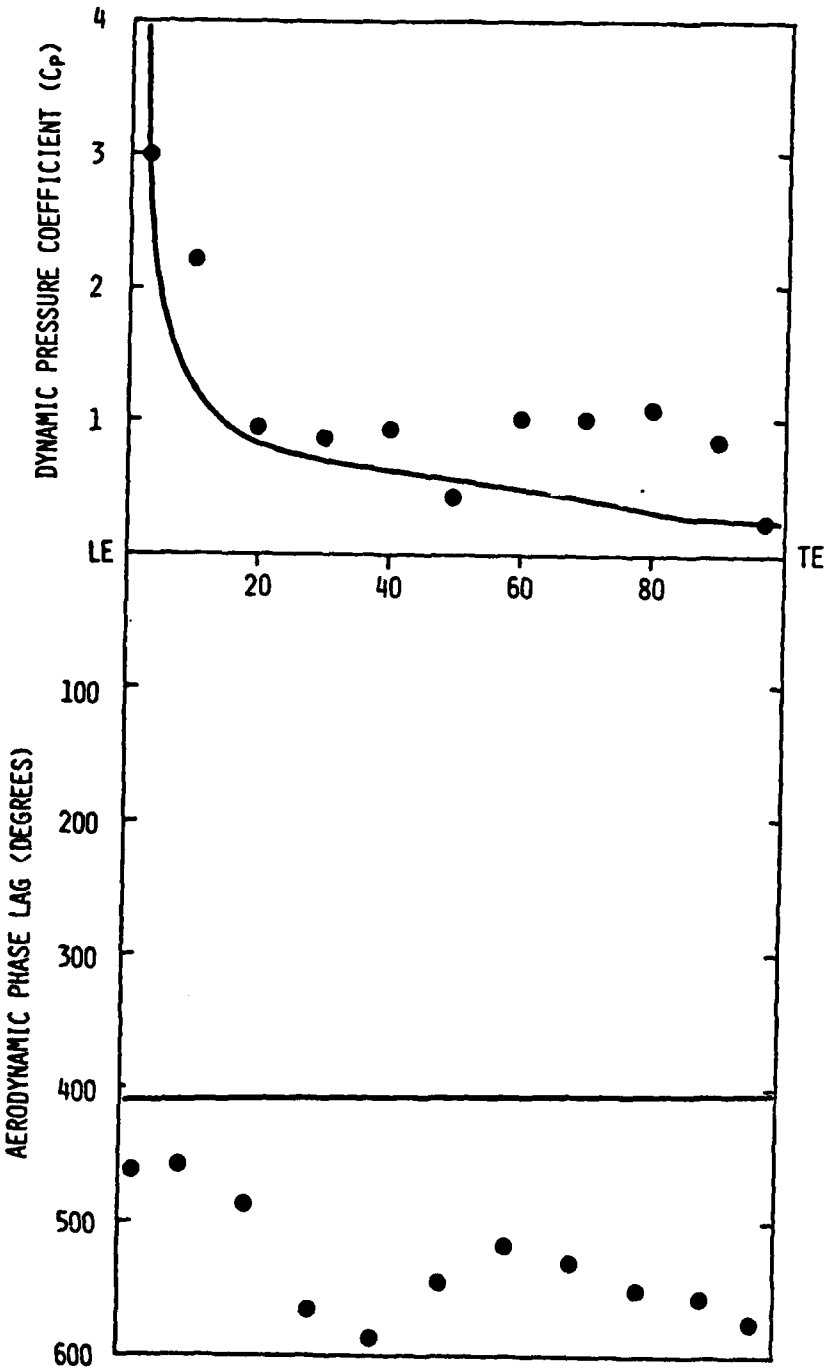

Figure 71. Chordwise data for first harmonic pressure difference and phase lag and prediction from reference 6 for point 32.

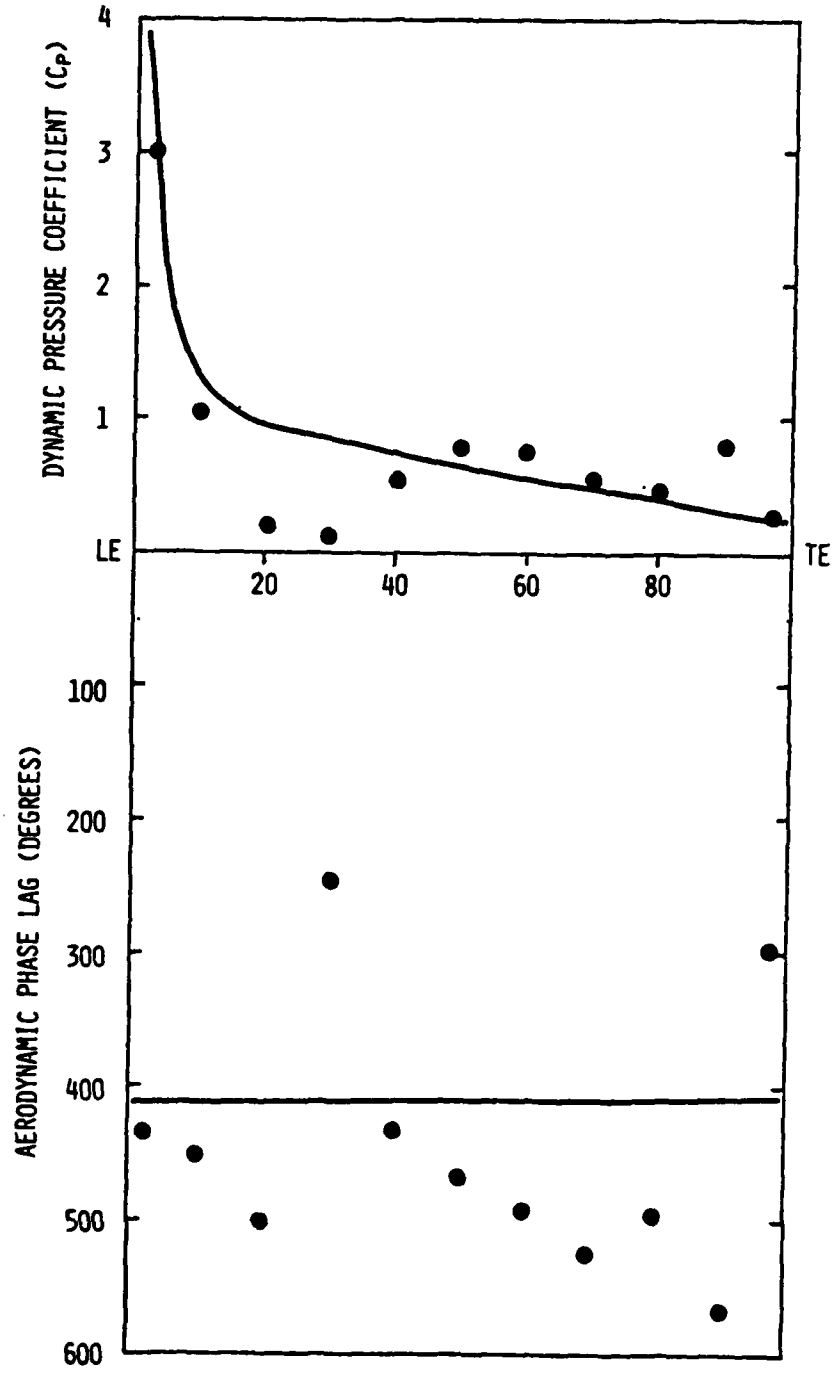

Figure 72. Chordwise data for first harmonic pressure difference and phase lag and prediction from reference 6 for point 33.

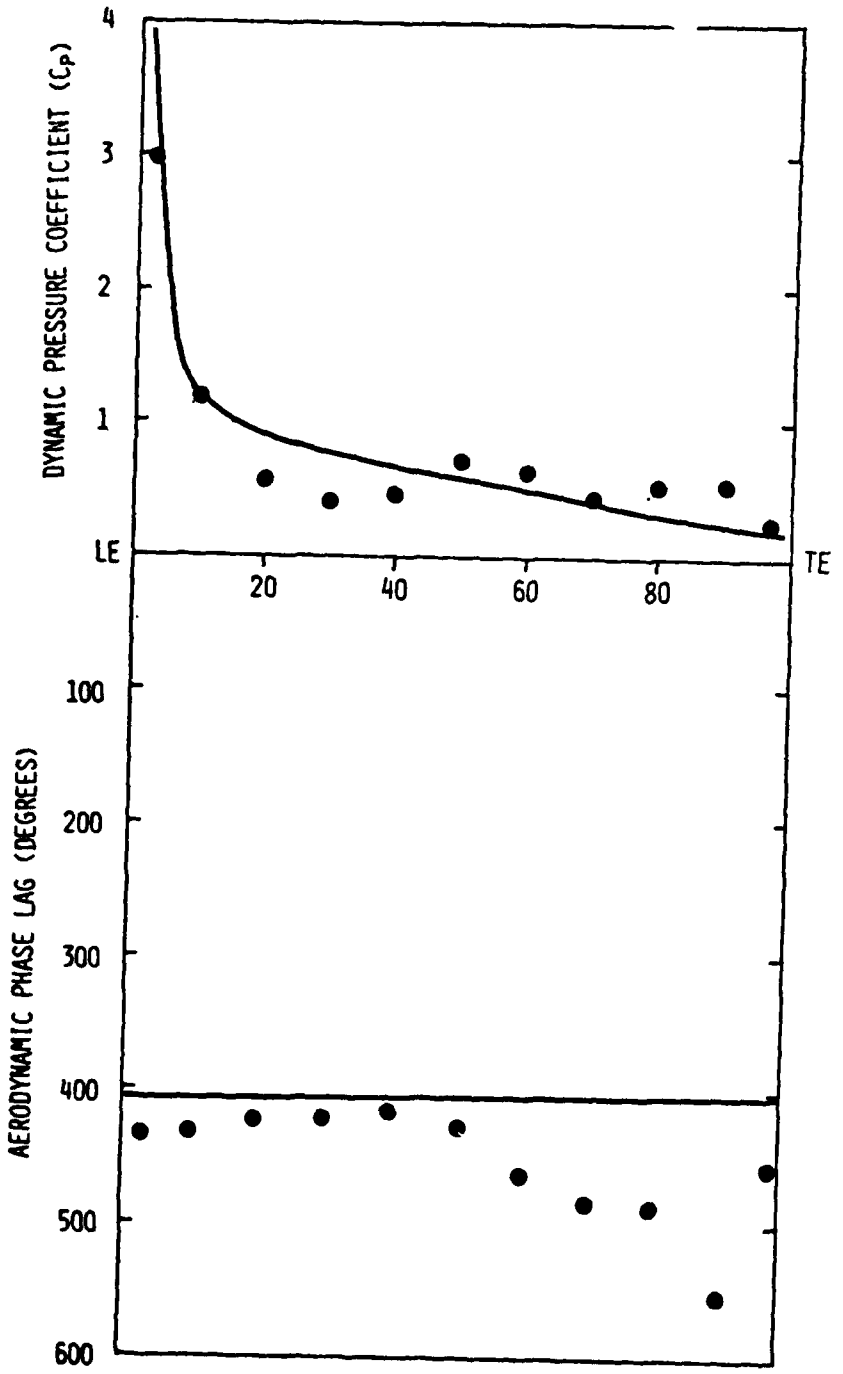

Figure 73. Chordwise data for first harmonic pressure difference and phase lag and prediction from reference 6 for point 34.

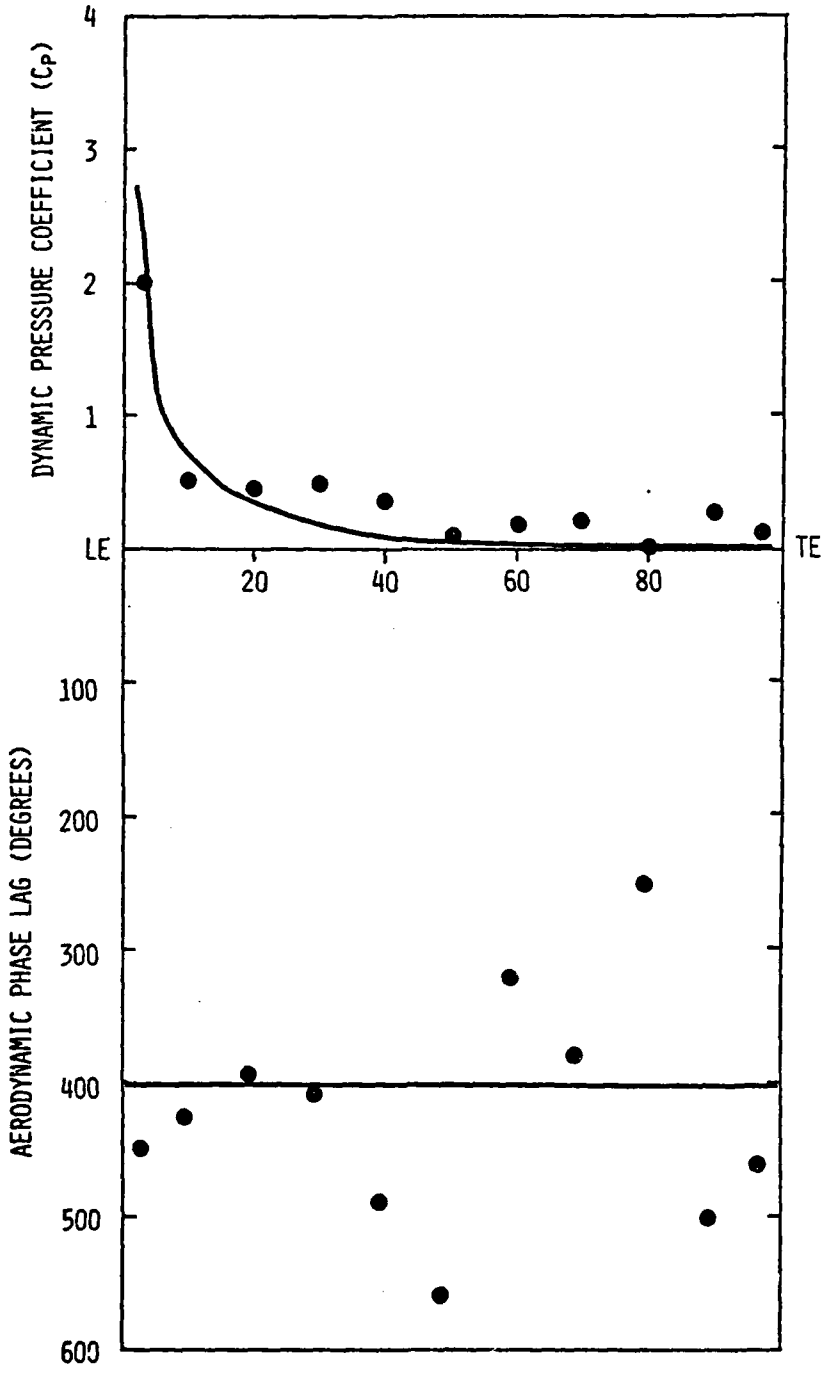

Figure 74. Chordwise data for second harmonic pressure difference and phase lag and prediction from reference 6 for point 31.

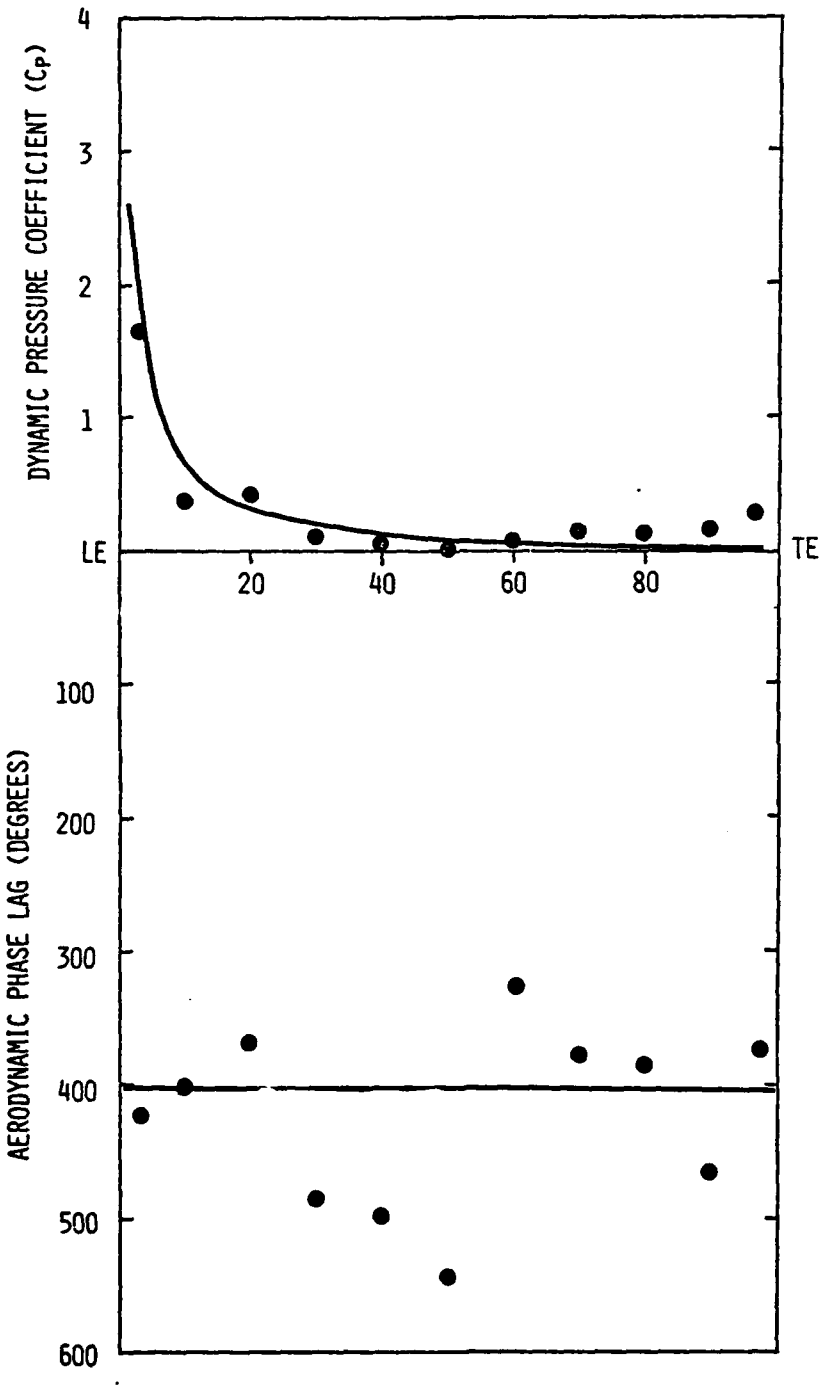

Figure 75. Chordwise data for second harmonic pressure difference and phase lag and prediction from reference 6 for point 32.

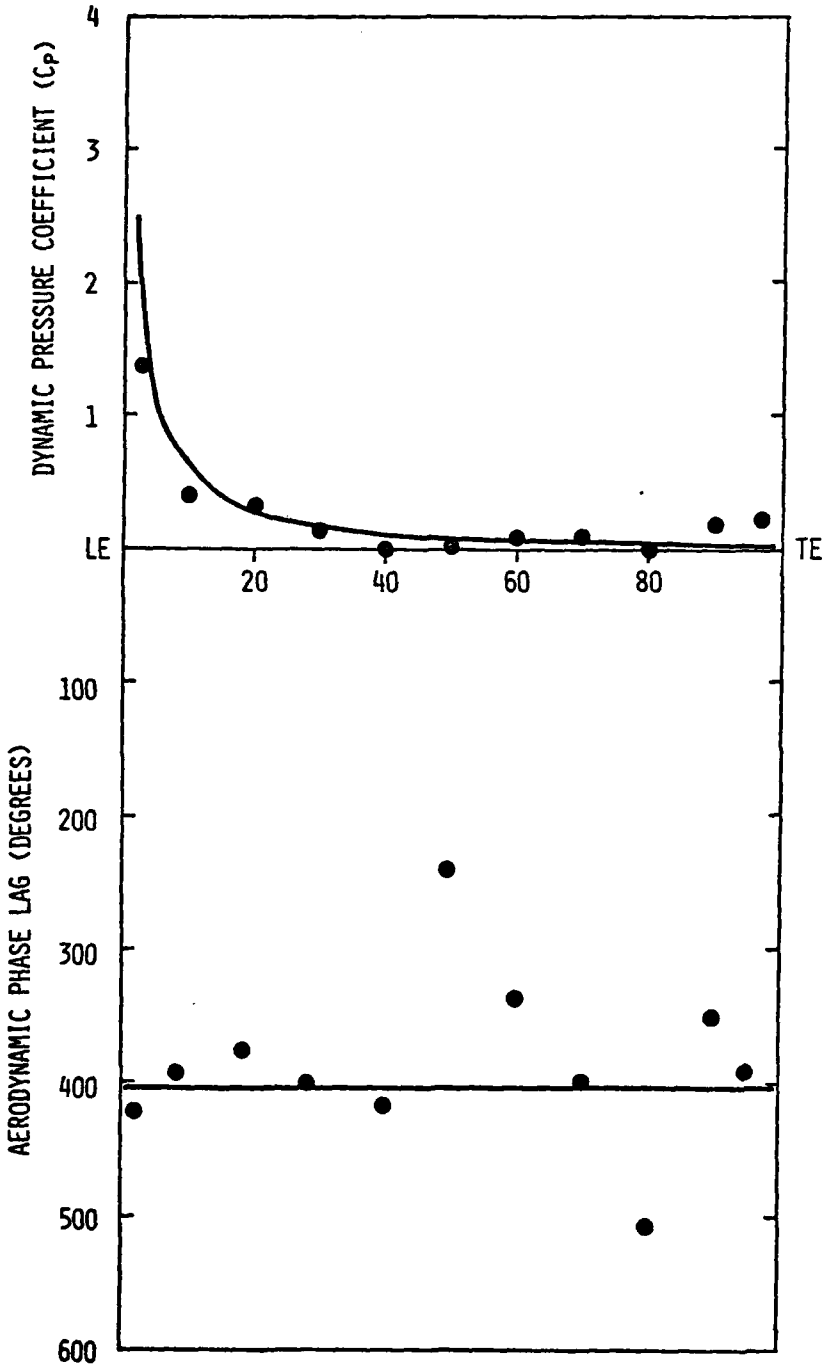

Figure 76. Chordwise data for second harmonic pressure difference and phase lag and prediction from reference 6 for point 33.

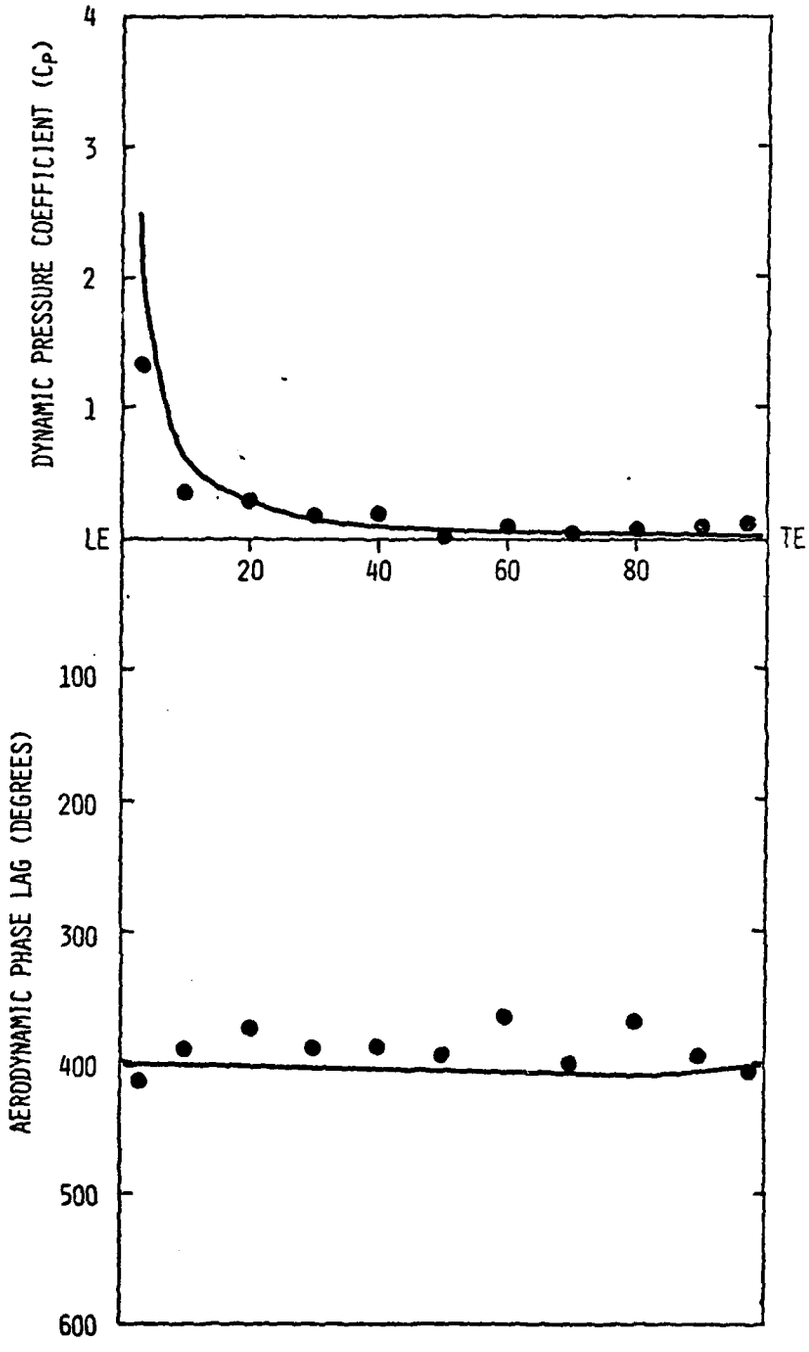

Figure 77. Chordwise data for second harmonic pressure difference and phase lag and prediction from reference 6 for point 34.

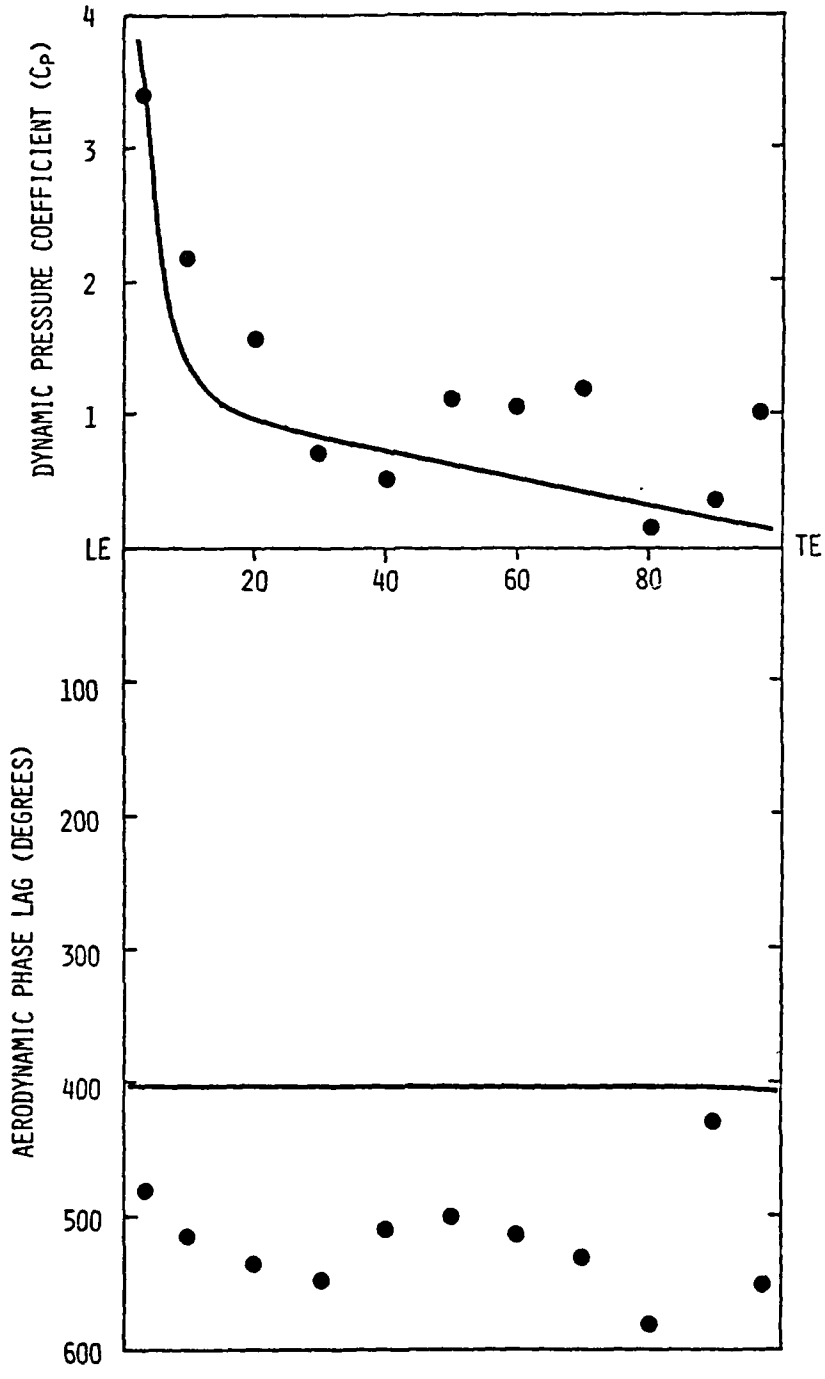

Figure 78. Chordwise data for first harmonic pressure difference and phase lag and prediction from reference 6 for point 35.

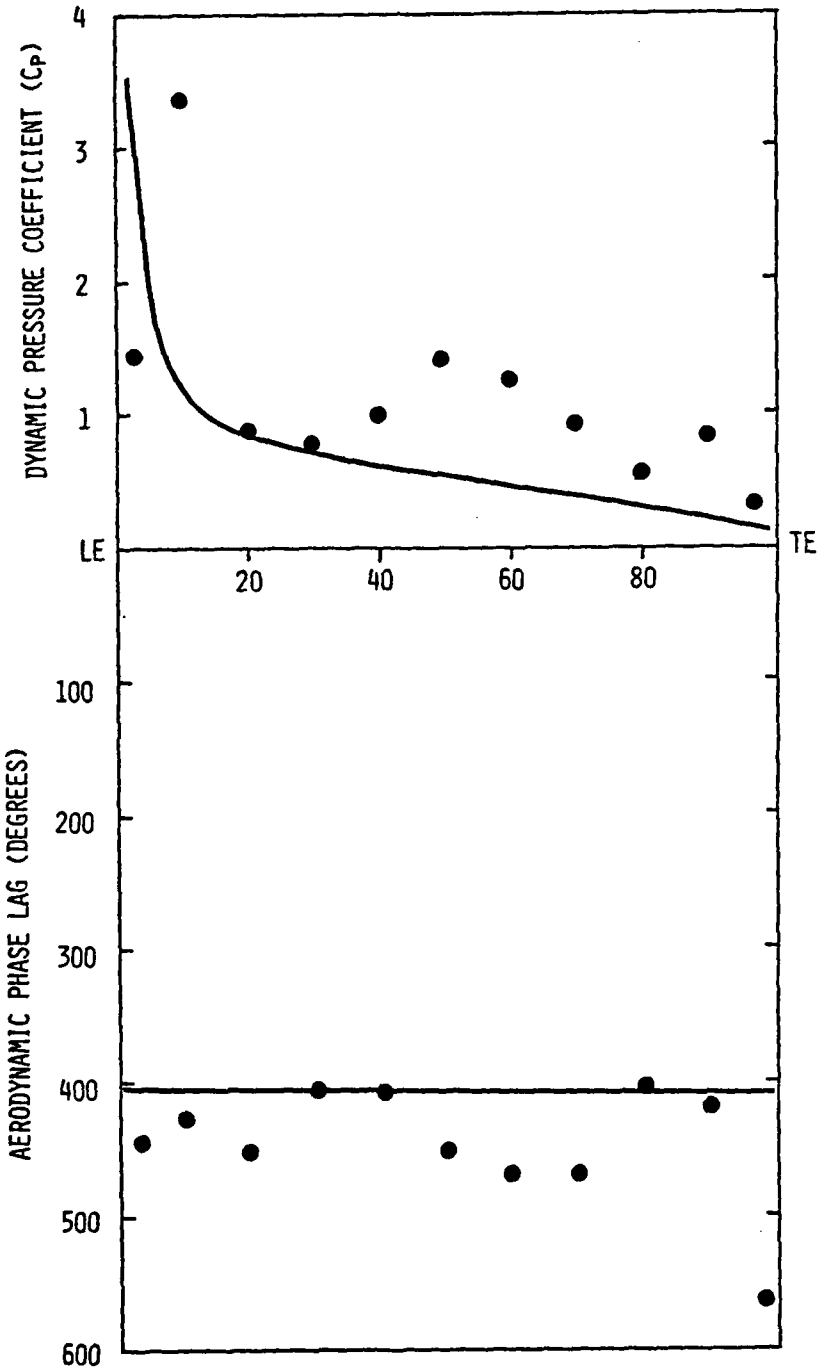

Figure 79. Chordwise data for first harmonic pressure difference and phase lag and prediction from reference 6 for point 36.

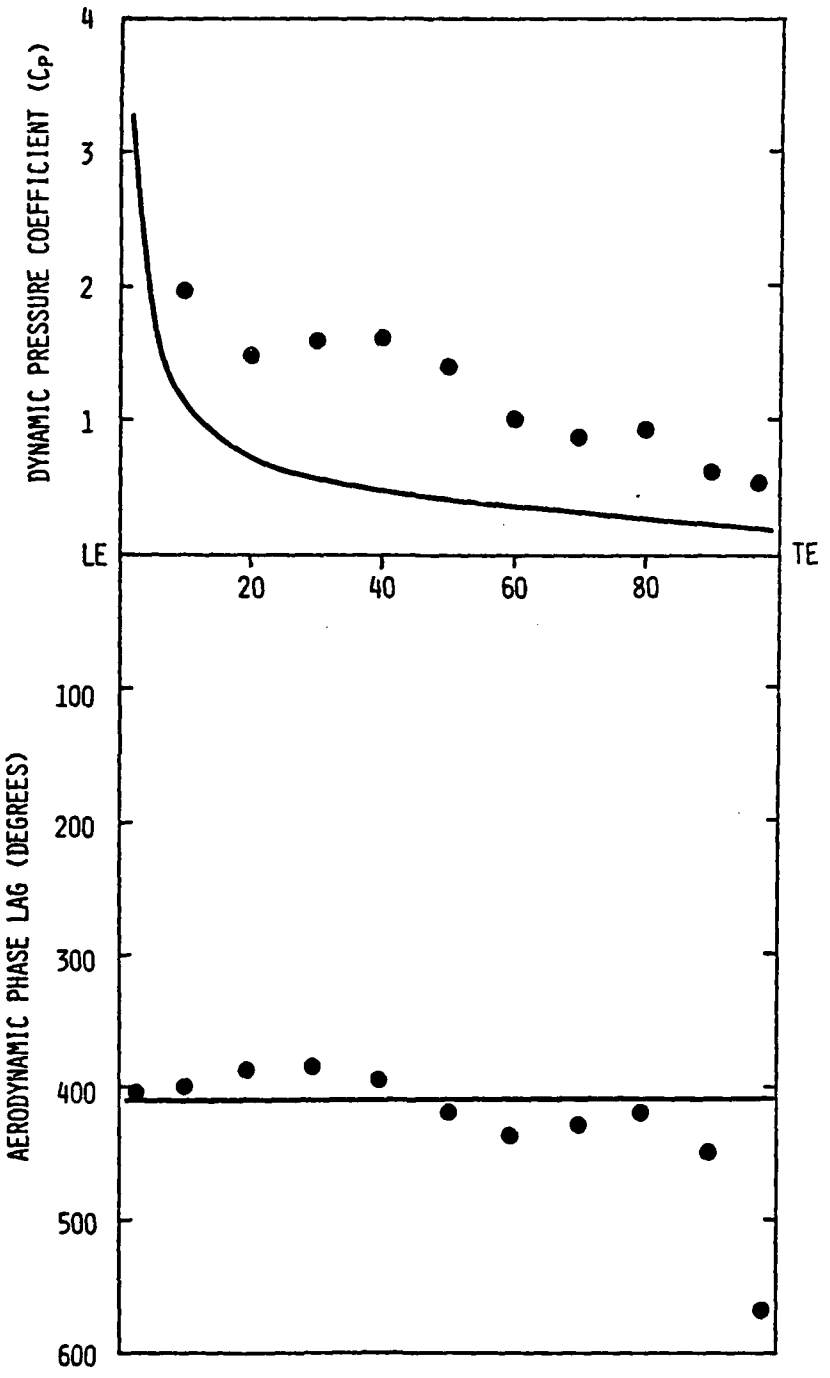

Figure 80. Chordwise data for first harmonic pressure difference and phase lag and prediction from reference 6 for point 37.

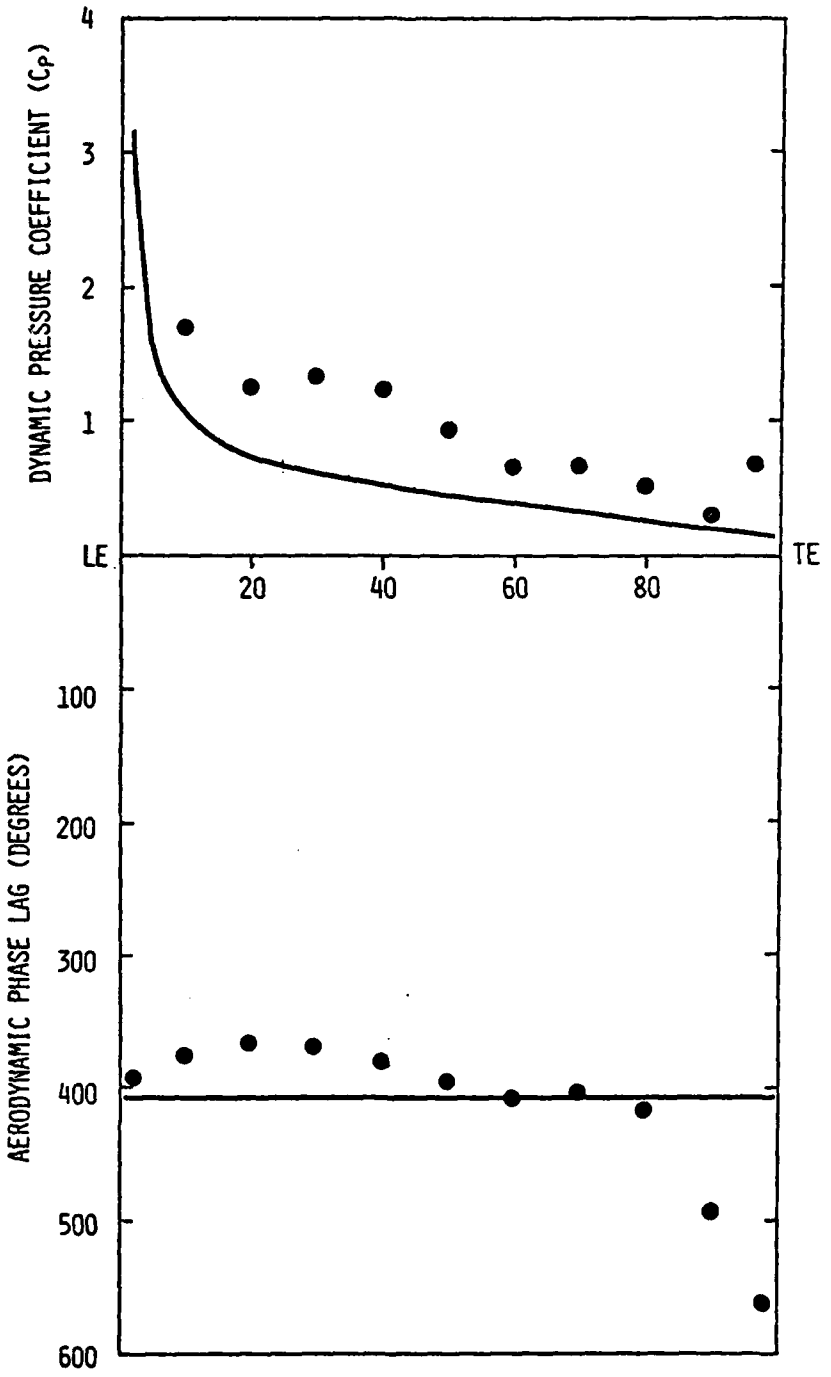

Figure 81. Chordwise data for first harmonic pressure difference and phase lag and prediction from reference 6 for point 38.

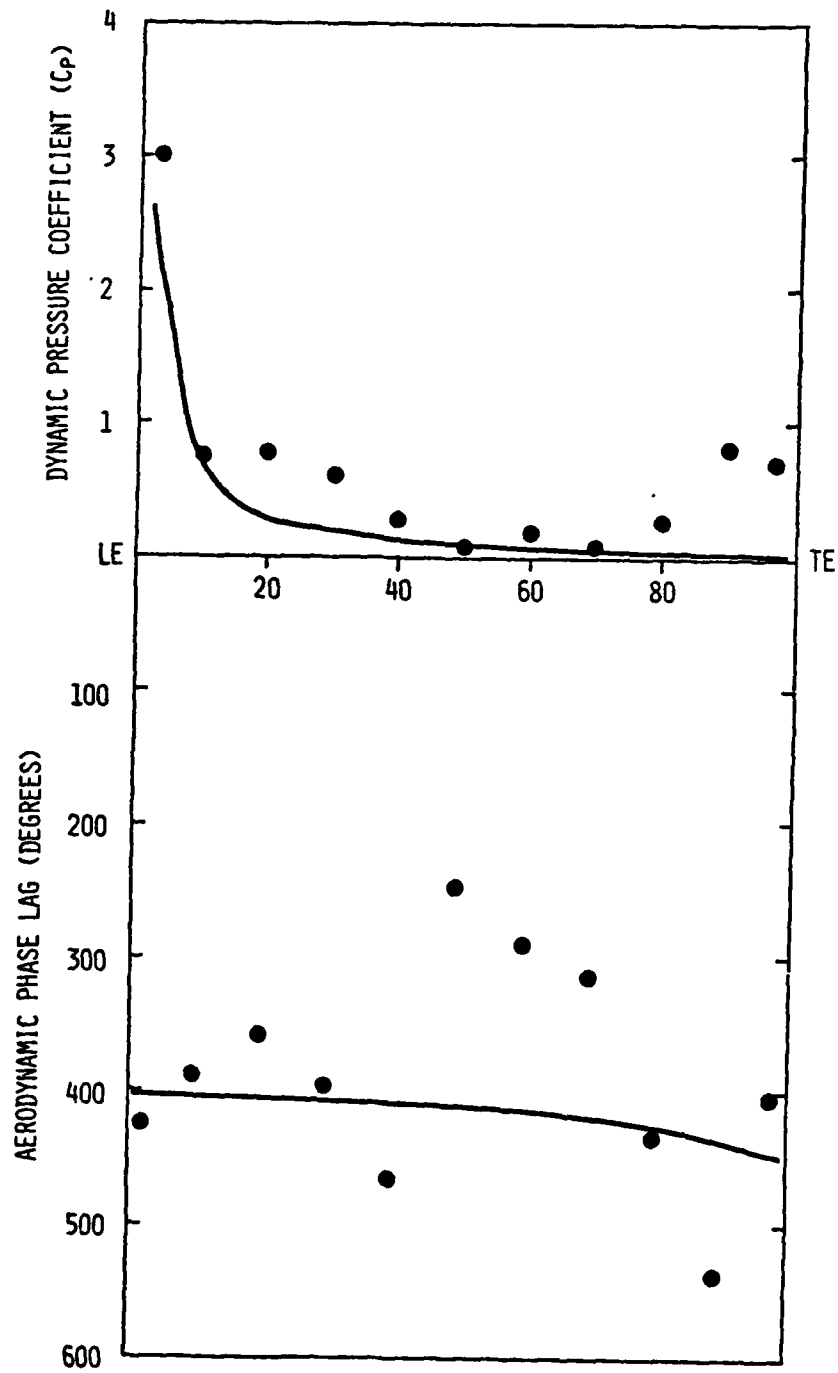

Figure 82. Chordwise data for second harmonic pressure difference and phase lag and prediction from reference 6 for point 35.

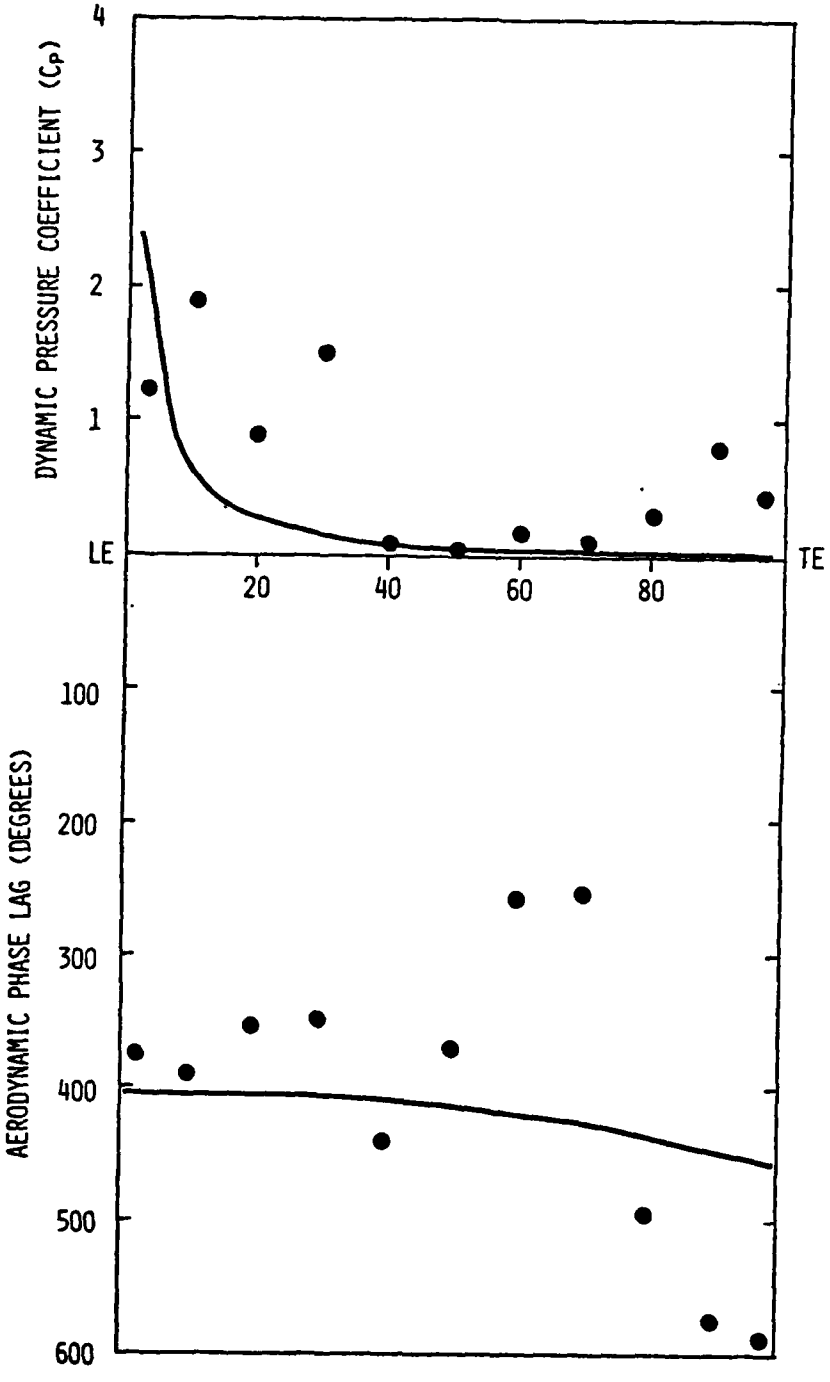

Figure 83. Chordwise data for second harmonic pressure difference and phase lag and prediction from reference 6 for point 36.

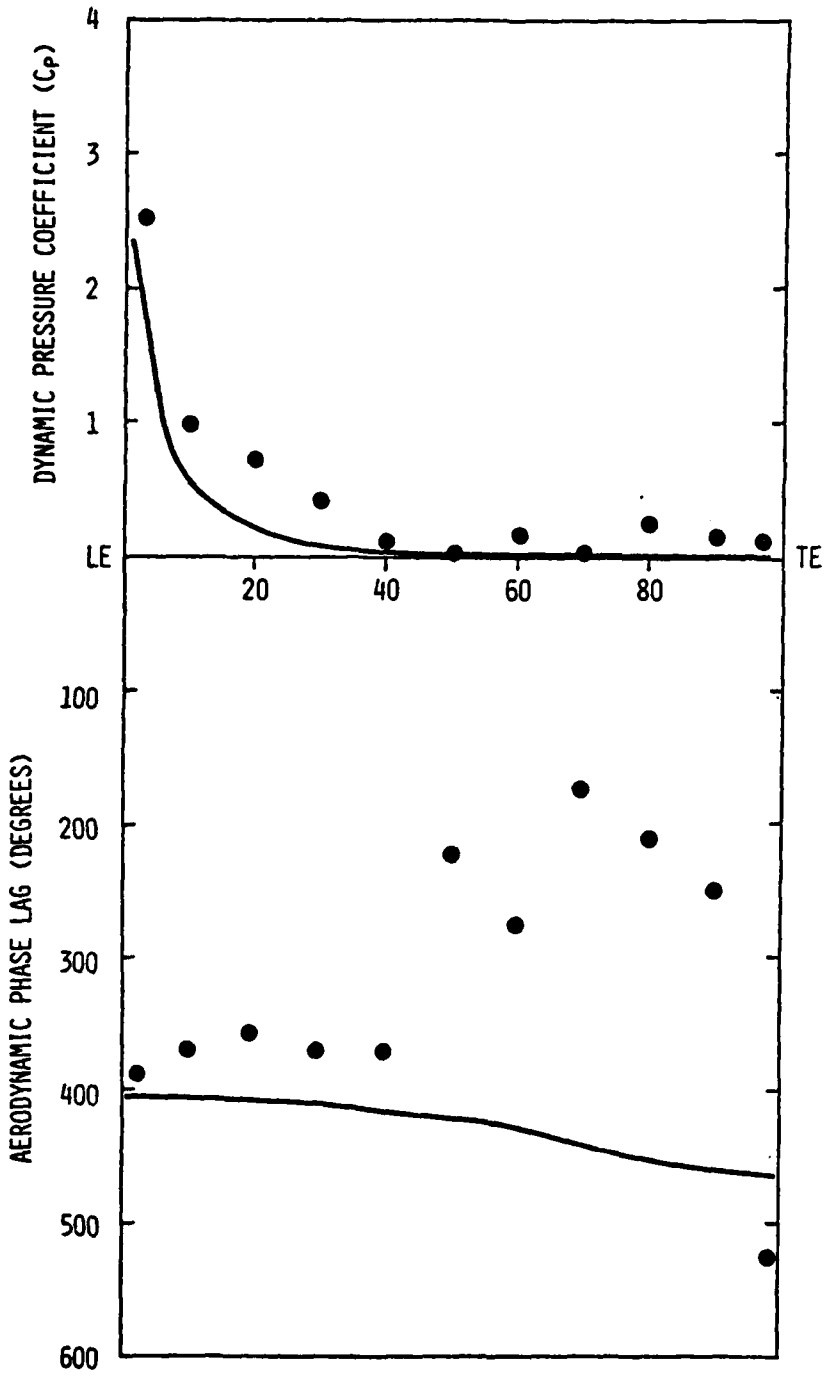

Figure 84. Chordwise data for second harmonic pressure difference and phase lag and prediction from reference 6 for point 37.

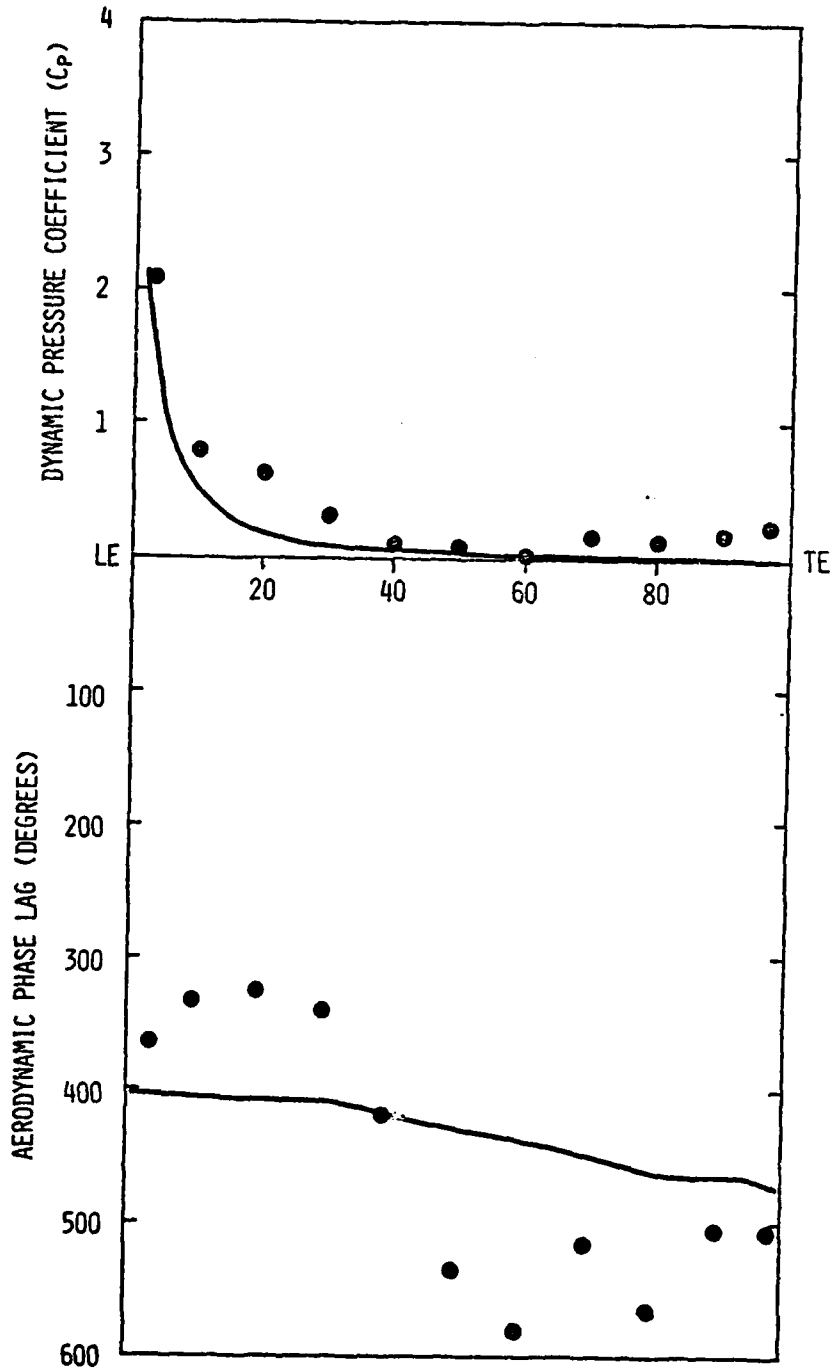

Figure 85. Chordwise data for second harmonic pressure difference and phase lag and prediction from reference 6 for point 38.

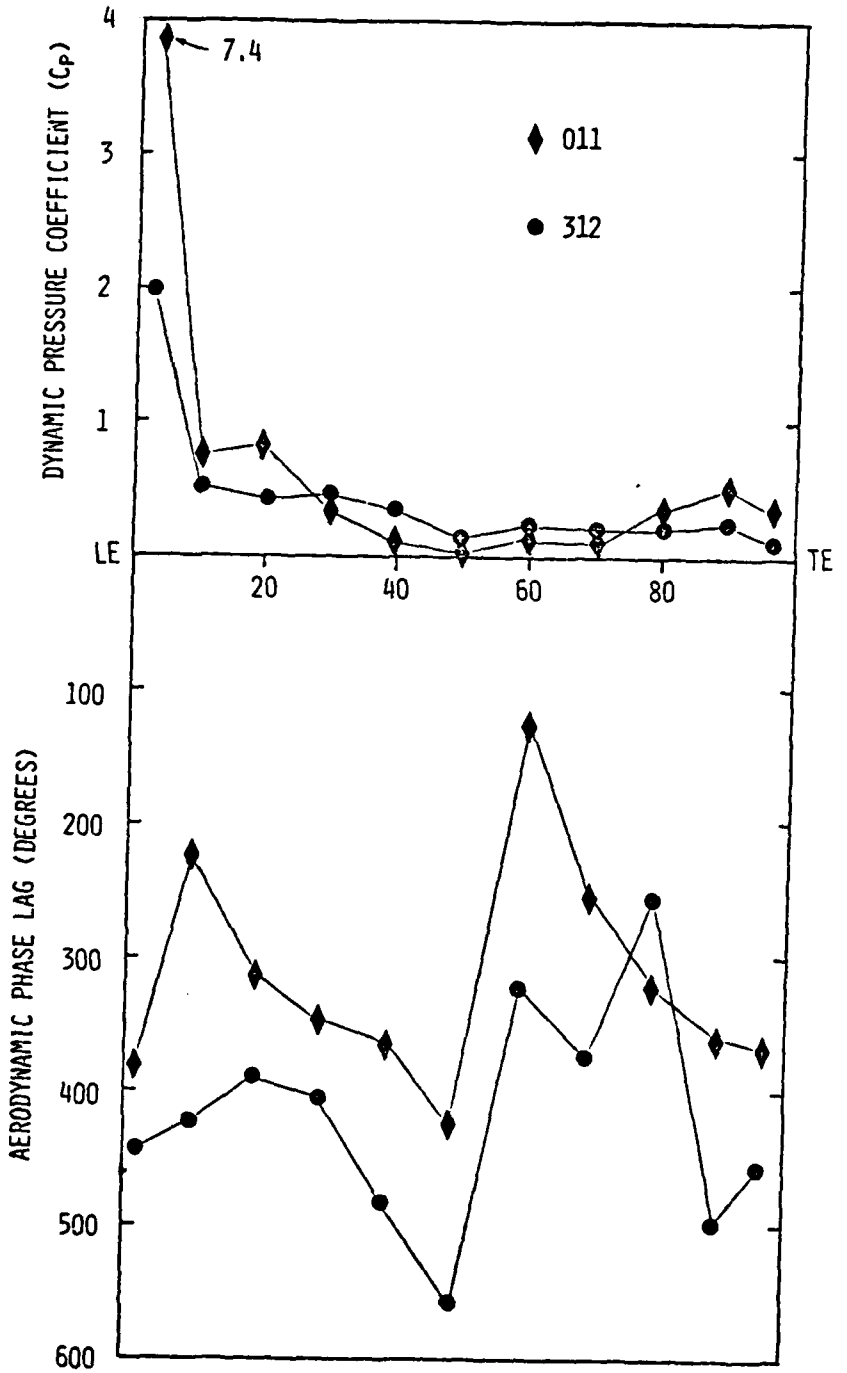

Figure 86. Baseline, data point 1, first harmonic compared to configuration 1, point 1, second harmonic.

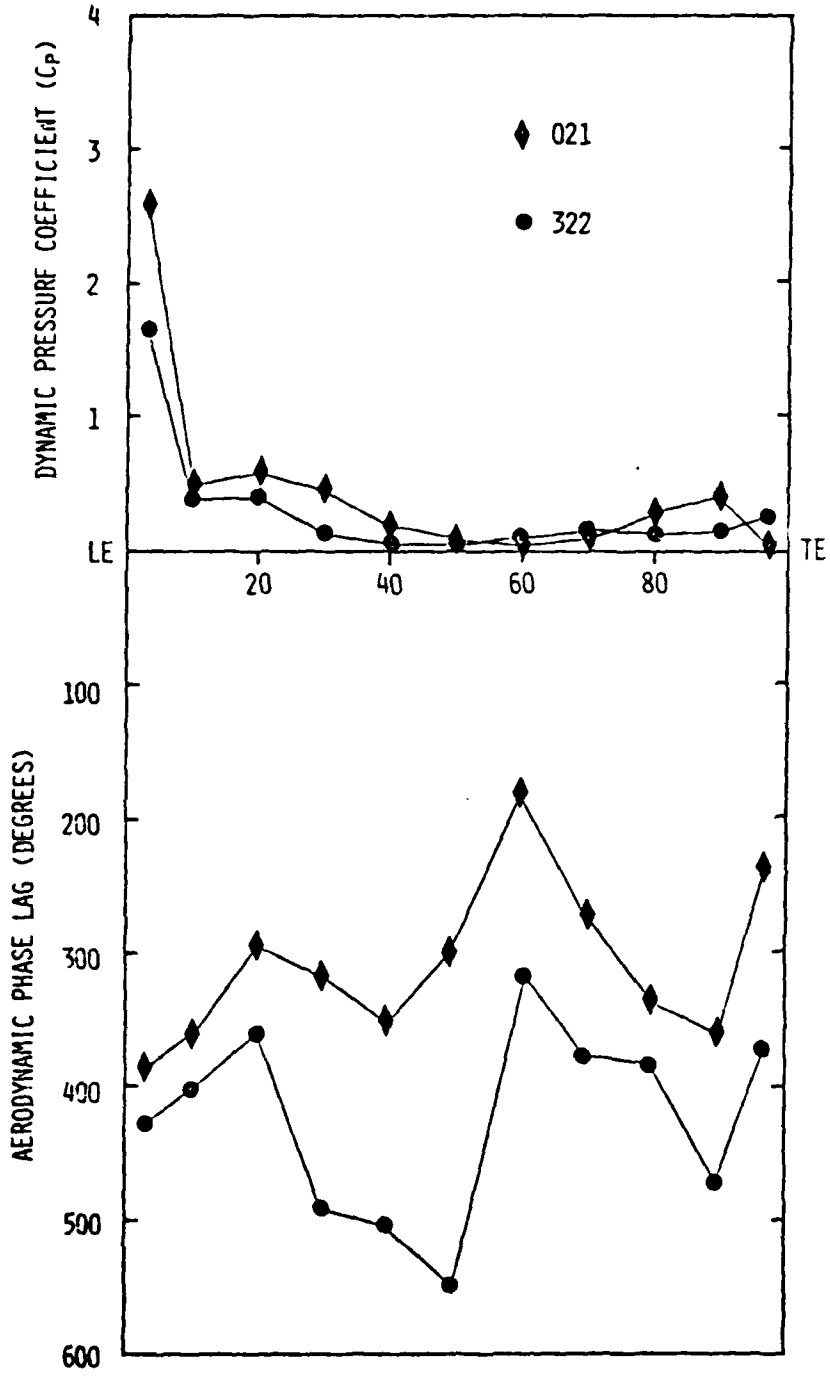

Figure 87. Baseline, data point 2, first harmonic compared to configuration 1, point 2, second harmonic.

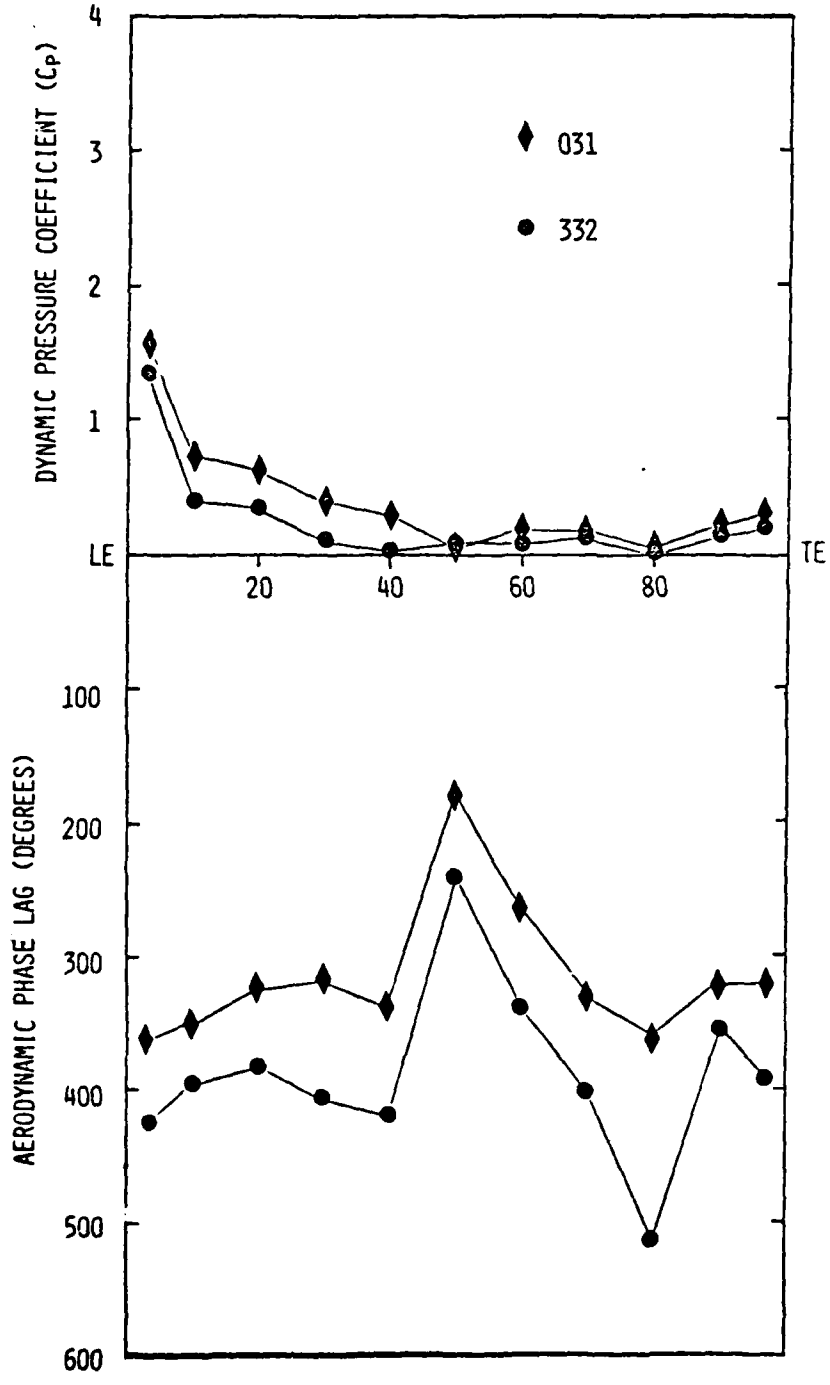

Figure 88. Baseline, data point 3, first harmonic compared to configuration 1, point 3, second harmonic.

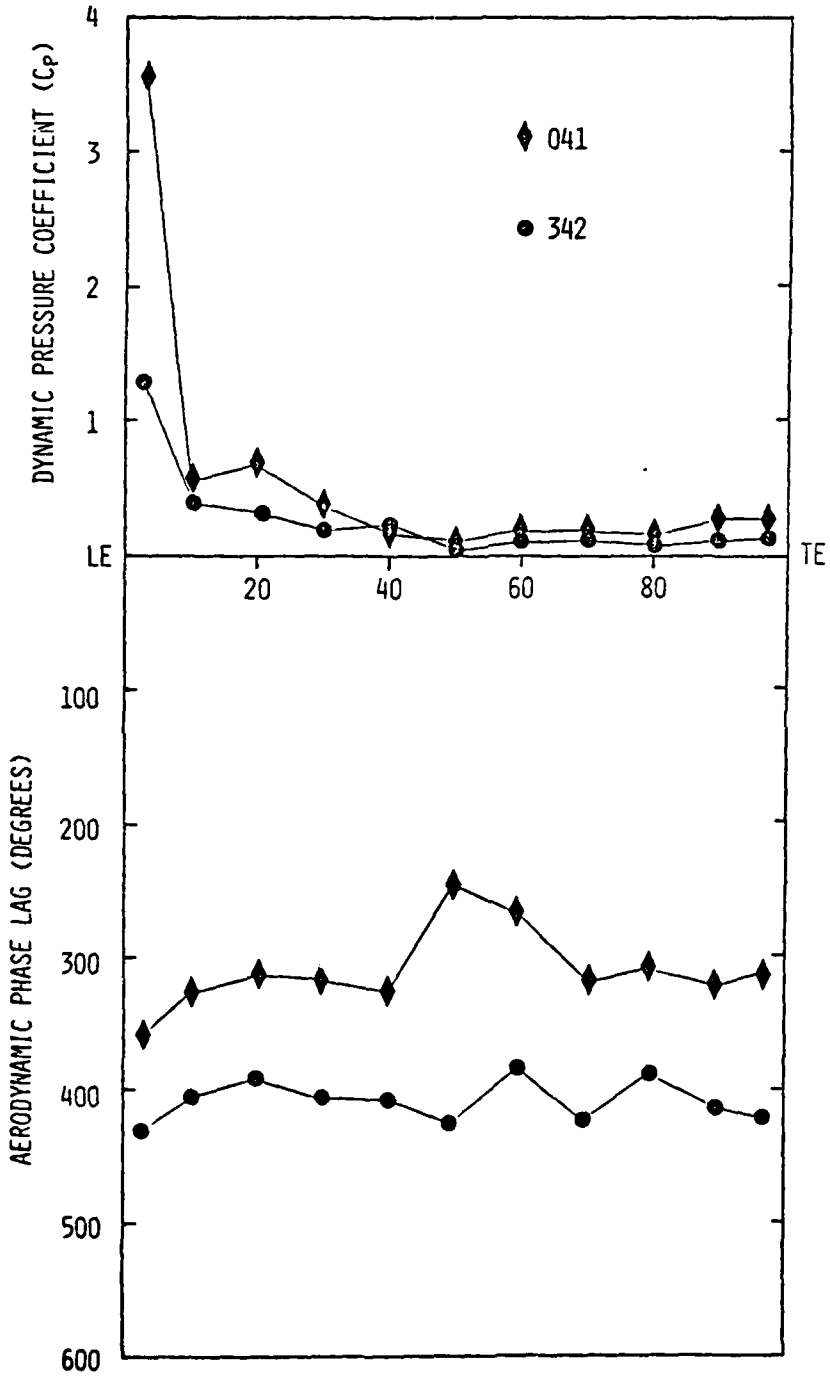

Figure 89. Baseline, data point 4, first harmonic compared to configuration 1, point 4, second harmonic.

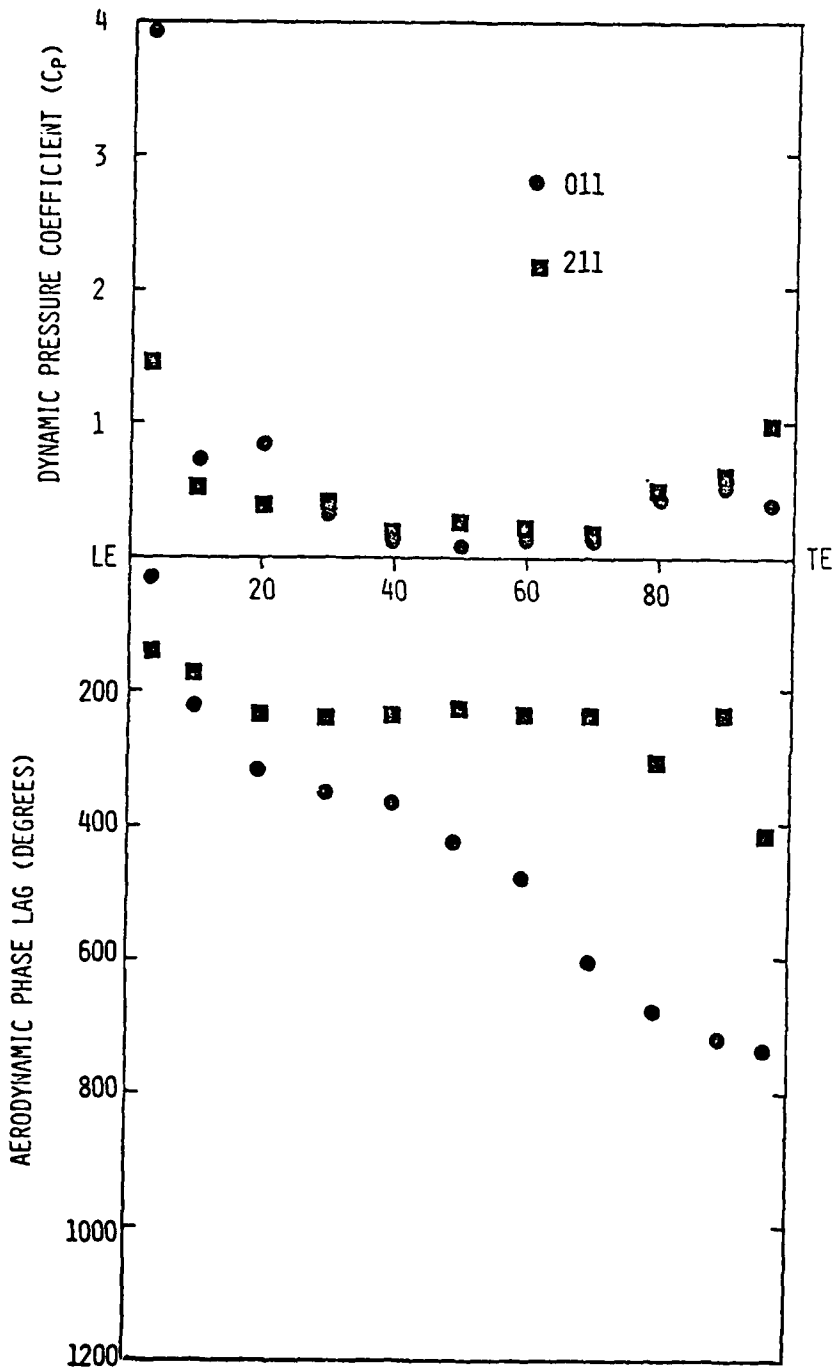

Figure 90. Baseline, data point 1, first harmonic compared to configuration 2, point 1, first harmonic.

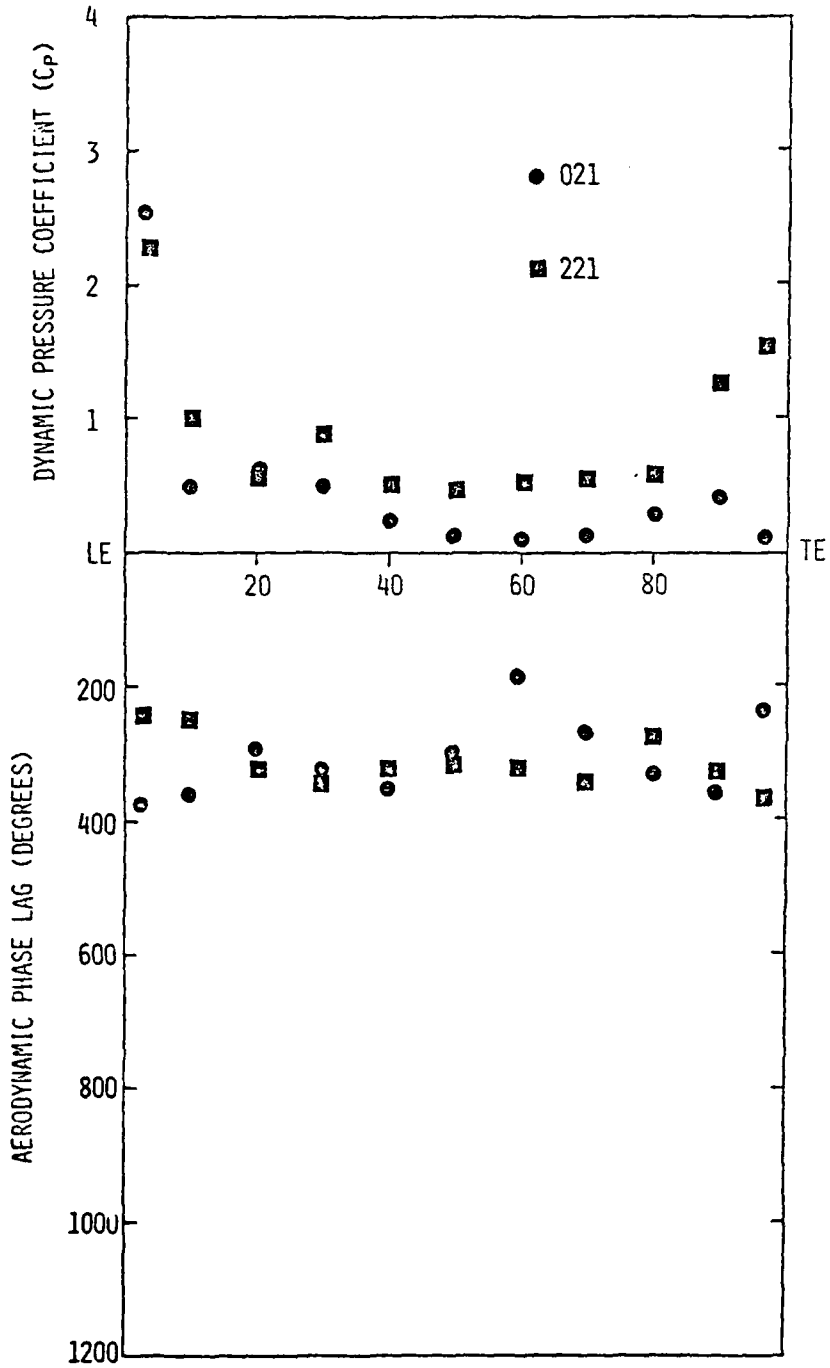

Figure 91. Baseline, data point 2, first harmonic compared to configuration 2, point 2, first harmonic.

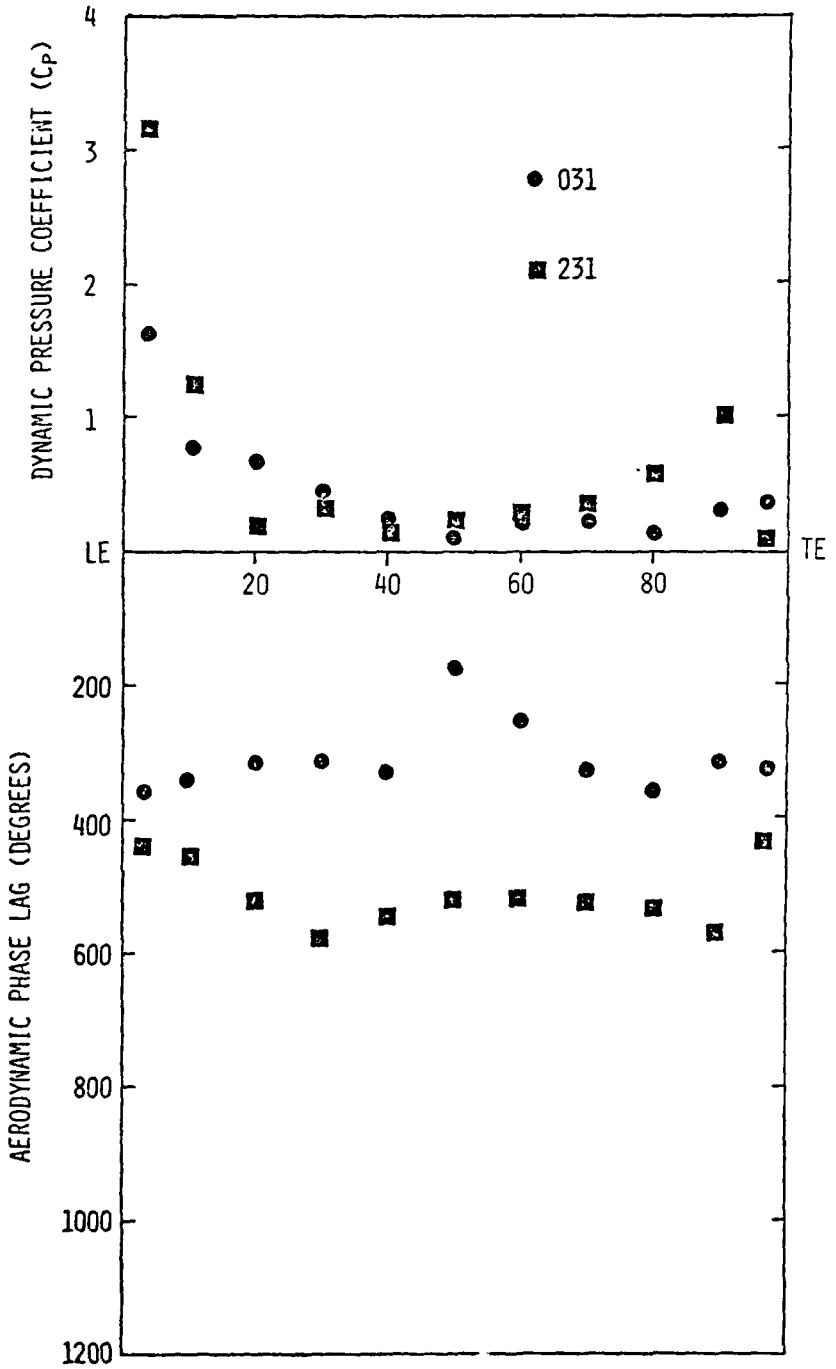

Figure 92. Baseline, data point 3, first harmonic compared to configuration 2, point 3, first harmonic.

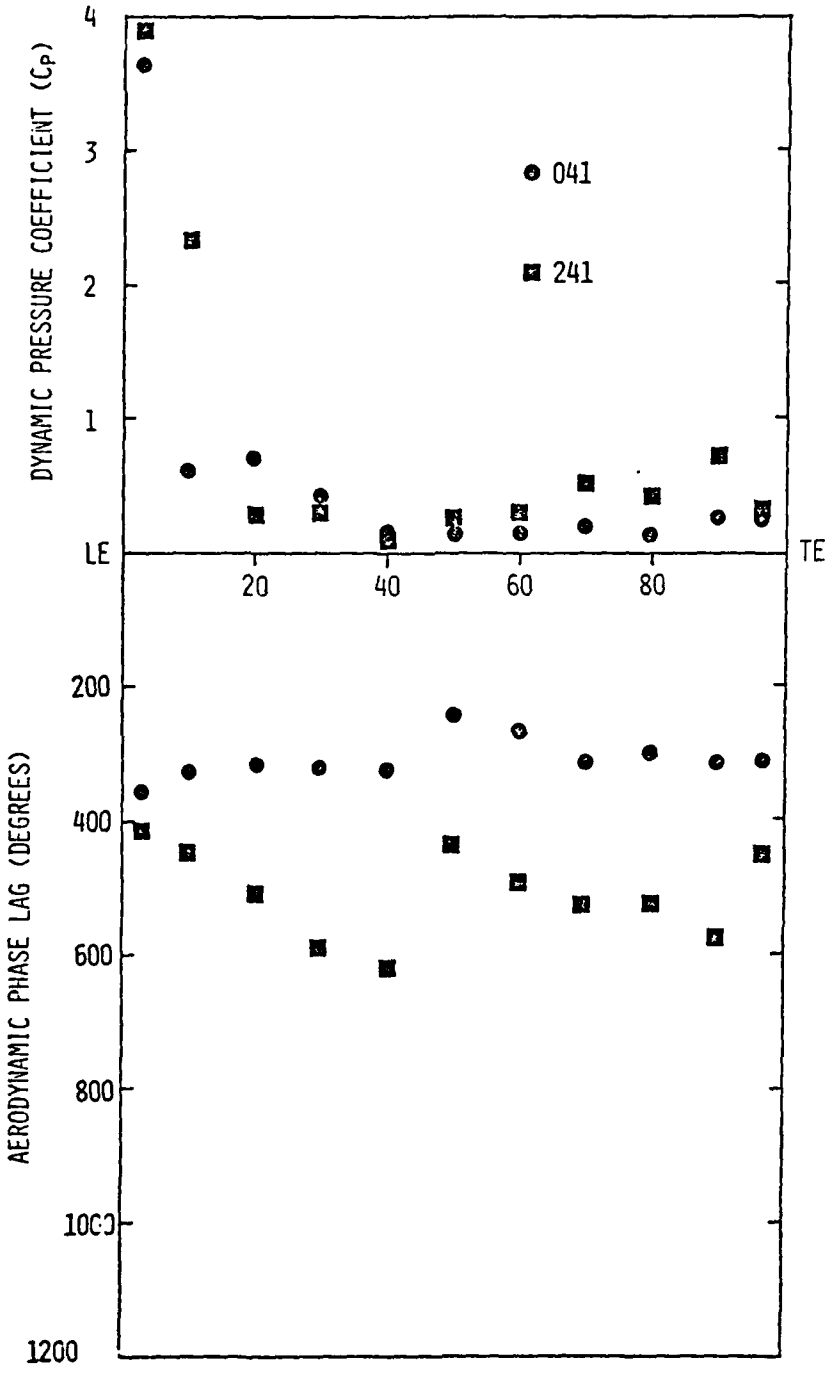

Figure 93. Baseline, data point 4, first harmonic compared to configuration 2, point 4, first harmonic.

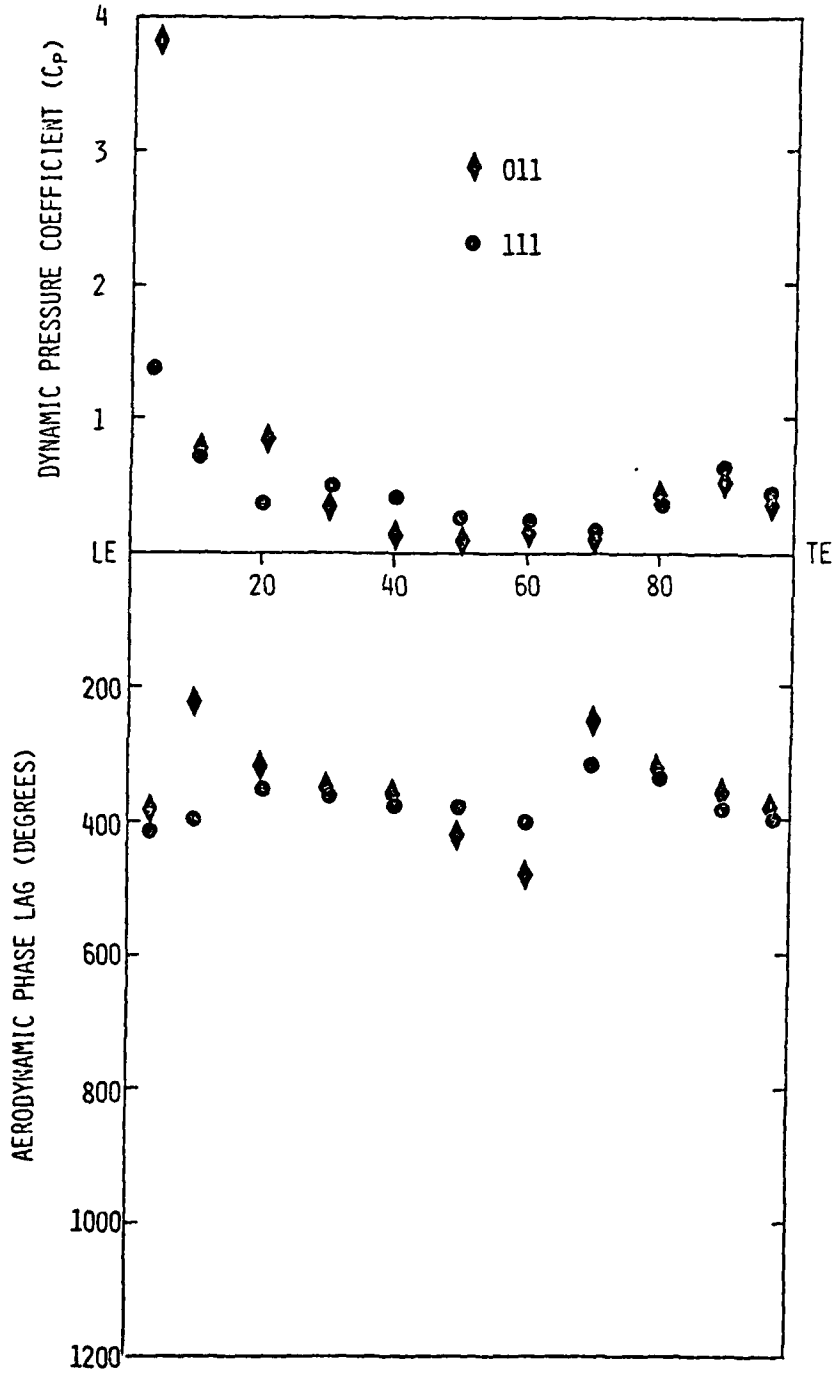

Figure 94. Baseline, data point 1, first harmonic compared to configuration 1, point 1, first harmonic.

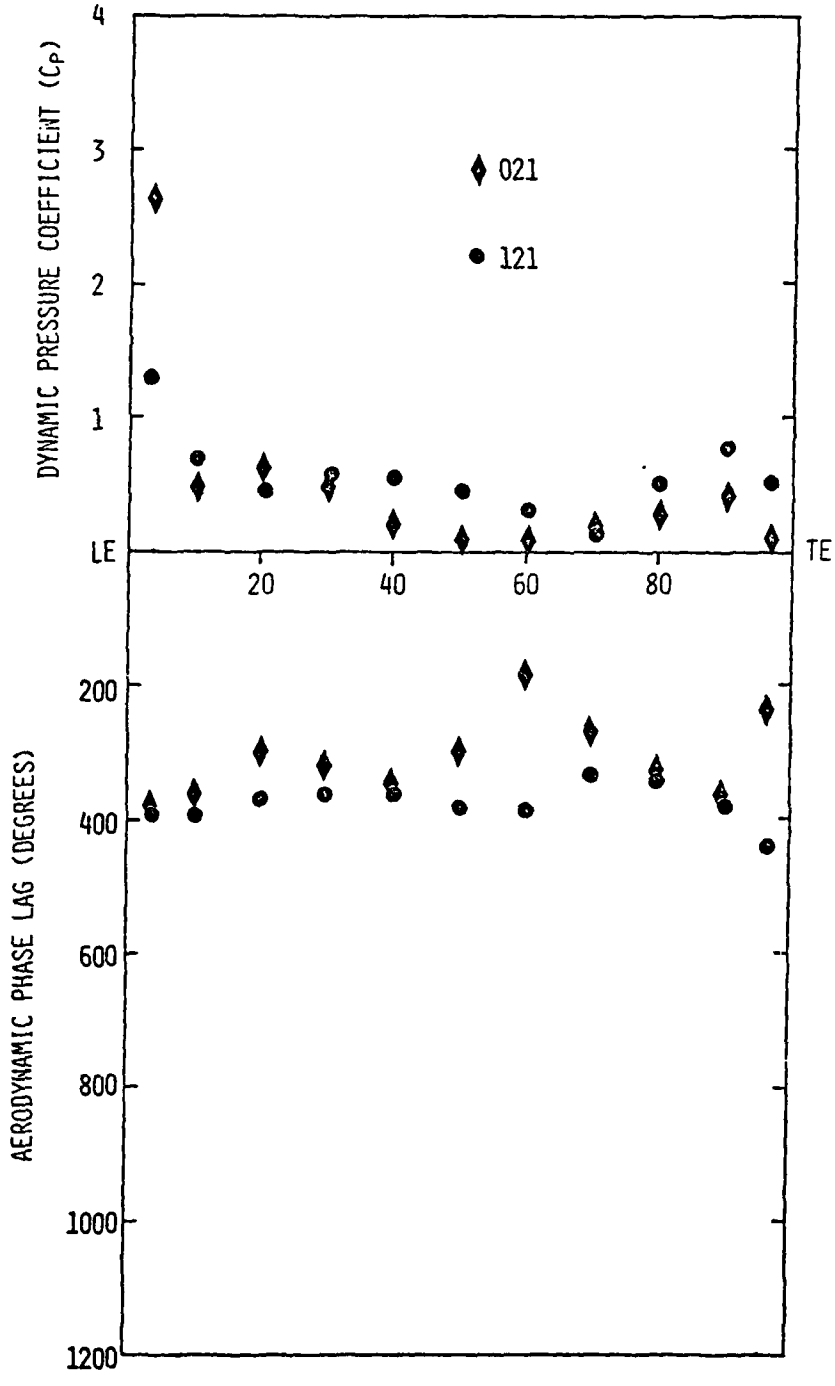

Figure 95. Baseline, data point 2, first harmonic compared to configuration 1, point 2, first harmonic.

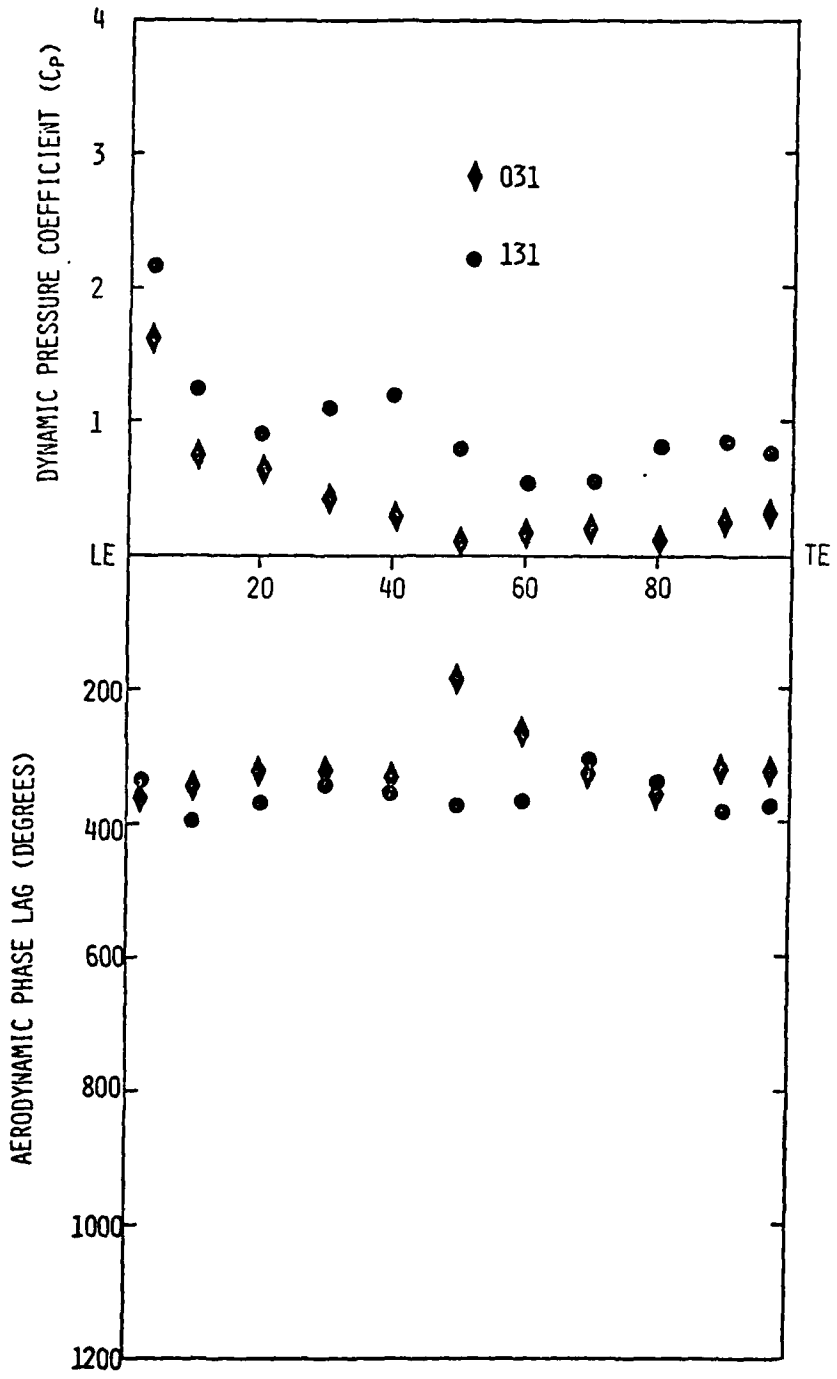

Figure 96. Baseline, data point 3, first harmonic compared to configuration 1, point 3, first harmonic.

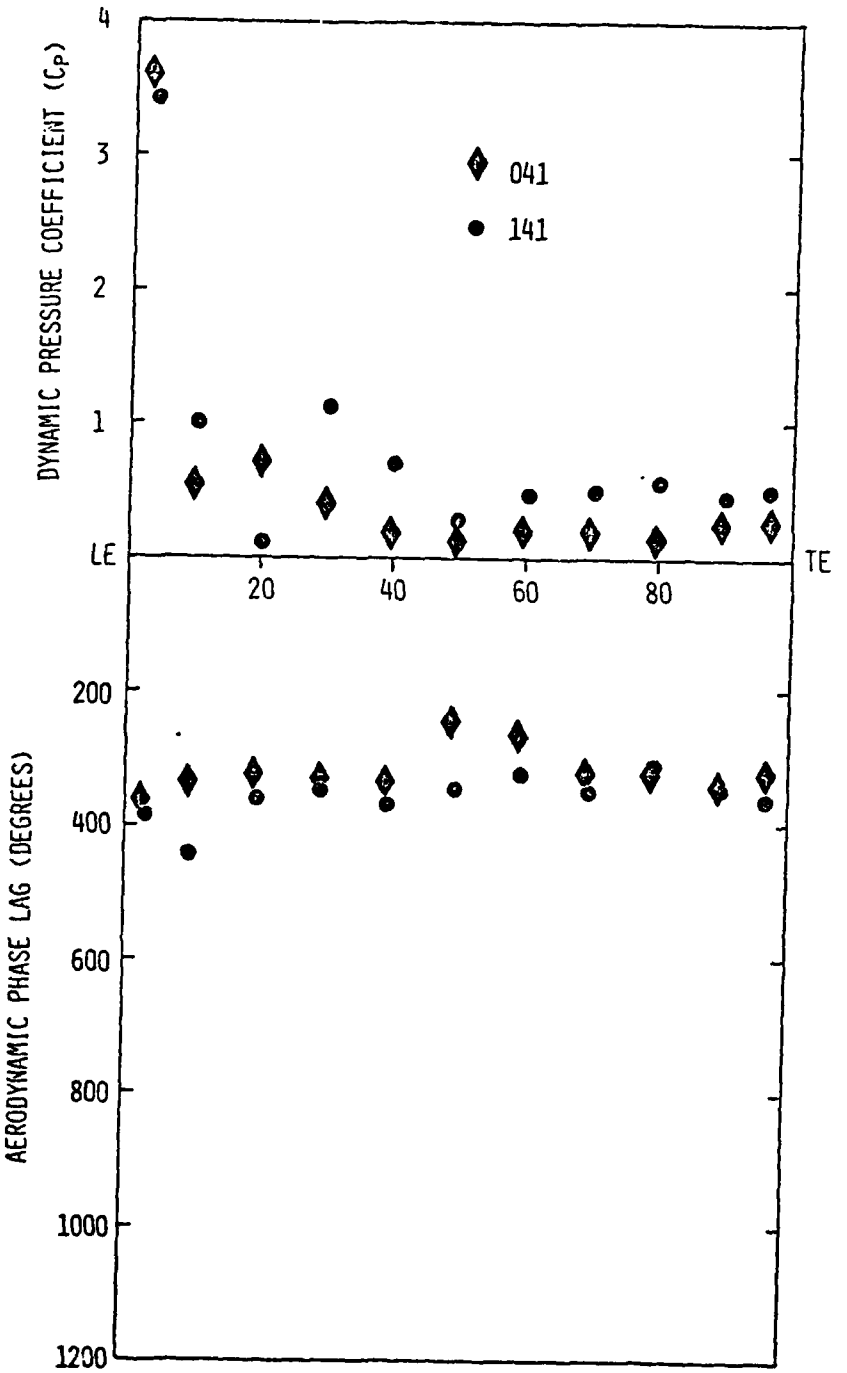

Figure 97. Baseline, data point 4, first harmonic compared to configuration 1, point 3, first harmonic.

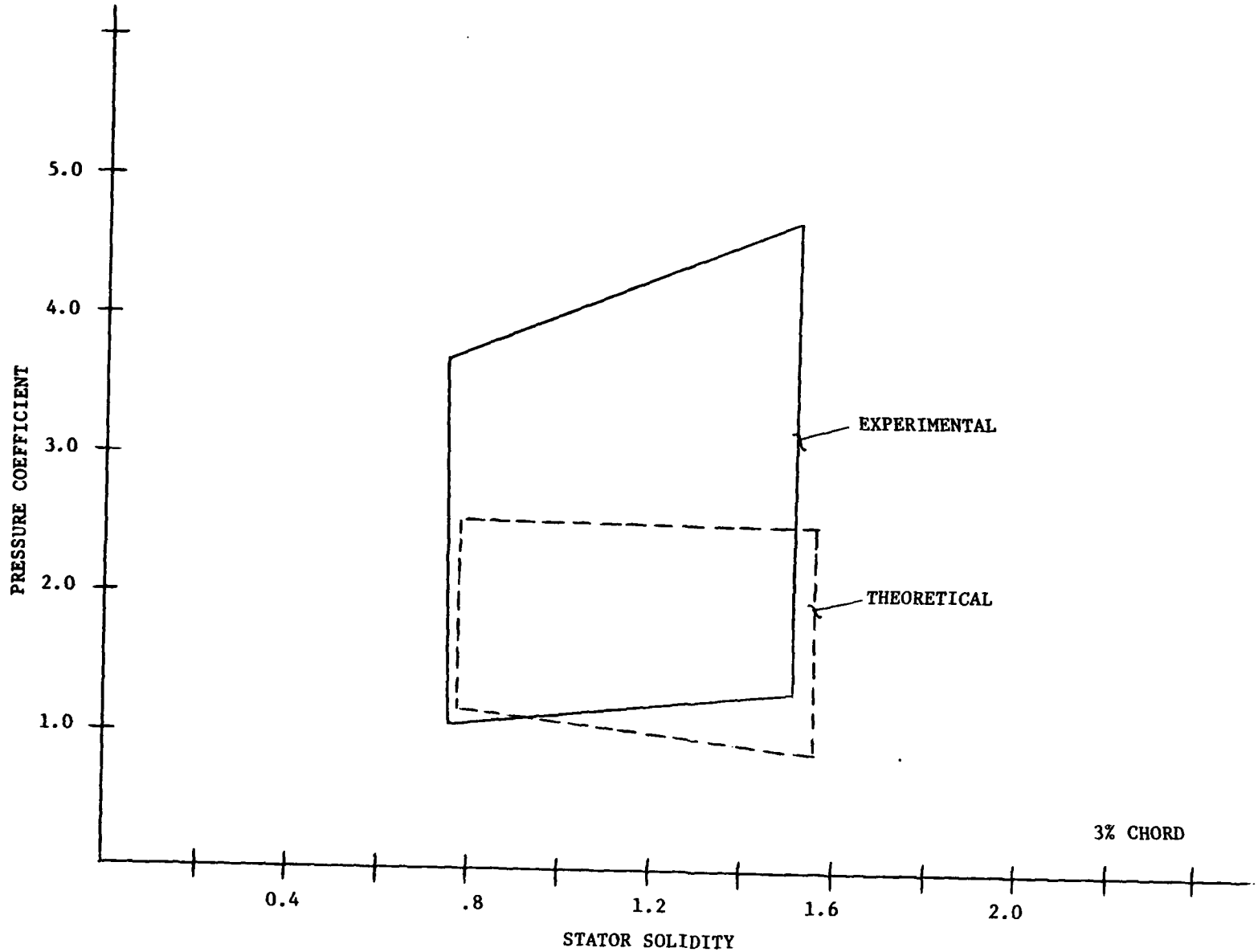

Figure 98. Variation in pressure coefficient at 3% chord due to solidity changes.

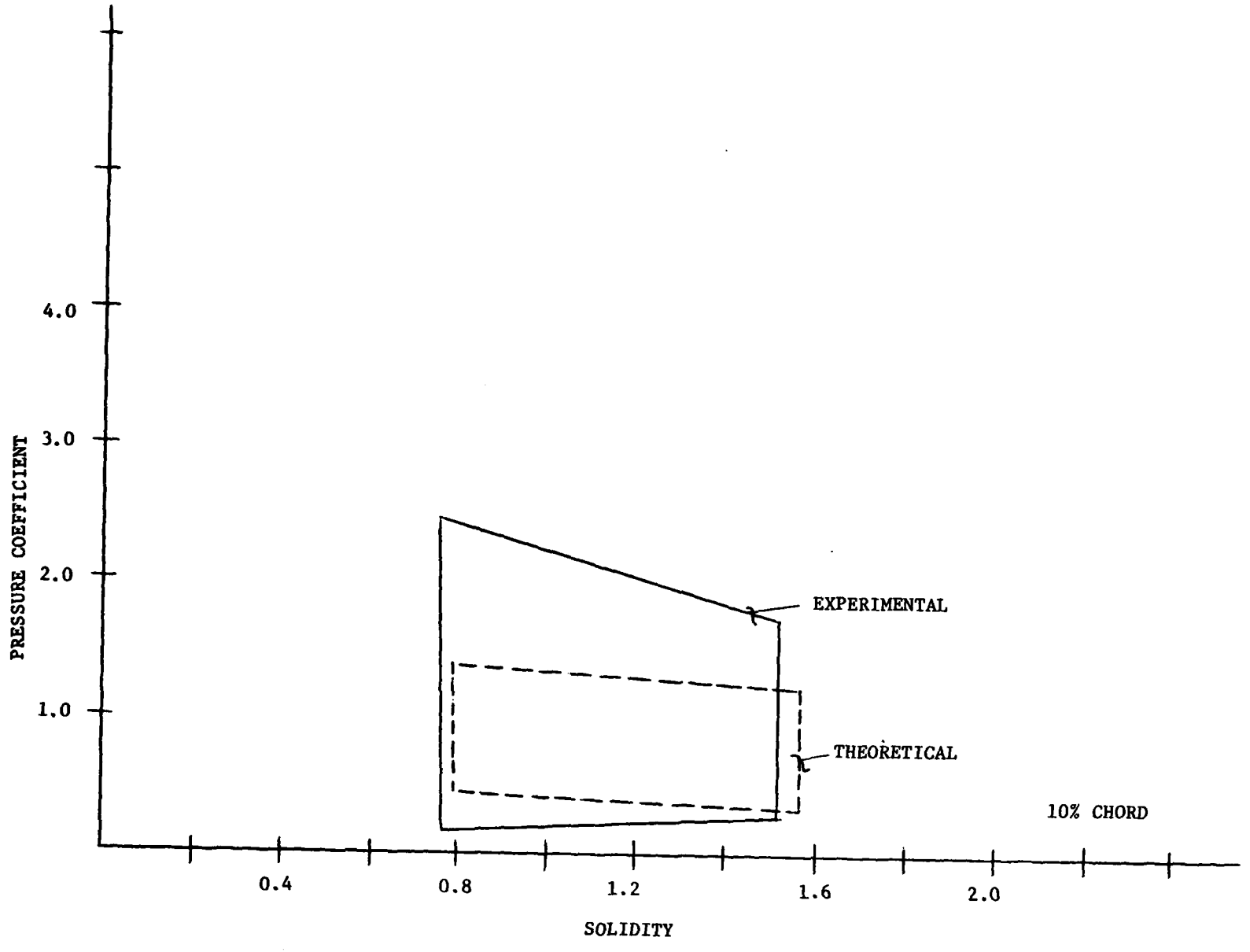

Figure 99. Variation in pressure coefficient at 10% chord due to solidity changes.

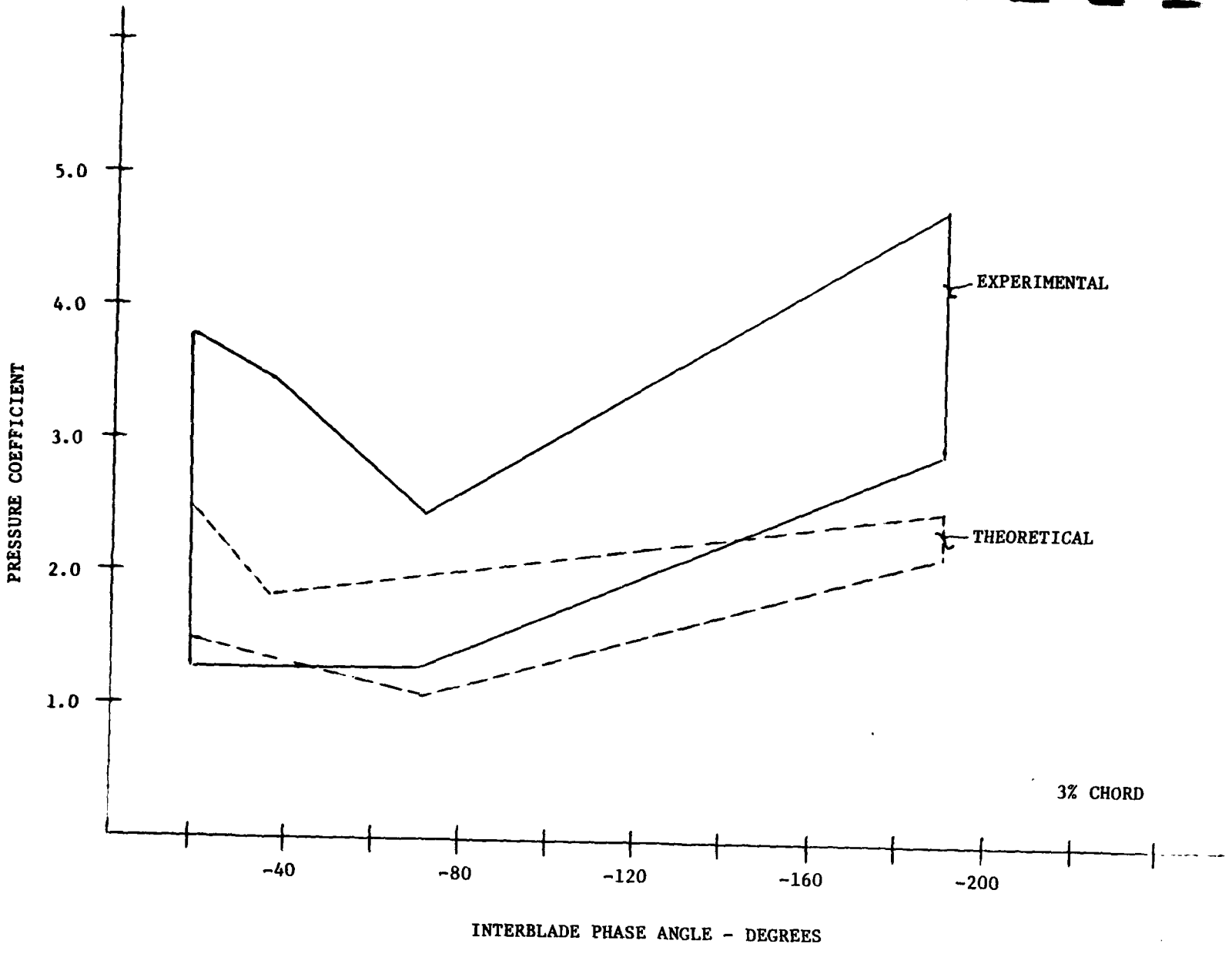

Figure 100. Variation in pressure coefficient at 3% chord due to interblade phase angle changes.

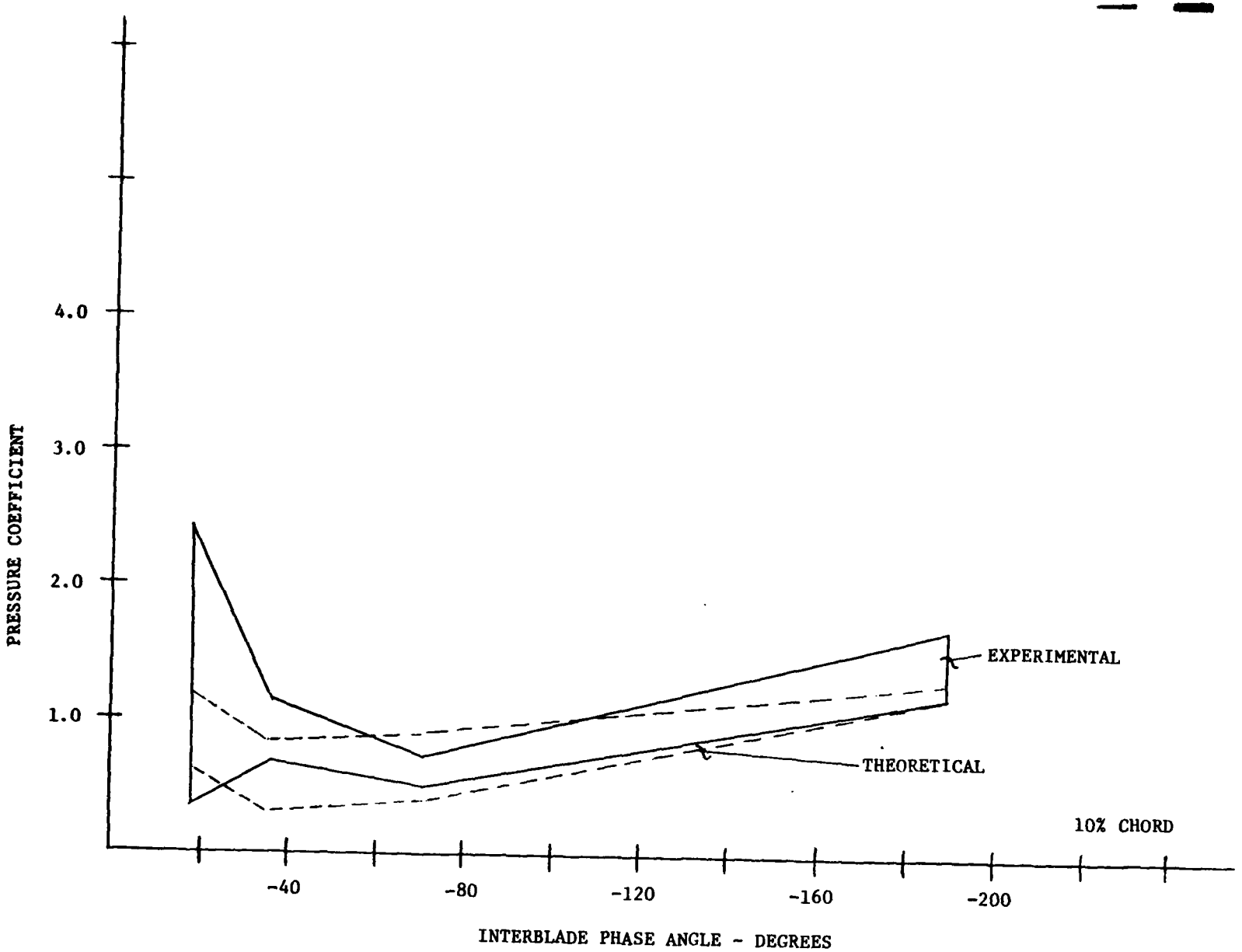

Figure 101. Variation in pressure coefficient at 10% chrod due to interblade phase angle changes.

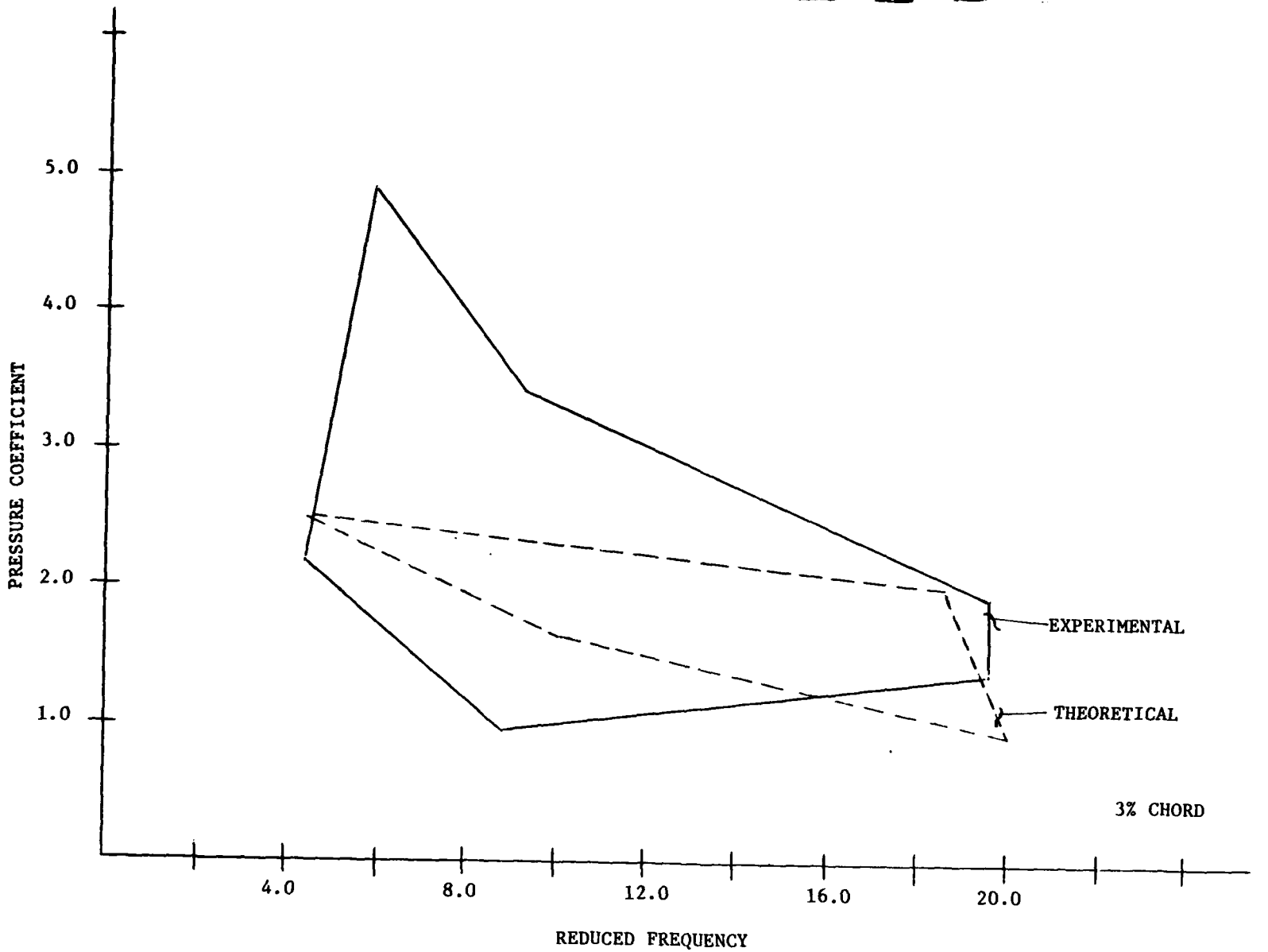

Figure 102. Variation in pressure coefficient at 3% chord due to reduced frequency changes.

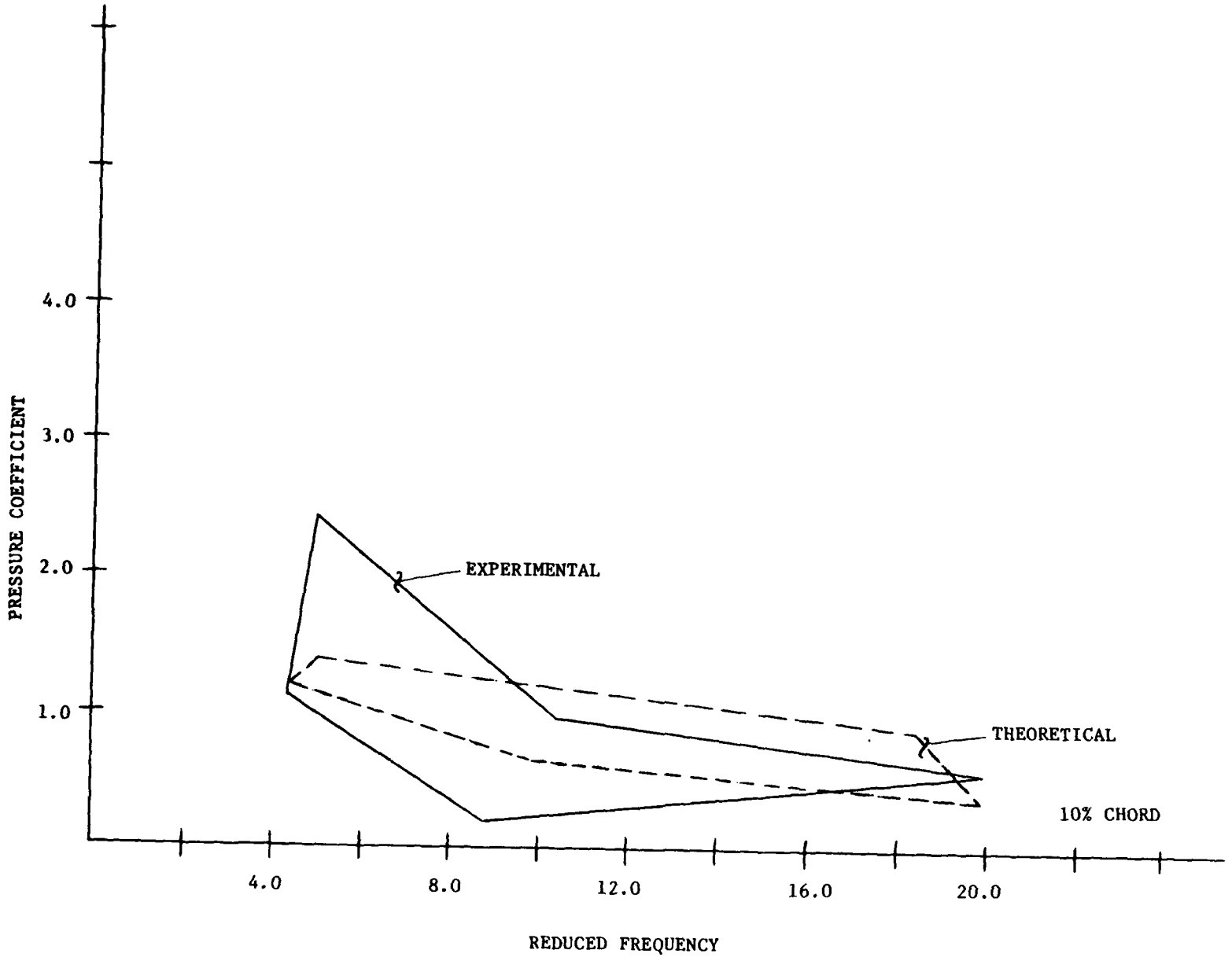

Figure 103. Variation in pressure coefficient at 10% chord due to reduced frequency changes.

APPENDIX A

PRESSURE AND SUCTION SURFACE TIME-VARIANT PRESSURE DATA

AFOSR-3 [illegible]-1 1ST HARMONIC 11/21/78

ROTOR SPEED = 889.

AXIAL LOCATION	SUCTION SURFACE		PRESSURE SURFACE	
PERCENT OF CHORD	AMPLITUDE	PHASE	AMPLITUDE	PHASE
2.94	.815	-222.	.568	-57.
10.00	.258	-241.	.293	-21.
20.00	.065	-130.	.316	-7.
30.00	.249	-161.	.272	-16.
40.00	.199	-210.	.189	-9.
50.00	.101	-251.	.220	-353.
60.00	.117	-299.	.212	-6.
70.00	.136	-31.	.167	-10.
80.00	.213	-137.	.171	-353.
90.00	.410	-214.	.258	-352.
97.06	.324	-205.	.332	-356.

AFOSR-3 BUILT-1 PT-1 2ND HARM. 11/22//8

ROTOR SPEED = 889.

AXIAL LOCATION	SUCTION SURFACE		PRESSURE SURFACE	
PERCENT OF CHORD	AMPLITUDE	PHASE	AMPLITUDE	PHASE
2.94	.496	-281.	.325	-94.
10.00	.078	-290.	.218	-83.
20.00	.210	-295.	.123	-98.
30.00	.144	-346.	.124	-108.
40.00	.043	-223.	.087	-101.
50.00	.190	-301.	.094	-114.
60.00	.148	-12.	.098	-114.
70.00	.137	-263.	.097	-110.
80.00	.065	-355.	.086	-109.
90.00	.115	-300.	.062	-128.
97.00	.089	-4.	.083	-106.

AFOSR-3 BUILD-1 PT-2 1ST HARM. 11/22/78

ROTOR SPEED = 889.

AXIAL LOCATION	SUCTION SURFACE		PRESSURE SURFACE	
PERCENT OF CHORD	AMPLITUDE	PHASE	AMPLITUDE	PHASE
2.94	.569	-187.	.777	-41.
14.00	.230	-221.	.463	-27.
24.00	.154	-148.	.458	-30.
34.00	.312	-135.	.351	-30.
44.00	.252	-106.	.324	-21.
54.00	.125	-185.	.312	-24.
64.00	.033	-315.	.306	-23.
74.00	.211	-61.	.271	-26.
84.00	.335	-135.	.267	-22.
94.00	.433	-210.	.330	-12.
97.00	.226	-275.	.435	-16.

AFOSR-3 BUILD-1 PT-2 2ND HARM. 11/21/78

ROTOR SPEED = 849.

AXIAL LOCATION	SUCTION SURFACE		PRESSURE SURFACE	
PERCENT OF CHORD	AMPLITUDE	PHASE	AMPLITUDE	PHASE
2.94	.556	-238.	.486	-88.
10.00	.056	-304.	.246	-86.
20.00	.258	-296.	.194	-82.
30.00	.108	-335.	.141	-93.
40.00	.016	-124.	.154	-90.
50.00	.191	-303.	.142	-96.
60.00	.087	-354.	.129	-103.
70.00	.132	-285.	.102	-112.
80.00	.050	-300.	.095	-107.
90.00	.122	-302.	.049	-141.
97.00	.048	-322.	.066	-144.

AFOSR-3 BUILD-1 PT-3 1ST HARM. 11/21/78

ROTOR SPEED = 689.

AXIAL LOCATION	SUCTION SURFACE		PRESSURE SURFACE	
PERCENT OF CHORD	AMPLITUDE	PHASE	AMPLITUDE	PHASE
2.94	1.327	-139.	1.353	-34.
10.00	.339	-227.	.991	-29.
20.00	.394	-115.	.864	-33.
30.00	.695	-129.	.716	-23.
40.00	.538	-154.	.750	-19.
50.00	.201	-155.	.674	-23.
60.00	.126	-78.	.610	-21.
70.00	.407	-87.	.549	-17.
80.00	.441	-140.	.485	-16.
90.00	.322	-198.	.501	-9.
97.00	.254	-191.	.502	-7.

AFOSR-3 BUILD-1 PT-3 2ND HARM. 11/21/78

ROTOR SPEED = 689.

AXIAL LOCATION	SUCTION SURFACE		PRESSURE SURFACE	
PERCENT OF CHORD	AMPLITUDE	PHASE	AMPLITUDE	PHASE
2.94	1.675	-248.	.987	-82.
10.00	.139	-182.	.576	-78.
20.00	.629	-92.	.594	-82.
30.00	.368	-309.	.540	-87.
40.00	.233	-264.	.549	-93.
50.00	.421	-280.	.541	-92.
60.00	.292	-282.	.496	-94.
70.00	.383	-273.	.499	-93.
80.00	.287	-276.	.394	-91.
90.00	.287	-285.	.324	-91.
97.00	.362	-289.	.245	-71.

AFOSR-3 BUILD-1 PT-4 1ST HARM. 11/21/78

ROTOR SPEED = 889.

AXIAL LOCATION	SUCTION SURFACE		PRESSURE SURFACE	
PERCENT OF CHORD	AMPLITUDE	PHASE	AMPLITUDE	PHASE
2.34	2.371	-202.	1.099	-25.
10.00	1.011	-312.	.800	-17.
20.00	.054	-351.	.178	-354.
30.00	.653	-153.	.542	-3.
40.00	.179	-208.	.546	-5.
50.00	.185	-29.	.428	-2.
60.00	.262	-85.	.393	-359.
70.00	.149	-138.	.375	-2.
80.00	.433	-102.	.303	-360.
90.00	.133	-159.	.302	-350.
97.00	.232	-185.	.262	-346.

AFOSR-3 BUILD-1 PT-4 2.0 MAR4, 11/21/78

ROTOR SPEED = 889.

AXIAL LOCATION	SUCTION SURFACE		PRESSURE SURFACE	
PERCENT OF CHORD	AMPLITUDE	PHASE	AMPLITUDE	PHASE
2.94	1.655	-243.	.799	-76.
10.00	.999	-108.	.567	-65.
20.00	.212	-267.	.093	-214.
30.00	.084	-198.	.522	-71.
40.00	.344	-298.	.521	-74.
50.00	.170	-276.	.492	-74.
60.00	.397	-288.	.497	-69.
70.00	.346	-272.	.451	-60.
80.00	.383	-273.	.359	-53.
90.00	.360	-209.	.289	-46.
97.00	.415	-275.	.277	-26.

AFOSR-3 BLU-1 PT-5 1ST HARM.

ROTOR SPEED = 613.

AXIAL LOCATION	SUCTION SURFACE		PRESSURE SURFACE	
PERCENT OF CHORD	AMPLITUDE	PHASE	AMPLITUDE	PHASE
2.94	.959	-221.	.802	-44.
10.00	.389	-244.	.349	-8.
20.00	.042	-82.	.124	-7.
30.00	.256	-175.	.224	-16.
40.00	.232	-206.	.147	-2.
50.00	.124	-225.	.150	-355.
60.00	.112	-278.	.156	-4.
70.00	.207	-4.	.076	-3.
80.00	.312	-98.	.086	-352.
90.00	.348	-183.	.110	-329.
97.00	.165	-269.	.151	-337.

AFOSR-3 BLD-1 PT-5 2ND HARM.

ROTOR SPEED = 613.

AXIAL LOCATION PERCENT OF CHORD	SUCTION SURFACE AMPLITUDE	SUCTION SURFACE PHASE	PRESSURE SURFACE AMPLITUDE	PRESSURE SURFACE PHASE
2.94	.543	-256.	.278	-69.
10.00	.075	-244.	.168	-40.
20.00	.029	-319.	.060	-13.
30.00	.120	-323.	.031	-37.
40.00	.089	-142.	.046	-348.
50.00	.172	-270.	.036	-337.
60.00	.123	-46.	.033	-334.
70.00	.110	-247.	.037	-343.
80.00	.087	-59.	.031	-332.
90.00	.099	-292.	.026	-339.
97.00	.108	-46.	.018	-74.

APOS4=3 SLO=1 PT=0 1ST HARM.

ROTOR SPEED = 613.

AXIAL LOCATION	SUCTION SURFACE		PRESSURE SURFACE	
PERCENT OF CHORD	AMPLITUDE	PHASE	AMPLITUDE	PHASE
2.94	.445	-218.	.876	-14.
10.00	.211	-232.	.576	-1.
20.00	.172	-178.	.396	-13.
30.00	.234	-121.	.339	-8.
40.00	.184	-143.	.328	-10.
50.00	.097	-171.	.282	-14.
60.00	.106	-339.	.279	-19.
70.00	.305	-31.	.199	-33.
80.00	.355	-101.	.209	-29.
90.00	.200	-207.	.227	-44.
97.00	.315	-341.	.324	-32.

AFOSR-3 BLC-1 PT-C 2ND HARM.

ROTOR SPEED = 613.

AXIAL LOCATION	SUCTION SURFACE		PRESSURE SURFACE	
PERCENT OF CHORD	AMPLITUDE	PHASE	AMPLITUDE	PHASE
2.94	.462	-224.	.363	-54.
10.00	.044	-227.	.147	-35.
20.00	.064	-153.	.106	-13.
30.00	.109	-312.	.080	-343.
40.00	.107	-118.	.090	-340.
50.00	.127	-267.	.078	-329.
60.00	.104	-47.	.076	-337.
70.00	.062	-271.	.075	-323.
80.00	.074	-76.	.063	-324.
90.00	.081	-339.	.052	-310.
97.00	.085	-107.	.048	-247.

AFOSR-3 BLD-1 PT-7 1ST HARM.

ROTOR SPEED = 613.

AXIAL LOCATION	SUCTION SURFACE		PRESSURE SURFACE	
PERCENT OF CHORD	AMPLITUDE	PHASE	AMPLITUDE	PHASE
2.94	.507	-188.	.964	-16.
10.00	.261	-227.	.745	-12.
20.00	.200	-108.	.501	-26.
30.00	.262	-133.	.430	-8.
40.00	.162	-142.	.379	-12.
50.00	.370	-122.	.316	-19.
60.00	.243	-22.	.295	-17.
70.00	.326	-49.	.162	-23.
80.00	.225	-66.	.197	-22.
90.00	.261	-24.	.080	-81.
97.00	.393	-33.	.105	-92.

AOISR=3 FL=1 PT=7 [illegible].

ROTOR SPEED = 513.

AXIAL LOCATION	SUCTION SURFACE		PRESSURE SURFACE	
PERCENT OF CHORD	AMPLITUDE	PHASE	AMPLITUDE	PHASE
2.00	.049	-234.	.043	-61.
10.00	.106	-108.	.174	-46.
20.00	.038	-213.	.111	-25.
30.00	.050	-311.	.144	-2.
40.00	.053	-104.	.131	-360.
50.00	.049	-277.	.126	-3.
60.00	.027	-80.	.107	-308.
70.00	.016	-302.	.096	-356.
80.00	.053	-171.	.082	-356.
90.00	.010	-41.	.064	-353.
97.00	.017	-211.	.057	-355.

AFOSR-3 SL.-1 PT-8 1ST HARM

ROTOR SPEED = 614.

AXIAL LOCATION	SUCTION SURFACE		PRESSURE SURFACE	
PERCENT OF CHORD	AMPLITUDE	PHASE	AMPLITUDE	PHASE
2.94	1.460	-213.	.884	-21.
10.00	.591	-295.	.649	-11.
20.00	.034	-97.	.112	-9.
30.00	.257	-167.	.399	-360.
40.00	.083	-256.	.320	-1.
50.00	.171	-3.	.262	-360.
60.00	.251	-36.	.254	-356.
70.00	.148	-42.	.141	-346.
80.00	.205	-18.	.144	-351.
90.00	.294	-26.	.065	-259.
97.00	.309	-28.	.056	-270.

AFOSR-3 BLD-1 PT-B 2ND HARM.

ROTOR SPEED = 613.

AXIAL LOCATION	SUCTION SURFACE		PRESSURE SURFACE	
PERCENT OF CHORD	AMPLITUDE	PHASE	AMPLITUDE	PHASE
2.94	1.066	-250.	.262	-74.
10.00	.567	-101.	.123	-39.
20.00	.045	-251.	.036	-44.
30.00	.074	-176.	.073	-18.
40.00	.120	-268.	.077	-10.
50.00	.012	-146.	.060	-7.
60.00	.071	-297.	.049	-4.
70.00	.004	-275.	.044	-7.
80.00	.030	-296.	.036	-9.
90.00	.019	-314.	.031	-29.
97.00	.022	-294.	.026	-27.

AFOSR3 BLD2 DATA POINT 1 FIRST HARM. ALP=25

ROTOR SPEED = 903.

AXIAL LOCATION	SUCTION SURFACE		PRESSURE SURFACE	
PERCENT OF CHORD	AMPLITUDE	PHASE	AMPLITUDE	PHASE
2.94	1.608	-314.	.493	-186.
10.00	.869	-334.	.339	-255.
20.00	.659	-28.	.336	-294.
30.00	.060	-38.	.336	-307.
40.00	.452	-20.	.356	-302.
50.00	.703	-6.	.438	-301.
60.00	.748	-7.	.530	-307.
70.00	.733	-17.	.590	-301.
80.00	.455	-344.	.620	-333.
90.00	.763	-2.	.673	-344.
97.00	.819	-325.	.851	-347.

AFOSR3 BL02 DATA POINT 1 SECOND HARM, ALPH=25

ROTOR SPEED = 903.

AXIAL LOCATION	SUCTION SURFACE		PRESSURE SURFACE	
PERCENT OF CHORD	AMPLITUDE	PHASE	AMPLITUDE	PHASE
2.94	1.123	-270.	.690	-80.
10.00	.207	-265.	.318	-64.
20.00	.246	-168.	.287	-83.
30.00	.263	-219.	.136	-100.
40.00	.260	-283.	.146	-67.
50.00	.132	-292.	.140	-96.
60.00	.027	-86.	.086	-116.
70.00	.140	-149.	.089	-88.
80.00	.331	-47.	.086	-99.
90.00	.374	-324.	.141	-102.
97.00	.245	-79.	.216	-119.

AFDSR3--BLD2 DATA POINT 2 FIRST HARM. ALPHA=27

ROTOR SPEED = 902.

AXIAL LOCATION	SUCTION SURFACE		PRESSURE SURFACE	
PERCENT OF CHORD	AMPLITUDE	PHASE	AMPLITUDE	PHASE
2.94	1.259	-65.	1.036	-246.
10.00	.584	-59.	.459	101.
20.00	.508	-168.	.241	102.
30.00	.684	-182.	.299	71.
40.00	.146	-200.	.392	40.
50.00	.312	-79.	.464	8.
60.00	.520	-93.	.442	-15.
70.00	.540	-161.	.415	-25.
80.00	.784	-75.	.344	-25.
90.00	1.119	-139.	.391	-30.
97.00	1.200	-176.	.494	-38.

AFUSR3--BLD2 DATA POINT2 SECOND HARM. ALPHA=27

ROTOR SPEED = 902.

AXIAL LOCATION	SUCTION SURFACE		PRESSURE SURFACE	
PERCENT OF CHORD	AMPLITUDE	PHASE	AMPLITUDE	PHASE
2.94	.566	-266.	.521	-82.
14.00	.050	-324.	.266	-73.
20.00	.241	-161.	.158	-96.
30.00	.186	-212.	.068	-60.
40.00	.084	-287.	.110	-71.
50.00	.050	-3.	.050	-86.
60.00	.084	-136.	.032	-55.
70.00	.136	-190.	.047	-47.
80.00	.865	-276.	.009	-58.
90.00	.130	-151.	.016	-39.
97.00	.085	-267.	.025	-51.

AFOSR3--BL02 DATA POINT 3 FIRST HARM. ALPHA=33

ROTOR SPEED = 901.

AXIAL LOCATION	SUCTION SURFACE		PRESSURE SURFACE	
PERCENT OF CHORD	AMPLITUDE	PHASE	AMPLITUDE	PHASE
2.94	2.420	-258.	.787	-105.
10.00	.680	-282.	.588	-103.
20.00	.415	-82.	.477	-108.
30.00	.572	-88.	.421	-129.
40.00	.242	-146.	.372	-163.
50.00	.203	-225.	.337	-193.
60.00	.178	-267.	.240	-208.
70.00	.274	-314.	.195	-218.
80.00	.384	-319.	.371	-221.
90.00	.643	-41.	.371	-221.
97.00	.524	-238.	.452	-233.

AFOSR3--BLD2 DATA POINT 3 SECOND HARM. ALPHA=33

ROTOR SPEED = 901.

AXIAL LOCATION	SUCTION SURFACE		PRESSURE SURFACE	
PERCENT OF CHORD	AMPLITUDE	PHASE	AMPLITUDE	PHASE
2.94	2.023	-260.	.408	-74.
10.00	.233	-49.	.235	-76.
20.00	.341	-172.	.120	-92.
30.00	.225	-226.	.077	-80.
40.00	.078	-291.	.095	-79.
50.00	.041	-67.	.516	-92.
60.00	.097	-172.	.046	-81.
70.00	.109	-217.	.054	-84.
80.00	.049	-216.	.031	-87.
90.00	.097	-206.	.051	-49.
97.00	.122	-229.	.613	-34.

AFOSR3--5L02 DATA POINT 4 FIRST HARM. ALPHA=36

ROTOR SPEED = 898.

AXIAL LOCATION	SUCTION SURFACE		PRESSURE SURFACE	
PERCENT OF CHORD	AMPLITUDE	PHASE	AMPLITUDE	PHASE
2.94	3.182	-229.	.742	-91.
10.00	1.530	-291.	.936	-90.
20.00	.415	-50.	.499	-99.
30.00	.597	-86.	.377	-125.
40.00	.348	-141.	.305	-159.
50.00	.346	-220.	.244	-187.
60.00	.282	-270.	.183	-202.
70.00	.320	-322.	.198	-207.
80.00	.191	-320.	.220	-199.
90.00	.433	-45.	.331	-217.
97.00	.557	-237.	.415	-228.

AFOSR3--SLL2 DATA POINT4 SECOND HARM. ALPHA=36

ROTOR SPEED = 898.

AXIAL LOCATION	SUCTION SURFACE		PRESSURE SURFACE	
PERCENT OF CHORD	AMPLITUDE	PHASE	AMPLITUDE	PHASE
2.94	2.100	-250.	.449	-95.
10.00	.936	-179.	.220	-95.
20.00	.577	-183.	.125	-104.
30.00	.295	-277.	.077	-105.
40.00	.110	-30.	.081	-102.
50.00	.150	-150.	.056	-110.
60.00	.118	-239.	.042	-102.
70.00	.008	-343.	.478	-109.
80.00	.047	-197.	.028	-104.
90.00	.059	-227.	.037	-71.
97.00	.089	-254.	.036	-50.

AFOSR3--BLD2 DATA POINT 5 FIRST HARM. ALPHA=25

ROTOR SPEED = 630.

AXIAL LOCATION	SUCTION SURFACE		PRESSURE SURFACE	
PERCENT OF CHORD	AMPLITUDE	PHASE	AMPLITUDE	PHASE
2.94	.745	-303.	.758	-168.
10.00	.495	-313.	.401	-272.
20.00	.242	-332.	.375	-287.
30.00	.135	-292.	.375	-283.
40.00	.251	-266.	.397	-280.
50.00	.297	-294.	.361	-276.
60.00	.357	-298.	.353	-277.
70.00	.310	-317.	.337	-278.
80.00	.293	-246.	.328	-282.
90.00	.459	-279.	.337	-292.
97.00	.625	-294.	.388	-295.

AFOSR3--BLD2 DATA POINT 5 SECOND HARM. ALPHA=25

ROTOR SPEED = 63M.

AXIAL LOCATION	SUCTION SURFACE		PRESSURE SURFACE	
PERCENT OF CHORD	AMPLITUDE	PHASE	AMPLITUDE	PHASE
2.94	1.001	-305.	2.083	-157.
10.00	.393	-327.	.482	-64.
20.00	.092	-192.	.518	-96.
30.00	.249	-255.	.266	-101.
40.00	.296	-339.	.250	-90.
50.00	.228	-52.	.248	-96.
60.00	.320	-108.	.215	-107.
70.00	.212	-131.	.114	-114.
80.00	.433	-200.	.157	-100.
90.00	.435	-341.	.093	-127.
97.00	.476	-57.	.160	-135.

AFUSR3--BL02 DATA POINT 6 FIRST HARM. ALPHA=27

ROTOR SPEED = 630.

AXIAL LOCATION	SUCTION SURFACE		PRESSURE SURFACE	
PERCENT OF CHORD	AMPLITUDE	PHASE	AMPLITUDE	PHASE
2.94	1.151	-272.	.322	-160.
10.00	.577	-278.	.515	-215.
20.00	.282	-221.	.467	-220.
30.00	.548	-215.	.451	-224.
40.00	.548	-215.	.432	-220.
50.00	.448	-254.	.491	-224.
60.00	.427	-247.	.454	-227.
70.00	.368	-244.	.387	-233.
80.00	.760	-213.	.303	-239.
90.00	.862	-243.	.213	-248.
97.00	.730	-273.	.217	-273.

-PUSR3--BLDZ DATA POINTS SECOND HARM. ALPHA=27

ROTOR SPEED = 630.

AXIAL LOCATION	SUCTION SURFACE		PRESSURE SURFACE	
PERCENT OF CHORD	AMPLITUDE	PHASE	AMPLITUDE	PHASE
2.94	.950	-253.	.205	-118.
10.00	.198	-307.	.486	-59.
20.00	.252	-158.	.500	-68.
30.00	.183	-215.	3.188	-82.
40.00	.207	-329.	.237	-69.
50.00	.090	-49.	.265	-80.
60.00	.283	-76.	.203	-90.
70.00	.283	-106.	.124	-93.
80.00	3.191	-206.	.145	-95.
90.00	.047	-350.	.184	-138.
97.00	.078	-62.	.261	-130.

AFOSR3--BLD2 DATA POINT / FIRST HARM. ALPHA=32

ROTOR SPEED = 634.

AXIAL LOCATION	SUCTION SURFACE		PRESSURE SURFACE	
PERCENT OF CHORD	AMPLITUDE	PHASE	AMPLITUDE	PHASE
2.94	1.176	-304.	1.388	-109.
10.00	.223	-186.	.961	-163.
20.00	.590	-126.	.926	-102.
30.00	.672	-142.	.978	-105.
40.00	.659	-159.	.912	-115.
50.00	.479	-160.	.757	-119.
60.00	.348	-159.	.621	-116.
70.00	.316	-146.	.588	-108.
80.00	.144	-147.	.613	-112.
90.00	.341	-100.	.637	-115.
97.00	.640	-123.	.672	-111.

AF0SR3--BLO2 DATA POINT 7 SECOND HARM, ALPHA=32

ROTOR SPEED = 634.

AXIAL LOCATION	SUCTION SURFACE		PRESSURE SURFACE	
PERCENT OF CHORD	AMPLITUDE	PHASE	AMPLITUDE	PHASE
2.94	.697	-295.	.562	-78.
10.00	.101	-335.	.345	-70.
20.00	.147	-176.	.234	-73.
30.00	.083	-257.	.161	-54.
40.00	.107	-351.	.135	-53.
50.00	.126	-35.	.108	-55.
60.00	.140	-89.	.103	-52.
70.00	.050	-97.	.059	-32.
80.00	.119	-42.	.053	-39.
90.00	.150	-98.	.038	-307.
97.00	.086	-91.	.054	-284.

AFOSR3--0L02 DATA POINT 8 FIRST HARMONIC ALPHA=35.5

ROTOR SPEED = 630.

AXIAL LOCATION	SUCTION SURFACE		PRESSURE SURFACE	
PERCENT OF CHORD	AMPLITUDE	PHASE	AMPLITUDE	PHASE
2.34	.949	-243.	1.464	-105.
14.00	.224	-304.	.981	-89.
20.00	.275	-118.	.945	-92.
30.00	.304	-134.	.939	-98.
40.00	.277	-146.	.847	-103.
50.00	.242	-153.	.725	-104.
60.00	.173	-151.	.665	-104.
70.00	.125	-126.	.603	-98.
80.00	.168	-104.	.607	-102.
90.00	.216	-112.	.569	-108.
97.00	.274	-121.	.589	-109.

AFOSR3--CLOD DATA POINT 8 SECOND HARMONIC ALPHA=35.5

ROTOR SPEED = 630.

AXIAL LOCATION	SUCTION SURFACE		PRESSURE SURFACE	
PERCENT OF CHORD	AMPLITUDE	PHASE	AMPLITUDE	PHASE
2.94	.783	-291.	.204	-139.
10.00	.206	-64.	.308	-88.
20.00	.133	-211.	.214	-87.
30.00	.084	-302.	.154	-74.
40.00	.064	-28.	.120	-70.
50.00	.056	-95.	.107	-74.
60.00	.029	-132.	.091	-68.
70.00	.039	-59.	.067	-52.
80.00	.055	-92.	.060	-54.
90.00	.043	-105.	.041	-3.
97.00	.048	-99.	.039	-9.

AFOSR-3 PI=1 1ST HARM 21/47

ROTOR SPEED = 885.

AXIAL LOCATION	SUCTION SURFACE		PRESSURE SURFACE	
PERCENT OF CHORD	AMPLITUDE	PHASE	AMPLITUDE	PHASE
2.94	.981	-222.	1.401	-358.
10.00	.662	-175.	1.316	-40.
20.00	.626	-246.	1.116	-49.
30.00	1.241	-297.	1.005	-61.
40.00	.938	-319.	.777	-82.
50.00	.645	-240.	.795	-41.
60.00	.808	-228.	.701	-54.
70.00	1.091	-253.	.693	-59.
80.00	.693	-82.	.701	-63.
90.00	1.060	-293.	.612	-95.
97.00	.645	-158.	.522	-120.

AFOSR-3 FT-1 2:D HARM 21/4U

ROTOR SPEED = 865.

AXIAL LOCATION	SUCTION SURFACE		PRESSURE SURFACE	
PERCENT OF CHORD	AMPLITUDE	PHASE	AMPLITUDE	PHASE
2.94	1.160	-244.	1.036	-112.
10.00	.317	-249.	.194	-51.
20.00	.310	-189.	.203	-62.
30.00	.336	-217.	.166	-72.
40.00	.369	-348.	.016	-309.
50.00	.107	-6.	.027	-289.
60.00	.189	-130.	.039	-51.
70.00	.224	-190.	.026	-112.
80.00	.035	-147.	.040	-193.
90.00	.290	-339.	.087	-50.
97.00	.097	-150.	.222	-120.

AFOSR-3 PT-2 1ST HARM 21/44

ROTOR SPEED = 845.

AXIAL LOCATION PERCENT OF CHORD	SUCTION SURFACE AMPLITUDE	SUCTION SURFACE PHASE	PRESSURE SURFACE AMPLITUDE	PRESSURE SURFACE PHASE
2.94	1.169	-272.	1.880	-109.
10.00	1.403	-263.	.902	-125.
20.00	.394	58.	.571	-137.
30.00	.879	-56.	.466	-129.
40.00	1.169	-74.	.514	-125.
50.00	.475	-81.	.563	-129.
60.00	.461	15.	.555	-149.
70.00	.091	2.	.371	-158.
80.00	.775	-23.	.383	-161.
90.00	.679	-24.	.197	-173.
97.00	.404	-10.	.222	-342.

AFOSR-3 FT-2 2ND HARM 21/4N

ROTOR SPEED = 885.

AXIAL LOCATION	SUCTION SURFACE		PRESSURE SURFACE	
PERCENT OF CHORD	AMPLITUDE	PHASE	AMPLITUDE	PHASE
2.00	.940	-247.	.723	-65.
14.00	.073	-204.	.321	-45.
20.00	.319	-153.	.271	-59.
30.00	.118	-36.	.167	-87.
40.00	.119	-11.	.086	-45.
50.00	.135	-43.	.109	-51.
60.00	.122	-121.	.055	-86.
70.00	.112	-194.	.043	-36.
80.00	.106	-204.	.032	-36.
90.00	.163	-306.	.035	-29.
97.00	.326	-201.	.052	-241.

AFOSR-3 PT-3 1ST HARM 21/40

ROTOR SPEED = 685.

AXIAL LOCATION	SUCTION SURFACE		PRESSURE SURFACE	
PERCENT OF CHORD	AMPLITUDE	PHASE	AMPLITUDE	PHASE
2.94	1.351	-251.	1.687	-84.
10.00	.228	83.	.843	-88.
20.00	.508	-66.	.637	-83.
30.00	.721	-79.	.613	-81.
44.00	.254	-145.	.651	-90.
50.00	.235	62.	.560	-106.
60.00	.362	24.	.439	-120.
70.00	.386	-14.	.277	-124.
80.00	.289	20.	.197	-110.
90.00	.869	-36.	.148	-81.
97.00	.356	-102.	.129	-59.

AFOSR-3 FT-3 200 HARM 21/40

ROTOR SPEED = 885.

AXIAL LOCATION PERCENT OF CHORD	SUCTION SURFACE AMPLITUDE	SUCTION SURFACE PHASE	PRESSURE SURFACE AMPLITUDE	PRESSURE SURFACE PHASE
2.94	.702	-249.	.692	-62.
10.00	.086	-173.	.346	-46.
20.00	.253	-150.	.272	-67.
30.00	.079	-158.	.142	-75.
40.00	.108	-50.	.130	-51.
50.00	.169	-60.	.141	-60.
60.00	.109	-116.	.074	-65.
70.00	.034	-219.	.073	-44.
80.00	.077	-30.	.070	-40.
90.00	.153	-160.	.061	-33.
97.00	.194	-230.	.078	-342.

AFOSR-3 PT-4 1ST HARM 21/40

ROTOR SPEED = 885.

AXIAL LOCATION PERCENT OF CHORD	SUCTION SURFACE AMPLITUDE	SUCTION SURFACE PHASE	PRESSURE SURFACE AMPLITUDE	PRESSURE SURFACE PHASE
2.94	1.526	-255.	1.461	-71.
10.00	.264	-257.	.921	-70.
20.00	.276	-82.	.813	-67.
30.00	.374	-88.	.764	-72.
40.00	.428	-87.	.855	-72.
50.00	.191	-197.	.590	-84.
60.00	.241	67.	.386	-103.
70.00	.212	23.	.268	-101.
80.00	.305	26.	.263	-96.
90.00	.555	-40.	.178	-112.
97.00	.201	-249.	.130	-155.

AFOSR-3 [illegible] PART 2174[illegible]

ROTOR SPEED = 685.

AXIAL LOCATION	SUCTION SURFACE		PRESSURE SURFACE	
PERCENT OF CHORD	AMPLITUDE	PHASE	AMPLITUDE	PHASE
2.34	.745	-259.	.588	-65.
10.00	.1?2	-171.	.333	-59.
20.00	.222	-167.	.223	-76.
30.00	.187	-178.	.139	-75.
40.00	.103	-173.	.161	-77.
50.00	.094	-70.	.120	-69.
60.00	.069	-126.	.087	-69.
70.00	.040	-83.	.087	-72.
80.00	.047	-142.	.067	-66.
90.00	.031	-202.	.072	-68.
97.00	.002	-245.	.063	-60.

APOSR-3 P-3 1ST HARM 21/40

ROTOR SPEED = 62[illegible].

AXIAL LOCATION	SUCTION SURFACE		PRESSURE SURFACE	
PERCENT OF CHORD	AMPLITUDE	PHASE	AMPLITUDE	PHASE
2.94	2.189	-292.	1.315	-142.
10.00	1.418	-315.	1.027	-185.
20.00	.809	20.	.864	-204.
30.00	.452	-320.	.554	-226.
40.00	.570	-294.	.350	-233.
50.00	1.092	-309.	.174	-220.
60.00	.961	-324.	.198	-207.
70.00	.847	16.	.357	-187.
80.00	.135	-204.	.288	-215.
90.00	.543	-264.	.216	-288.
97.00	.636	-42.	.529	-166.

APOSR-3 PT=3 2ND HARM 2140

ROTOR SPEED = 524.

AXIAL LOCATION	SUCTION SURFACE		PRESSURE SURFACE	
PERCENT OF CHORD	AMPLITUDE	PHASE	AMPLITUDE	PHASE
2.94	1.260	-235.	1.756	-67.
10.00	.263	-242.	.543	-17.
20.00	.361	-141.	.568	-26.
30.00	.249	-199.	.392	-44.
40.00	.188	-357.	.294	-70.
50.00	.344	-59.	.256	-56.
60.00	.474	-80.	.309	-61.
70.00	.308	-102.	.301	-94.
80.00	.112	-172.	.290	-94.
90.00	.735	-25.	.424	-112.
97.00	.748	-178.	.581	-114.

[illegible]

ROTOR SPEED = 62[illegible].

AXIAL LOCATION	SUCTION SURFACE		PRESSURE SURFACE	
PERCENT OF CHORD	AMPLITUDE	PHASE	AMPLITUDE	PHASE
2.04	.266	-187.	1.691	-87.
10.00	2.625	-236.	.911	-98.
20.00	.341	-245.	.523	-104.
30.00	.091	-207.	.312	-109.
40.00	.946	-210.	.331	-124.
50.00	1.144	-254.	.447	-140.
60.00	.925	-267.	.542	-151.
70.00	.835	-279.	.322	-137.
80.00	.537	-216.	.267	-128.
90.00	.915	-254.	.188	-302.
97.[illegible]	.456	62.	.546	-264.

AFOSR-3 PT-3 2ND YEAR 21/40

ROTOR SPEED = 620.

AXIAL LOCATION	SUCTION SURFACE		PRESSURE SURFACE	
PERCENT OF CHORD	AMPLITUDE	PHASE	AMPLITUDE	PHASE
2.94	.303	-154.	1.028	-23.
10.00	1.175	-220.	.798	-11.
20.00	.412	-121.	.733	-18.
30.00	1.272	-154.	.424	-36.
40.00	.196	-18.	.255	-38.
50.00	.268	-47.	.315	-42.
60.00	.445	-63.	.291	-55.
70.00	.346	-86.	.196	-92.
80.00	.215	-6.	.225	-84.
90.00	.739	-53.	.324	-132.
97.00	.527	-92.	.374	-148.

AD-A090 546 GENERAL MOTORS CORP INDIANAPOLIS IN DETROIT DIESEL A--ETC F/G 21/5
THE EFFECTS OF SOLIDITY, INTERBLADE PHASE ANGLE AND REDUCED FRE--ETC(U)
JUN 80 R L JAY, W A BENNETT F49620-78-C-0070
UNCLASSIFIED DDA-EDR-10339 AFOSR-TR-80-1041 NL

Cont

AFOSR-3 PT-7 1ST HARM 21/40

ROTOR SPEED = 620.

AXIAL LOCATION	SUCTION SURFACE		PRESSURE SURFACE	
PERCENT OF CHORD	AMPLITUDE	PHASE	AMPLITUDE	PHASE
2.94	2.905	-226.	2.291	-45.
10.00	.787	-217.	1.185	-43.
20.00	.443	-190.	1.065	-35.
30.00	.874	-189.	.813	-42.
40.00	1.129	-200.	.617	-64.
50.00	1.024	-225.	.499	-92.
60.00	.767	-238.	.372	-116.
70.00	.594	-243.	.283	-77.
80.00	.619	-244.	.319	-51.
90.00	.474	83.	.158	-62.
97.00	.242	-32.	.285	-205.

AFUSR-3 PT-7 2ND HARM 21/40

ROTOR SPEED = 620.

AXIAL LOCATION	SUCTION SURFACE		PRESSURE SURFACE	
PERCENT OF CHORD	AMPLITUDE	PHASE	AMPLITUDE	PHASE
2.94	1.230	-224.	1.390	-12.
10.00	.128	-194.	.882	-7.
20.00	.241	-102.	.714	-15.
30.00	.074	-87.	.445	-20.
40.00	.249	-8.	.364	-12.
50.00	.394	-23.	.364	-21.
60.00	.378	-44.	.312	-19.
70.00	.229	-18.	.200	-21.
80.00	.477	-33.	.243	-33.
90.00	.273	-67.	.130	-57.
97.00	.212	-17.	.138	-43.

AFOSR-3 PT-B 1ST HARM 21/40

ROTOR SPEED = 620.

AXIAL LOCATION	SUCTION SURFACE		PRESSURE SURFACE	
PERCENT OF CHORD	AMPLITUDE	PHASE	AMPLITUDE	PHASE
2.94	3.049	145.	1.757	-27.
10.00	.751	156.	.973	-8.
20.00	.397	-170.	.876	-12.
30.00	.697	-178.	.651	-23.
40.00	.871	-187.	.443	-48.
50.00	.749	164.	.310	-75.
60.00	.584	150.	.220	-110.
70.00	.475	137.	.191	-57.
80.00	.321	111.	.209	-39.
90.00	.169	26.	.136	-111.
97.30	.287	-60.	.465	-182.

AFUSR-3 PT-8 2ND HARM 21/40

ROTOR SPEED = 620.

AXIAL LOCATION	SUCTION SURFACE		PRESSURE SURFACE	
PERCENT OF CHORD	AMPLITUDE	PHASE	AMPLITUDE	PHASE
2.94	1.238	-223.	1.324	-331.
10.00	.081	-269.	.842	-328.
20.00	.070	-84.	.606	-332.
30.00	.138	-310.	.440	-331.
40.00	.339	39.	.341	-335.
50.00	.403	15.	.308	-342.
60.00	.276	8.	.252	-345.
70.00	.330	18.	.172	-351.
80.00	.313	-5.	.193	-358.
90.00	.238	15.	.097	-20.
97.00	.274	6.	.132	-54.

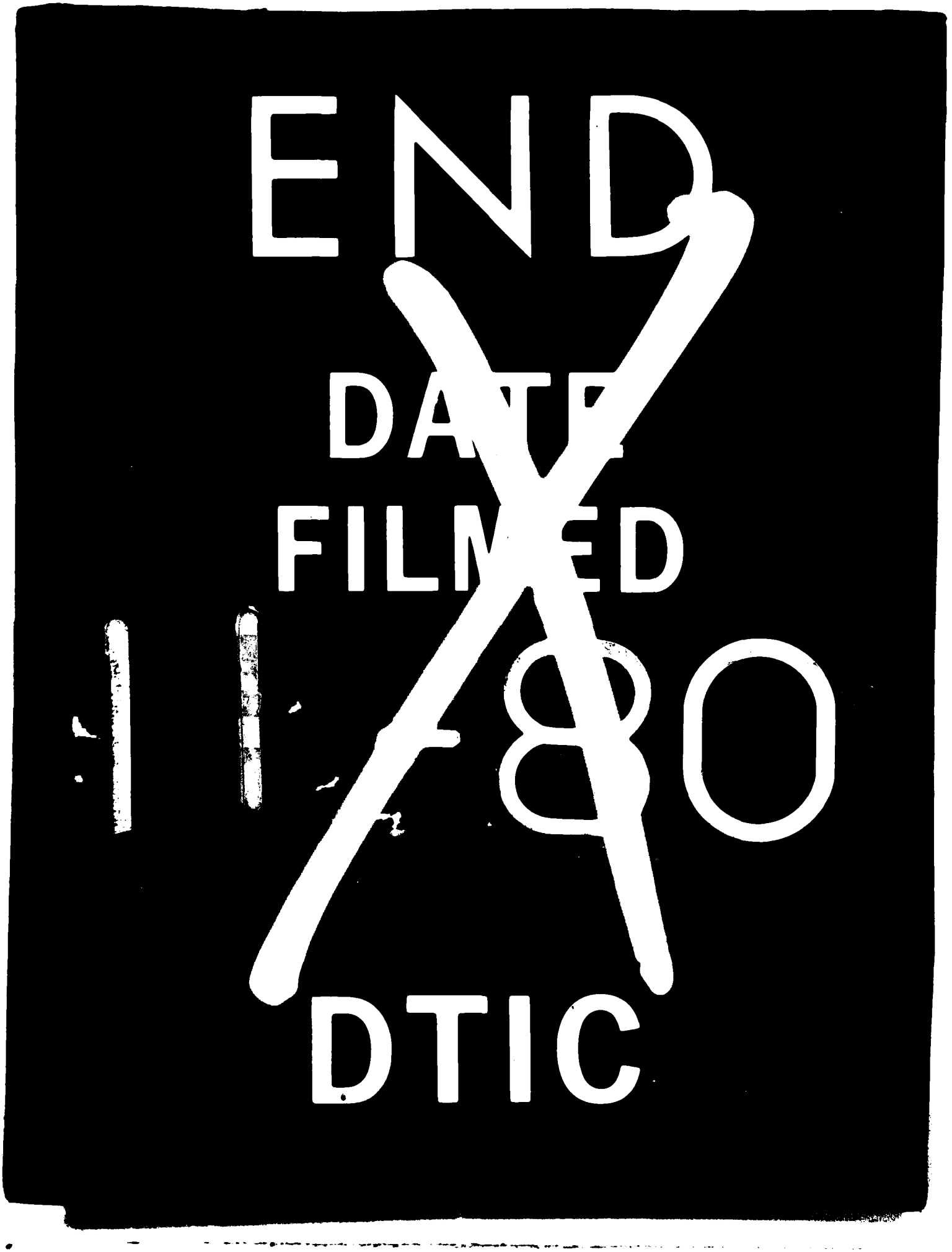
END
DATE
FILMED
80
DTIC

AD-A090 546 THE EFFECTS OF SOLIDITY INTERBLADE PHASE ANGLE AND REDUCED FREQUENCY ON T..(U) GENERAL MOTORS CORP INDIANAPOLIS IN DETROIT DIESEL ALLISON DI..

UNCLASSIFIED R L JAY ET AL. JUN 80 DDA-EDR-10339 F/G 21/5 NL

4/4

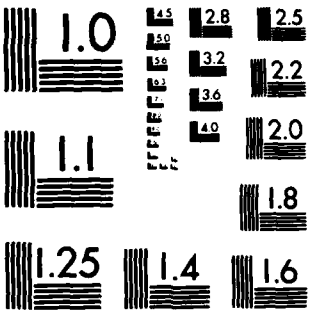

SUPPLEMENTARY

INFORMATION

Correction

SECURITY CLASSIFICATION OF THIS PAGE (When Data Entered)

REPORT DOCUMENTATION PAGE

REPORT NUMBER: AFOSR-TR-80-1041	2. GOVT ACCESSION NO.: AD-A090546
3. RECIPIENT'S CATALOG NUMBER: Change to Final	
TITLE (and Subtitle): THE EFFECTS OF SOLIDITY, INTERBLADE PHASE ANGLE AND REDUCED FREQUENCY ON THE TIME-VARIANT AERODYNAMIC RESPONSE OF A COMPRESSOR STATOR	5. TYPE OF REPORT & PERIOD COVERED: INTERIM ~~(ANNUAL)~~ Final, 1 May 1979 - 1 May 1980
	6. PERFORMING ORG. REPORT NUMBER
AUTHOR(s): ROBERT L JAY, WILLIAM A BENNETT	8. CONTRACT OR GRANT NUMBER(s): F49620-78-C-0070
PERFORMING ORGANIZATION NAME AND ADDRESS: DETROIT DIESEL ALLISON, P.O. BOX 894, INDIANAPOLIS, INDIANA 46206	10. PROGRAM ELEMENT, PROJECT, TASK AREA & WORK UNIT NUMBERS: 2307A4, 61102F
CONTROLLING OFFICE NAME AND ADDRESS: AIR FORCE OFFICE OF SCIENTIFIC RESEARCH/NA, BLDG 410, BOLLING AIR FORCE BASE, DC 20332	12. REPORT DATE: June 1980
	13. NUMBER OF PAGES: 103
MONITORING AGENCY NAME & ADDRESS (if different from Controlling Office)	15. SECURITY CLASS. (of this report): UNCLASSIFIED
	15a. DECLASSIFICATION DOWNGRADING SCHEDULE

DISTRIBUTION STATEMENT (of this Report)

Approved for public release; distribution unlimited

DISTRIBUTION STATEMENT (of the abstract entered in Block 20, if different from Report)

SUPPLEMENTARY NOTES

KEY WORDS (Continue on reverse side if necessary and identify by block number)

FORCED VIBRATION
AERODYNAMICALLY INDUCED VIBRATION
TURBO MACHINERY
UNSTEADY FLOW
AXIAL FLOW COMPRESSOR

ABSTRACT (Continue on reverse side if necessary and identify by block number)

An experimental investigation was conducted to provide basic unsteady pressure distributions on a stationary vane row, with the primary source of excitation being the wakes generated from an upstream rotor. This was accomplished over a wide range of key parameters in a large-scale, low-speed, single stage compressor. The excitation, the velocity defect created by the rotor blade wakes, was measured with a crossed hot wire. The resulting time-variant aerodynamic response was measured by means of flush mounted high response

DD FORM 1 JAN 73 1473

UNCLASSIFIED

SECURITY CLASSIFICATION OF THIS PAGE (When Data Entered)